

9. SITE 829¹

Shipboard Scientific Party²

HOLE 829A

Date occupied: 27 October 1990
Date departed: 4 November 1990
Time on hole: 7 days, 12 hr, 45 min
Position: 15°18.96'S, 166°20.7'E
Bottom felt (rig floor; m; drill-pipe measurement): 2916.2
Distance between rig floor and sea level (m): 11.0
Water depth (drill-pipe measurement from sea level, m): 2905.2
Total depth (rig floor; m): 3506.5
Penetration (m): 590.3
Number of cores (including cores with no recovery): 64
Total length of cored section (m): 590.3
Total core recovered (m): 197.44
Core recovery (%): 33.4
Oldest sediment cored:
Depth below seafloor (m): 495.0
Nature: foraminiferal chalk
Age: Oligocene
Measured velocity (km/s): 2.187
Hard rock:
Depth below seafloor (m): 532.8
Nature: basalt
Measured velocity (km/s): 5.358

HOLE 829B

Date occupied: 4 November 1990
Date departed: 4 November 1990
Time on hole: 7 hr, 15 min
Position: 15°18.97'S, 166°20.7'E
Bottom felt (rig floor; m; drill-pipe measurement): 2920.0
Distance between rig floor and sea level (m): 11.0
Water depth (drill-pipe measurement from sea level, m): 2909.0
Total depth (rig floor; m): 2939.5
Penetration (m): 19.5
Number of cores (including cores with no recovery): 3
Total length of cored section (m): 19.5
Total core recovered (m): 15.59
Core recovery (%): 80
Oldest sediment cored:
Depth below seafloor (m): 19.5
Nature: volcanic silt
Age: Pleistocene to Holocene
Measured velocity (km/s): 1.660

HOLE 829C

Date occupied: 4 November 1990
Date departed: 5 November 1990
Time on hole: 21 hr
Position: 15°18.96'S, 166°20.7'E
Bottom felt (rig floor; m; drill-pipe measurement): 2921.7
Distance between rig floor and sea level (m): 11.0
Water depth (drill-pipe measurement from sea level, m): 2910.7
Total depth (rig floor; m): 2980.1
Penetration (m): 58.4
Number of cores (including cores with no recovery): 11
Total length of cored section (m): 58.4
Total core recovered (m): 52.67
Core recovery (%): 90.2
Oldest sediment cored:
Depth below seafloor (m): 58.4
Nature: foraminiferal chalk
Age: Miocene
Measured velocity (km/s): 1.717

Principal results: We arrived at Site 829 on 27 October 1990 at 1930 hr Universal Time Coordinated (UTC). After 10 days and 1.5 hr on site drilling three holes (Holes 829A, 829B, and 829C) we departed Site 829 at 1230 UTC on 5 November 1990. We were forced to abandon Hole 829A at 590.3 meters below seafloor (mbsf) because of hole collapse and filling problems. Hole 829B was aborted because a core barrel bent on the steeply sloping seafloor. Hole 829C was completed in a hard horizon (58.4 mbsf) where the advanced piston coring (APC) system could penetrate no farther.

Site 829 (proposed Site DEZ-2) is located within the collision zone of the d'Entrecasteaux Zone (DEZ) along the forearc slope of the New Hebrides Island Arc where the North d'Entrecasteaux Ridge (NDR) impinges upon the arc slope, approximately 3 km south of Site 827 and about 35 km west of Espiritu Santo Island, Vanuatu. This site was located very close to the original proposed site (DEZ-2) along a single-channel seismic reflection line surveyed by the *JOIDES Resolution* prior to spudding in at Site 827. The site selected lies on a very narrow (~200-m-wide) shelf protruding out from a 10° slope. We were able to spud in without difficulty on our first try and cored to 590.3 mbsf, recovering 197.44 m of core for a recovery rate of 33.4%. Hole 829B was drilled and cored to 19.5 mbsf, recovering 15.59 m for an 80% recovery rate; Hole 829C was drilled and cored to 58.4 mbsf, recovering 52.67 m of core for a 90.2% recovery rate. The purpose of drilling a second hole at this site was to recover cores with the APC in the upper 100 m of section that was poorly recovered during drilling with the rotary core barrel in Hole 829A. Oriented cores for paleomagnetic analyses and structural examinations were taken and whole-round core samples for both fluid analyses and physical properties measurements were obtained. This was our second attempt to drill to the décollement in the DEZ–New Hebrides Island Arc collision zone. Although hole collapse prevented the penetration of the décollement, we successfully cored the overlying thrust sheets and accretionary prism and may have entered the upper reaches of the décollement zone. Tectonic

¹ Collot, J.-Y., Greene, H. G., Stokking, L. B., et al., 1992. *Proc. ODP, Init. Repts.*, 134: College Station, TX (Ocean Drilling Program).

² Shipboard Scientific Party as is given in the list of participants preceding the contents.

setting and objectives of this site are given in the Site 827 report and therefore will not be repeated here.

Lithostratigraphic examination of the 590.3 m of sedimentary and igneous rocks cored at Site 829 indicate that the sequence can be divided into 21 lithostratigraphic units (Units I–XXI) that represent repeated lithologies throughout the core. Because of these repetitions, the lithostratigraphic units can be divided into four composite units (Bigwan Wan, Bigwan Tu, Bigwan Tri, and Bigwan Fo). These composite units are defined on the basis of age and lithologies. Bigwan Wan is a Pleistocene volcanic silt, sandstone or gray silty chalk. Bigwan Tu is an upper Oligocene to lower Miocene, foraminiferal or calcareous chalk. Bigwan Tri is an upper Pliocene or Pleistocene chalk breccia with upper Oligocene to lower Miocene clasts. Bigwan Fo is an igneous breccia of unknown age with clasts of basalt, diabase, microgabbro, gabbro, pyroxenite, and serpentinite. At least six major thrust faults and seven minor thrust faults separate the lithostratigraphic units within the sequence and seven of them bound eight tectonic units (A–H); tectonic Unit E is subdivided into two subunits (Subunits E₁ and E₂), based on the presence of major thrust faults. These tectonic units become progressively more intensively deformed downhole.

The lithostratigraphic units are defined on the basis of lithology, carbonate vs. volcanic composition, and structural relationships. Lithostratigraphic units are numbered consecutively starting with Hole 829A and ending with Hole 829C. In Hole 829A, lithostratigraphic Unit I (0–60.5 mbsf; Bigwan Wan, tectonic Unit A) is composed of Pleistocene clayey volcanic silt, siltstone, and sandstone. Lithostratigraphic Unit II (60.5–99.4 mbsf; Bigwan Tu, tectonic Unit A), based on fragments from a poorly recovered zone, is an upper Oligocene to lower Miocene foraminiferal chalk. Lithostratigraphic Unit III (99.4–171.9 mbsf; Bigwan Wan, tectonic Unit B) is a Pleistocene clayey volcanic silt and sandstone. Lithostratigraphic Unit IV (171.9–205.2 mbsf; Bigwan Tri, tectonic Unit C) is a siltstone chalk breccia composed of angular clasts of calcareous volcanic sandy siltstone and calcareous chalk that is separated from the overlying Unit III by a minor thrust-faulted contact.

Lithostratigraphic Unit V (205.2–311.3 mbsf; Bigwan Tri, tectonic Unit C) consists of upper Pliocene or Pleistocene breccia with upper Oligocene to lower Miocene clasts. Lithostratigraphic Unit VI (311.3–398.9 mbsf; Bigwan Tu, tectonic Unit D) consists of middle Oligocene to lower Miocene calcareous chalk that is separated from underlying Unit VII by brown clay laminae.

Lithostratigraphic Unit VII (398.9–407.4 mbsf; Bigwan Fo, tectonic Unit D), a volcanic breccia of unknown age, is composed of igneous rock clasts in a matrix of calcareous silty clay with sedimentary fragments. The igneous clasts include aphyric to sparsely phryic basalts, pyroxenite, and serpentinite. It is a poorly recoverable zone that appears to be highly sheared and fractured, exhibiting microfolds and reverse faults with a major thrust located near the base of the unit.

Lithostratigraphic Unit VIII (407.4–407.8 mbsf; tectonic Unit E₁) is a small (0.4-m-thick) sliver of lower Pliocene chalk. Lithostratigraphic Unit IX (407.8–421.6 mbsf; Bigwan Tu, tectonic Unit E₁) is a Pleistocene calcareous silty mixed sediment. Lithostratigraphic Unit X (421.6–427.3 mbsf; Bigwan Tu, tectonic Unit E₁) is a highly tectonized pale brown Oligocene chalk with a 14-cm-thick brown clay layer that marks a thrust fault at the base of the unit.

Lithostratigraphic Unit XI (427.3–445.9 mbsf; Bigwan Wan, tectonic Unit E₂) is an upper Pliocene(?) or Pleistocene dark gray silty chalk. Lithostratigraphic Unit XII (445.9–462.9 mbsf; Bigwan Tu, tectonic Unit E₂) is an Oligocene, pale brown chalk with brown clay laminae at its base, and lies within a major northeast-dipping thrust fault zone. Beneath this thrust contact lies lithostratigraphic Unit XIII (462.9–484.5 mbsf; Bigwan Wan, tectonic Unit F), an upper Pliocene or Pleistocene calcareous volcanic sandstone with sand-sized clasts of pumice, wood, and chalk, some of Oligocene age. Lithostratigraphic Unit XIV (484.5–495.6 mbsf; Bigwan Tu, tectonic Unit F) is an Oligocene, brown, white, and pale brown chalk and brown mixed sediment with a major thrust fault at its base that separates this unit from the underlying Unit XV. Lithostratigraphic Unit XV (495.6–517.2 mbsf; Bigwan Wan, tectonic Unit G) is a sandy volcanic siltstone of Pliocene or

Pleistocene age and is separated from the underlying Unit XVI by an interval of sandy brown clay.

The final unit in Hole 829A is lithostratigraphic Unit XVI (517.2–590.3 mbsf; Bigwan Fo, tectonic Units G and H), an interval of unknown age that is composed of alternating layers of sed-lithic breccia and intervals of ig-lithic breccia containing fragments of basalt, diabase, microgabbro, and gabbro. Preliminary geochemical studies suggest affinities with the igneous rocks from Site 828 on the NDR. Thus, we suspect that the drill may have penetrated the upper surface of the décollement or was quite close to it.

Lithostratigraphic Unit XVII (0–19.5 mbsf; Bigwan Wan, tectonic Unit A), the only unit defined in Hole 829B, is a Pleistocene clayey sandy volcanic silt that may be correlated with lithostratigraphic Unit I of Hole 829A.

In Hole 829C, four additional lithostratigraphic units are defined (Units XVIII–XXI). Lithostratigraphic Unit XVIII (0–54.6 mbsf) contains Pleistocene clayey, sandy, volcanic silt and clayey volcanic silt with a basal interval of silty foraminiferal mixed sediment; this unit correlates with Unit I of Hole 829A and is a member of Bigwan Wan and tectonic Unit A. Lithostratigraphic Unit XIX (54.6–57.3 mbsf) is a lower Miocene foraminiferal ooze; this unit is correlatable with lithostratigraphic Unit II in Hole 829A and is a member of Bigwan Tu and tectonic Unit A. Lithostratigraphic Unit XX (57.3–58.3 mbsf) is a Pliocene(?) silty foraminiferal mixed sediment that belongs to Bigwan Wan and tectonic Unit A. Lithostratigraphic Unit XXI (58.3–58.4 mbsf) is a foraminiferal chalk found at the total depth of Hole 829C.

Initial interpretations of the cores suggest that many of the units identified in Hole 829A are similar to those observed in Hole 828A. For example, the calcareous chalk and the pale brown chalk of Bigwan Tu are similar in age and lithology to the nannofossil chalk of lithostratigraphic Unit III from Hole 828A. Igneous rocks collected at both Site 828 and 829 are similar. Therefore, we tentatively conclude that we drilled through an accretionary prism that is composed in part of offscraped rocks and sediments from the downgoing NDR. As at Site 828, a middle to upper Miocene hiatus appears to exist at Site 829.

Foraminifers and nannofossils were the best source of age information, based primarily on core-catcher samples. Unconsolidated samples recovered were principally of Pleistocene age; some material of Pliocene age was also found. The more lithified samples of calcareous chalk revealed an age of Oligocene to possible early Miocene and Eocene. Paleomagnetic polarity is normal (Brunhes Chron) from 0–50 mbsf; below this depth cores were too tectonically deformed for accurate measurements to be made. At 100–150 mbsf the volcanic silt showed very high magnetic susceptibility values; susceptibilities of different lithostratigraphic units are quite distinct.

Analyses of fluids from whole-round samples of the core indicate a sharp decrease in magnesium concentration within the upper 10 m, suggesting a high fluid flux up through the sediments. Chloride was constant from 0–250 mbsf. Solutes related to organic carbon appear low in the upper 100 m of core (in lithostratigraphic Units II and III), but increase in concentration beneath the thrust fault that separates Units I and II. Beneath this fault, to a depth of about 500 mbsf the core is extremely dry and devoid of water. However, below this depth, the fluid content increases, minor amounts of methane occur, and chloride concentrations are low. Initial interpretations indicate that Hole 829A may have terminated close to the décollement because the fluid chemistry, showing an increase in methane accompanying low chloride concentration, is similar to that found along other subduction zones (i.e., Barbados and Nankai). The brecciated sequence (Unit XVI, 517.2–590.3 mbsf) may then represent the sheared and deformed rocks that lie within the décollement just above the basement rocks of the NDR. Above the wet zone, the area of dry rocks suggests that dewatering has taken place, the result of compressional pressures exerted onto the forearc slope by the impingement of the NDR. Fluid migration may be taking place along the thrust fault (100 mbsf) that separates Unit II from Unit III.

The most notable feature of the physical properties at Site 829 is the distinctly sharp decrease in porosity and water content at the contact between lithostratigraphic Unit IV and lithostratigraphic

Unit V (205.2 mbsf) and below. Porosity and water content range from 29.4% to 37.3% and 14.6% to 18.4%, respectively, from 205.2 mbsf to the bottom of Hole 829A (590.3 mbsf). These ranges are significantly lower than Sites 827 and 828 and probably result from the collision of the North d'Entrecasteaux Ridge. Sudden anomalous increases or decreases of porosity and water content were also observed at the locations of major thrust planes and overthrust faults. For example, porosity and water content suddenly increased by about 20%–25% in the overthrust zone at 397.8–399.9 mbsf.

Logging of Hole 829A was extensive and provided excellent results. The digital borehole televiewer and magnetic susceptibility tool were run for the first time in Ocean Drilling Program and resulted in the collection of good data that appear to correlate well with the formation microscanner (FMS) and other logging tools. The FMS, seismic stratigraphy combination, and geochemical tools correlated very well with each other and with the lithostratigraphic units. Thrust faults and lithologic contacts were well defined in all logs. Physical properties measurements of the cores in Hole 829A also correlate well with the lithostratigraphic units. Calcium carbonate measurements correlate well with water-rich zones defined by the fluid analyses.

BACKGROUND AND OBJECTIVES

Site 829 was chosen to penetrate the décollement as well as a series of thrust sheets that have been severely deformed by the collision of the North d'Entrecasteaux Ridge (NDR) with the New Hebrides Island Arc. Specific objectives for drilling at Site 829 are identical to those for drilling at Site 827. Site 829 was located away from the terrace-like feature at Site 827 to avoid drilling troubles related to the unstable, poorly lithified conglomerate encountered at that site. On the basis of seismic reflection profiles collected during the pre-site geophysical survey, we located the site on a small flat area along a slope that dips 10° west, where rocks overlying the décollement are thinner than at Site 827 (Fig. 1). Site 829 lies only 2 km east of the trace of the subduction zone, at a depth of 2916 m below sea level (mbsl).

At the toe of the arc slope, near Sites 827 and 829, a Seabeam bathymetric map indicates several narrow flat areas separated by 100-m-high scarps that converge southward near Site 829 (Fig. 2) (Collot and Fisher, 1991). These morphologic features may be the trace of thrust faults that dip arcward in the accretionary wedge and separate possible thrust sheets.

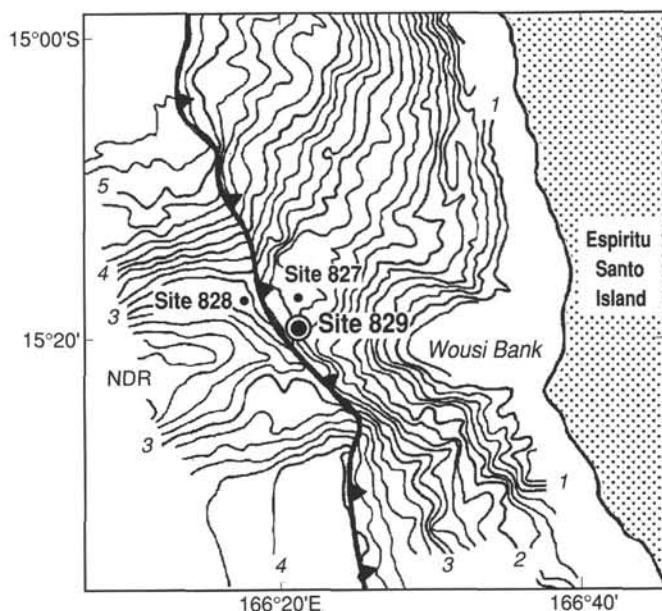


Figure 1. Location of Leg 134 drilling sites in the collision zone between the North d'Entrecasteaux Ridge (NDR) and the New Hebrides Island Arc (modified after Collot et al., 1989). Bathymetry in kilometers; contour interval is 200 m.

Multichannel seismic reflection data collected across the arc slope near Site 829 indicate a strong, low-frequency reflector that extends below the arc slope, 15 km arcward from the trench (Fisher et al., 1986). This reflector has been interpreted as the interplate décollement between the NDR and the New Hebrides Island Arc. However arc-slope rocks above the décollement are poorly reflective and do not show clear evidence of thrust faulting (Fisher et al., 1991). A reconnaissance of the seafloor was conducted near Site 829 with the deep submersible *Nautilé* (Collot et al., 1989). Observations made during the dives revealed a smooth seafloor that dips locally 25° westward and is draped with Pleistocene grayish

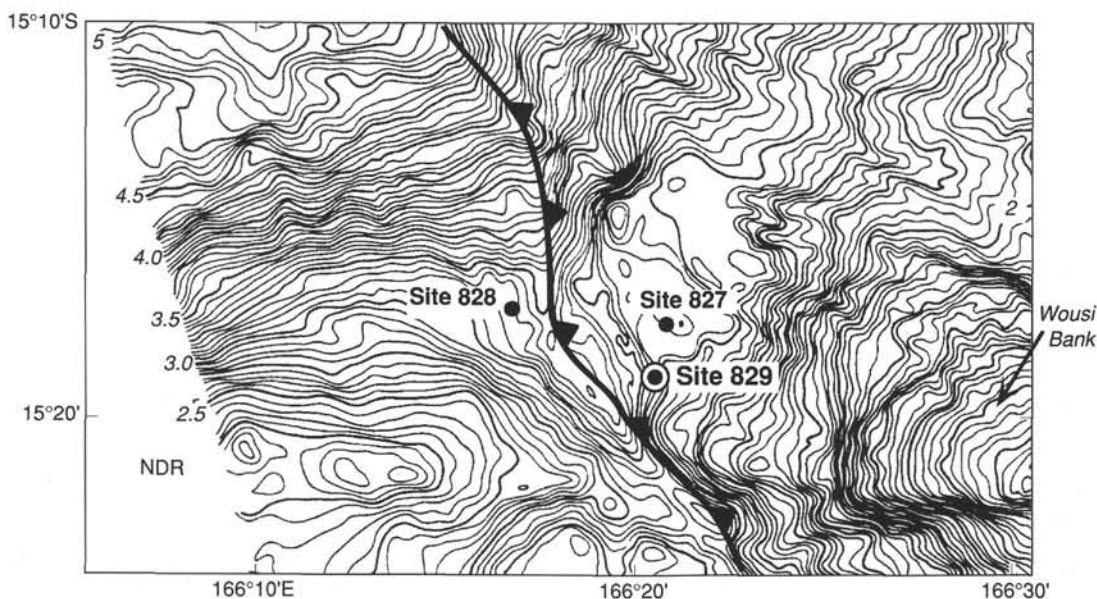


Figure 2. Detailed Seabeam bathymetry of the collision zone between the North d'Entrecasteaux Ridge and the New Hebrides Island Arc (modified after Collot and Fisher, 1991). Bathymetry in kilometers, contour interval is 50 m.

green mud. The trace of the subduction zone was tentatively identified as a west-facing scarp, 1–2 m high, that extends along the morphologic depression between the NDR and the lower arc slope.

SEISMIC STRATIGRAPHY

Multichannel Seismic Data

The description of the multichannel seismic data from near this site is included in the description of Site 827 and is summarized here. A reflection from the top of the colliding north ridge can be traced beneath the arc's lower slope (Fig. 3 and 4), and under the arc slope this reflection may be from the subducted top of the ridge sediment or from the contact between this sediment and the underlying, putative igneous basement. In either case, we interpret this reflection to be from the interplate décollement, but neither at Site 829 nor at Site 827 did the drill penetrate this reflector. The poor acoustic image of rocks near these sites suggests that considerable disruption of forearc strata has attended insertion of the north ridge; in particular, the low number of diffractions and reflections from within the slope rocks may indicate that the coherent rock bodies are substantially smaller than the area of the first Fresnel zone.

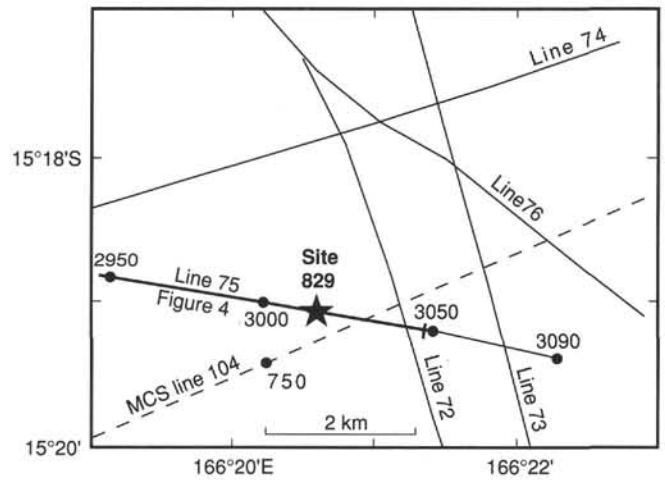


Figure 3. Trackline map showing the locations of Site 829, single-channel seismic line 75 (Fig. 4) and multichannel seismic line 104 (USGS, L5-84-SP).

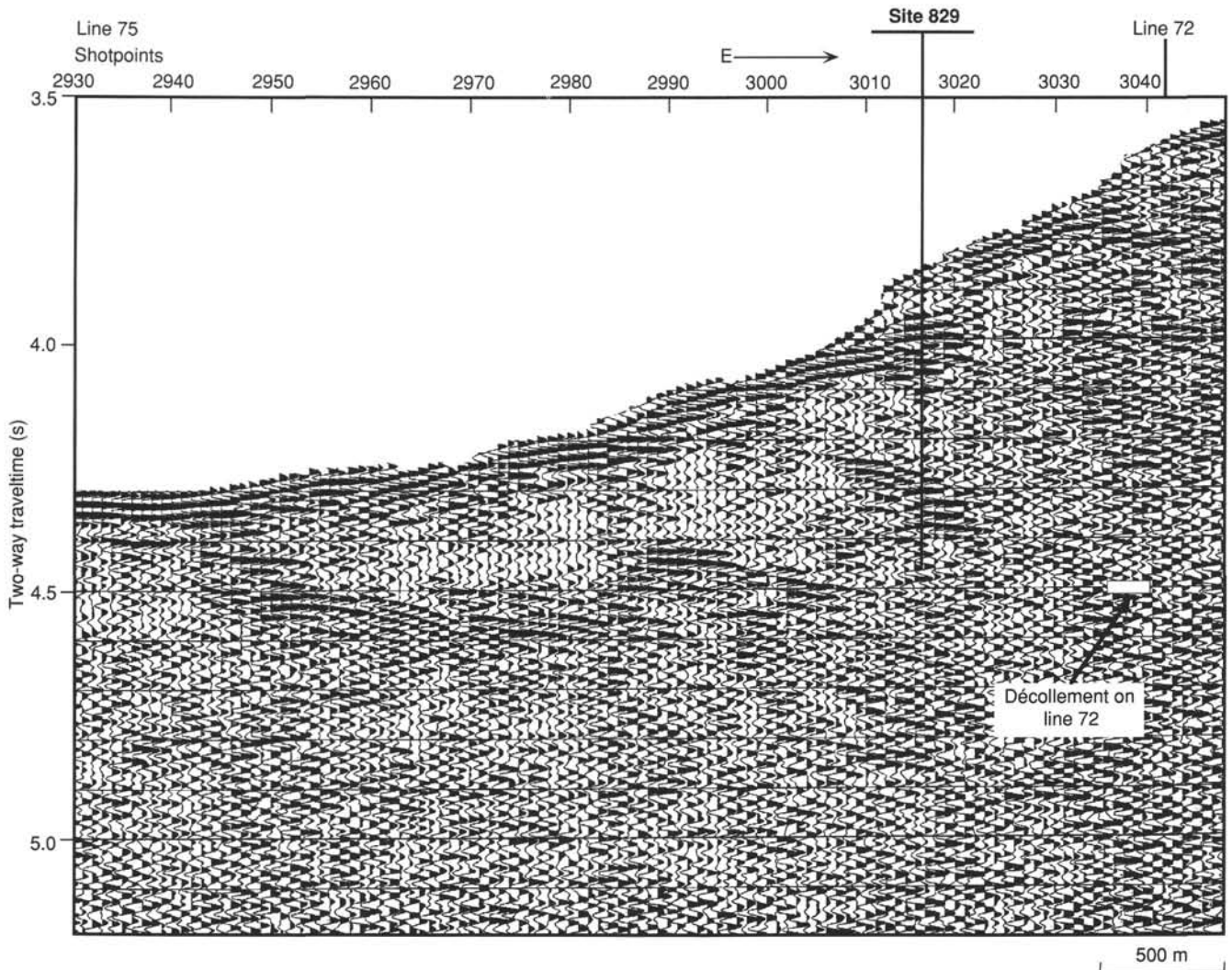


Figure 4. Part of single-channel seismic line 75 that crosses the arc slope near Site 829.

Single-Channel Seismic Data

Single-channel seismic (SCS) reflection data were collected over Site 829 using two 80-in.³ water guns for the source and a streamer that has a 100-m-long active section. Processing aboard ship included predictive deconvolution, bandpass filtering, and automatic gain control.

Seismic line 75 (Figs. 3 and 4) crosses over Site 829 and seismic line 72 crosses line 75 just east of the site. Together with one multichannel seismic section, these two single-channel lines indicate that the reflector presumed to be the interplate décollement underlies the site at a sub-bottom time of about 0.62 seconds (s).

Velocity data used to convert depth in the hole to travel-time come primarily from the velocity log and partly from physical properties measurements, which were used where well-log data are not available from the very shallowest and the deeper parts of the hole.

The comparison of the lithologic boundaries determined from core analysis with single-channel seismic reflection data (Fig. 5) shows that the upper two lithostratigraphic units correlate with seismic reflections that dip northwest. Lithostratigraphic Unit I is a Pleistocene silt and Unit II is an Oligocene chalk. Some of the high-frequency apparent reflections that parallel and lie within about 0.08 s of the seafloor are actually residual peaks in the outgoing seismic pulse that remain after deconvolution and filtering. Nevertheless, some reflections appear to be from geologic features, and the reflections end on the west at a seafloor scarp. This seafloor scarp is one of several extensive features that appear to have formed at the toes of thrust faults, which crop out at the base of each scarp, as interpreted from combined Seabeam and seismic reflection data.

Lithostratigraphic Unit III is a Pleistocene silt; the top of Unit III is a biostratigraphically determined thrust fault (see "Biostratigraphy" section, this chapter), the contact between an upper Oligocene to lower Miocene chalk above the fault and a Pleistocene silt below. Well-log data indicate that this contact should be a good reflector. The seismic data of Figure 5 show that, unlike the reflections of Units I and II which dip northwest, reflections at the traveltime of Unit III dip southeast. In fact, the most apparent reflection from Unit III extends southeastward from the base of the seafloor scarp that lies just northwest of the site. Because this reflection conforms to the relationship between thrust faults and seafloor scarps, we believe that it is from a thrust fault. We cannot yet explain why the reflection stems from an interface lying nearly halfway down Unit III: the reflection crosses Hole 829A at a traveltime greater than that of the fault observed in cores and well logs.

The lithostratigraphic Units IV through XIV fall in an area of the seismic section that includes primarily short discontinuous reflections. The significance of these reflections cannot be judged at this stage.

A good reflection crosses Hole 829A at about 4.77 s (Fig. 5). This reflection also dips southeast from the foot of a seafloor scarp, and we propose that it, too, is a thrust fault. This fault crosses Hole 829A below the base of the logged section, just below 480 mbsf. Numerous thrust faults have been interpreted from analysis of cores from near this depth (see "Structural Studies" section, this chapter).

OPERATIONS

Site 829 represented a second attempt to penetrate the décollement near proposed site DEZ-2. The new site was located away from sediment ponds revealed on the seismic reflection profiles, in an area where the section

overlying the décollement was considerably thinner than at Site 827.

Hole 829A

During the round trip of the drill string the vessel was moved in dynamic positioning mode to a location about 4.1 nautical miles (nmi) southeast of Site 828 and 2.3 nmi south of Site 827. Because the precision depth recorder displayed multiple reflections, the top drive was deployed well before the bit reached the shallowest echo (2852 mbsl). After several joints of "feeling for bottom" and one "water core," a core containing the mudline finally determined the depth to be 2905.2 mbsl.

Continuous rotary core barrel (RCB) cores then were taken through an alternating series of Pleistocene clayey silt and older fractured carbonate rocks separated by thrust faults (see "Lithostratigraphy" and "Structural Studies" sections, this chapter). The rate of penetration was generally low but the hole remained remarkably stable throughout the highly fractured and unstable tectonized section. The first signs of torque, fill, and sticking began at about 525 mbsf and became progressively worse with depth despite mud flushes and short trips. Because of the risk of hole collapse, coring operations ceased at 590.4 mbsf, before fully penetrating the décollement and basement targets, and preparations were made for logging.

The Schlumberger "quad combo," FMS, and geochemical combination logs were recorded successfully from about 460 mbsf. From about 430 mbsf, the LDGO digital borehole televiwer (BHTV) and the magnetic susceptibility logs then were successfully recorded (see "Downhole Measurements" section, this chapter). A total of 197.44 m of core were recovered; recovery averaged 33.4% (Table 1).

Hole 829B

Hole 829B was attempted 10 m south of Hole 829A to recover oriented advanced piston coring system (APC) cores from the uppermost tectonized slab of carbonate rocks at 60–100 mbsf. Three attempts to spud with the APC on the sloping seabed resulted in a total of 15.59 m of soft surficial sediment and a badly bent core barrel.

Hole 829C

The rig was repositioned to a point 10 m east of Hole 829A for another try at recovering oriented APC cores. Although the spud in was successful, the sediment proved to be exceptionally firm and incomplete strokes began with the second core. Short cores were taken to 52 mbsf, with broken liners and some core disturbance, where a chalky ooze was encountered in which little APC progress could be made. In an attempt to make a second temperature measurement at 58 mbsf with the water sample temperature probe (WSTP), the thermistor probe tip was broken off and left in the hole. The hole was then terminated because of the ineffectiveness of the APC to core well in the hard formation and the presence of pieces of the thermistor in the bottom of the hole. Eleven APC cores retrieved a total of 52.67 m for a recovery of 90.2% (Table 1).

LITHOSTRATIGRAPHY

Sedimentary Units

Sedimentologic data combined with biostratigraphic (see "Biostratigraphy" section, this chapter) and structural data (see "Structural Studies" section, this chapter) suggest that the stratigraphic sequence at Site 829 is structurally complex. Thrust faulting has placed older units over younger, causing

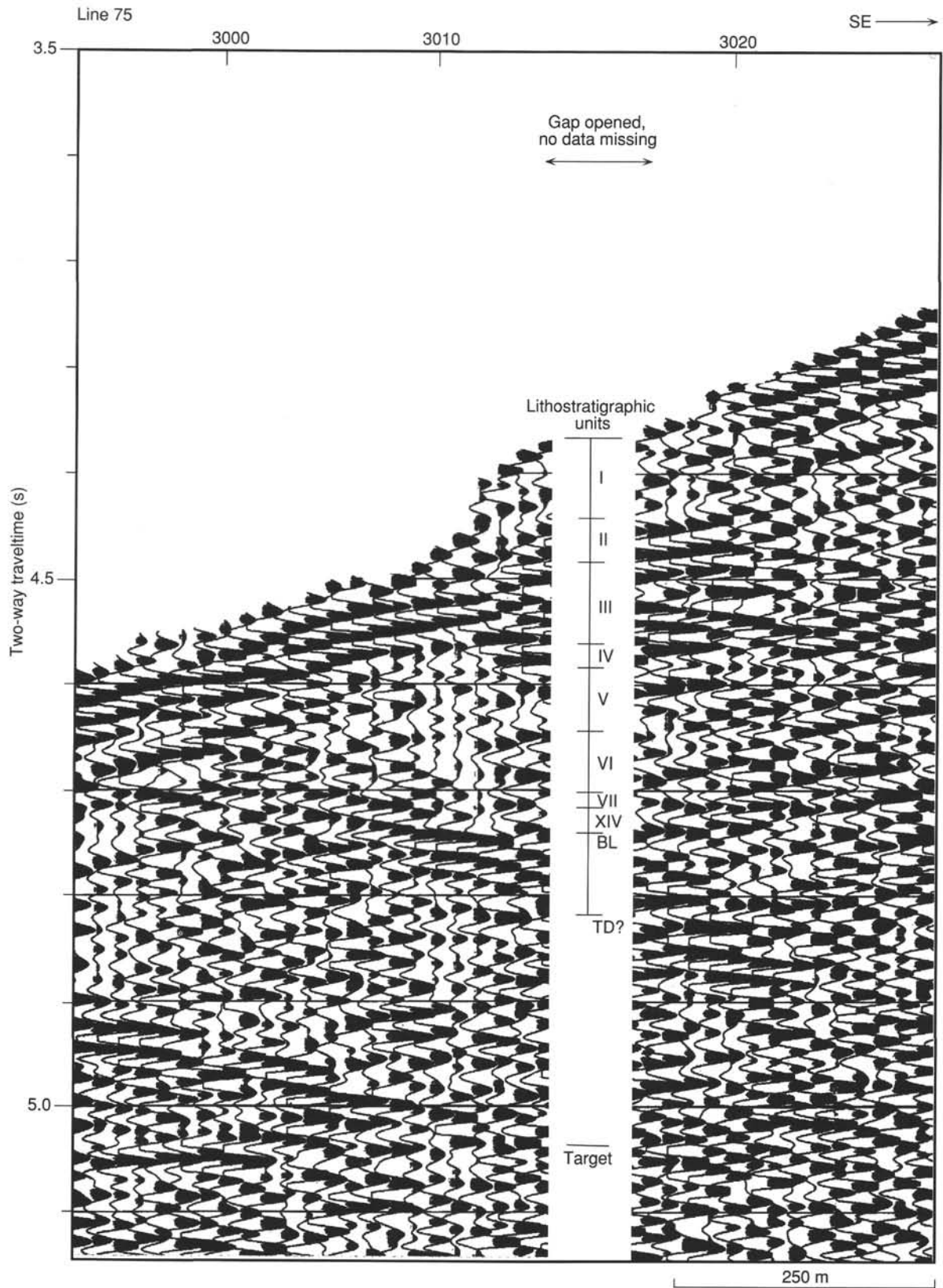


Figure 5. Detailed part of single-channel seismic line 75 that crosses Site 829. Lithostratigraphic units are explained in the "Lithostratigraphy" section (this chapter). Vertically along the line in the gap at the center of the section are numbers that stand for the lithostratigraphic units, and the short, horizontal bars indicate the bottom of the numbered units; "BL" shows the bottom of the logged interval; "TD?" indicates the approximate total depth of this hole.

Table 1. Coring summary, Holes 829A, 829B, and 829C.

Core	Date (1990)	Time (UTC)	Depth (mbsf)	Length cored (m)	Length recovered (m)	Recovery (%)	Age
134-829A-							
1R	28 October	0530	0.0–2.8	2.8	2.79	99.6	Pleistocene
2R	28 October	0620	2.8–12.3	9.5	4.02	42.3	Pleistocene
3R	28 October	0655	12.3–21.6	9.3	4.17	44.8	Pleistocene
4R	28 October	0740	21.6–31.0	9.4	6.73	71.6	Pleistocene
5R	28 October	0830	31.0–41.1	10.1	9.18	90.9	Pleistocene
6R	28 October	0920	41.1–50.8	9.7	9.72	100.0	Pleistocene
7R	28 October	1020	50.8–60.5	9.7	3.30	34.0	Pleistocene
8R	28 October	1140	60.5–70.1	9.6	0.35	3.6	Miocene-Oligocene
9R	28 October	1235	70.1–79.7	9.6	0.12	1.3	Miocene-Oligocene
10R	28 October	1400	79.7–89.3	9.6	0.85	8.9	Miocene-Oligocene
11R	28 October	1525	89.3–99.0	9.7	0.12	1.2	Miocene-Oligocene
12R	28 October	1650	99.0–108.6	9.6	9.83	102.0	Pleistocene
13R	28 October	1810	108.6–118.2	9.6	9.79	102.0	?Pliocene
14R	28 October	2000	118.2–127.9	9.7	9.75	100.0	?Pliocene
15R	28 October	2130	127.9–137.5	9.6	9.72	101.0	Pleistocene
16R	28 October	2300	137.5–147.2	9.7	9.69	99.9	Pleistocene
17R	29 October	0015	147.2–156.8	9.6	9.70	101.0	Pleistocene
18R	29 October	0200	156.8–166.5	9.7	9.25	95.3	Pleistocene
19R	29 October	0350	166.5–176.1	9.6	7.65	79.7	Pleistocene
20R	29 October	0520	176.1–185.8	9.7	3.36	34.6	Pleistocene
21R	29 October	0650	185.8–195.5	9.7	4.60	47.4	Pliocene
22R	29 October	0820	195.5–205.2	9.7	2.42	24.9	Pliocene
23R	29 October	1020	205.2–214.9	9.7	1.91	19.7	Pliocene
24R	29 October	1155	214.9–224.6	9.7	1.90	19.6	Pliocene + Oligocene
25R	29 October	1400	224.6–234.3	9.7	0.69	7.1	Miocene-Oligocene
26R	29 October	1555	234.3–243.9	9.6	1.34	13.9	Miocene-Oligocene
27R	29 October	1755	243.9–253.6	9.7	2.14	22.0	Miocene-Oligocene
28R	29 October	2000	253.6–263.1	9.5	1.25	13.1	Miocene-Oligocene
29R	29 October	2215	263.1–272.8	9.7	0.64	6.6	Pliocene
30R	30 October	0015	272.8–282.4	9.6	0.96	10.0	Pliocene
31R	30 October	0215	282.4–292.1	9.7	2.15	22.1	Pliocene + Oligocene
32R	30 October	0410	292.1–301.8	9.7	0.92	9.5	Miocene
33R	30 October	0550	301.8–311.3	9.5	0.95	10.0	early Miocene
34R	30 October	0805	311.3–320.5	9.2	1.17	12.7	Oligocene
35R	30 October	1010	320.5–330.2	9.7	1.13	11.6	Miocene-Oligocene
36R	30 October	1200	330.2–339.8	9.6	0.21	2.2	Miocene-Oligocene
37R	30 October	1415	339.8–349.5	9.7	0.99	10.2	Miocene-Oligocene
38R	30 October	1640	349.5–359.1	9.6	0.36	3.8	early Miocene
39R	30 October	1910	359.1–368.8	9.7	0.68	7.0	Oligocene
40R	30 October	2200	368.8–378.4	9.6	1.29	13.4	Oligocene
41R	31 October	0015	378.4–388.1	9.7	2.49	25.7	Oligocene
42R	31 October	0250	388.1–397.7	9.6	1.69	17.6	Oligocene
43R	31 October	0510	397.7–407.4	9.7	4.84	49.9	—?
44R	31 October	0645	407.4–416.6	9.2	3.03	32.9	
45R	31 October	0810	416.6–421.6	5.0	1.29	25.8	Pleistocene
46R	31 October	0925	421.6–426.6	5.0	0.45	9.0	early Pliocene
47R	31 October	1140	426.6–436.3	9.7	1.64	16.9	Pleistocene
48R	31 October	1340	436.3–445.9	9.6	1.55	16.1	late Pliocene
49R	31 October	1540	445.9–455.6	9.7	0.24	2.5	Miocene-Oligocene
50R	31 October	1740	455.6–460.1	4.5	0.75	16.6	Oligocene
51R	31 October	1950	460.1–465.2	5.1	4.06	79.6	Pliocene
52R	31 October	2200	465.2–474.8	9.6	2.10	21.9	Pliocene
53R	31 October	2350	474.8–484.5	9.7	1.64	16.9	Pleistocene
54R	1 November	0230	484.5–494.1	9.6	0.90	9.4	Oligocene
55R	1 November	0550	494.1–503.8	9.7	1.57	16.2	Pleistocene + Oligocene
56R	1 November	0800	503.8–513.5	9.7	7.57	78.0	Pliocene?
57R	1 November	1110	513.5–523.2	9.7	5.01	51.6	?
58R	1 November	1430	523.2–532.9	9.7	1.87	19.3	?
59R	1 November	1655	532.9–542.6	9.7	1.04	10.7	
60R	1 November	2050	542.6–552.3	9.7	1.87	19.3	
61R	1 November	2315	552.3–561.8	9.5	0.49	5.2	
62R	2 November	0130	561.8–571.5	9.7	0.25	2.6	
63R	2 November	0415	571.5–581.2	9.7	1.51	15.5	
64R	2 November	0735	581.2–590.3	9.1	1.80	19.8	
Coring totals				590.3	197.44	33.4	

repetition of some sequences. Because interpreting relations between noncontiguous intervals is subjective, we have chosen to represent each downhole lithologic change as a new unit. These units are referred to as “primary units” and are assigned consecutive roman numerals. Sixteen primary units are recognized in Hole 829A (Units I to XVI; Fig. 6, Table 2),

one in Hole 829B (Unit XVII), and four in Hole 829C (Units XVIII to XXI; Fig. 7, Table 2). The primary units are grouped into four composite units, which are assigned names in Bislama, the native language of Vanuatu (Bigwan Wan, Bigwan Tu, Bigwan Tri, and Bigwan Fo; Crowley, 1990) to distinguish them from the primary units.

Table 1 (continued).

Core	Date (1990)	Time (UTC)	Depth (mbsf)	Length cored (m)	Length recovered (m)	Recovery (%)	Age
134-829B-							
1H	4 November	1400	0.0–0.5	0.5	0.53	100.0	Pleistocene-Holocene
2H	4 November	1500	0.5–10.0	9.5	5.21	54.8	
3H	4 November	1730	10.0–19.5	9.5	9.85	103.0	
Coring totals				19.5	15.59	80.0	
134-829C-							
1H	4 November	1900	0.0–8.3	8.3	8.23	99.1	Pleistocene
2H	4 November	1950	8.3–17.8	9.5	9.42	99.1	Pleistocene-Holocene
3H	4 November	2040	17.8–27.3	9.5	9.86	104.0	Pleistocene
4H	4 November	2115	27.3–30.3	3.0	2.91	97.0	Pleistocene
5H	4 November	2345	30.3–38.0	7.7	7.64	99.2	Pleistocene
6H	5 November	0045	38.0–47.5	9.5	0.02	0.2	Pleistocene
7H	5 November	0230	47.5–50.0	2.5	2.52	101.0	Pleistocene
8H	5 November	0315	50.0–52.0	2.0	1.85	92.5	Pleistocene
9H	5 November	0415	52.0–57.3	5.3	9.08	171.0	Miocene
10H	5 November	0500	57.3–58.3	1.0	1.01	101.0	Pleistocene
11H	5 November	0715	58.3–58.4	0.1	0.13	130.0	
Coring totals				58.4	52.67	90.2	

Because of poor recovery in many cores (Fig. 6), lithologies have commonly been extrapolated from sparse samples. Where a compositional change occurs between recovered intervals, we have arbitrarily chosen to place the lithologic boundary at the top of the lower core. In effect, we assume that the missing interval has the same composition as the bottom of the upper core. Lithostratigraphic units are described below proceeding on a hole-by-hole basis, beginning with Hole 829A; each hole is described from top to bottom.

Hole 829A

Unit I

Depth: 0–60.5 mbsf

Interval: Sections 134-829A-1R-1, 0 cm, to 134-829A-8R-1, 0 cm

Thickness: 60.5 m

Age: Pleistocene

Unit I consists of Pleistocene, very dark greenish gray (10Y 3/1), clayey volcanic silt. The silt contains abundant volcanogenic minerals including plagioclase, pyroxenes, amphiboles, and opaque minerals (e.g., magnetite and pyrite), as well as 10%–20% foraminifers and calcite of uncertain origin (Fig. 8). Interbeds of sandy volcanic silt, 1–4 cm thick, and pumice fragments are common. Foraminifers increase in the lower 10 m of the unit, forming foraminiferal silty mixed sediment. The contact between Units I and II was not recovered.

Unit II

Depth: 60.5–99.4 mbsf

Interval: Sections 134-829A-8R-1, 0 cm, to 134-829A-12R-1, 40 cm

Thickness: 38.9 m

Age: late Oligocene to early Miocene

Unit II consists of very pale brown (10YR 8/3) foraminiferal chalk. Foraminifers comprise about 50% of the sediment and nannofossils about 5%; the remainder is fine silt- and clay-sized calcite that may represent recrystallized microfossils. In places, the chalk shows millimeter-scale laminations, some of which are cross-bedded. Such laminations may reflect subtle differences in grain size. A 10-cm interval of brown zeolitic clay occurs at a depth of 99 mbsf (interval 134-829-12R-1, 0–10 cm), about 30 cm above an abrupt contact between Unit II and the Pleistocene siltstone of Unit III.

Unit III

Depth: 99.4–171.9 mbsf

Interval: Sections 134-829A-12R-1, 40 cm, to 134-829A-19R-4, 88 cm

Thickness: 72.5 m

Age: Pleistocene

Unit III consists of very dark greenish gray (10Y 3/1) clayey volcanic silt and, below about 125 mbsf (Section 134-829A-15R-1, 0 cm), partially lithified siltstone. The silt and siltstone contain abundant volcanogenic minerals (e.g., plagioclase, pyroxenes, and amphiboles) and variable amounts of carbonate. Burrows and fecal pellets are abundant in this heavily bioturbated unit. Interbeds of volcanic sand, generally <4 cm but up to 28 cm thick, are common; some interbeds contain volcanic glass and some are normally graded. Granule- to pebble-sized clasts of chalk, pumice, and brown clay occur throughout the unit.

Grain size increases in the lower 15 m of Unit III. Clayey siltstone grades to sandy siltstone and silty sandstone with intervals of foraminiferal sandy mixed sediment. The contact between Units III and IV is gradational.

Unit IV

Depth: 171.9–205.2 mbsf

Interval: Sections 134-829A-19R-4, 88 cm, to 134-829A-23R-1, 0 cm

Thickness: 33.3 m

Age: late Pliocene or early Pleistocene

Unit IV consists of intensely deformed siltstone-chalk breccia. Angular clasts of dark greenish gray (10Y 5/1 to 4/1), partially lithified sandy volcanic siltstone and very pale brown (10YR 7/3) and white (10YR 8/1) chalk occur in a gray (5Y 6/1) chalk matrix (Fig. 9). Clasts are foraminiferal and calcareous chalk; the matrix is calcareous chalk (note: “calcareous” designates chalk composed mainly of calcite of uncertain origin). Clast size ranges from 1 mm to at least 14 cm. Intervals of siltstone up to 1 m thick—for example, 178.5–179.5 mbsf (Sections 134-829A-20R-2, 75 cm, to -20R-CC, 25 cm)—could be boulder-sized clasts or interbeds. Some clasts are themselves pieces of brecciated siltstone, and most of the unit displays signs of intense shearing and tectonic brecciation (see “Structural Studies” section, this chapter). Siltstone becomes less abundant below 195.5 mbsf (Section 134-829A-22R-1, 0 cm), with a gradual transition to chalk breccia without siltstone in Unit V.

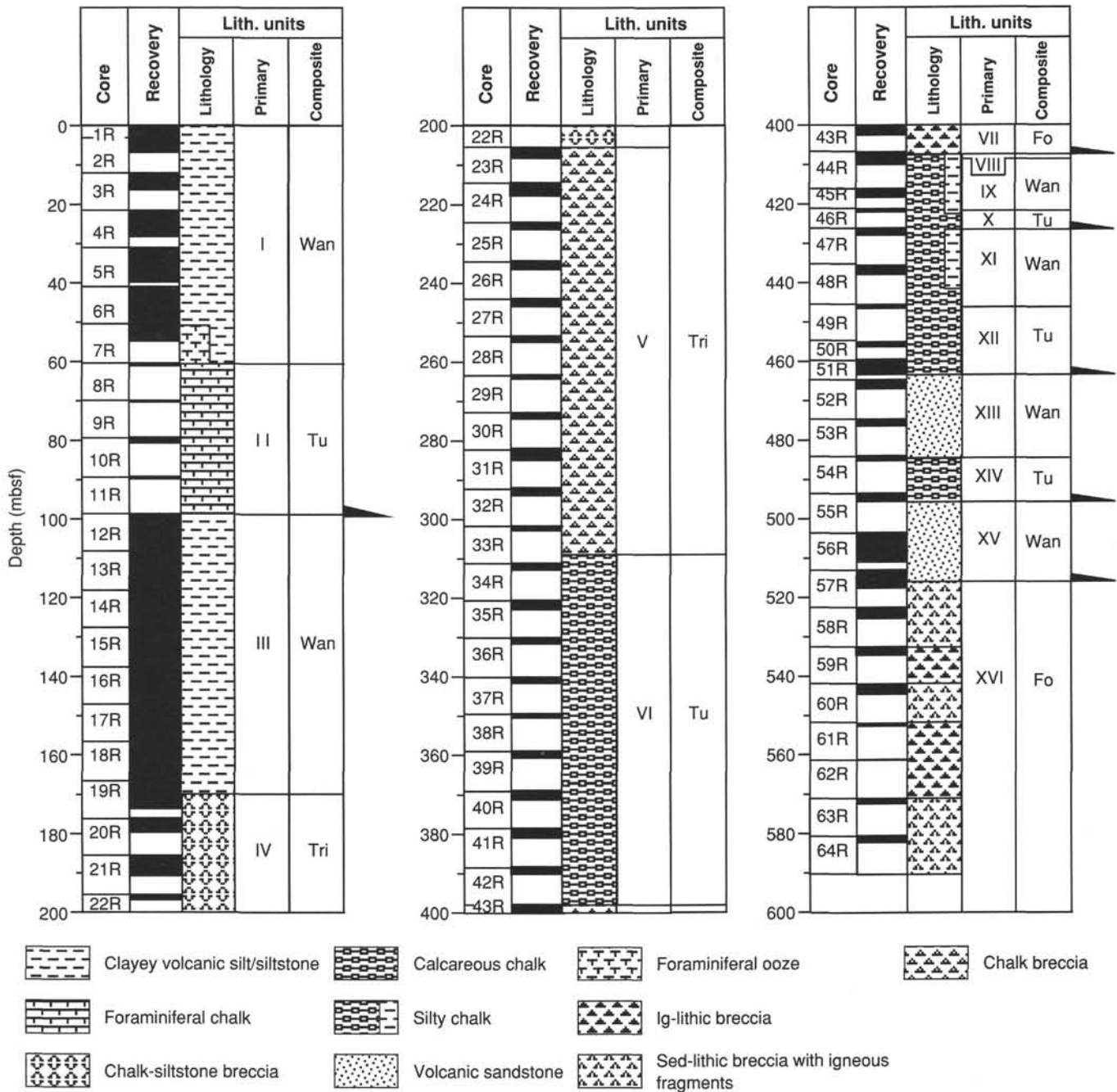


Figure 6. Diagram depicting the primary and composite (Bigwan) lithostratigraphic units of Hole 829A. Arrows denote lithostratigraphically defined thrust faults.

Biostratigraphic data indicate that the breccia was deposited during the late Pliocene or early Pleistocene (see "Biostratigraphy" section, this chapter). In contrast, the chalk clasts are late Oligocene to early Miocene in age.

Unit V

Depth: 205.2–311.3 mbsf
 Interval: Sections 134-829A-23R-1, 0 cm, to 134-829A-34R-1, 0 cm
 Thickness: 106.1 m
 Age: late Pliocene or early Pleistocene

Unit V is chalk breccia consisting of angular, granule- to pebble-sized clasts of very pale brown (10YR 8/1), white (10YR

8/1), and light gray (10YR 7/2) chalk in a light gray (10YR 7/1) to gray (10YR 6/1) chalk matrix (Fig. 10). Clasts and matrix are predominantly calcareous chalk, with some clasts of foraminiferal chalk. Some of the clasts are themselves pieces of breccia, and evidence of structural deformation, such as microfaults and scaly fabric, is common (see "Structural Studies" section, this chapter). Sand- to gravel-sized fragments of shells and volcanic fragments occur throughout the unit. The breccia was deposited during the late Pliocene or early Pleistocene (see "Biostratigraphy" section, this chapter), whereas the chalk clasts are late Oligocene to early Miocene in age. The contact between Units V and VI was not recovered.

Table 2. Primary lithostratigraphic units, Site 829.

Unit	Interval	Depth (mbsf)	Dominant lithology	Age
Hole 829A				
I	Sections 134-829A-1R-1, 0 cm, to 134-829A-8R-1, 0 cm	0–60.5	Clayey volcanic silt	Pleistocene
II	Sections 134-829A-8R-1, 0 cm, to 134-829A-12R-1, 40 cm	60.5–99.4	Foraminiferal chalk	late Oligocene to early Miocene
III	Sections 134-829A-12R-1, 40 cm, to 134-829A-19R-4, 88 cm	99.4–171.9	Clayey volcanic silt	Pleistocene
IV	Sections 134-829A-19R-4, 88 cm, to 134-829A-23R-1, 0 cm	171.9–205.2	Siltstone–chalk breccia	late Pliocene or Pleistocene
V	Sections 134-829A-23R-1, 0 cm, to 134-829A-34R-1, 0 cm	205.2–311.3	Chalk breccia	late Pliocene or Pleistocene
VI	Sections 134-829A-34R-1, 0 cm, to 134-829A-43R-1, 120 cm	311.3–398.9	Calcareous chalk	middle Oligocene to early Miocene
VII	Sections 134-829A-43R-1, 120 cm, to 134-829A-44R-1, 0 cm	398.9–407.4	Volcanic breccia	Indeterminate
VIII	Sections 134-829A-44R-1, 0 cm, to 134-829A-44R-1, 40 cm	407.4–407.8	Foraminiferal chalk	early Pliocene
IX	Sections 134-829A-44R-1, 40 cm, to 134-829A-46R-1, 0 cm	407.8–421.6	Silty chalk	Pleistocene
X	Sections 134-829A-46R-1, 0 cm, to 134-829A-47R-1, 67 cm	421.6–427.3	Calcareous chalk and foraminiferal chalk	middle to late Oligocene
XI	Sections 134-829A-47R-1, 67 cm, to 134-829A-49R-1, 0 cm	427.3–445.9	Silty chalk	late Pliocene to Pleistocene
XII	Sections 134-829A-49R-1, 0 cm, to 134-829A-51R-3, 10 cm	445.9–462.9	Calcareous chalk	early Oligocene (or late Eocene?) to late Oligocene
XIII	Sections 134-829A-51R-3, 10 cm, to 134-829A-54R-1, 0 cm	462.9–484.5	Volcanic sandstone	late Pliocene or Pleistocene
XIV	Sections 134-829A-54R-1, 0 cm, to 134-829A-55R-CC, 15 cm	484.5–495.6	Chalk and mixed sediment	early to late Oligocene
XV	Sections 134-829A-55R-CC, 15 cm, to 134-829A-57R-3, 72 cm	495.6–517.2	Sandy volcanic siltstone	late Pliocene to Pleistocene
XVI	Sections 134-829A-57R-3, 72 cm, to 134-829A-64R-CC, 27 cm	517.2–590.3	Igneous sed-lithic breccia	Indeterminate
Hole 829B				
XVII	Sections 134-829B-1H-1, 0 cm, to 134-829B-3H-CC, 50 cm	0–19.5	Clayey sandy volcanic silt	Pleistocene
Hole 829C				
XVIII	Sections 134-829C-1H-1, 0 cm, to 134-829C-9H-4, 0 cm	0–54.6	Clayey sandy volcanic silt	Pleistocene
XIX	Sections 134-829C-9H-4, 0 cm, to 134-829C-10H-1, 0 cm	54.6–57.3	Foraminiferal ooze	early Miocene
XX	Sections 134-829C-10H-1, 0 cm, to 134-829C-11H-1, 0 cm	57.3–58.3	Foraminiferal silty mixed sediment	Pleistocene
XXI	Sections 134-829C-11H-1, 0 cm, to 134-829C-11H-CC, 15 cm	58.3–58.4	Foraminiferal chalk	Pleistocene

Unit VI

Depth: 311.3–398.9 mbsf

Interval: Sections 134-829A-34R-1, 0 cm, to 134-829A-43R-1, 120 cm

Thickness: 87.6 m

Age: middle Oligocene to early Miocene

Unit VI consists of light greenish gray (10Y 7/1), very pale brown (10YR 7/3), white (5Y 8/1), and light gray (5Y 7/2) calcareous chalk with intervals of nanofossil and foraminiferal chalk. This unit has been highly sheared and fractured (see “Structural Studies” section, this chapter). Calcareous chalk with 10%–20% sponge spicules occurs from 320.5 to 359.1 mbsf (Sections 134-829A-35R-1, 0 cm, to -39R-1, at 0 cm). The upper 58.7 m of Unit VI is late Oligocene to early Miocene in age; the remainder, 370 mbsf (Section 134-829A-40R-1, 0 cm), is middle Oligocene in age.

Carbonate content decreases in the lowermost 1.2 m of the unit (Section 134-829A-43R-1, 0–120 cm) in an interval char-

acterized by tectonic shearing (Fig. 35, “Structural Studies” section, this chapter) and abundant wavy laminations in light brown clayey calcareous chalk.

Unit VII

Depth: 398.9–407.4 mbsf

Interval: Sections 134-829A-43R-1, 120 cm, to 134-829A-44R-1, 0 cm

Thickness: 8.5 m

Age: Indeterminate

Unit VII consists of matrix-supported ig-lithic breccia. The contact with overlying chalk is marked by abrupt color and compositional changes. The upper 30 cm of Unit VII (Section 134-829A-43R-1, 120–150 cm), consists of granule- to pebble-sized clasts of chalk and basalt in a brown (10YR 5/3) clay matrix. Below this, the breccia consists of basalt and, less commonly, plutonic rock fragments in greenish gray (10Y 4/1) and dark bluish gray (5G 4/1) volcanic silt. Several zones of

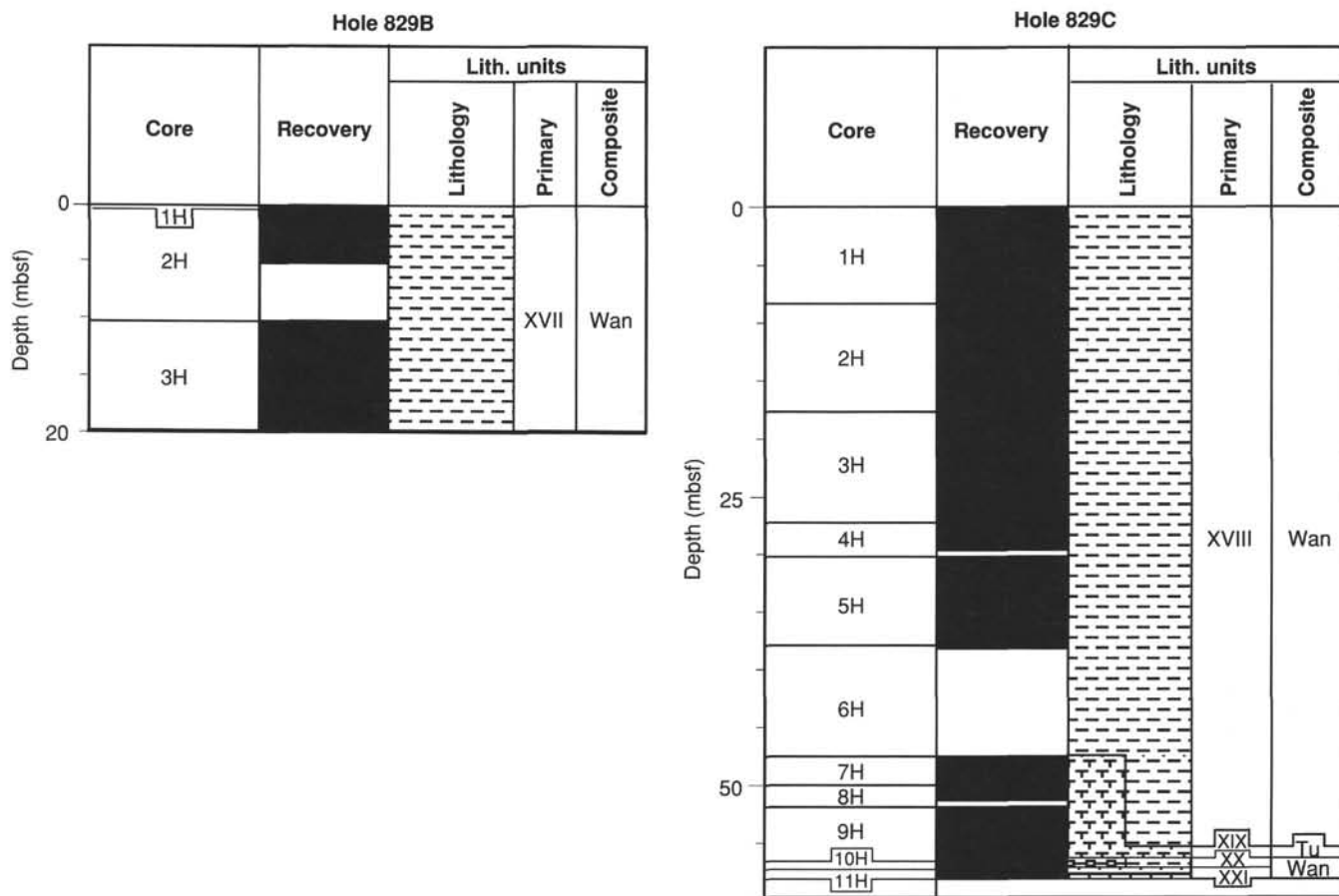


Figure 7. Diagram depicting the primary and composite (Bigwan) lithostratigraphic units of Holes 829B and 829C. For key to lithology symbols, see Figure 6.

shear deformation are observed (see “Structural Studies” section, this chapter). The contact between the ig-lithic breccia and the chalk of Unit VIII was not recovered.

Unit VIII

Depth: 407.4–407.8 mbsf
Interval: Section 134-829A-44R-1, 0–40 cm
Thickness: 0.4 m
Age: early Pliocene

Unit VIII consists of lower Pliocene, very pale brown (10YR 7/3) foraminiferal chalk. The chalk was recovered only as fragments at the top of Core 134-829-44R. Contacts of the Pliocene chalk with overlying breccia (Unit VII) and underlying Pleistocene chalk (Unit IX) were not recovered.

Unit IX

Depth: 407.8–421.6 mbsf
Interval: Sections 134-829A-44R-1, 40 cm, to 134-829A-46R-1, 0 cm
Thickness: 13.8 m
Age: Pleistocene

Unit IX consists of dark gray (5Y 4/1) and dark greenish gray (10Y 4/1) volcanic silty chalk of Pleistocene age. Some of the chalk is foraminiferal, some is calcareous, and plagioclase is also a common constituent. The chalk occurs as angular fragments, some with slickensides, which appear to result

from brittle deformation (see “Structural Studies” section, this chapter).

Unit X

Depth: 421.6–427.3 mbsf
Interval: Sections 134-829A-46R-1, 0 cm, to 134-829A-47R-1, 67 cm
Thickness: 5.7 m
Age: middle to late Oligocene

Unit X occurs as rounded and angular pieces of middle to upper Oligocene, very pale brown (10YR 7/3) calcareous chalk and light gray (10YR 7/1) foraminiferal chalk (Fig. 10). Unit X is separated from Unit XI by 14 cm of light yellowish brown (10YR 6/4) calcareous clay with wavy laminae and dendritic structures.

Unit XI

Depth: 427.3–445.9 mbsf
Interval: Sections 134-829A-47R-1, 67 cm, to 134-829A-49R-1, 0 cm
Thickness: 18.6 m
Age: late Pliocene to early Pleistocene

Unit XI consists of gray (10Y 5/1), silty foraminiferal chalk with a 0.5-m intercalation of light gray (10Y 7/1) foraminiferal chalk. Much of the gray silty chalk occurs as centimeter-sized angular fragments of drilling breccia. The unit was deposited during the late Pliocene to early Pleistocene.

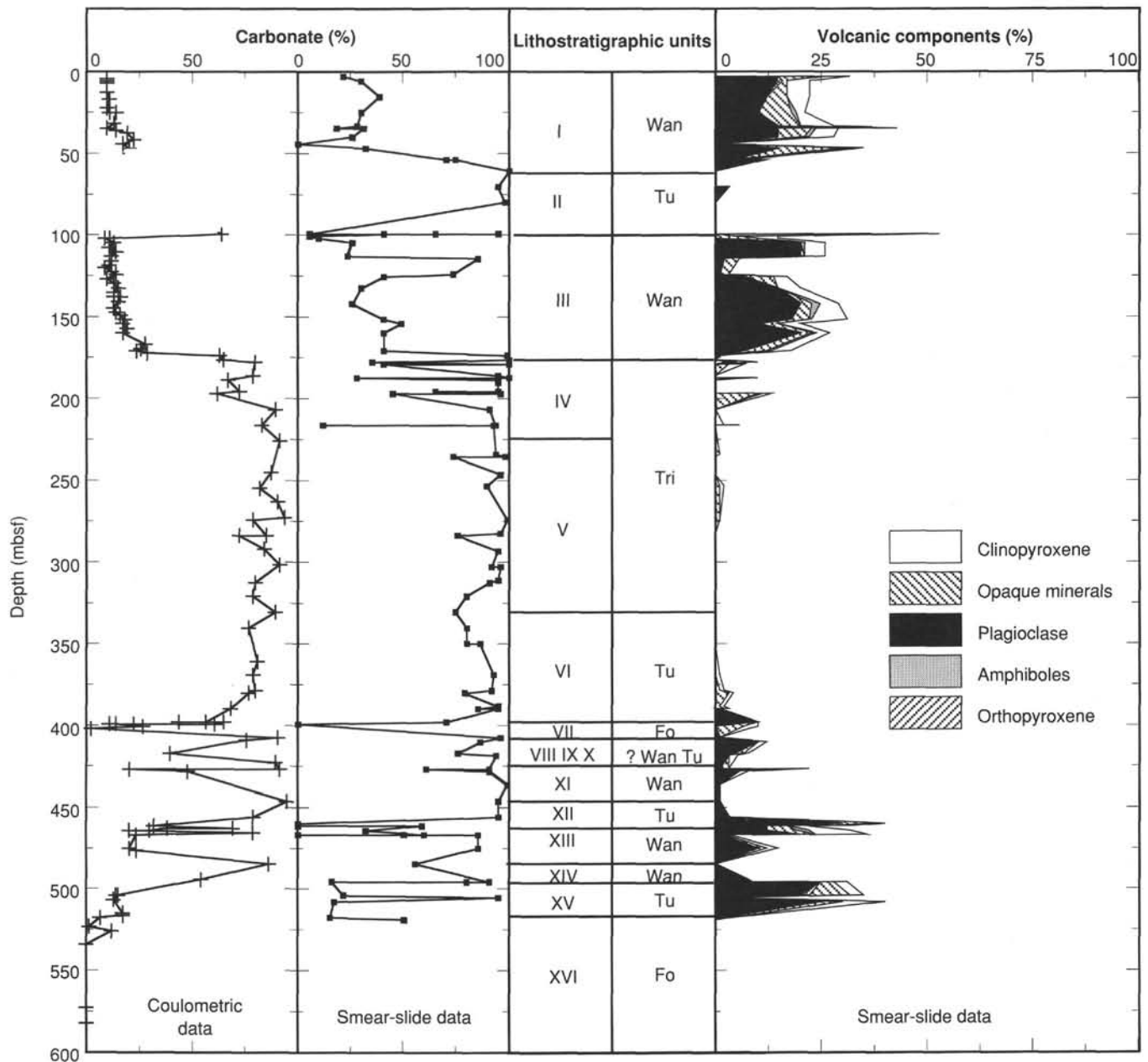


Figure 8. Percentage of carbonate and volcanic mineral components plotted vs. depth for Hole 829A.

Unit XII

Depth: 445.9–462.9 mbsf
 Interval: Sections 134-829A-49R-1, 0 cm, to 134-829A-51R-3, 10 cm
 Thickness: 17 m
 Age: early Oligocene (or late Eocene?) to late Oligocene

Unit XII consists of pale brown (10YR 6/3) and very pale brown (10YR 8/3) calcareous chalk. The chalk is primarily early to late Oligocene in age, but one sample contains an upper Eocene assemblage (interval 134-829A-51R-1, 105–107 cm) that occurs between upper Oligocene chalk and lower Oligocene chalk (see "Biostratigraphy" section, this chapter).

The lower 3 m of this unit (Sections 134-829A-51R-1, 0 cm, to -51R-3, 10 cm) are characterized by decreased carbonate content, laminations, some of them wavy, layers up to 50 cm thick of brown (10YR 5/3) calcareous clay and clayey chalk (Fig. 11),

and shear bands and folds indicative of shearing (see Figs. 37, 38, and 41; "Structural Studies" section, this chapter). The clay-rich interval occurs directly above an abrupt contact between chalk and underlying volcanic sandstone of Unit XIII.

Unit XIII

Depth: 462.9–484.5 mbsf
 Interval: Sections 134-829A-51R-3, 10 cm, to 134-829A-54R-1, 0 cm
 Thickness: 21.6 m
 Age: late Pliocene or early Pleistocene

Unit XIII consists of partially lithified, black (5Y 5/1) volcanic sandstone deposited in the late Pliocene or early Pleistocene. Plagioclase is abundant in the sandstone; pyroxenes, amphiboles, and opaque minerals such as magnetite are common. The sandstone contains variable amounts of carbonate, with common foraminifers that often occur as

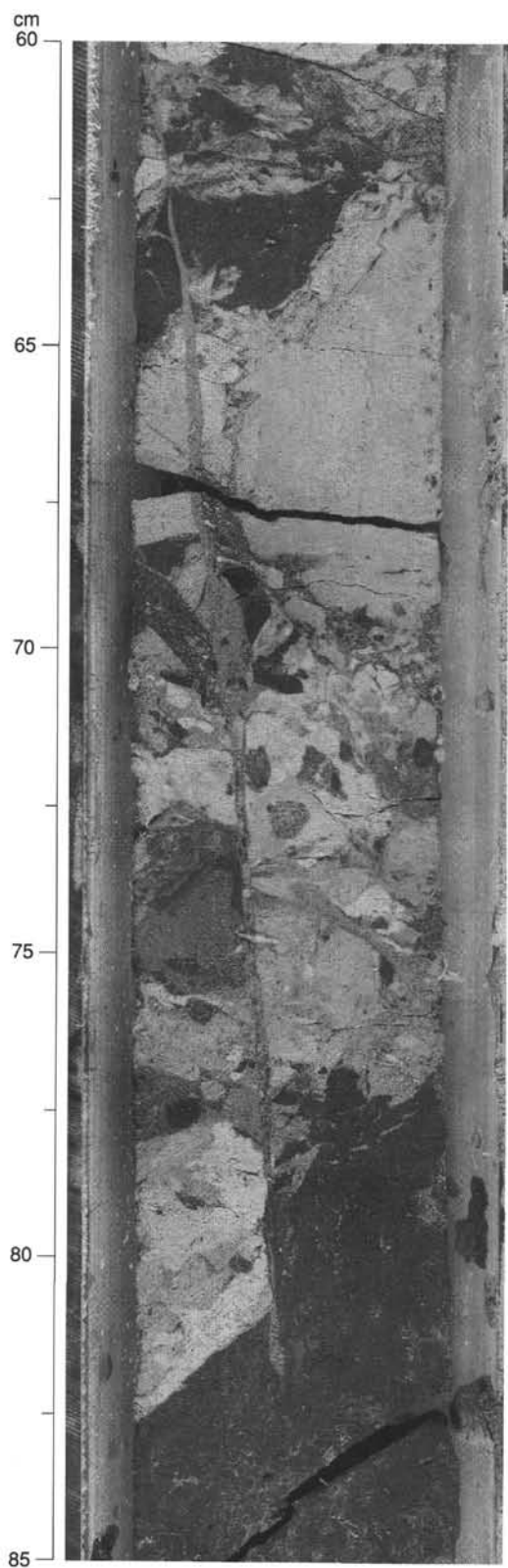


Figure 9. Photograph of interval 134-829A-20R-1, 60-85 cm, showing the sheared chalk and siltstone clasts of the sed-lithic breccia of Unit IV.

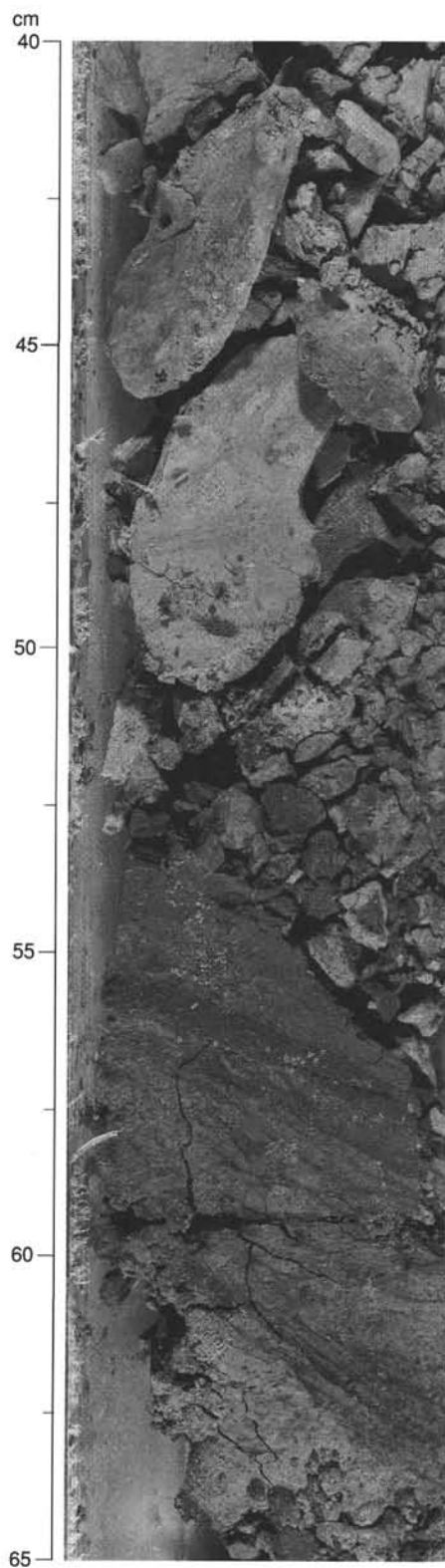


Figure 10. Photograph of interval 134-829A-47R-1, 40-65 cm, showing the fragments of pale brown limestone of Unit X (40-52 cm) and the light yellowish brown calcareous clay with wavy laminae and dendritic structures (53-65 cm).

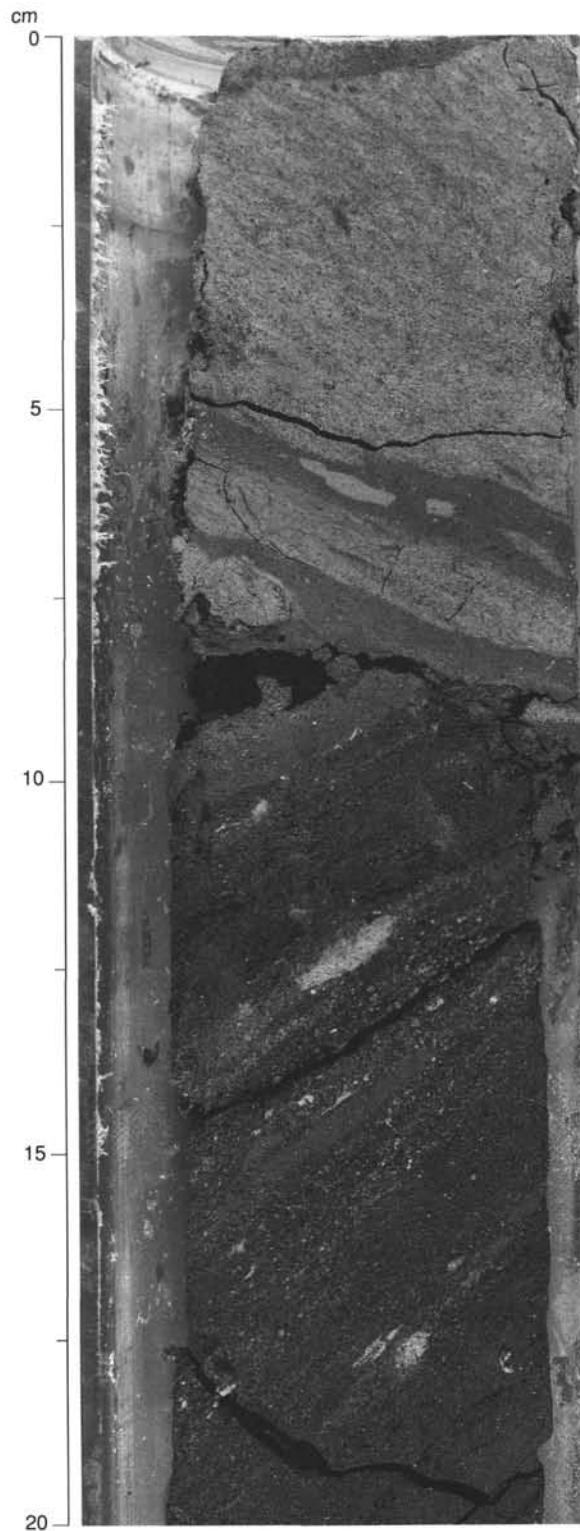


Figure 11. Photograph of interval 134-829A-51R-3, 0–20 cm, showing contact between Oligocene chalk of Unit XII that overlies upper Pliocene or lower Pleistocene calcareous volcanic sandstone of Unit XIII (at 9 cm). Calcareous brown clay occurs as dipping beds at the contact between the two units and within the chalk. Elongate (sheared?) clasts of white chalk are present in the sandstone (at 12.5 and 17.5 cm).

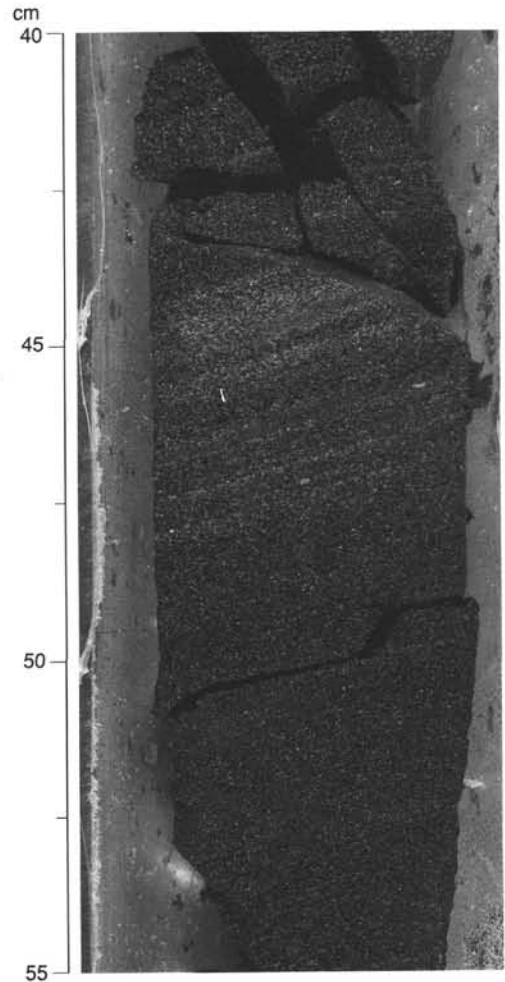


Figure 12. Photograph of interval 134-829A-53R-1, 40–55 cm, showing white foraminifer-rich laminations in the black volcanic sandstone of Unit XIII.

white laminations (Fig. 12). Intervals of nannofossil chalk up to 20 cm thick, wood fragments, and gravel- to sand-sized clasts of pumice and chalk occur throughout the unit. The contact between volcanic sandstone and the chalk of Unit XIV was not recovered.

Unit XIV

Depth: 484.5–495.6 mbsf
 Interval: Sections 134-829A-54R-1, 0 cm, to 134-829A-55R-CC, 15 cm
 Thickness: 11.1 m
 Age: early to late Oligocene

Unit XIV contains intervals of brown (10YR 4/3) nannofossil chalk, brown (10YR 5/3) clayey chaly mixed sedimentary rocks, light brownish gray (10YR 6/2) foraminiferal chalk and white (10YR 8/2) nannofossil chalk. The recovery was nearly all angular fragments, the size of which varied with lithology. The mixed sedimentary rock fragments were mostly less than 1 cm in diameter; the chalk fragments were up to 5 cm across. An abrupt contact between white nannofossil chalk and volcanic siltstone (Unit XV) marks the lower boundary of Unit XIV.

Unit XV

Depth: 495.6–517.2 mbsf
 Interval: Section 134-829A-55R-CC, 15 cm, to 134-829A-57R-3, 72 cm
 Thickness: 21.6 m
 Age: late Pliocene or early Pleistocene

Unit XV is very dark gray (5Y 3/1), massive, partially lithified, sandy volcanic siltstone deposited in the late Pliocene or early Pleistocene. The siltstone is bioturbated, with horizons of abundant fecal pellets. Chalk clasts occur throughout the unit. The interval from 504.7 to 506.7 mbsf (Section 134-829A-56R-1, 87 cm, to -56R-2, 137 cm, contains contorted lenses and layers of gray (5Y 6/1) chalk with rounded siltstone clasts. The lower contact of Unit XV is marked by a layer of normally graded, calcareous volcanic sand that abruptly overlies the lithic breccia of Unit XVI.

Unit XVI

Depth: 517.2–590.3 mbsf
 Interval: Sections 134-829A-57R-3, 72 cm, to 134-829A-64R-CC, 27 cm
 Thickness: 73.1 m
 Age: Indeterminate

Unit XVI consists of matrix- to grain-supported sed-lithic breccia interspersed with intervals of ig-lithic breccia. Most of the unit is composed of clasts of siltstone and claystone with rare igneous fragments and possible chert in a matrix of calcareous clay and silt (Fig. 13). The ig-lithic breccias contain fragments of gabbro, diabase, and basalt (see "Igneous Petrology" section, this chapter). Clasts are typically less than 1 cm in size, but some are as large as 3 cm. The upper 6 cm of the unit consists of yellowish brown (10YR 3/4) sandy clay with granules of dark gray siltstone. Changes in matrix color define layers 10–60 cm thick, ranging from weak red (10R 4/3) to light greenish gray (10Y 3/1), pale brown (10YR 7/3), and light gray (5Y 7/2). Clasts are typically darker than the matrix.

Hole 829B**Unit XVII**

Depth: 0–19.5 mbsf
 Interval: Sections 134-829B-1H-1, 0 cm, to 134-829B-3H-CC, 50 cm
 Thickness: 19.5 m
 Age: Pleistocene

Unit XVII of Hole 829B consists of Pleistocene, very dark greenish gray (10Y 3/1), clayey sandy volcanic silt with interbeds, 1 cm thick, of normally graded sand.

Hole 829C**Unit XVIII**

Depth: 0–54.6 mbsf
 Interval: Sections 134-829C-1H-1, 0 cm, to 134-829C-9H-4, 0 cm
 Thickness: 54.6 m
 Age: Pleistocene

Unit XVIII consists of Pleistocene, very dark greenish gray (10Y 3/1) volcanic silt with variable amounts of clay and sand. Poorly defined ash layers and pumice fragments occur throughout. Foraminifers increase in the lower 7 m of the unit, forming foraminiferal silty mixed sediment.

Unit XIX

Depth: 54.6–57.3 mbsf
 Interval: Sections 134-829C-9H-4, 0 cm, to 134-829C-10H-1, 0 cm
 Thickness: 2.7 m
 Age: latest early Miocene

Unit XIX consists of soupy, pale yellowish white (2.5Y 8/3) foraminiferal ooze of latest early Miocene age; these rocks do

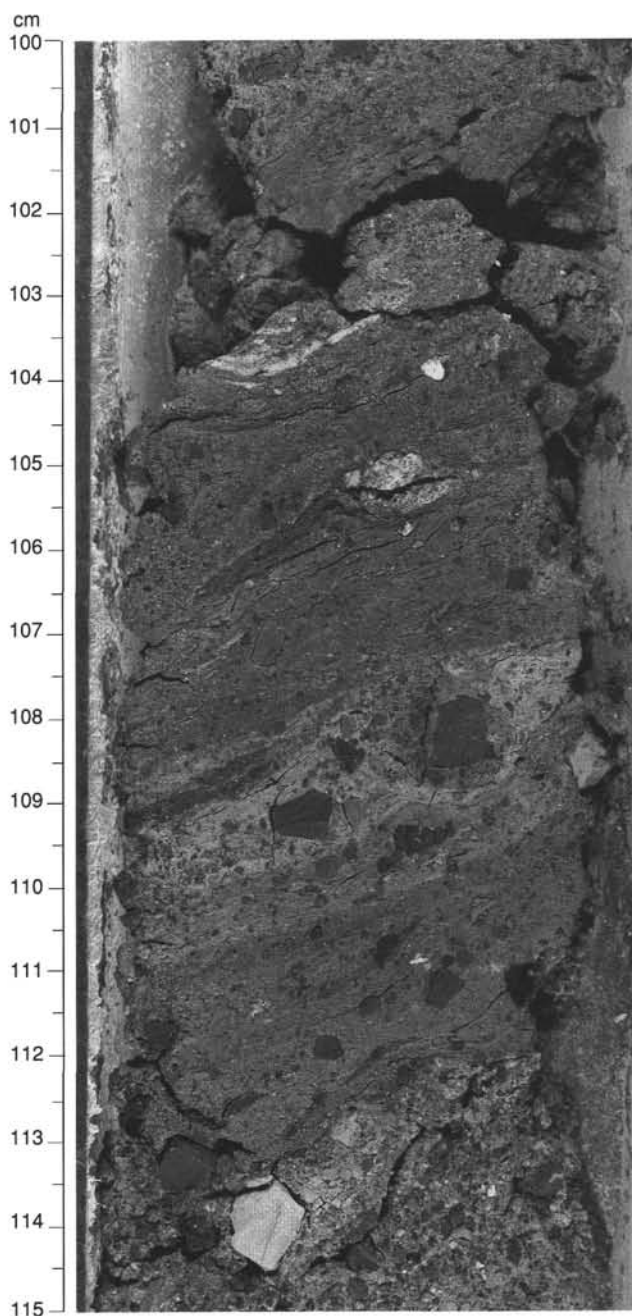


Figure 13. Photograph of interval 134-829A-58R-1, 100–115 cm, showing breccia from Unit XVI. Clasts are mainly siltstone and claystone, although the clast at 105 cm is gabbro. Breccia is matrix-supported with a calcareous clay matrix from 104–114 cm.

not correlate in age with the lower Miocene intervals of Hole 829A (see "Biostratigraphy" section, this chapter). The contacts of this unit are poorly defined because of drilling disturbance. For example, ooze flowed into the core barrel with Pleistocene silt and recovery was greater than the cored interval. The contact between Unit XIX and the Pleistocene mixed sediment of Unit XX was not recovered.

Unit XX

Depth: 57.3–58.3 mbsf
 Interval: Sections 134-829C-10H-1, 0 cm, to 134-829C-11H-1, 0 cm
 Thickness: 1 m
 Age: Pleistocene

Unit XX consists of Pleistocene, gray to greenish gray (2.5Y 5/0 to 10Y 5/1), foraminiferal silty mixed sediment containing 1.5 cm clasts of volcanic silt and pale yellowish white calcareous chalk. The contact between Unit XX and the chalk of Unit XXI was not recovered.

Unit XXI

Depth: 58.3–58.4 mbsf
Interval: Section 134-829C-11H-CC, 0–15 cm
Thickness: 0.15 m
Age: Pleistocene

Unit XXI consists of light gray (5Y 7/1) foraminiferal chalk of Pleistocene age. This unit was defined based on the 15 cm of homogeneous rubble found in the core catcher of Core 134-829C-11H.

Discussion

The primary units at Site 829 can be grouped into four composite lithostratigraphic units (assigned Bislama names) as follows:

1. Bigwan Wan, which consists of dark greenish gray to gray, upper Pliocene to Pleistocene volcanic silt, siltstone, sandstone, silty chalk, and mixed sediment (Hole 829A—Units I, III, IX, XI, XIII, and XV; Hole 829B—Unit XVII; and Hole 829C—Units XVIII, XX and XXI);
2. Bigwan Tu, consisting of light brown to gray, lower Oligocene (or upper Eocene?) to lower Miocene chalk (Hole 829A—Units II, VI, X, XII, and XIV; and Hole 829C—Unit XIX);
3. Bigwan Tri, which is upper Pliocene or lower Pleistocene sed-lithic (chalk and chalk-siltstone) breccia (Hole 829A—Units IV and V) with clasts that vary in color from white to dark-greenish gray and a light gray matrix; and
4. Bigwan Fo, which is red to gray and brown igneous sed-lithic breccia of unknown age (Hole 829A—Units VII and XVI).

The four Bigwan units include all primary units except Unit VIII in Hole 829A, which is the only occurrence of lower Pliocene chalk at Site 829.

Distinct depositional processes and environments are suggested by the lithologies of the four Bigwan units. The upper Pliocene to Pleistocene sediments of Bigwan Wan are interpreted as hemipelagic and turbidite deposits, with texture and composition varying from volcanic sand (Hole 829A—Units XIII and XV), to clayey volcanic silt and mixed sediment (Hole 829A—Units I and III; Hole 829B—Unit XVII; and Hole 829C—Units XVIII and XX) to silty chalk (Hole 829A—Units IX and XI), depending on the proximity of volcanic sources. In contrast to Bigwan Wan, the Oligocene to lower Miocene chalks of Bigwan Tu lack volcanoclastic sediment and are considered to be pelagic deposits. The sheared and fractured chalk-rich breccias of Bigwan Tri, deposited in the late Pliocene or early Pleistocene, are interpreted as a tectono-sedimentary deposit consisting of Bigwan Wan- and Bigwan Tu-type rocks that have been eroded, deposited, and sheared (see “Structural Studies” section, this chapter). The igneous component of the breccias of Bigwan Fo suggests erosion of a basement rock that is transitional between mid-ocean ridge basalt (MORB) and island-arc tholeiite (IAT) (see “Igneous Geochemistry” section, this chapter).

The stratigraphic section in Hole 829A includes several intervals of Bigwan Wan and Bigwan Tu, one interval of Bigwan Tri, and two intervals of Bigwan Fo (Fig. 6). Oligocene to lower Miocene chalk (Bigwan Tu) overlies upper Pliocene to Pleistocene sediments (Bigwan Wan) at five hori-

zons in Hole 829A: 99.4 mbsf, 398.9 mbsf (at this horizon, Bigwan Tu and Wan are separated by 8.5 m of volcanic breccia in Bigwan Fo), 427.3 mbsf, 462.9 mbsf, and 495.6 mbsf. Occurrences of Oligocene to lower Miocene rocks stratigraphically above upper Pliocene to Pleistocene Bigwan Wan rocks suggests the presence of thrust faults (see “Structural Studies” section, this chapter). Lower Miocene ooze (Unit XIX) also overlies Pleistocene silt (Unit XX) in Hole 829C, but severe drilling disturbance makes interpretation of a thrust in this interval equivocal.

Thrust fault zones identified in Hole 829A are typically associated with layers of brown clay. For example, 10 cm of brown clay occurs at 99 mbsf in Unit II, 30 cm above the contact between upper Oligocene to lower Miocene chalk and the Pleistocene siltstone of Unit III. In addition, brown clay occurs at the base of Unit VI and forms the matrix of the upper 30 cm of the breccia of Unit VII. A 14-cm layer of brown clay with wavy laminae marks the contact between the Oligocene chalk of Unit X and upper Pliocene or lower Pleistocene silty chalk of Unit XI (Fig. 10). Thin layers of brown clay also occur in Unit XII, above the contact between Oligocene chalk and the upper Pliocene or lower Pleistocene volcanic sandstone in Unit XIII (Fig. 11). Brown clay was not recovered in Unit XIV at the contact between Oligocene chalk and the upper Pliocene or lower Pleistocene siltstone of Unit XV, but some chalk in Unit XIV is brown. An additional occurrence of brown clay matrix at the top of and within the igneous sed-lithic breccia of Unit XVI may also be related to thrusting (see “Structural Studies” section, this chapter).

BIOSTRATIGRAPHY

The application of foraminiferal and nannofossil biostratigraphy to Holes 829A, 829B, and 829C was greatly constrained by sediment reworking within the Pleistocene intervals and intensive tectonic mixing within the Pliocene to Eocene intervals. Hole 829A was particularly complex because of the mixing of different lithologies and ages within a single core, frequently preventing the separation of assemblages. Because of the structural complexities in Hole 829A, micropaleontological dating was undertaken with a certain degree of interpretation. Based on information provided by the sedimentologists and structural geologists, an interpretation must be made as to the processes (faulting or reworking) that result in the mixing of specimens from various ages. Such is the case with Samples 134-829A-13R-CC and -14R-CC, where a Pliocene to Pleistocene(?) foraminiferal fauna was recorded, whereas in the underlying interval (Samples 134-829A-15R-CC to -19R-CC) a typical Pleistocene assemblage was identified. In the absence of data indicating a fault, reworking appears to explain this abnormal relationship despite the absence of Pleistocene marker species.

In general, planktonic foraminifers and nannofossils are abundant and well preserved throughout Holes 829A, 829B, and 829C. Exceptions are in the interval between Samples 134-829A-21R-CC and -38R-CC, where preservation of nannofossils is poor, and in samples collected at the base of major thrust faults (e.g., Sample 134-829A-43R-CC), where dissolution is common and affects mainly the planktonic population (foraminifers and nannofossils). Similarly, the middle to late Oligocene foraminiferal faunas were sometimes difficult to extract due to the fairly indurated character of the chalks. Barren samples were found below 517 mbsf.

Benthic foraminiferal faunas were also affected by mixing and reworking, making it possible only to suggest wide paleobathymetric ranges for the whole sequence. Furthermore, due to the long stratigraphic range of Cenozoic benthic species, it was common to find together assemblages of the

same paleobathymetry but of different ages (e.g., lower bathyal Oligocene species together with lower bathyal Pleistocene species). A distinction in age in this case was possible only where preservation was markedly different.

Figures 14, 15, and 16 summarize the nannofossil and foraminiferal biostratigraphy and the benthic foraminiferal assemblages and paleodepths of Holes 829A, 829B, and 829C, respectively.

Calcareous Nannofossils

Extensive diversity is found in both the ages and preservational quality of nannofossils at Site 829. Rapid changes in ages of the sediments as well as complex, inverted age relationships are evidenced by nannofossil biostratigraphy.

Pleistocene

The interval from Samples 134-829A-1R-CC to -3R-CC contains an assemblage typified by the presence of *Emiliania huxleyi*, *Gephyrocapsa oceanica*, *G. caribbeanica*, *Ceratolithus telesmus*, *Rhabdosphaera claviger*, and *Helicosphaera kamptneri* and have thus been placed within Zone CN15. From Sections 134-829A-RH-CC through -7R-CC a typical middle Pleistocene assemblage is represented by *G. oceanica*, *G. caribbeanica*, *H. kamptneri*, and *Calcidiscus leptoporus*. This floral assemblage is repeated several times in Hole 829A: Sections 134-829A-12R-CC through -20R-CC; Samples 134-829A-44R-CC and -45R-CC; Samples 134-829A-47R-CC and -48R-CC; Sample 134-829A-51R-CC; Sample 134-829A-53R-CC; Samples 134-829A-55R-CC and -56R-CC (Fig. 14). In Holes 829B and 829C, nannofossil assemblages nearly identical to the middle Pleistocene Zone CN14 found in Hole 829A are recorded in all cores except in Section 134-829C-9R-CC (Figs. 15 and 16).

Miocene

Although lower Miocene nannofossil specimens have been recorded as reworked components throughout Pleistocene sediments, only one sample at Site 829 has been interpreted as being latest early Miocene in age (Zone CN3). Sample 134-829C-9R-CC contains a lower Miocene assemblage typified by *Sphenolithus heteromorphus*, *Cyclocargolithus floridanus*, *Discoaster deflandrei*, and *Cyclocargolithus abisectus*. Nannofossils indicative of the earliest Miocene have been recorded from Samples 134-829A-8R-CC through 134-829A-11R-CC. A diagnostic nannofossil assemblage including *C. abisectus*, *C. floridanus*, and *D. deflandrei*, coincident with the absence of *Dictyococcites bisectus* and *Sphenolithus ciperoensis*, requires the zonal determination CN1 for this interval.

Early Miocene or Late Oligocene

Nannofossil biostratigraphy in the interval from Section 134-829A-21R-CC through Section 134-829A-38R-CC is problematic because of the poor preservation of *Cyclocargolithus abisectus* and *C. floridanus* and severely overgrown discoasters are typical of this interval. The lack of age-diagnostic markers in this interval prevents precise zonal determination, but the assemblages are representative of the early Miocene or late Oligocene and are, therefore, tentatively placed into Zone CN1/CP19.

Oligocene

From Section 134-829A-39R-CC through Section 134-829A-43R-CC the presence of *D. bisectus* together with *C. abisectus*, *C. floridanus*, and *Discoaster deflandrei* indicates a zonal designation of CP19. This upper Oligocene assemblage is repeated numerous times downhole: Sample 134-829A-

46R-CC; Samples 134-829A-49R-CC and -50R-CC; and Sample 134-829A-54R-CC (Fig. 14).

A lower Oligocene assemblage typified by *Ericsonia formosa*, *Reticulofenestra umbilica*, *C. floridanus*, *D. bisectus*, *Clausicoccolithus fenestrata*, *D. deflandrei*, and *Dictyococcites scrippsae* is recorded in the following samples: 134-829A-51R-2, 66–68 cm, 134-829A-51R-3, 4–6 cm; 134-829A-52R-1, 83–85 cm; and 134-829A-55R-1, 81–83 cm.

Eocene

Only one Eocene sample was found at Site 829. In Sample 134-829A-51R-1, 105–107 cm, the presence of *Discoaster saipanensis* and *Discoaster barbadiensis* indicates a zonal designation of CP15. Also found in this sample were *R. umbilica*, *E. formosa*, *D. bisectus*, *Coccolithus miopelagicus*, *D. scrippsae*, and medium-sized reticulofenestrids (<7 μ m).

Planktonic Foraminifers

A brief description of the planktonic foraminiferal assemblages is given below under each time segment recognized throughout the sequence, as follows:

Pleistocene

Pleistocene (Zone N22) foraminiferal assemblages were found at the following intervals in Hole 829A: (1) 0 to 60 mbsf (Samples 134-829A-1R-CC to -7R-CC), (2) 99 to 185 mbsf (Samples 134-829A-12R-CC to -20R-CC), (3) 397 to 517 mbsf (Samples 134-829A-43R-CC to -57R-CC), (4) 416 mbsf (Sample 134-829A-44R-CC), (5) 436 mbsf (Sample 134-829A-47R-CC), and (6) 503 to 513 mbsf (Samples 134-829A-55R-CC to -56R-CC). In addition, all of Hole 829B (Samples 134-829B-1H-CC to -3H-CC) and most of Hole 829C (Samples 134-829C-1H-CC to -9H-5, 100–101 cm, and 134-829C-10H-CC to -11H-CC) yielded a similar assemblage. The most characteristic species determined at these intervals are *Globorotalia truncatulinoides*, *Globorotalia crassaformis*, *Globorotalia menardii*, *Neoglobobiquadrina dutertrei*, *Globigerinoides conglobatus*, and *Globorotalia tumida*. Some reworking of Pliocene material is found in the uppermost part of the sequence (e.g., *Dentoglobigerina altispira*, *Sphaeroidinellopsis kochi*, and *Sphaeroidinellopsis paenedehiscens* in Sample 134-829A-7R-CC).

Late Pliocene or Early Pleistocene

Foraminiferal faunas of this age are commonly found mixed with late Oligocene or early Miocene species. This is the case in the interval between 185 and 310 mbsf (Samples 134-829A-21R-CC to -33R-CC), where an assemblage composed of *S. paenedehiscens*, *D. altispira*, *G. tosaensis*, *G. tumida flexuosa*, *S. kochi*, and *Globigerinoides obliquus* was identified in a grayish marlstone matrix containing abundant clasts of upper Oligocene to lower Miocene creamy foraminiferal chalk. The intensive mixing, together with the questionable chronostratigraphic value of the first occurrence of *G. truncatulinoides*, did not permit us to distinguish clearly between latest Pliocene and earliest Pleistocene time. Similarly, the interval between 410 and 510 mbsf (Samples 134-829A-44R-CC to -56R-CC), where there is no record of mixing with Oligocene to Miocene faunas, shows an uppermost Pliocene and/or lowermost Pleistocene sequence indistinguishable on the basis of the occurrence or apparent absence of *G. truncatulinoides*.

In addition to these assemblages, samples from 416 mbsf (Sample 134-829A-44R-1, 20–25 cm) and from 465 to 474 mbsf (Samples 134-829A-51R-CC and -52R-CC) yielded foraminiferal faunas that can be assigned to the late early Pliocene (Zone N20). These samples contain *S. paenedehiscens*, *G.*

Depth (mbsf)	Core	Recovery	Lith. unit	Nannofossil zone	Planktonic foraminifer zone	Benthic foraminifers		Age
						Assemblage	Paleodepth	
0	1-2 R		I	CN15	N22	I	M./L. bathyal	Pleistocene
20	3 R							
30	4 R							
40	5 R							
50	6 R							
60	7 R		II	CN1	N3-N4	IIa	Lower bathyal	late Oligocene(?) to early Miocene
80	8 R							
90	9 R							
100	10 R							
110	11 R							
120	12 R		III	CN14	N22	IIb	Lower bathyal	Pleistocene
130	13 R							
140	14 R							
150	15 R							
160	16 R							
170	17 R		IV	CN1/CP19 ?	N21/N22 + N3-N4	Barren	Middle bathyal	late Pliocene to early Pleistocene + late Oligocene/early Miocene (Tectonic mixing)
180	18 R							
190	19 R							
200	20 R							
210	21 R							
220	22 R		V	CN1/CP19 ?	N21/N22 + N3-N4	IIc	Middle bathyal	late Pliocene to early Pleistocene + late Oligocene/early Miocene (Tectonic mixing)
230	23 R							
240	24 R							
250	25 R							
260	26 R							
270	27 R		VI	CP19	P22	Barren	Lower bathyal	late Oligocene to (early Miocene?)
280	28 R							
290	29 R							
300	30 R							
310	31 R							
320	32 R		VII	CP19 ?	P19-P20	Barren	Lower bathyal	middle Oligocene
330	33 R							
340	34 R							
350	35 R							
360	36 R							
370	37 R		IX	CN14	N22	IV	Lower bathyal	Pliocene to Pleistocene + some Oligocene intervals (Tectonic mixing)
380	38 R							
390	39 R							
400	40 R							
410	41 R							
420	42 R		X	CP19	P 21	IV	Lower bathyal	Pliocene to Pleistocene + some Oligocene intervals (Tectonic mixing)
430	43 R							
440	44 R							
450	45-46							
460	46 R							
470	47 R		XI	CN14	N21/N22	III	M. bathyal	Pliocene to Pleistocene + some Oligocene intervals (Tectonic mixing)
480	48 R							
490	49 R							
500	50-51R							
510	51 R							
520	52 R		XIII	CP16*	N20-N22	Barren	?	Pliocene to Pleistocene + some Oligocene intervals (Tectonic mixing)
530	53 R							
540	54 R							
550	55 R							
560	56 R							
570	57 R		XIV	CN14	?	II	L. bathyal	Pliocene to Pleistocene + some Oligocene intervals (Tectonic mixing)
580	58 R							
590	59 R							
600	60 R							
610	61 R							
620	62 R		XVI	Barren	Barren	Barren	?	?
630	63 R							
640	64 R							
650								
660								

Figure 14. Biostratigraphic summary of Hole 829A. * = includes Eocene; # = includes Oligocene. Intervals are too small to be represented at this scale.

Depth (mbsf)	Core	Recovery	Nannofossil zone	Planktonic foraminifer zone	Benthic foraminifer assemblage (paleodepth)	Age
0	1H				I	Pleistocene
10	2H		CN14	N22	(Lower/middle bathyal)	
20	3H				II (Lower bathyal)	

Figure 15. Biostratigraphic summary of Hole 829B.

Depth (mbsf)	Core	Recovery	Nannofossil zone	Planktonic foraminifer zone	Benthic foraminifer assemblage (paleodepth)	Age
0	1H				I	Pleistocene
10	2H		CN14	N22	II (Lower bathyal)	
20	3H					
30	4H					
40	5H					
50	6H					
55	7H					
58	8H		CN3	N7-N8	IIIb (Middle bathyal)	
60	9H		CN14	N22		Pleistocene
61	11H					
62	10H					

Figure 16. Biostratigraphic summary of Hole 829C.

tumida tumida, *D. altispira*, *Globigerina nepenthes*, and *Globigerina apertura*, among others.

Early Miocene

Late early Miocene faunas were found in Hole 829C (Samples 134-829C-9H-6, 100 cm, to -9H-CC). Characteristic species found in this interval include *Globoquadrina dehiscens*, *D. altispira*, *Globigerina brazieri*, *Globoquadrina fohsi peripheroronda*, and *Globigerina druryi*, forms that can be assigned to Zone N8 (cf. Kennett and Srinivasan, 1983).

Late Oligocene to Early Miocene

Assemblages assigned to this age were identified in Hole 829A from 60 to 99 mbsf (Samples 134-829A-8R-CC to -11R-CC), as well as from 205 to 360 mbsf (Samples 134-829A-24R-CC to -39R-CC), and at 426 mbsf (Sample 134-829A-46R-CC) and 455 mbsf (Sample 134-829A-49R-CC). Among the foraminiferal species found are *Globoquadrina kugleri*, *Globoquadrina binaiensis*, *Globoquadrina dehiscens*, *Dentoglobigerina altispira*, *Catasyndrax dissimilis*, *Globigerina tripartita*, and *Globigerina venezuelana*. These are assigned to the foraminiferal Zones N3-N4 (Bolli and Saunders, 1985). No

major apparent change in the foraminiferal composition of these samples was observed, although Miocene markers (e.g., *G. dehiscens*) were absent between 310 and 370 mbsf (Samples 134-829A-34R-CC to -39R-CC). In this case, a late Oligocene age could be assigned (Zones P22/N3; cf. Bolli and Saunders, 1985).

Middle Oligocene

A middle Oligocene age was assigned to foraminiferal assemblages found between 378 and 397 mbsf (Samples 134-829A-40R-CC to -42R-CC). These samples are assigned to the middle Oligocene (Zones P19/20) on the basis of the presence of *Globigerina tripartita* and *Globigerina gortanii*. Apparently a continuous sequence is present connecting the upper and the middle Oligocene, though the poor recovery and foraminiferal preservation did not permit us to resolve the biostratigraphy in greater detail. In a preliminary survey, Sample 134-829A-42R-CC provided very few planktonic foraminifers that were found forming the nuclei of the abundant sand-sized carbonate nodules characteristic of this sample. Marker species for the early Oligocene were absent, but this age is not completely rejected, particularly in Samples 134-829A-49R-CC to -50R-CC (Fig. 14).

Benthic Foraminifers

Benthic foraminifers occur from the top of the sequence down to 510 mbsf (Sample 134-829A-56R-CC). Few to common, moderately well-preserved specimens occur from Sections 134-829A-1R-CC to -16R-CC. This contrasts with the rare and poorly preserved specimens present in the lower part of Hole 829A (Samples 134-829A-21R-CC to -50R-CC). Barren horizons were found between Sections 134-829A-9R-CC and -11R-CC; in Section 134-829A-20R-CC; between Sections 134-829A-35R-CC and -36R-CC; between Sections 134-829A-41R-CC and -43R-CC; between Sections 134-829A-51R-CC and -55R-CC, and below Section 134-829A-57R-CC.

Several species assemblages were determined as follows (Figs. 14, 15, and 16):

Assemblage Unit I (Sections 134-829A-1R-CC and -6R-CC, Samples 134-829B-1H-CC and -2H-CC, and Sections 134-829C-1H-CC to -3H-CC). Assemblage I is characterized by the co-occurrence of *Globobulimina pupoides*, *Melonis pacificus*, and *Uvigerina hispidocostata*. Along with these species some characteristic deep-water forms such as *Cassidulina carinata*, *Chilostomella oolina*, and *Cibicides wuellerstorfi* are also present (cf. Akimoto, 1990). The abundance of *M. pacificus* increases toward the lower part (between Samples 134-829A-1R-CC to -6R-CC), suggesting a subtle paleobathymetric change from the middle to lower bathyal zone boundary during the late Pleistocene to the lower bathyal zone during the early Pleistocene (Fig. 14). In addition, the presence of *G. pupoides* in the upper Pleistocene interval (Sections 134-829A-1R-CC to -5R-CC, Sections 134-829B-1H-CC to -3H-CC, and Sections 134-829C-1H-CC to -3H-CC) suggests low oxygen conditions at the sediment-water interface.

Assemblage Unit II. This assemblage has been divided into three subassemblage Units IIa, IIb, and IIc (Fig. 14), according to the state of preservation or mixing of faunas of different ages. Subassemblage Unit IIa, for example, shows a poor state of preservation related to the fairly indurated character of the upper Oligocene to lower Miocene chinks, compared to subassemblage Unit IIb, where a well-preserved microfauna was recovered. Subassemblage Unit IIc is a zone of mixing in which the faunas present in subassemblage Units IIa and IIb are found together. In spite of these differences, a similar assemblage is found from Sections 134-829A-7R-CC to -23R-CC, in Samples 134-829A-56R-CC and 134-829B-3H-CC, and

in Sections 134-829C-4H-CC to -6H-CC. The assemblage Unit II is characterized by the presence of *Bulimina aculeata*, *Cibicides wuellerstorfi*, *Melonis pacificus*, *Melonis sphaeroides*, and *Uvigerina hispidocostata*. *M. sphaeroides* found sporadically in this assemblage suggesting lower bathyal depths (cf. Akimoto, 1990).

The species *Cassidulina? perumbonata*, which is found in assemblage Unit III, also occurs in the uppermost part of assemblage Unit II (Sample 134-829A-8R-CC). *Bulimina* sp. and *Rectuvigerina prisca* occur in both assemblage Unit III and in the lower part of assemblage Unit II (Samples 134-829-21R-CC and -23R-CC). These occurrences suggest reworking from the Oligocene to Miocene deposits.

Assemblage Unit III (Sections 134-829A-23R-CC to -39R-CC, Samples 134-829A-49R-CC and -50R-CC, and Sections 134-829C-7H-CC to -9H-CC). Assemblage Unit III includes *Pleurostomella alternans*, *Bulimina* sp., *Cibicides aknerianus*, *C. wuellerstorfi*, *Gyroidina soldanii*, *Karriella bradyi*, *Oridorsalis umbonatus*, and *Stilostomella* sp. This assemblage exists in a zone of intensive deformation and mixing where it was impossible to separate species belonging to different ages due to their long stratigraphic ranges. Nonetheless, the assemblage in general suggests a middle bathyal depth of deposition.

Assemblage Unit IV (Samples 134-829A-40R-CC to -48R-CC). Assemblage Unit IV includes *Bulimina* sp. *Cibicides wuellerstorfi*, *Hoeglundina elegans*, *Gyroidina altiformis*, *Gyroidina soldanii*, *Melonis barleeanus*, *M. sphaeroides*, *Oridorsalis umbonatus*, and *Stilostomella* sp. This interval was deposited in the lower bathyal zone on the basis of the occasional occurrence of *M. sphaeroides*. The presence of species belonging to Zones II and III in this assemblage supports the idea of mixing between Oligocene and Pleistocene sediments as has been discussed above.

Figure 14 summarizes the paleobathymetric interpretation of Hole 829A based on the occurrence of deep-water species of benthic foraminifers. The first part of the hole (Cores 134-829A-1R to -3R) was deposited in the boundary between the middle and lower bathyal zone, whereas the assemblages between Cores 134-829A-4R and -23R suggest slightly deeper conditions (lower bathyal). Down to this depth (~215 mbsf) the oxygen conditions at the sediment-water interface vary from low in the first 40 mbsf (occurrence of *Globobulimina pupoides*) to normal in the next 175 m. Middle bathyal conditions are suggested from Core 134-829A-24R to -39R, whereas alternating lower to middle bathyal conditions are characteristic of the lowermost part of the sequence (Cores 134-829A-40R to -56R).

Summary and Discussion

Six biostratigraphic intervals were distinguished in Hole 829A based on planktonic foraminifers and nannofossils (Fig. 14). These intervals are informal units that contain sets of strata whose fossil assemblages are of a related age (e.g., the Pleistocene interval) or a different age (e.g., the upper Pliocene or lower Pleistocene with some Oligocene intervals). In the second case reworking and/or tectonic mixing is suggested to explain the complex array of lithologies and ages. The relationship between the different intervals is defined by either a fault plane (e.g., upper Oligocene to lower Miocene overlying the Pleistocene at 308 mbsf), or a zone of intensive tectonic deformation (e.g., Pleistocene overlying the upper Pliocene plus upper Oligocene to lower Miocene at 185 mbsf). As a consequence of this intensive tectonic deformation the stratigraphic relationship between these units is normally masked. Figure 14 depicts the age of the sequence (biostratigraphic intervals), along with the lithostratigraphic units as they have been defined by the shipboard sedimentologists. In

spite of some differences in the boundaries, the biostratigraphic intervals generally agree with the lithostratigraphic units. We therefore interpret the sequence in Hole 829A as the result of thrusting (at least two major faults at 99 and 410 mbsf) cutting a sedimentary sequence that basically consists of two time-rock units: (1) middle Oligocene to lowest Miocene and (2) upper Pliocene(?) to Pleistocene. Furthermore, the few late early Pliocene faunas (contained in creamy foraminiferal chalk fragments) may represent a third time-rock unit, commonly highly deformed and containing a mixture of material of different ages. In the same way, the unique late Eocene and the sparse early Oligocene flora could represent slabs of the lower part of a more complete sequence of time-rock unit (1). This means a time interval ranging from the late Eocene to the lowest Miocene.

Finally, the biostratigraphic correlation between Holes 829A and 829C is hampered by the difference in age found at 55–60 mbsf in the two holes. A time span of approximately 2 m.y. appears from the comparison between nannofossil Zones CN1 (Hole 829A) and CN3 (Hole 829C), or foraminiferal Zones N3–N4 (Hole 829A) and N7–N8 (Hole 829C). In other words, the difference accounts for the middle lower Miocene between the two holes, so that a structural explanation rather than a stratigraphic explanation is suggested here. Tectonic squashing (and missing) of the upper lower Miocene in Hole 829A is a possible explanation, as this unit is “soupy” in Hole 829C. Similarly a structural explanation is suggested here to explain the occurrence of the sand-sized carbonate nodules of Sample 134-829A-42R-CC. The major thrust fault at 410 mbsf and its related shearing zone appears to be the pathway to fluids that partially dissolved planktonic foraminifers and nannofossils, precipitating a thin crust of carbonate minerals. The nuclei of these nodules are not only planktonic foraminifers but also quartz, plagioclase, and heavy mineral grains.

IGNEOUS PETROLOGY

Igneous rocks were encountered at two levels in the lowermost part of Hole 829A (399–407 mbsf and 517–590 mbsf; see “Lithostratigraphy” section, this chapter). Both groups of rocks are assigned to composite Unit Bigwan Fo, the repetition being attributed to thrusting. The igneous rocks occur as clasts in a matrix of calcareous silty clay with sedimentary fragments. While there are some similarities, the assemblages of igneous clasts at the two levels are not identical, perhaps due either to lateral variation in the original deposit or to incomplete sampling or recovery.

The upper occurrence extends over a thickness of 7 m where igneous clasts 1–5 cm in maximum diameter are thinly dispersed throughout the unconsolidated breccia. The composition of the igneous fragments ranges from aphyric basalt through sparsely phytic basalt to pyroxenite and serpentinite, although only solitary small (1–2 cm) pieces of the latter two categories were found. The basalt clasts are pale gray with a slightly greenish tinge due to alteration. One small (2.5-cm) fragment from Section 134-829A-43R-CC is a very fine-grained aphanitic basalt with a thin (1-mm) rind of fresh black glass and is presumably derived from pillow lava or hyaloclastite. The pyroxenite fragment is very small (1.5 cm) but coarse-grained, being composed of a few dark green to black crystals. The gravel-sized serpentinite clast is distinctive, mainly because of one or two reflective bastite pseudomorphs.

The aphyric to sparsely porphyritic basalts contain occasional subhedral microphenocrysts of clinopyroxene (0.1–0.5 mm) and in one instance (interval 134-829A-43R-2, 145–147 cm), olivine. In each case the groundmass is similar and is dominated by plagioclase laths (0.01–0.4 mm) with intergranular clinopyroxene, which together constitute between 55%

and 80% of the rock. Opaque minerals and glass make up the remainder. In one of the specimens (Sample 134-829A-43R-2, 145–147 cm) some of the plagioclase and opaque minerals have characteristic quench morphology. Glass appears to have formed between 13% and 30% of the original lavas, though much of it has now devitrified and altered to a mixture of clay minerals, chlorite, and oxide minerals. The specimen with quenched phases referred to above contains a small cognate inclusion of darker, more vesicular and more markedly quenched nature, which probably represents a piece of its own scoriaceous crust ingested during flow. All of the lava samples examined are vesicular (15%–30% of the total rock) and one (Sample 134-829A-43R-3, 132–133 cm) has flow banding defined by the subparallel orientation of plagioclase laths. The single small pyroxenite fragment (Sample 134-829A-43R-1, 133–135 cm) has an allotriomorphic-granular texture and is composed largely of clinopyroxene (80%) accompanied by orthopyroxene (15%) and serpentinized olivine (5%). The clinopyroxene, probably diopsidic augite, forms anhedral crystals up to 8 mm across: there is conspicuous exsolution of orthopyroxene lamellae and some alteration to serpentine minerals and iron oxide minerals. The orthopyroxene crystals are smaller (1–2 mm) and of a similar size to the olivines, which have been completely pseudomorphed by serpentine and oxide minerals. The serpentinite fragment (Sample 134-829A-44R-1, 1–4 cm) has a coarse to medium seriate texture. Most (65%) of the specimen appears to have been olivine originally, although again it has been almost entirely serpentinized. There are very occasional relict grains of olivine, but elsewhere pseudomorphs retain the distinctive fracture pattern of the mineral emphasized by residual iron oxide minerals. Orthopyroxene, which originally made up about 20% of the rock, forms large crystals about 7 mm in maximum diameter, which are now partially serpentinized. These bastite pseudomorphs are the most conspicuous feature of the hand specimen. Subhedral clinopyroxene and anhedral spinel crystals (<0.6 mm) make up the rest of the rock (12%) apart from about 3% secondary calcite.

After a gap of 110 m, represented by calcareous silty mixed sediments, igneous rocks were again recovered between 518.40 and 581.43 mbsf. The hole terminated in sheared breccia at 583 mbsf. This second appearance of igneous material, also ascribed to Unit XVI, is dominated by microgabbro and diabase together with less abundant basalt and gabbro. The basalt is light greenish gray, aphyric and nonvesicular, containing about 1% irregular fractures filled with calcite. The typical diabase or microgabbro is a medium gray rock without veins or fractures and in which plagioclase and pyroxene crystals may be distinguished without the aid of a hand lens. Apart from a coarser grain size, the gabbros closely resemble their finer-grained counterparts in hand specimen. There has been significant alteration of pyroxene and development of secondary pyrite: olivine crystals show characteristic fracturing and are strongly serpentinized. A feature of samples in Core 134-829A-62R is that all seven pieces of gabbro have a yellowish to pale brown weathering or alteration rind.

In thin section, the basalt from the lower part of Unit XVI (Sample 134-829A-59R-1, 1–4 cm) differs from samples found in the upper part of the unit in that it is devoid of clinopyroxene phenocrysts and instead contains sparse (1%) microphe-nocrysts of plagioclase. The groundmass is dominated by plagioclase laths, sometimes showing quench morphology, and anhedral clinopyroxene. Apart from about 5% opaque minerals the remainder of the rock (<20%) is composed of devitrified glass. A typical diabase (Sample 134-829A-59R-1, 45–50 cm) has medium grain size and characteristic subophitic

texture. The dominant mineral (50%) is elongate, euhedral to subhedral plagioclase (<1 mm). The plagioclase is partially enclosed by anhedral clinopyroxene (36%, 0.1–0.4 mm in diameter), about half of which has altered to chlorite and actinolite. Olivine (10%, 0.1–0.6 mm in diameter) and small opaque minerals (4%) make up the rest of the rock. A typical microgabbro (interval 134-829A-61R-1, 49–53 cm) shows similar modal proportions to the diabase and ophitic texture, with the main difference being an increase in grain size (in the range of 1–4 mm).

There is a further increase in grain size to an average of about 5 mm for the primary phases of the gabbro. The texture continues to be ophitic or poikilitic, though clinopyroxene now tends to be slightly more abundant than plagioclase (40% clinopyroxene and 35% plagioclase in gabbro; Sample 134-829A-59R-1, 15–18 cm). In this sample, and also in the microgabbro (Sample 134-829A-61R-1, 1–5 cm), a number of additional features were evident. Firstly, the clinopyroxene crystals have a moderately strong grayish to pale brown color in plane-polarized light and some are distinctly zoned to a thin green margin; there are also smaller pyroxene laths showing pleochroism in shades of green to yellow green. Small crystals of apatite are quite widely distributed throughout these two specimens. Also, a zeolite mineral occurs in cavities and there is a late-stage mineral with negative relief and very low birefringence which may be analcite.

Despite differences, the igneous rocks recovered from the two levels are treated as belonging to the same unit. In the upper group they are manifestly present as clasts in a breccia and this is also true of the specimens from near the top of the lower group. However, most of the lower group were recovered as pieces of igneous rock without any matrix. One possibility is that the unconsolidated matrix was washed out during drilling, and in this respect it is perhaps significant that breccia was sampled once again from the bottom of Hole 829A. Even in cores without any matrix (e.g., Core 134-829A-62R), microgabbro pieces sometimes have weathered or altered rims suggesting an origin as clasts rather than fragmentation and rounding during drilling. The conclusion is that none of the material described here represents a primary igneous body. Hole 829A evidently penetrated a breccia containing igneous clasts of quite varied lithology within the basic-ultrabasic range. The igneous rocks were probably brecciated prior to their incorporation in the collision complex. They lack the obvious arc signature of the brecciated material from Hole 827B and preliminary geochemical studies point to a composition transitional between mid-ocean ridge basalt and island-arc tholeiite. In this respect there are similarities to the clasts recovered from Site 828 on the North d'Entrecasteaux Ridge.

IGNEOUS GEOCHEMISTRY

Igneous rocks were recovered from the two levels of volcanic breccia comprising composite Unit Bigwan Fo at Site 829 (see "Lithostratigraphy" and "Igneous Petrology" sections, this chapter). Seven samples of basalt, gabbro, microgabbro, and diabase from Hole 829A were selected for shipboard analysis of major and trace elements by X-ray fluorescence (XRF) (see "Explanatory Notes" chapter, this volume). The results are presented in Table 3.

Sample 134-829A-43R, 94–96 cm, is a clast of sparsely aphyric basalt from 406 mbsf. Compared with the gabbro and diabase pieces from the same composite unit, concentrations of SiO₂, K₂O, Rb, and Sr in the basalt are higher, although concentrations of CaO, Cr, and Ni are lower (Table 3). A chondrite-normalized trace-element pattern for this basalt is shown in Figure 17 where distributions for typical MORB and

Table 3. Shipboard XRF analyses of samples from Hole 829A.

Core, section	43R-3	59R-1	59R-1	61A-1	61A-1	61A-1	64R-1
Sample interval (cm)	94–96	45–50	105–108	3–4	56–59	80–86	10–13
Piece number		5	13	1	7	10	1
Depth (mbsf)	401.5	533.50	534.00	552.50	552.90	553.10	581.30
Unit	VII	XVI	XVI	XVI	XVI	XVI	XVI
Lithology	Basalt	Gabbro	Gabbro	Gabbro	Gabbro	Gabbro	Diabase
Major elements (wt%)							
SiO ₂	50.24	48.81	47.33	47.58	47.35	47.78	48.74
TiO ₂	0.85	0.97	1.86	1.14	0.96	0.92	0.73
Al ₂ O ₃	17.70	16.62	16.85	16.33	17.32	17.86	17.33
Fe ₂ O ₃	10.51	10.27	12.70	11.72	11.37	11.18	9.58
MnO	0.17	0.18	0.20	0.22	0.22	0.16	0.18
MgO	7.58	9.85	6.19	7.41	8.35	8.58	6.78
CaO	9.04	11.96	10.45	12.82	11.92	10.56	13.82
Na ₂ O	2.35	2.03	4.40	2.73	2.27	3.38	2.30
K ₂ O	1.10	0.04	0.13	0.03	0.05	0.07	0.06
P ₂ O ₅	0.15	0.06	0.18	0.05	0.04	0.06	0.03
Total	99.67	100.78	100.28	100.03	99.85	100.55	99.55
LOI	4.37	2.68	3.93	1.05	3.21	4.62	4.00
Trace elements (ppm)							
Rb	11	0	3	0	1	1	0
Ba	22	30	59	20	25	22	24
Nb	0	2	5	1	1	1	1
Ce	11	0	1	11	7	3	1
Sr	248	63	124	88	114	126	94
Zr	62	49	96	53	51	49	41
Ti	5455	5815	11540	7014	5845	5588	4496
Y	31	27	40	33	30	28	26
V	244	286	267	288	229	205	212
Ni	43	132	145	106	189	202	177
Cr	78	323	154	303	395	336	450
Cu	122	132	137	141	146	140	168
Zn	57	54	79	56	72	67	52

Note: LOI = loss on ignition.

IAT are illustrated for comparison. The righthand part of the basalt pattern, from Ce to V, is similar to MORB, but the basalt is relatively enriched in Rb and K and has a conspicuous negative niobium anomaly, features which are characteristic of island-arc basalts. Overall, this sample may be regarded as transitional between MORB and IAT.

Analyses were made on five pieces of gabbro and microgabbro and one of diabase, all of which were from the interval 517 to 590 mbsf. These samples have relatively uniform

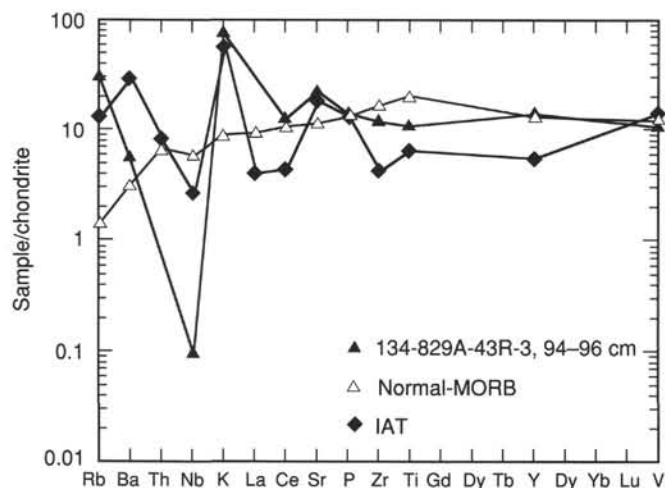


Figure 17. Chondrite-normalized trace-element distribution patterns of incompatible elements for a basalt, Sample 134-829A-43R-3, 94–96 cm (Table 3), normal-type MORB (N-MORB), and island-arc tholeiite (IAT) (data from Sun, 1980).

major-element chemistry with rather low SiO₂ (approximately 48%). The MgO content, which is usually a more reliable index of differentiation, varies from 6.2% to 9.9%. Al₂O₃ is in the range 16.3%–17.9% and both K₂O (0.03%–0.13%), and P₂O₅ (0.03%–0.18%) are at low concentrations. Site 829 samples are generally less altered than those from the previous site as apparent from differences in loss on ignition (1.0%–4.6% for Site 829 samples and 3.3%–6.7% for Site 828 samples).

Chondrite-normalized incompatible trace-element patterns are presented on two separate diagrams (Fig. 18). On each diagram Site 829 samples are shown in conjunction with spectra from typical MORB and IAT. The “normal-type” MORB (data from Sun, 1980) is characterized by progressive depletion of the more mobile elements. In contrast the IAT pattern shows relative depletion of the high field strength elements (Zr, Ti, and Y) and enrichment in the large ion lithophile (LIL) elements; it also exhibits the pronounced negative niobium anomaly regarded as a characteristic subduction zone signature (Briqueu et al., 1984). Although the Ba and Ce values obtained are plotted on the diagrams, their concentrations are very low and must be regarded as unreliable; they are therefore omitted from the following discussion.

Despite some perturbations, the patterns of samples cored at Site 829 show a broad resemblance to MORB (e.g., Sample 134-829A-59R-1, 105–108 cm), although the negative phosphorus anomaly in Sample 134-829A-61R-1, 3–4 cm, represents a deviation from typical MORB. Three specimens (e.g., Sample 134-829A-61R-1, 56–59 cm) have conspicuous negative niobium anomalies, typical of IAT, but lack the enrichment in LIL elements associated with island-arc volcanic rocks. In general terms the righthand portions of these patterns, relating to the heavier elements, are similar to MORB,

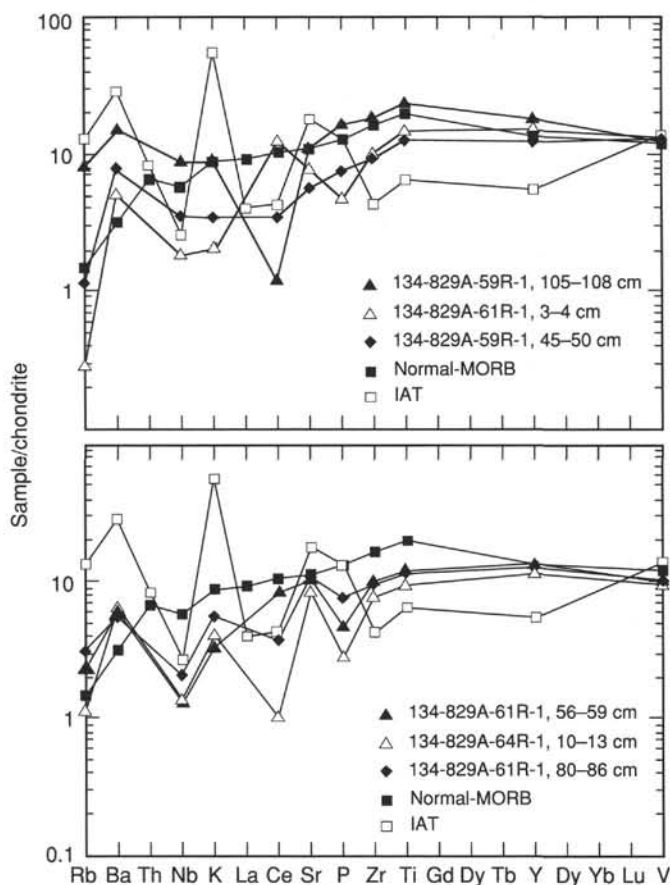


Figure 18. Comparison of chondrite-normalized trace element distribution patterns of gabbro, microgabbro, and diabase collected at Hole 829A with N-MORB and typical island-arc tholeiite (IAT) (Sun, 1980).

whereas the more incompatible elements on the left are more erratic in distribution and more difficult to interpret. Considerable importance is attached to the Nb anomalies in attempting to arrive at a classification. On this basis the six analyzed samples are divided into two groups, one with MORB affinity (Fig. 18) and the other with island-arc characteristics (Fig. 18).

A plot of Nb vs. Zr (Fig. 19) is used in a further effort to establish the affinities of these samples. The Site 829 analyses are plotted on the diagram, which shows for comparison suites of "normal-MORB" from the Atlantic ($Zr/Nb = 9$) and IAT from Vanuatu ($Zr/Nb = 40$). All the samples from Site 829 follow the island-arc trend. Unfortunately, this is not entirely decisive in view of the findings from Deep Sea Drilling Project (DSDP) Legs 69/70 (Etoubleau et al., 1983) and ODP Leg 111 (Shipboard Scientific Party, 1988) on the Costa Rica Rift, where highly depleted MORB had the same Zr/Nb ratio as island-arc volcanics.

The Ni vs. Ti diagram (Fig. 20) illustrates the MORB affinities of the gabbro, microgabbro, and diabase from Hole 829A (Cores 134-829A-59R to -64R). MORB analyses from the Famous area (Bougault et al., 1980) and the Costa Rica Rift (Etoubleau et al., 1983) define a field that is distinct from that of the Central Chain (Epi Island) of the New Hebrides Island Arc (Dupuy et al., 1982; Briquieu et al., 1984).

Figure 21 is a chondrite-normalized trace-element distribution diagram on which average gabbro, microgabbro, and diabase from Hole 829A are compared with normal-type MORB and a gabbro from Malakula Island. The Hole 829A

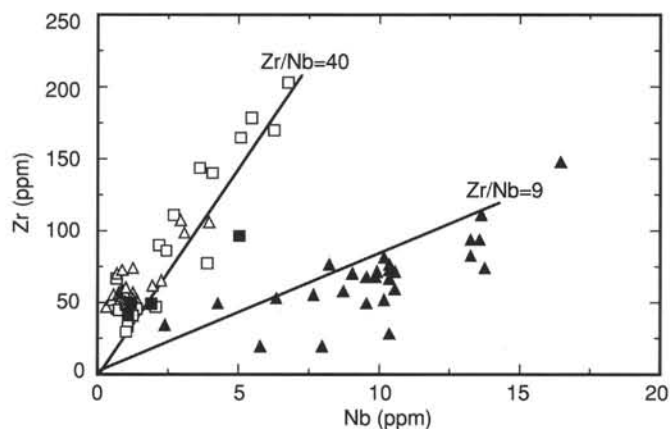


Figure 19. Plot of Zr vs. Nb. The Zr/Nb ratio of N-MORB (solid triangles) is about 9, that of depleted MORB from Costa Rica (open triangles) and of the Central Chain of New Hebrides Island Arc series (open squares) is about 40. The Zr/Nb ratios of gabbro, microgabbro, and diabase collected at Hole 829A (solid squares) are similar to ratios in basalts from the Costa Rica Rift zone (Etoubleau et al., 1983; Shipboard Scientific Party, 1988) and island-arc magmatic suites (Dupuy et al., 1982; Briquieu et al., 1984).

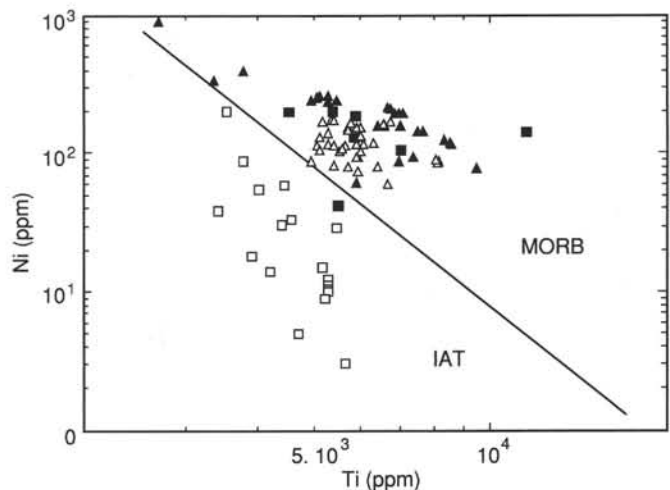


Figure 20. $\log(Ti)$ vs. $\log(Ni)$. Points plotted include normal-type MORB of the Atlantic Ocean, depleted-type MORB of the Costa Rica Rift, island-arc tholeiitic suites (Central Chain–New Hebrides Island Arc), and gabbro, microgabbro, and diabase collected at Hole 829A (same symbols as in Fig. 19).

average shows a relatively systematic pattern that is more depleted than MORB. It could be argued that it was derived from a MORB-type magma with relatively low K_2O and TiO_2 but rather high MgO and Al_2O_3 . These are geochemical characteristics indicative of high degrees of partial melting of peridotitic mantle. They could equally well, of course, be produced by the dilution effects resulting from crystal accumulation. In contrast, the lower Miocene gabbro from Malakula (Gorton, 1974) has an island-arc signature.

There appear to be two possible origins for the volcanic breccias of Site 829. They may have been derived from the New Hebrides Island Arc, especially from Espiritu Santo Island, in which case they will have island-arc affinities and will be situated above the décollement. Alternatively, they may have been detached from the subducting NDR and incorporated into the accretionary prism at the base of the

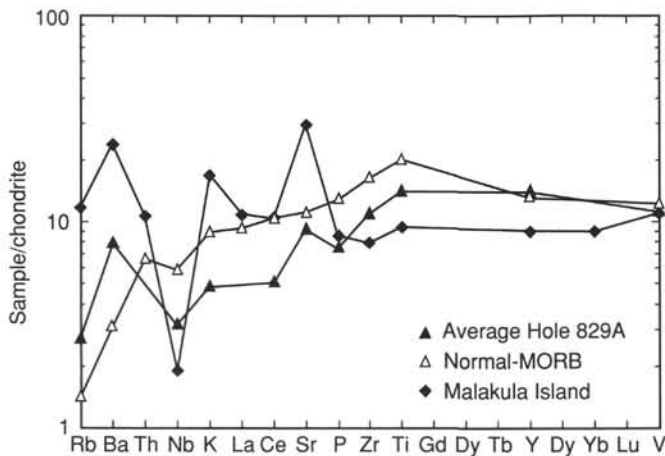


Figure 21. Chondrite-normalized trace element distribution patterns for the average composition of gabbroic material cored at Hole 829A, a normal-type MORB, and an island-arc gabbro sampled at Malakula Island (Gorton, 1974).

forearc. In this case there should be similarities to material recovered from Site 828 on the NDR. The available analyses, which have MORB characteristics, suggest that the NDR is the more likely provenance of the Site 829 breccia clasts. The basalt clast with transitional MORB-IAT affinities (Sample 134-829A-43R, 94–96 cm) also resembles basalt clasts from Site 828 on the NDR.

SEDIMENT AND FLUID GEOCHEMISTRY

Drilling in several accretionary prisms suggests that the sediment dewatering by a variety of processes; for example, fluid flow is confined to thrust faults in the fine-grained sediment of the Barbados accretionary prism (Masle, Moore, et al., 1988; Gieskes et al., 1990a, 1990b), whereas fluid flow appears to be more diffuse or may only flow episodically in the coarser sediment of the Nankai prism (Taira, Hill, Firth, et al., 1991). The Barbados and Nankai accretionary prisms differ tectonically from the New Hebrides Island Arc where collision of the d'Entrecasteaux Zone (DEZ) causes severe deformation (Collot et al., 1985). The New Hebrides Island Arc may therefore dewater by processes different from either the Barbados or Nankai accretionary prisms.

The objectives for measuring pore-fluid geochemistry at Site 829 were similar to the objectives at Site 827 and include determining the alteration of pore-fluid chemistry by diagenetic reactions and identifying by using solute concentrations as chemical tracers those horizons through which fluids flow. Extreme diagenetic reactions apparently control the pore-fluid chemistry at Site 827 and similar reactions were expected at Site 829, located just 2.5 km south of the first site (see "Operations" section, this chapter). Subtle chemical anomalies, which may have originated from fluid flow from the décollement, were observed in the pore-fluid gradients in shallow sediments at Site 827 and thus one specific objective at Site 829 was to further define the chemistry and origin of that horizon.

Methods and Sample Handling

A total of 21 whole-round samples were collected from Holes 829A, 829B, and 829C (Tables 4 and 5). Portions of each sample were removed if they were disturbed by drilling or had been invaded by drilling mud. Two samples (134-829A-60R-1, 120–150 cm, and 134-829C-9H-4, 135–140 cm), however, were soft and friable throughout and contained more water

than shallower samples (Table 5). These samples are characterized by anomalous concentrations of chloride, sodium, potassium, and magnesium, suggesting that they had been contaminated by drilling mud and therefore no data are reported for them. No other samples appear to be contaminated with the drill fluid.

The yield of fluid dropped as the sediments became progressively indurated with depth (Fig. 22). Two samples (134-829A-41R-1, 77–90 cm, and 134-829A-51R, 120–150 cm; Table 5) yielded no water although they were squeezed for ~3 hr at 35,000 pounds per square inch. Data from these samples, therefore, do not appear in Table 4.

The magnesium concentrations in samples from the upper 200 m at Hole 829A were measured by both titration and by atomic absorption spectroscopy (AAS), yielding consistent results (Fig. 23). The deepest samples at Site 829 were therefore measured only by AAS to preserve the small volumes of fluids comprising the samples (Gieskes and Gamo, in press). The concentrations of calcium, alkalinity, ammonia, phosphate, and silica also were not measured in these deep samples because of the volume of fluids required.

The samples that were measured for their carbon content were residues of the physical properties measurements and a few additional samples selected by the sedimentology group. The results are reported in Table 6, the carbonate content is plotted against depth in the "Lithostratigraphy" section of this chapter, and the organic carbon content is plotted against depth in Figure 24.

Results

The organic carbon content is consistently ~0.4% in the sediments of Units I, II, and III to a depth of 175 mbsf (Fig. 24), but decreases below this depth. Within Units IV and V, the organic carbon content varies, ranging from 0% to 0.4%. Almost no organic carbon is contained within the calcareous chalk in Unit VI between 310 and 400 mbsf. Three samples contain >1% organic carbon but the origin of the carbon is unknown.

The amount of water yielded by the sediments appears to decrease in a series of steps (Fig. 22). The upper hundred meters of sediment yielded ~6 cm³/cm of fluid, but below a major thrust fault recognized at 99 mbsf (see "Structural Studies" section, this chapter) the fluid yield dropped from 4 to 0.5 cm³/cm. No samples were taken between 178.9 and 379.2 mbsf, and below this depth only five samples were taken. The sediments at 379.2 and 461.3 mbsf provided no fluid; low water contents were also measured in this interval (see "Physical Properties" section, this chapter). Below 379.2 mbsf, fluid was obtained only from samples at depths of 408.2, 507.1, and 515.0 mbsf. These depths correspond to the locations of major thrust faults, implying that fluids may be concentrated along structural features. The sample taken at a depth of 461.3 mbsf also corresponds to the location of a major thrust fault but is located directly above the thrust fault whereas the samples containing fluid are located below faults.

Chloride and Salinity

The chloride concentrations exhibit little change except for a slight increase to a depth of ~200 mbsf. In samples below 400 mbsf, however, the chloride concentrations are much lower, exhibiting a maximum value of 408.8 mM, ~30% lower than seawater values. Low chloride concentrations also occur at other convergent margins; the chloride concentration decreases to 505 mM in the décollement at the Barbados prism (Masle, Moore, et al., 1988; Gieskes et al., 1990a, 1990b) and a minimum value of 451 mM was observed below the décollement at the Nankai Trough (Taira, Hill, Firth, et al., 1991).

Table 4. Pore-fluid chemistry, Site 829.

Core, section, interval (cm)	Depth (mbsf)	pH	Salinity (‰)	Chloride (mM)	Sodium (mM)	Potassium (mM)	Magnesium (mM)	Calcium (mM)	Sulfate (mM)	Alkalinity (mM)	Phosphate (μM)	Ammonia (μM)	Silica (μM)
134-829A-													
1R-1, 146-150	1.5	7.8	35.0	558	487	11.3	45.0	9.3	23.2	5.9	13.2	246	422
3R-2, 145-150	15.3	8.0	35.5	561	488	11.6	42.2	8.9	16.8	9.0	12.9	676	450
5R-5, 145-150	38.5	7.8	34.0	561	490	10.7	38.0	11.1	16.5	5.0	5.8	729	543
7R-1, 145-150	52.3	7.8	34.0	562	485	10.6	34.6	14.6	20.0	2.2	1.3	459	501
12R-5, 140-150	106.4	8.0	32.5	564	477	10.4	38.9	4.8	1.6	14.3	24.4	1319	531
14R-4, 135-150	124.1	8.0	32.5	568	482	10.3	37.2	5.0	3.8	12.0	24.3	1482	475
16R-4, 135-150	143.4	8.1	33.0	565	482	11.0	35.8	7.3	9.0	7.7	11.0	1521	527
18R-3, 135-150	161.2	8.2	34.0	564	479	10.6	34.4	12.3	14.6	4.4		1163	482
20R-2, 130-150	178.9			565	470	10.1	38.2	15.6	20.0			674	283
44R-1, 123-140	408.6			424	396	7.7	16.5		12.2				
56R-3, 130-150	508.1			409	362	7.2	20.2		4.5				
57R-2, 0-33	515.0			417	365	7.6	21.5		7.3				
134-829B-													
2H-2, 145-150	3.5	7.9	34.5	554	470	11.3	42.6	9.2	21.5	6.6	16.1	403	334
134-829C-													
1H-2, 145-150	3.0	7.9	35.0	556	472	11.7	42.9	9.0	22.1	6.8	12.2	417	341
1H-4, 145-150	6.0	7.9	35.0	556	484	10.5	42.7	8.6	17.0		17.0	781	416
2H-2, 145-150	11.3	7.9	34.5	556	484	10.4	41.1	7.8	13.1		20.3	987	440
3H-6, 135-140	26.7	7.8	34.0	558	472	11.6	36.2	8.4	13.2	7.7	12.9	907	458

Note: Values in bold characters were measured by atomic absorption spectroscopy.

Table 5. Samples collected but not reported.

Core, section, interval (cm)	Depth (mbsf)	Problem
134-829A-		
41R-1, 77-90	379.2	No fluids
51R-1, 120-150	461.3	No fluids
60R-2, 120-150	545.3	Contaminated
134-829C-		
9H-4, 135-140	57.9	Contaminated

Low chloride concentrations have also been observed in diapiric structures at the Barbados and the Mariana convergent margins. At Barbados, the chloride concentration is ~ 250 mM by only 0.2 mbsf in mud diapirs (Le Pichon et al., 1990) and is ~ 230 mM at 50 mbsf (Mottl, in press) in serpentinite diapirs at the Mariana forearc.

Salinity varies with depth (Fig. 24) but exhibits a slight decrease to 52 mbsf. Below this depth, however, the salinity is lower overall, but increases from 32.5 to 35‰ from ~ 100 to ~ 160 mbsf. The variation in salinity probably results from changes in solute concentrations other than chloride because chloride concentrations are nearly constant with depth.

Sodium, Potassium, Calcium, and Magnesium

Both the sodium and potassium concentrations decrease with depth, although the potassium concentration is scattered (Fig. 25). The sodium concentration below 400 mbsf appears to decrease at the same rate as the sodium concentration above 200 mbsf, but because of the 200-m gap between the two sample groups, it is impossible to determine if the two trends are related. The low sodium and potassium concentrations may result from the same dilution that causes the low chloride concentration.

The concentrations of both magnesium and calcium exhibit discontinuities across the major thrust fault located at ~ 100 mbsf (Fig. 26; see also "Structural Studies" section, this chapter). Above this horizon, the magnesium concentration decreases linearly to 34.6 mM. Below the fault, the concentration is 38.9 mM and again decreases with depth. One sample located at 178.9 mbsf, the depth of a possible thrust

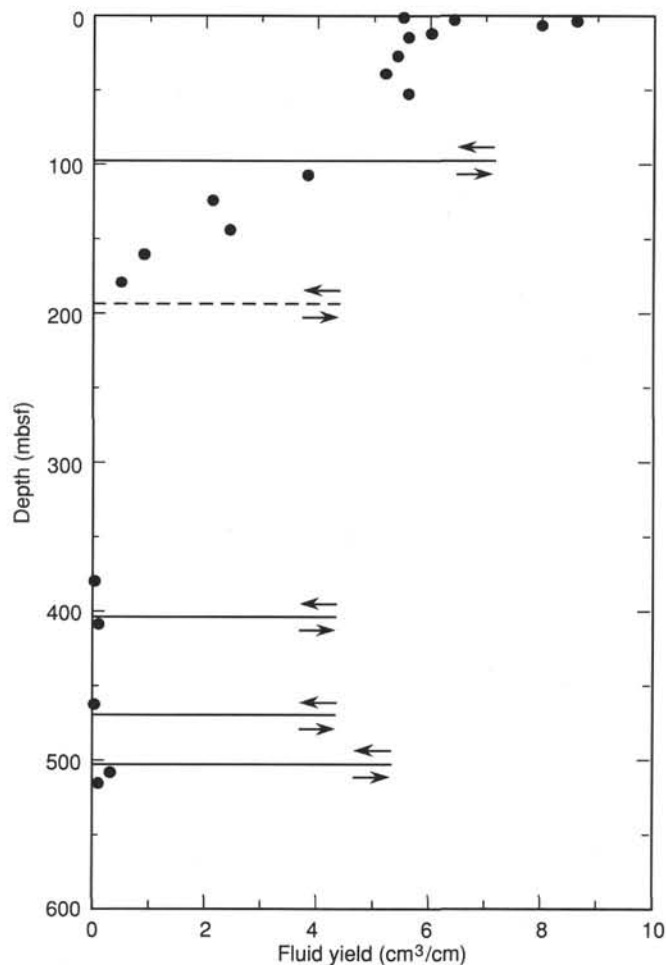


Figure 22. The yield of water per centimeter of core that was squeezed, Site 829. This value is only a qualitative measure of the water contained in the sediment because some variable amount of the sample was removed prior to squeezing. The heavy lines with arrows represent the locations of major thrust faults and the dashed line represents the location of an inferred thrust fault.

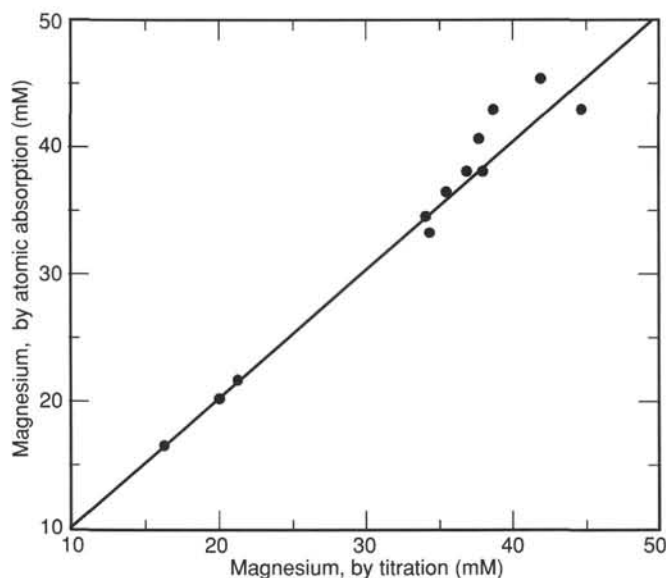


Figure 23. The magnesium concentration measured by titration plotted against the magnesium concentration measured by atomic absorption spectroscopy.

fault (see "Structural Studies" section, this chapter), shows a similar reversal in gradient.

The calcium concentration gradient exhibits similar profiles above and below the shallowest thrust fault (Fig. 26). Above the fault, the calcium concentration exhibits a minimum at 11 mbsf, increasing with depth to 52 mbsf. Below the fault, the fluid exhibits the lowest measured calcium concentration, but the concentration again increases with depth to the deepest measured sample at 179 mbsf.

The initial concentration of both magnesium and calcium are lower than seawater values (Fig. 26) and the concentrations from Hole 829A are higher than the concentrations at Holes 829B and 829C. Hole 829A was drilled in water ~5 m shallower than either Holes 829B or 829C, and when the concentrations are plotted against depth in meters below sea level, both the magnesium and calcium gradients are similar in all three holes (Fig. 27).

Ammonia, Phosphate, Alkalinity, Silica, Sulfate, and Methane

Because of the small volumes of fluid recovered in samples collected below 200 mbsf, ammonia, phosphate, alkalinity and silica concentrations were not measured. Where measured above 200 mbsf (Fig. 25), the ammonia, phosphate, and alkalinity concentrations are characterized by distinct and sharp maxima at ~10 mbsf. The maxima correspond to the sulfate minimum, but the maxima and minimum are shallower than those observed at Site 827. The ammonia, phosphate, alkalinity, and sulfate concentrations exhibit discontinuities across the thrust fault at ~100 mbsf, similar to the calcium and magnesium gradients.

The sulfate concentration decreases to 16.5 mM at 38.5 mbsf, but the concentration increases below this depth suggesting that sulfate is not completely reduced (Fig. 25). Below the fault at 100 mbsf, there is almost no sulfate, but the concentration increases linearly with depth to 178.9 mbsf. Sulfate is present at depths below 400 mbsf although the concentration is low. The lack of samples between 200 and 400 mbsf prevents comparison between the upper and lower samples.

Methane concentrations are near zero except at a depth of ~510 mbsf, where the headspace samples contained 2600

parts per million (ppm) methane (Fig. 28). Two samples contain >1% total organic carbon at this depth (Fig. 24), which may provide a source for the methane. This methane maximum corresponds to a zone of high water content (see "Physical Properties" section, this chapter) and the location of chloride-depleted water fluid.

Discussion

The sediments between ~200 and 400 mbsf contain little water (Fig. 22; see also "Physical Properties" section, this chapter), and some of the original fluid may have flowed from the sediments during tectonic compression caused by subduction of the NDR. Variations in solute concentrations and water content at fault boundaries (Figs. 22 and 26) suggest that these structural horizons may be conduits for the fluid flow. Alternatively, the thrust fault at ~100 mbsf may be impermeable, thereby preventing diffusive and advective exchange across the boundary. Fault-controlled hydrology characterizes the fine-grained sediments at the Barbados prism (Gieskes et al., 1990a, 1990b), but the sediments there have greater water contents than at Site 829 (e.g., Mascle, Moore, et al., 1988). The sediments at Site 829 are also fine grained and are thus probably characterized by low permeabilities, which may force the fluids to flow along fault planes.

Fluids are also associated with faults in the deeper sediments, and based on the locations of samples containing fluids and the thrust faults below 400 mbsf (Fig. 22), the sediments appear to contain less fluid above the faults than below them. The fluids below the faults may facilitate motion along the fault plane, and possibly represent vertically flowing fluids that are trapped below an impermeable fault barrier. The fluids below 400 mbsf exhibit chemical compositions different from the shallower fluids (e.g., low chloride and high methane concentrations), indicating that at least two fluid sources may be present. Because of their similarity in chemistry to fluids sampled from the décollement at the Barbados prism, the deep fluids may have been derived from a source within the décollement.

The magnesium gradient across the sediment-water interface (Fig. 26) could result from rapid diagenesis of volcanic ash (e.g., Gieskes, 1981) or may be maintained by rapid, upward flow of magnesium-poor fluids. The difference in concentration across the interface, however, is probably too large to result solely from diagenesis of the shallow sediment. Rapid upward flow of magnesium-poor fluid could overwhelm diffusive exchange of magnesium from seawater into the sediments but should produce an exponential curve in the concentration gradients which is not observed.

Figure 27 shows that the calcium and magnesium gradients at Holes 829A, 829B, and 829C are essentially the same when plotted using the sea surface as a reference plane, suggesting that the modern sediment-water interface is not the horizon at which these diffusional profiles were established. Similarly, the initial ammonia, alkalinity, and phosphate concentrations are greater, and their maxima occur at shallower depths below seafloor than at Site 827, implying that part of the shallow sediments may have been removed through erosion. Extrapolating the alkalinity, calcium, and magnesium gradients to seawater concentrations suggests that 25 to 50 m of sediment is missing from this location. The removal must have occurred rapidly and recently to prevent diffusion from altering the sharp gradients at the sediment-water interface and probably indicates that the erosion occurred as a slump. Slumping may be a common process in areas with rapid vertical fluid flow that would alter sediment physical properties and facilitate mass wasting.

Table 6. Sediment carbon contents, Site 829.

Core, section, interval (cm)	Depth (mbsf)	Total carbon (wt%)	Inorganic carbon (wt%)	TOC (wt%)	CaCO ₃ (wt%)
134-829A-					
2R-1, 87-90	3.7		1.2		9.7
2R-2, 87-90	5.2	1.4	1.1	0.3	9.2
2R-3, 87-90	6.7		1.2		9.7
3R-1, 100-103	13.3	1.6	1.2	0.4	10.1
3R-3, 100-103	16.3		1.3		10.5
4R-1, 38-40	22.0		1.1		9.2
4R-3, 38-40	25.0	1.7	1.3	0.4	10.7
4R-3, 71-73	25.3		1.7		14.2
4R-5, 38-40	28.0				
5R-1, 38-40	31.4	1.8	1.5	0.3	12.3
5R-3, 38-40	34.4		1.1		9.2
5R-4, 69-71	36.2		1.7		13.7
5R-5, 38-40	37.4		2.3		19.5
6R-1, 38-40	41.5		2.7		22.1
6R-3, 38-40	44.5		2.1		17.2
6R-5, 38-40	47.5	2.6	2.4	0.2	20.3
6R-7, 38-40	50.5		2.4		20.3
12R-1, 27-30	99.3		7.7		63.7
12R-2, 138-140	101.9		1.3		10.7
12R-3, 37-39	102.4	1.4	1.1	0.3	8.7
12R-5, 37-39	105.4		1.6		13.1
12R-7, 37-39	108.4		1.3		10.7
13R-1, 120-123	109.8		1.6		13.5
13R-3, 120-123	112.8	1.7	1.4	0.3	11.9
13R-5, 120-123	115.8		1.3		11.2
13R-7, 65-67	118.3		1.3		10.7
14R-1, 130-133	119.5		1.0		8.3
14R-3, 130-133	122.5	1.7	1.4	0.3	11.6
14R-4, 130-133	124.0		1.6		13.4
14R-6, 130-133	127.0		1.2		10.0
15R-1, 115-118	129.1		1.5		12.5
15R-3, 115-118	132.1	2.1	1.8	0.3	15.3
15R-5, 115-118	135.1		1.6		13.2
15R-7, 60-62	137.5		1.5		12.7
16R-1, 57-61	138.1		2.0		16.4
16R-3, 57-61	141.1	2.1	1.8	0.3	14.6
16R-5, 57-61	144.1		1.6		13.2
16R-7, 57-61	147.1		1.7		14.1
17R-1, 55-58	147.8		1.9		16.2
17R-3, 55-58	150.8	2.5	2.2	0.3	18.3
17R-5, 55-58	153.8		2.0		16.5
17R-7, 55-58	156.8		2.3		19.0
18R-2, 137-140	159.7	2.4	2.1	0.4	17.1
18R-6, 137-140	165.7		3.3		27.4
19R-2, 97-100	169.0		3.0		25.0
19R-3, 97-100	170.5	3.2	2.9	0.3	23.8
19R-4, 97-100	172.0		3.4		28.6
19R-5, 97-100	173.5		7.6		63.1
20R-1, 26-29	176.4		7.8		65.1
20R-2, 23-26	177.8	9.6	9.6	0.0	80.2
21R-1, 24-25	186.0		9.4		78.6
21R-3, 28-30	189.1	8.0	8.1		67.1
22R-1, 37-39	195.9		8.6		72.0
22R-2, 36-37	197.4	7.5	7.5	0.1	62.1
23R-1, 33-35	205.5	10.9	10.8	0.1	89.5
24R-1, 85-87	215.8	10.2	10.0	0.2	83.4
25R-1, 28-31	224.9	11.3	10.9	0.3	91.1
27R-1, 133-136	245.2	10.7	10.5	0.2	87.6
28R-1, 27-30	253.9	10.0	9.9	0.2	82.1
29R-1, 34-37	263.4	11.0	10.9	0.1	90.6
30R-1, 30-31	273.1		11.2		93.6
30R-1, 90-92	273.7	11.3	9.4	1.9	78.3
31R-1, 23-24	282.6	10.8	10.2	0.6	84.9
31R-2, 15-16	284.0		8.7		72.2
32R-1, 31-36	292.4	10.1	10.1	0.0	84.5
33R-1, 44-46	302.2	11.0	11.0	0.0	92.0
34R-1, 33-34	311.6	9.6	9.6	0.0	80.1
36R-CC, 14-15	330.3	9.4	9.5	0.0	78.7

Table 6 (continued).

Core, section, interval (cm)	Depth (mbsf)	Total carbon (wt%)	Inorganic carbon (wt%)	TOC (wt%)	CaCO ₃ (wt%)
37R-1, 28-31	340.1	10.8	10.8	0.0	89.7
39R-1, 40-43	359.5	9.2	9.2	0.0	76.9
40R-1, 34-37	369.1	9.7	9.7	0.0	80.5
41R-1, 30-33	378.7	9.6	9.5	0.1	79.1
41R-3, 30-33	380.2		9.5		79.3
42R-1, 40-43	388.5	9.2	9.3	0.0	77.1
43R-1, 14-15	397.8		8.2		68.3
43R-1, 14-15	397.8		6.7		56.0
43R-1, 29-30	398.0		5.2		43.3
43R-1, 66-67	398.4		7.8		64.7
43R-1, 103-105	398.7		7.3		60.7
43R-1, 120-123	398.9	2.7	2.7	0.0	22.5
43R-1, 124-125	398.9		1.3		10.9
43R-1, 146-147	399.2		1.7		14.2
43R-1, 147-148	399.2		1.6		13.6
43R-2, 45-46	399.7		3.2		26.6
43R-3, 95-97	401.7		0.2		2.0
44R-1, 35-36	407.8		10.8		90.1
44R-2, 35-36	409.3	9.1	9.1	0.1	75.4
45R-1, 57-60	417.2	4.8	4.7	0.1	39.5
46R-1, 27-30	421.9	10.7	10.8	0.0	89.5
47R-1, 10-13	426.7		11.0		91.9
47R-1, 48-50	427.1		2.5		20.7
47R-1, 93-96	427.5		5.7		47.4
49R-CC, 10-13	446.0		11.3		94.4
50R-1, 20-23	455.8		9.5		78.9
51R-1, 100-103	461.1		3.8		31.7
51R-2, 72-75	462.3		8.3		69.1
51R-3, 0-3	463.1		4.6		38.7
51R-3, 72-75	463.8		3.6		29.7
51R-CC, 13-16	464.1		2.5		20.4
52R-1, 27-30	465.5		9.5		79.2
52R-2, 30-33	467.0		2.8		23.4
53R-1, 40-41	475.2		2.4		19.7
53R-1, 140-141	476.2		2.9		23.9
54R-1, 31-32	484.8		10.4		86.5
55R-1, 38-40	494.5		6.6		54.7
56R-1, 37-40	504.2		1.6		13.5
56R-1, 38-40	504.2		1.8		14.8
56R-3, 28-30	507.1		1.5		12.3
57R-1, 46-48	514.0		2.0		16.6
57R-2, 73-75	515.7	2.3	2.0	0.3	16.6
57R-3, 82-84	517.3		0.8		6.5
58R-1, 24-25	523.4	1.5	0.2	1.3	1.5
58R-1, 137-140	524.6		1.4		12.0
59R-1, 74-77	533.6	0.1	0.1	0.1	0.5
63R-1, 37-40	571.9	1.6	0.1	1.5	0.4
64R-1, 49-50	581.7	0.3	0.1	0.2	0.5
134-829C-					
1H-2, 60-63	2.1		1.1		8.7
1H-4, 60-63	5.1		1.2		10.0
2H-1, 140-143	9.7		1.4		11.8
2H-4, 140-143	14.2		1.3		10.8
2H-6, 140-143	17.2		1.3		10.8
3H-2, 125-128	20.6		1.0		8.7
3H-4, 135-138	23.7		1.3		10.4
3H-6, 140-143	26.7		1.2		10.2
4H-6, 110-113	29.9		2.3		18.9
5H-1, 130-133	31.6		2.2		18.2
5H-3, 120-123	34.5		2.2		18.2
5H-5, 120-123	37.5		1.8		15.1
7H-1, 105-108	48.6		6.4		53.1
8H-1, 135-138	51.4		5.4		45.0
9H-2, 130-133	54.8		7.3		60.6
9H-4, 132-135	57.8		8.6		71.8
9H-4, 76-79	58.8		11.1		92.6
10H-1, 42-45	57.7		6.5		53.8

Note: TOC = total organic carbon.

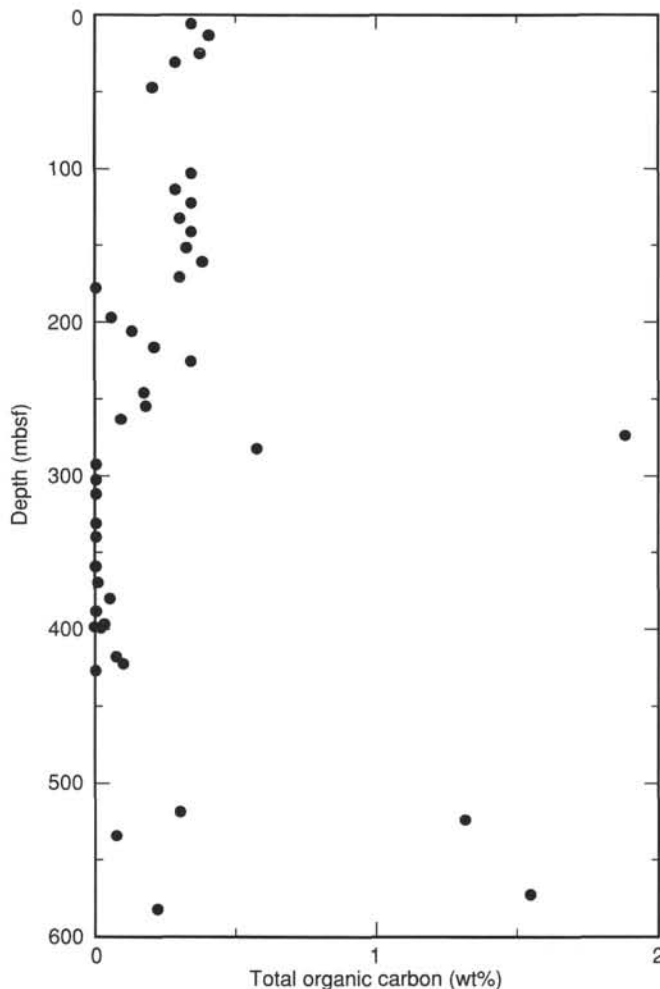


Figure 24. Plot of total organic carbon content vs. depth for sediments at Site 829.

Summary

The principal conclusion from the pore-fluid geochemistry at Site 829 is that the sediments have been rapidly and extensively dewatered, possibly a result of subduction of the NDR. Water contents in the sediments at Site 829 are lower than at either the Barbados or Nankai subduction zones which implies that some dewatering may result from compressional tectonics when positive topographic features impinge upon the margin.

Discontinuities in concentration gradients and in the water content of sediments indicate that the hydrology at Site 829 appears to be largely fault controlled, similar to the Barbados convergent margin. The fault control may result from the fine-grained, and thus probably impermeable, nature of the sediments at Site 829. Initial concentration gradients also suggest that 25 to 50 m of seafloor may have recently been removed, possibly by slumping. A flux of fluid across the sediment-water interface could alter the physical properties of the shallow sediment, making slumping more likely.

STRUCTURAL STUDIES

Several horizons of intense brittle and ductile deformation have been encountered in cores at Site 829. A summary of all structural data observed in Hole 829A is given in Figure 29; little structural information was obtained from Holes 829B and

829C. A plot of the rate of penetration of Hole 829A is included in Figure 29 to show the correlations between the depth of thrust planes and distinctive changes in drilling rate.

Attitudes of bedding planes downhole are poorly defined because many of the units lack distinct bedding planes. Bedding surfaces, where measurable, generally dip 30° to 60°. However, horizontal and nearly vertical bedding planes also occur.

Hole 829A is subdivided into eight tectonic units (A through H). This subdivision is based on structural, paleontological, and lithological observations. Repetition of the stratigraphic sequence defines five of these tectonic units; lithologic changes and degree of deformation define the rest.

Description of the Tectonic Units and Structural Features

Tectonic Unit A

This unit ranges from 0 to 99.4 mbsf (Cores 134-829A-1R through -11R and interval 134-829A-12R-1, 0–40 cm) and consists of structureless Pleistocene volcanic clayey silt (lithostratigraphic Unit I) underlain by upper Oligocene to lowermost Miocene foraminiferal chalk (lithostratigraphic Unit II). Despite significant disturbance by drilling, a few fault planes with polished surfaces were observed in the uppermost deformation zone of Hole 829A (Core 134-829A-10R). The base of this unit (99.4 mbsf, Section 134-829A-12R-1, 40 cm) is marked by a sharp contact along which pale brown upper Oligocene to lowermost Miocene chinks (lithostratigraphic Unit II) overlie the dark greenish gray Pleistocene volcanic silt (lithostratigraphic Unit III). A 1-cm-thick lens of light gray chalk underlies this contact. Paleontological and lithological evidence indicates that this contact must be a thrust plane, because the stratigraphy is inverted whereas there is no evidence for overturned beds, but the overthrust is not explicitly marked by strong tectonic deformation. Above the contact within the chinks, several fault planes dipping 30° to 50° and cutting across the bedding plane (dipping 10°–17°) can be interpreted as reverse faults. Below the contact a small-scale microshear fold also indicates a reverse sense of movement. Most of the deformation may have occurred in a shear zone above the top of Core 134-829A-12R. Poor (1.2%) recovery in Core 134-829A-11R directly above the contact hampered our ability to define the contact, but brown clay lies above the contact from 0–10 cm in Section 134-829A-12R-1. Similar layers of clay have been found downhole where inverted lithostratigraphic sections are observed together with overthrust planes and are clearly documented by structural evidence.

Tectonic Unit B

This unit includes the first repetition of Pleistocene volcanic silt and siltstone (lithostratigraphic Unit III). It ranges from 99.4 to 172 mbsf (from Section 134-829A-12R-1, 40 cm, to Section 134-829A-19R-4, 155 cm) and is about 10 m thicker than the Pleistocene volcanic silt of tectonic Unit A (lithostratigraphic Unit I). Down to 172 mbsf, faults of various dips are the only indicators of brittle deformation in Cores 134-829A-15R through -18R. The sense of faulting could not be obtained. A steeply dipping (82°), probably reverse, fault occurs from 80 to 105 cm in Section 134-829A-17R-5. Two horizons of disrupted strata 30 cm and 10 cm in thickness, respectively, are visible in Section 134-829A-18R-5, from 0 to 30 cm and from 50 to 60 cm. In Section 134-829A-14R-5, 32 cm, and in Section 134-829A-15R-1, 82 cm, pebbles of white chalk were found within the volcanic silt. The base of tectonic Unit B is not defined by a stratigraphic inversion but is marked

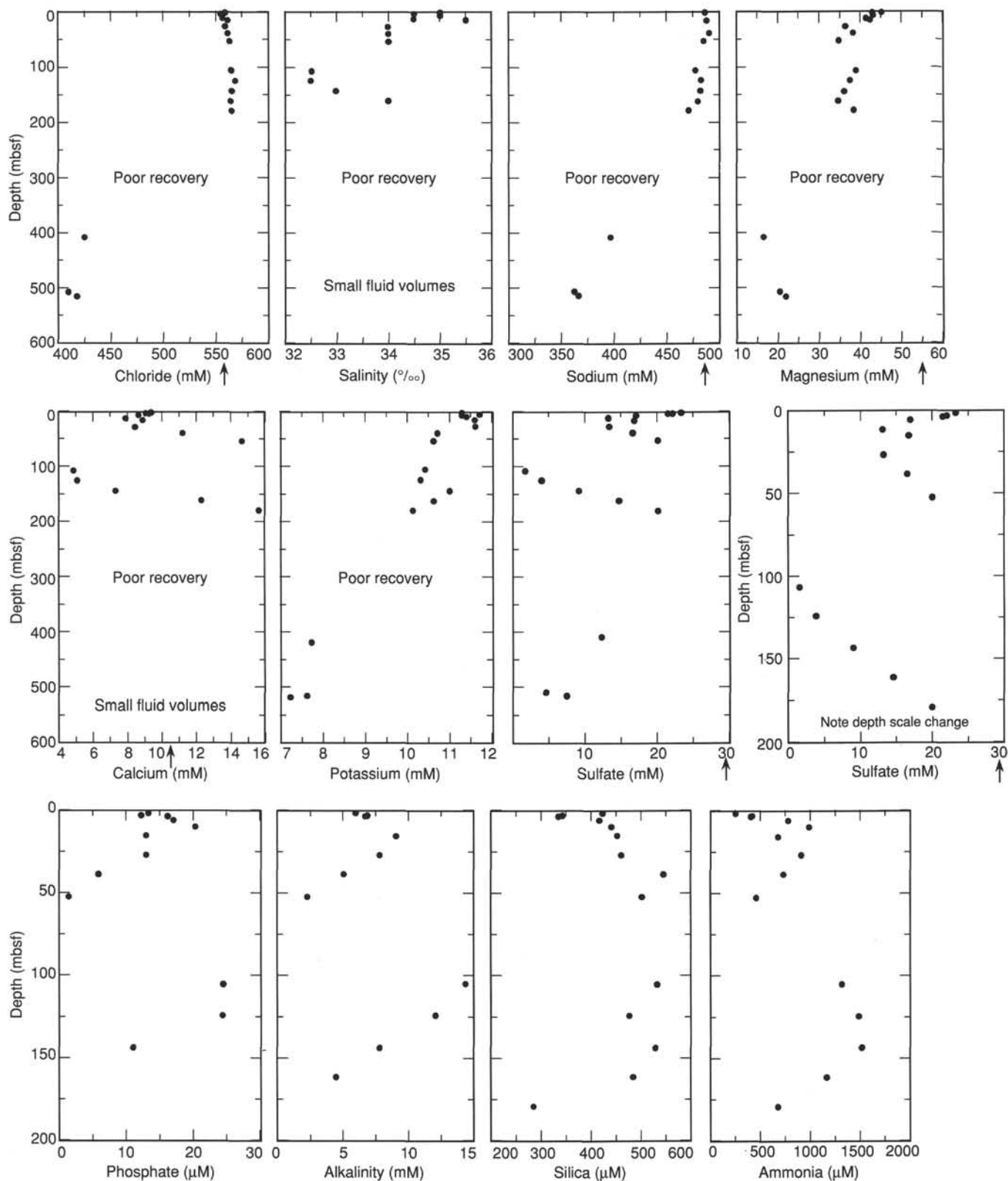


Figure 25. Pore-fluid gradients, Site 829. The arrows indicate seawater concentrations. No samples were measured between 200 and 400 mbsf because of low core recovery. Some solute concentrations in the samples from below 400 mbsf were not measured because of the limited sample size at that depth. The ammonia, phosphate, alkalinity, and silica concentrations are plotted only to 200 mbsf because no measurements were made below this depth. Sulfate is plotted at both scales.

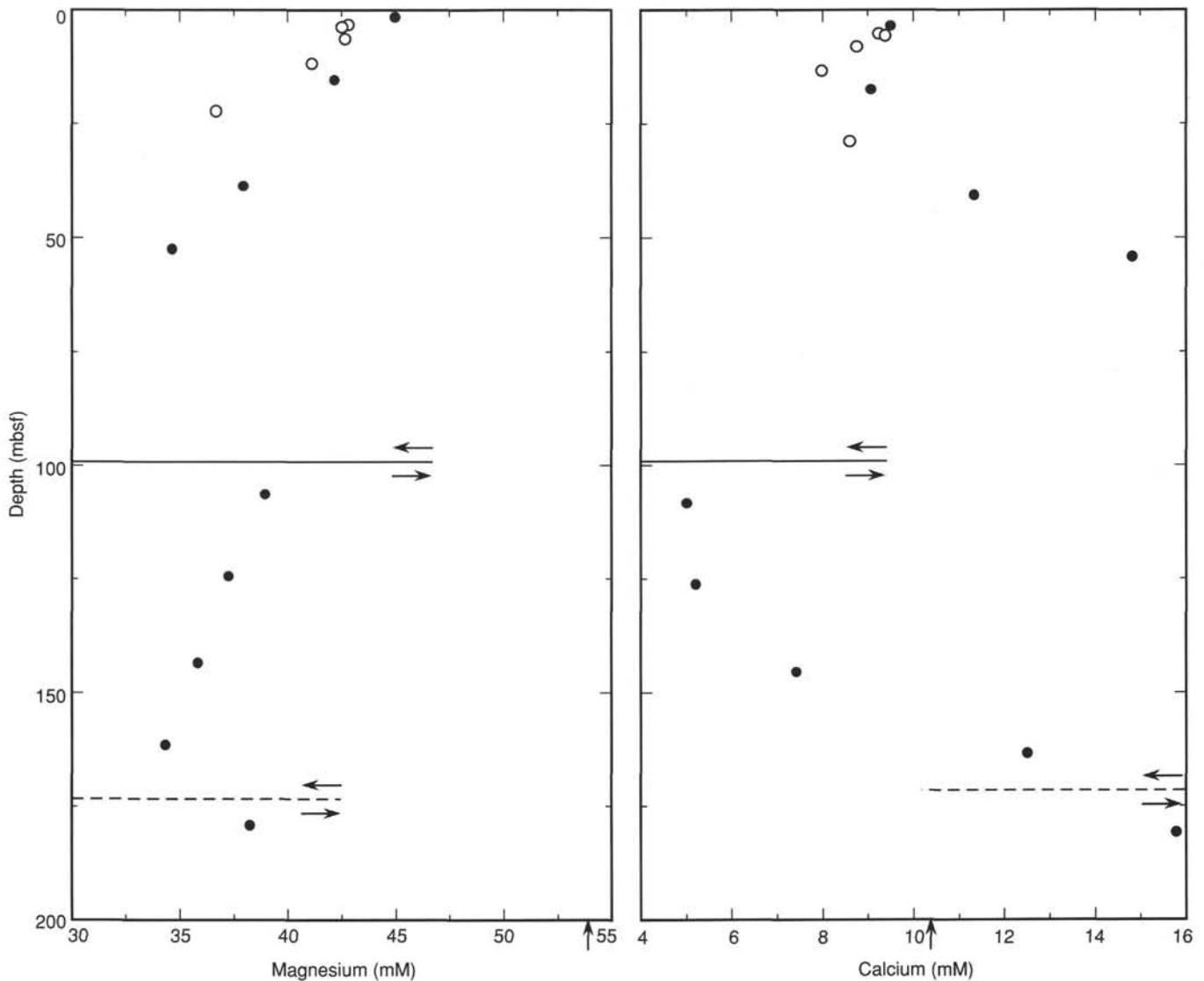


Figure 26. Magnesium and calcium concentrations from the upper 200 mbsf plotted against depth. Solid circles = Hole 829A; open circles = Holes 829B and 829C. The heavy line indicates the location of a major thrust fault and the dashed line indicates the location of an inferred minor thrust fault. The vertical arrows represent seawater concentrations.

by a lithologic change from Pleistocene volcanic silt to a sed-lithic breccia, which appears to be much more deformed than the overlying volcanic silt.

Tectonic Unit C

This unit ranges from 172 to 311 mbsf (Section 134-829A-19R-4, 115 cm, to the bottom of Core 134-829A-33R) and consists of a sed-lithic breccia with light gray matrix and clasts of chalk and volcanic siltstone (lithostratigraphic Units IV and V); the abundance of volcanic siltstone decreases downhole. The age of the breccia is late Pliocene to Pleistocene. Re-worked fossils of latest Oligocene to earliest Miocene age are also found (see "Biostratigraphy" section, this chapter).

Deformation is much greater in tectonic Unit C than in the overlying units. Near the top of tectonic Unit C (Sections 134-829A-19R-4 through 134-829A-21R-2) are numerous ductile microshear folds (Figs. 30 and 31) and shear-band structures (Fig. 32 and 33). Those structures that show evidence of movement are steeply dipping (50° – 80°) reverse thrust planes or shear zones (Fig. 32 and 33). Based on these faults and

shear zones, we suspect the presence of a major thrust plane within this zone between 172 and 189 mbsf. Below 189 mbsf the most obvious structures are faults and scaly fabric. In Section 134-829A-23R-1, a set of normal faults cuts a sand dike within the sed-lithic breccia (Fig. 34). A distinctive ductile shear zone 25 cm thick occurs at 244 mbsf (interval 134-829A-27R-1, 10–35 cm), and highly brecciated rocks resulting from brittle deformation were encountered in Core 134-829A-28R, from 253.6 to 254.9 mbsf. On the basis of these latter structural observations, we suggest that the deformed zone around 245–260 mbsf represents a second important thrust zone within tectonic Unit C, although we could not determine the sense of movement in the zone.

Tectonic Unit D

This unit ranges from 311 to 405 mbsf (Core 134-829A-34R to Section 134-829A-43R-3) and consists mainly of upper Oligocene chalk (lithostratigraphic Unit VI and upper part of VII). The rocks are characterized by a high degree of brecciation, probably from brittle deformation. Several polished

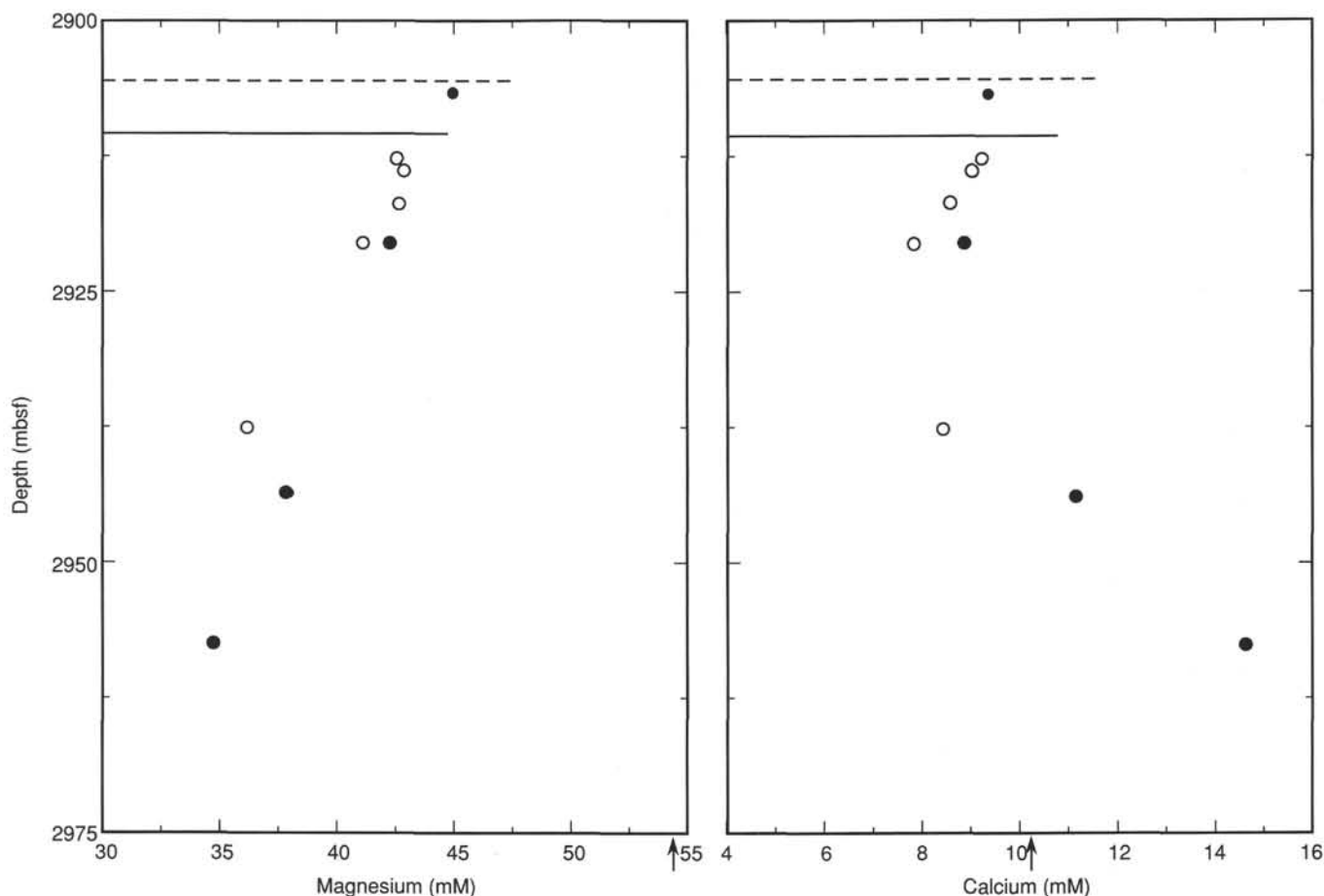


Figure 27. Magnesium and calcium concentrations from the upper 50 mbsf plotted against the depth below sea surface, or sea level (mbsl). Solid circles = Hole 829A; open circles = Holes 829B and 829C. The dashed line represents the location of the seafloor at Hole 829A and the dotted line represents the approximate location of the seafloor at Holes 829B and 829C. The arrows represent seawater concentrations.

surfaces with slickensides are present in most of the interval between Cores 134-829A-34R and -42R. The brecciation probably explains the poor recovery obtained in this part of Hole 829A.

In Core 134-829A-43R, at the base of this tectonic unit, the deformation regime changes from a brittle to a more ductile style. From 397.9 to 400.0 mbsf (from Section 134-829A-43R-1, 10 cm, to Section 134-829A-43R-2, 80 cm), we observed shear bands and microshear folds exhibiting a reverse sense of movement within a well-defined shear zone (Fig. 35). This 2-m-thick shear zone has a planar fabric that dips at an angle of 20° to 40° . A strong increase in clay content corresponds to the part of the zone in which planar fabric is best developed, perhaps the result of grain-size reduction produced by shearing. Igneous clasts occur for the first time in Hole 829A in a breccia at the base of tectonic Unit D (lithostratigraphic Unit VII). The structural features, distinct changes in lithology, and stratigraphic inversion in Core 134-829A-43R indicate a major zone of overthrusting.

Tectonic Unit E

This unit ranges from 405 to 463 mbsf (Sections 134-829A-43R-3 through 134-829A-51R-3). The unit has been subjected to intense brittle deformation; in its upper part (Cores 134-829A-44R through -47R) several faults with polished surfaces

and slickensides are present and in its lower part (Cores 134-829A-48R through -50R), scaly fabric that increases downhole.

Except for several pieces of lower Pliocene pale brown foraminiferal chalk recovered in the uppermost 30 cm, the main part of tectonic Unit E is subdivided into two similar tectonic subunits (E_1 and E_2), which both contain a sequence of dark gray Pleistocene silty chalk overlying pale brown upper Oligocene chalk. Tectonic Subunits E_1 and E_2 are separated by a shear zone in the interval 134-829A-47R-1, 45–60 cm, where Oligocene chinks overlie the Pleistocene sediments (lithostratigraphic Units X and XI). The shear zone between the two subunits dips about 20° and is mainly composed of yellow-brown clay. This zone is interpreted as a thrust plane; however, its thickness (15 cm) is much less than that of the other shear zones described above and below, which mark the top and base of tectonic Unit E.

Shear Zone at the Base of Tectonic Unit E

At the base of tectonic Unit E (460.1 to 463.0 mbsf) a well-preserved 3.1-m-thick shear zone was recovered (Section 134-829A-51R-1 to -51R-3, 10 cm) that is one of the major thrusts encountered at Site 829. The zone consists mainly of calcareous sandy siltstone with several distinct layers of clay and is identified by structural indications and a stratigraphic inversion.

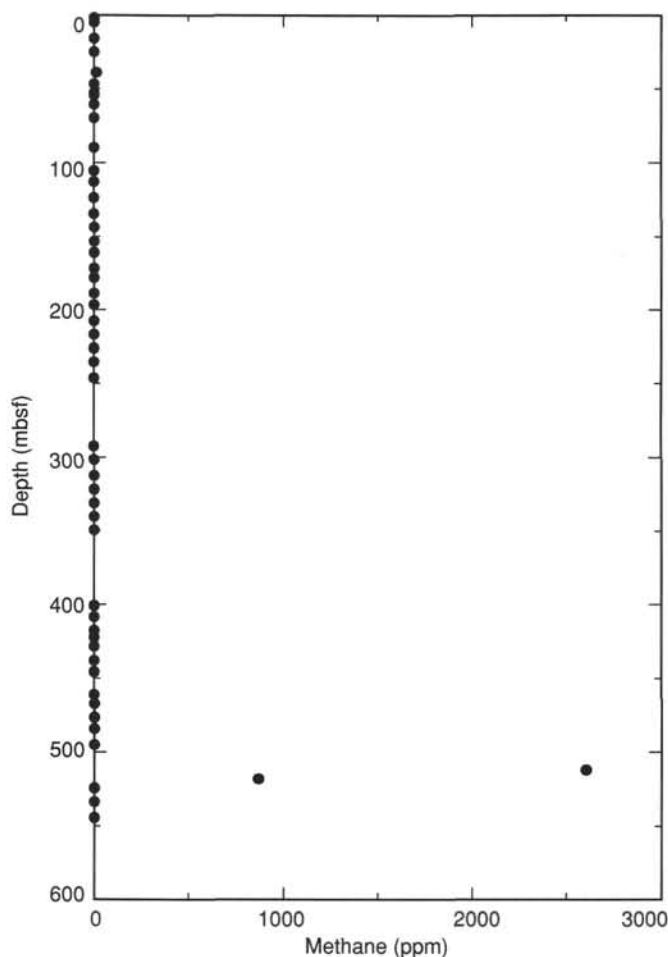


Figure 28. The concentration of methane in the headspace analyses plotted vs. depth below seafloor.

The shear zone can be subdivided into four parts (see Fig. 36):

1. The uppermost part (interval 134-829A-51R-1, 5–117 cm) shows a well-developed planar fabric dipping 20° to 30° east-northeast after paleomagnetic correction (see “Paleomagnetism” section, this chapter). Kinematic indicators including shear bands and rotated sigma clasts display a reverse sense of movement (Fig. 37).

2. The second part (interval 134-829A-51R-2, 0–55 cm) consists of the same material as the uppermost part, but the dip of the planar fabric changes downhole to 40° – 80° west-northwest after paleomagnetic correction without an interruption in the stratigraphic sequence. The kinematic indicators in this part of the shear zone including a microshear fold structure (interval 134-829A-51R-2, 46–57 cm; Fig. 37) show a normal sense of movement. However, the foliated rocks of the ductile shear zone are broken into several pieces and, therefore, have been deformed by a later brittle deformational event.

3. The third part of this shear zone is marked by a zone of intense brecciation (interval 134-829A-51R-2, 55–106 cm), which also indicates a later stage of tectonic deformation.

4. The lowermost part of the shear zone is similar to the uppermost one (Section 134-829A-51R-2, 106 cm, to Section 134-829A-51R-3, 10 cm); the planar fabric similarly dips 30° – 40° east after paleomagnetic correction and shows again a

reverse sense of movement (Fig. 38). Below the shear zone of tectonic Unit E the foliation parallels the bedding plane of the Pleistocene volcanic siltstone, dipping 30° – 40° north-northeast after paleomagnetic correction (interval 134-829A-51R-3, 10–60 cm).

Tectonic Unit F

This unit ranges from 463.0 to 494.4 mbsf and comprises a sequence of black Pleistocene volcanic sandstone underlain by upper Oligocene chalks (Sections 134-829A-52R-3, 10 cm, to 134-829A-55R-1, 30 cm; lithostratigraphic Units XIII and XIV). The volcanic sandstone is well stratified and inclined at an angle of 20° to 30° . At the top of this unit, directly below the major thrust zone of tectonic Unit E, the sandstone is strongly deformed and foliation planes appear to be parallel to bedding planes. This sandstone contains pebbles of white chalk, the largest occurring in Section 134-829A-52R-1, 82–98 cm. The sequence of chalks below the sandstone is highly brecciated and shows polished surfaces and slickensides (Core 134-829A-54R and interval 134-829A-55R-1, 0–30 cm). Within these chalks, a thrust plane separating the highly fractured rocks of this unit from less-deformed rocks of the unit below is postulated on the basis of another stratigraphic inversion.

Tectonic Unit G

This unit ranges from 494.4 to 524.6 mbsf (Sections 134-829A-55R-1, 30 cm, to 134-829A-58R-1, 140 cm) and is composed of black Pleistocene volcanic siltstone with a minor component of sed-lithic breccia (lithostratigraphic Unit XV and the upper part of Unit XVI). All cores in this tectonic unit contain several fractures. In addition, a few small-scale microshear folds are found in the breccia. However, a recumbent microfold, which occurs in Section 134-829A-56R-2, 105 cm, may result from a synsedimentary process because the abundant foraminifers in this layer are well preserved and undeformed.

A 3-m-thick shear zone marks the base of Unit G (Sections 134-829A-57R-3, 65 cm, to 134-829A-58R-1, 140 cm). This zone is composed of several horizons of intense deformation indicated by layers of brown clay (Fig. 39; see also Fig. 13, “Lithostratigraphy” section, this chapter). The primary rocks appear to comprise a breccia that contains clasts of mafic intrusive and volcanic rocks (see “Igneous Petrology” section, this chapter). The planar fabric in this shear zone, which is mainly subhorizontal, ranges in dip from 0° to 30° . This shear zone is considered a major overthrust.

Tectonic Unit H

This unit ranges from 524.6 mbsf to the base of Hole 829A at 590.6 mbsf (Section 134-829A-58R-1, 140 cm to the base of Core 134-829A-64R), and is composed of a sed-lithic breccia with fragments of gabbro and basalt (lithostratigraphic Unit XVI; see “Igneous Petrology” section, this chapter). The age of the breccia is unknown. Poor recovery prevented documentation of the structure of the unit, and no kinematic indicators were observed. At the base of Hole 829A in Cores 134-829A-63R and -64R are horizons in which planar fabric dips from 0° to 30° . However, it is not clear whether this planar fabric is a bedding plane or results from shearing.

Discussion and Interpretation

Structural observations of the cores from Hole 829A indicate that the rocks have been subjected to intense deformation. Numerous thrusts are documented by shear zones with a reverse sense of motion. Some of these shear zones are at least 3 m thick. The presence of most of these thrusts is indicated by repetitions of stratigraphic sequences. Pleis-

ocene sequences were penetrated at six different levels, five of them immediately underlying rocks of Oligocene age. A synthetic structural column of Hole 829A is shown in Figure 40. The type of deformation observed is typical of an accretionary wedge and the thrust planes are probably a consequence of the subduction of the NDR. However, the intensity of deformation, the thickness of shear zones, and the large number of thrust planes indicate that deformation at the front of an aseismic ridge may be more intense than in other accretionary wedges where an oceanic plate without substantial positive relief is being subducted (e.g., Barbados accretionary wedge drilled during Leg 110, Mascle, Moore, et al., 1988; Nankai accretionary wedge drilled during Leg 131; Taira, Hill, Firth, et al., 1991).

The orientations (see "Paleomagnetism" section, this chapter) of the parts of the shear zone at the base of tectonic Unit E (Fig. 36) indicate that (1) the thrust zone is dipping northeast (the true dip directions of the planar fabric of parts 1, 4, and the uppermost part of tectonic Unit F, where reverse motions have been observed, are east-northeast, east, and north-northeast, respectively); and (2) the variation in the direction of the dip of the planar fabric observed between part 1 and 2 of the shear zone results from tectonic deformation and not from drilling disturbance (the dip direction of the foliation of part 2 of the shear zone, where the apparent sense of motion is normal, is west-northwest).

The tectonic features observed in this shear zone are interpreted as the result of a two-stage deformation. The first stage formed planar fabric from a ductile shearing process. The second stage deformed the already existing planar fabric and formed structures with an apparent normal sense of movement within part 2 of the shear zone.

The northeast dip direction of the shear zone in Core 134-829A-51R (base of tectonic Unit E) agrees well with the geometry of the subduction zone (Fig. 41). Taking into account the eastward subduction of the NDR below the New Hebrides Island Arc and the shape of the NDR at the same latitude as Site 829, the décollement should be horizontal or have a northeast dip in this area. The dip angle of the shear zones decreases downhole from 50°–80° at 180 mbsf to 0°–30° at the bottom of Hole 829A (Fig. 40). This can be explained by the imbrication of several thrust sheets at the base of the accretionary wedge, if we consider that all thrust zones in the wedge dip in the same direction.

The style of deformation varies from brittle to ductile. Brittle deformation is characterized by faults and scaly fabric. The ductile behavior constitutes discrete shear zones with high contents of clay and several microshear folds. The plasticity of the shear zones is caused mainly by clay, which is the matrix for several clasts of different sizes and lithology. On a macroscopic scale, no deformation affected the clasts. However, the clasts rotated during shearing, which curved the foliation slightly around the grains (Fig. 38). These features, which resemble asymmetric recrystallization tails described from mylonitic and metamorphic rocks, are classified as asymmetric sigma clasts (Passchier and Simpson, 1986; Ramsay and Huber, 1987).

The lithostratigraphic Units of Hole 829A are further divided into four composite units (see "Lithostratigraphy" section, this chapter): upper Pliocene to Pleistocene sedimentary breccia (Bigwan Wan), Pleistocene volcanic silt-siltstone (Bigwan Tu), upper Oligocene to lowermost Miocene foraminiferal chalks (Bigwan Tri), and a breccia of unknown age that contains igneous clasts (Bigwan Fo). Moreover, lower Pliocene chalk has been found at the top of tectonic Unit E of Site 829. Lithologic sequences recovered from Hole 829A are similar to those encountered at Site 828 on the

northern flank of NDR (Fig. 36). The sequence in Hole 828A is composed of 60 m of Pleistocene to upper Pliocene volcanic siltstones, 10 m of lower Pliocene or upper Miocene foraminiferal oozes, 20 m of lower to upper Oligocene nannofossil chalks, and a volcanic breccia. The thicknesses of the volcanic siltstones and the nannofossil chalks at Site 828 are equivalent with those encountered in tectonic Unit A (60 m and 40 m, respectively) at Site 829. Although the age of the Oligocene chalks at Site 828 and Site 829 differs slightly, the successive tectonic units penetrated at Site 829 may result from accretion of the sedimentary rocks that cover the basement rocks of the NDR. This interpretation is supported by the fact that the upper Oligocene(?) to lower Miocene sequence on the western belt of the New Hebrides Island Arc is marked by an important volcanic eruption (Malakula and Espiritu Santo islands; Carney et al., 1985). Tectonic Unit D of Site 829, which comprises about 90 m of highly fractured Oligocene chalk, was probably thickened by thrust faulting.

The breccia of tectonic Unit C (172–311 mbsf), a primary sedimentary breccia later tectonized, is interpreted as a tectono-sedimentary melange formed in front of the accretionary complex and fed by erosion of previously accreted thrust sheets, and then deformed and emplaced within the accretionary wedge. This sedimentary breccia was probably deposited no earlier than the Pleistocene because it contains several reworked clasts of volcanic silt/siltstone that are similar in facies to Pleistocene siltstones.

The amount of reworked Oligocene chalk clasts within the repeated sequences of Pleistocene volcanic siltstones increases downhole. The first appearance of clasts of chalk within the Pleistocene sequences is in tectonic Unit B (124 mbsf). Clasts of chalks are more abundant in the Pleistocene sequence of Unit F (465 mbsf) and in the top of the Pleistocene sequence of Unit G (505 mbsf). The increase of chalky clasts downhole within the Pleistocene siltstone may suggest that levels of Oligocene chalks cropping out along the slope were more and more exposed during time. This can be explained by steepening of the arc slope and by the emplacement of successive slices that include Oligocene chalks.

Clasts of gabbros and basalts encountered at the base of a major thrust at 400 mbsf and then in a breccia at the base of Hole 829A from 518 to 590 mbsf may be derived either from volcanic arc rocks exposed on the neighboring Espiritu Santo Island or from the NDR. Petrological and geochemical analyses of these clasts and a comparison with both the igneous fragments recovered at the base of Hole 828A and the arc series exposed on Espiritu Santo Island are vital in addressing this problem.

PALEOMAGNETISM

Three holes were drilled at Site 829. Hole 829A was RCB-drilled to a depth of 590.3 mbsf. Holes 829B and 829C were drilled to recover oriented APC cores from the upper part of the sequence (see "Operations" section, this chapter). Results from the APC cores will be discussed first, after which results from the RCB cores of Hole 829A will be discussed.

Holes 829B and 829C

All APC archive halves from Holes 829B and 829C were measured in the cryogenic magnetometer. All cores recovered from Hole 829B were disturbed by drilling, as was Core 134-829C-9H. Thus, results from the upper part of Hole 829C are the most useful for paleomagnetic analyses (Fig. 42).

Fifty-four discrete samples have been alternating-field (AF)-demagnetized up to 40 mT. Most of the demagnetization

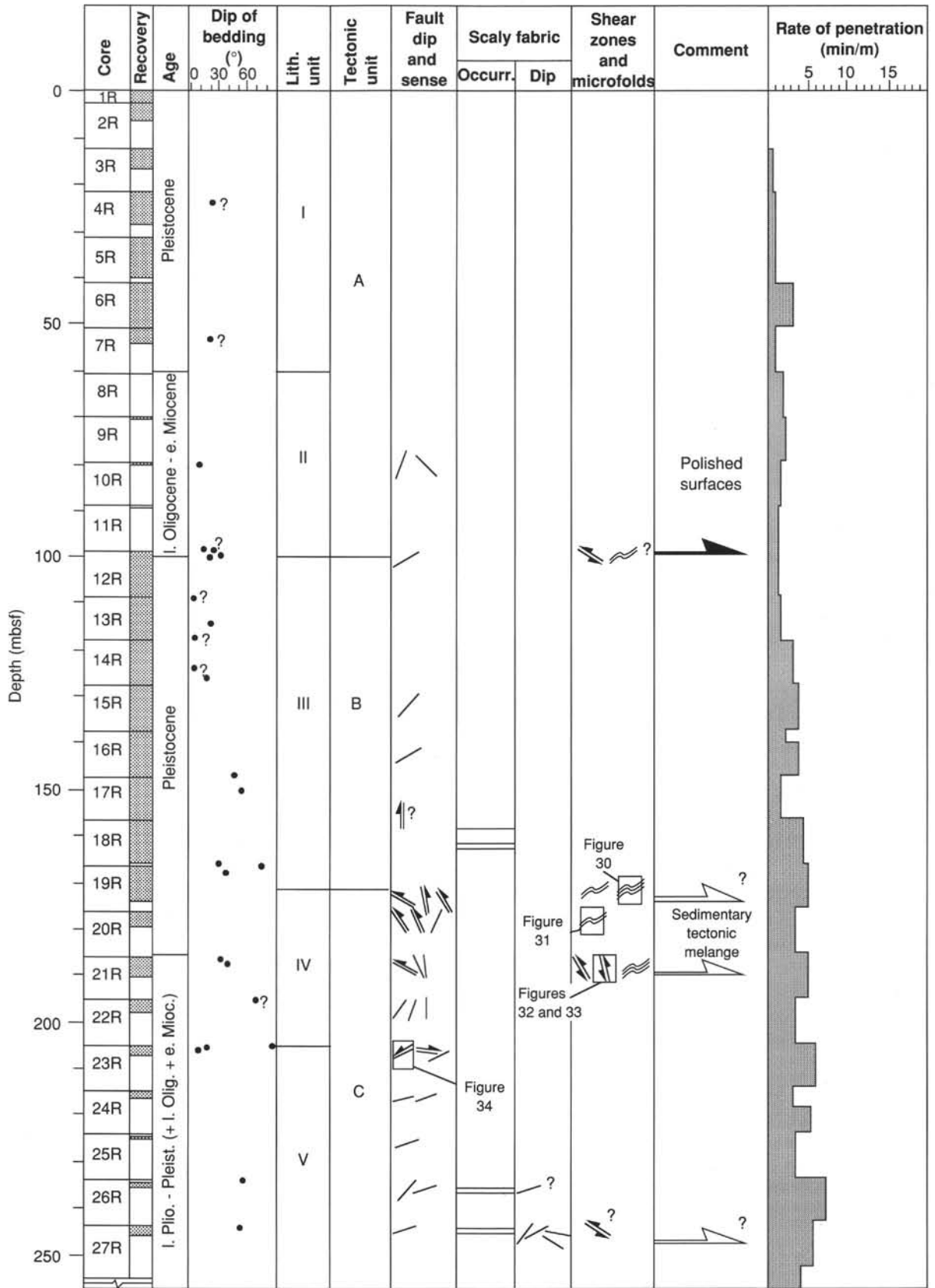


Figure 29. Structural data from Hole 829A. A legend for the symbols used to represent structural data is provided in the "Structural Studies" section, "Explanatory Notes" chapter (this volume).

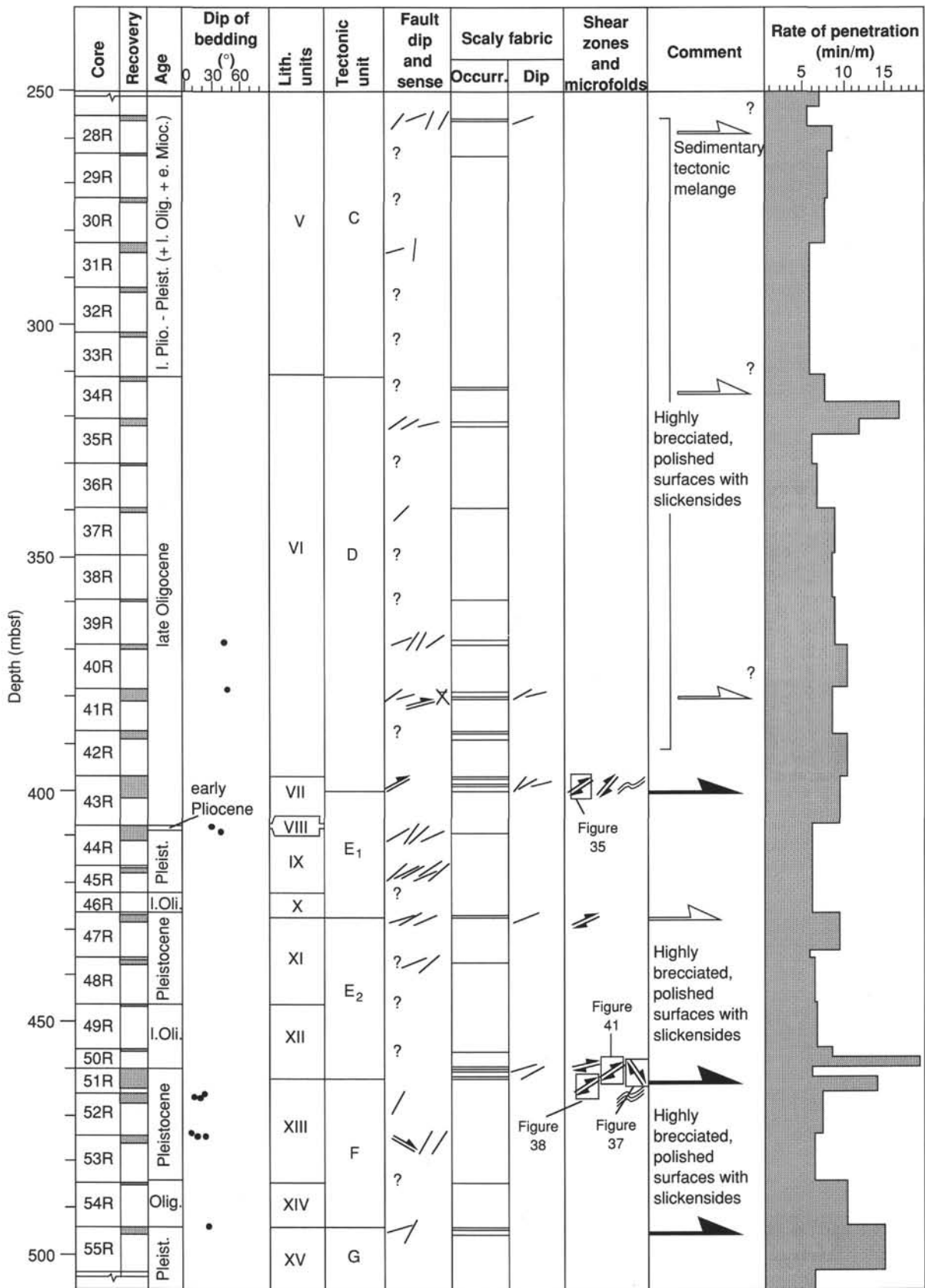


Figure 29 (continued).

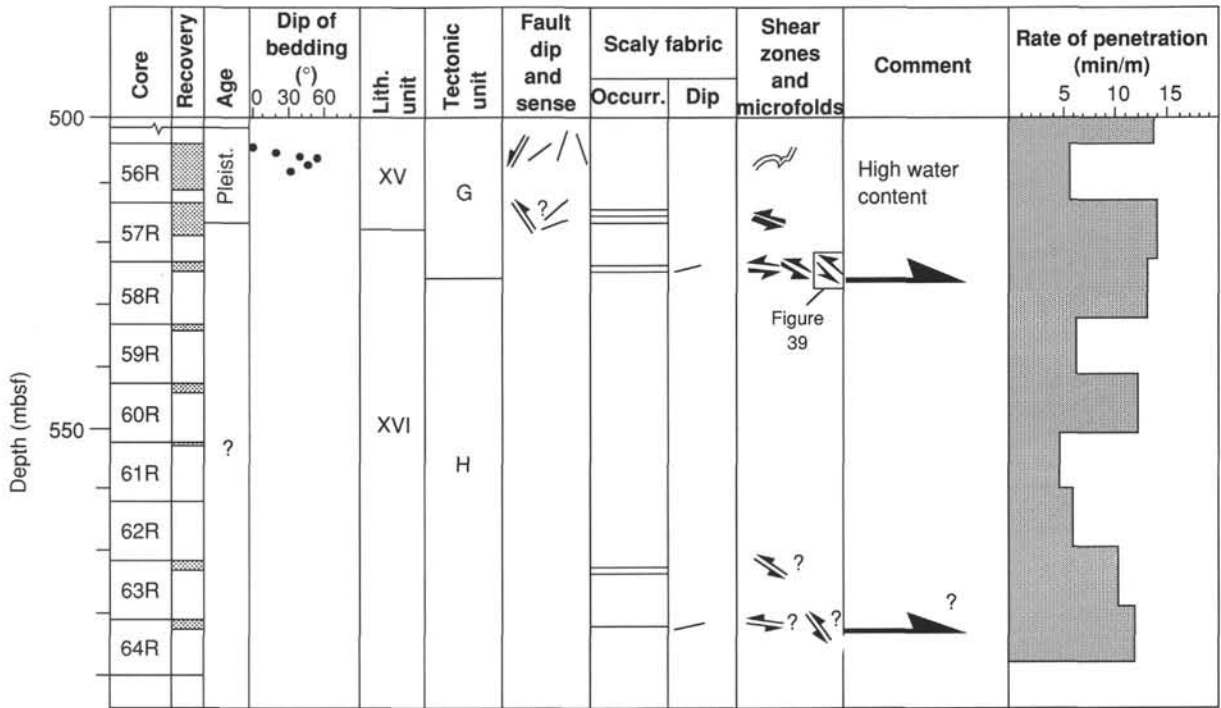


Figure 29 (continued).

paths correspond to great circles (Fig. 43) diverging from an initially steeply inclined, upward magnetization. All samples have median destructive fields (MDF) lower than 10 mT (Fig. 44) and it was not always possible to remove the secondary overprint induced by drilling (Fig. 45). The large deviations from the expected normal direction (declination = 0°; inclination = 29°) observed in data from oriented cores at Hole 829C may also result from an incomplete removal of the secondary overprint. For example, in Core 134-829C-5H, from 33.5 to 37.5 mbsf, the inclination is very steep and the declination is at about 80° from the expected geographic north. We observed no evidence for reversed polarities in lithostratigraphic Unit XVII (0–19.5 mbsf) from Hole 829B (see “Lithostratigraphy” section, this chapter, for a description of the units). Thus, in conjunction with the biostratigraphic data, we can assign this unit to the Brunhes Chron.

Hole 829A

Core recovery was sporadic in Hole 829A, although recovery was good in the unconsolidated Pleistocene sediments of Cores 134-829A-1R to -7R (1–60.5 mbsf) and Cores 134-829A-12R to -19R (99.0–176.1 mbsf). In addition, most cores were disturbed by drilling; thus, measurements by the cryogenic magnetometer were not reliable.

Most results from the 51 discrete samples that have been AF-demagnetized indicate a magnetic remanence whose inclination is negative (Fig. 45). Incomplete removal of drilling-induced remagnetization or a recent overprint acquired in the present-day field may explain this behavior.

Thermal demagnetization was performed on three samples of lithified siltstone from Core 134-829B-56R (503.8–513.5 mbsf) (Fig. 46) in order to test the stability of the magnetization vs. temperature. A secondary magnetic component is removed at low temperature (200°C) and a component of magnetization with higher unblocking temperatures can be identified. Unfortunately, despite the apparent sta-

bility of the magnetization of these samples, the lack of information about orientation and attitude of the bedding plane precludes a more detailed interpretation of the paleomagnetic data.

Core 134-829A-51R (460.1–465.2 mbsf) was the least disturbed of the cores recovered from Hole 829A and contains a shear zone with well-developed foliation (see “Structural Studies” section, this chapter). The natural remanent magnetization (NRM) and the remanent magnetization after AF demagnetization at 5, 10, and 15 mT were measured using the cryogenic magnetometer (Fig. 47). Intensity decreases after AF demagnetization, but the directional behavior is relatively stable. The lithology of Section 134-829A-51R-1 is homogeneous (see “Lithostratigraphy” section, this chapter); the paleomagnetic results are also homogeneous and have a mean declination of about 210°. From 463.2 to 463.9 mbsf, the lithology changes from pale brown chalk to calcareous volcanic sandstone, although the foliation appears to be the same (see “Structural Studies” section, this chapter). The paleomagnetic declination measured in Section 134-829A-51R-3 is about 45° (Fig. 47). However, the orientation of the foliation planes in Sections 134-829A-51R-1 and -51R-3 suggest that Section 134-829A-51R-3 was rotated about 180° in the plastic liner with respect to Section 134-829A-51R-1. By rotating Section 134-829A-51R-3 so that the attitude of the foliation plane is the same as that in Section 134-829A-51R-1, the declinations observed in both sections become similar. Results of AF demagnetization of discrete samples from Core 134-829A-51R agree with those obtained using the cryogenic magnetometer. These results suggest that the magnetization recorded in Core 134-829A-51R is homogeneous and was not produced during drilling. Because the inclination is similar to that of the present-day field, we may speculate that the recorded magnetization is either a viscous magnetization or was recently acquired during tectonic deformation. We oriented Core 134-829A-51R based on the assumption that this

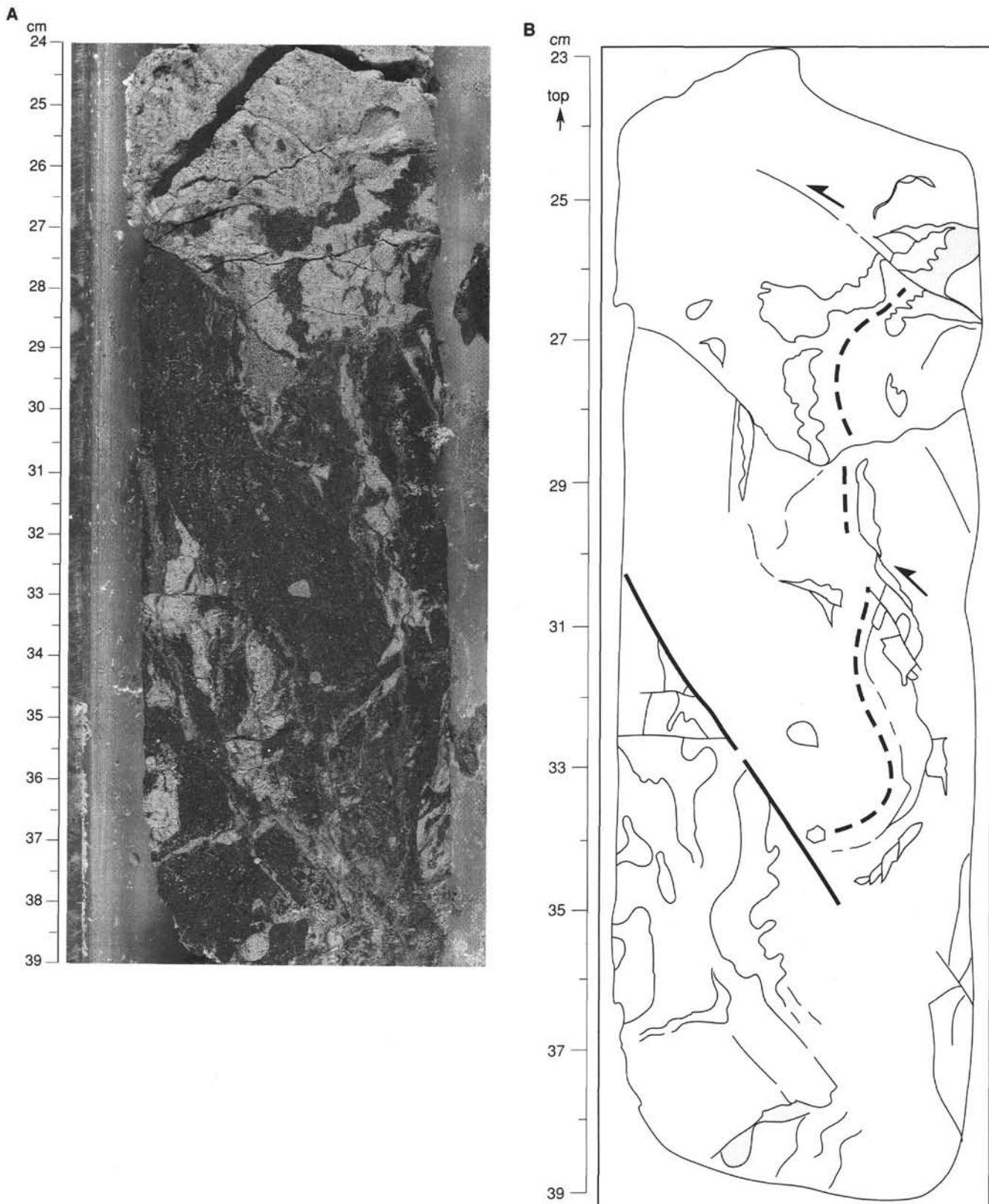


Figure 30. Photograph (A) and sketch (B) of microshear fold and fracture in the breccia of tectonic Unit C in interval 134-829A-20R-1, 24–39 cm. White pebbles are chalk and black pebbles are volcanic silt and siltstone. The location is indicated in Figure 29.

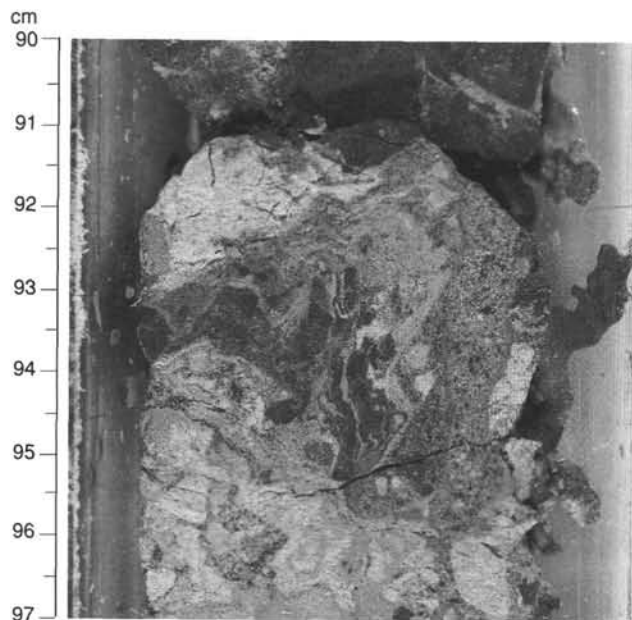


Figure 31. Photograph of a microfold in breccia of Unit C (interval 134-829A-20R-1, 90–97 cm). The location is indicated in Figure 29.

magnetization represents the direction of the actual geomagnetic field. After orientation, the attitude of the foliation plane is toward the northeast, which correlates well with the present tectonic setting (see “Structural Studies” section, this chapter). This hypothesis may be tested by using images from the FMS or BHTV to reorient the core.

Magnetic Susceptibility

Magnetic susceptibility was measured on all cores at Site 829. In addition, magnetic susceptibility logs were obtained from 50 to 425 mbsf.

Lithostratigraphic Unit I (0–60.5 mbsf; see “Lithostratigraphy” section, this chapter, and Figs. 48 and 49) consists of a volcanic siltstone whose magnetic susceptibility is high ($1.0\text{--}2.5 \times 10^{-2}$ SI), similar to that observed at Sites 827 and 828. Core recovery was too low in the foraminiferal chalk of Unit II (60.5–99.4 mbsf) to measure the susceptibility of the cores reliably; however, logging data indicate no high-susceptibility material in this interval (Fig. 49). The susceptibility of the volcanic silt in lithostratigraphic Unit III (99.4–171.9 mbsf) ranges from 1.0 to 2.5×10^{-2} SI. Data from susceptibility logs show a sharp contact between Unit II and Unit III which is interpreted as a thrust fault (see “Structural Studies” section, this chapter). Logging data show a poorly defined contact, however, between Units III and IV, a siltstone-chalk breccia that extends from 171.9 to 205.2 mbsf. A susceptibility maximum ($<2.0 \times 10^{-2}$ SI) at about 180 mbsf suggests that a layer of volcanic siltstone may be present near the top of Unit IV. Core recovery was poor from 180 to 590.3 mbsf, the bottom of Hole 829A. The susceptibility of all cores recovered from Units V (chalk breccia, 205.2–311.3 mbsf) and VI (calcareous chalk, 311.3–398.9 mbsf) was low ($<1.0 \times 10^{-2}$ SI); logging detected no high-susceptibility intervals (Fig. 49). Two susceptibility maxima are observed between 400 and 425 mbsf (Fig. 49), implying the presence of high-susceptibility material in the volcanic breccia of Unit VII (398.9–407.4 mbsf) as well as in the chinks of Units VIII–X (407.4–427.3 mbsf). Several susceptibility maxima are observed below 450 mbsf, some of

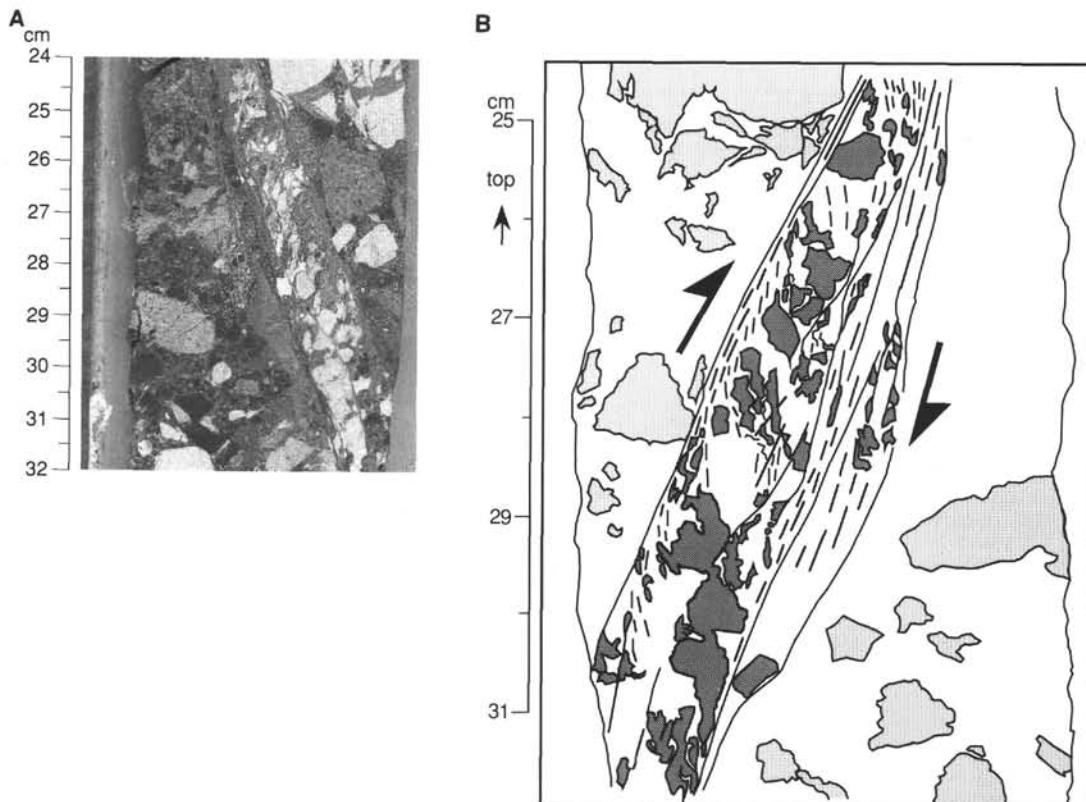


Figure 32. Photograph (A) and sketch (B) of a steeply dipping reverse shear zone in the breccia of tectonic Unit C (interval 134-829A-21R-2, 24–32 cm). The photograph is of the archive half of the core; the sketch represents the working half. The location is indicated in Figure 29.

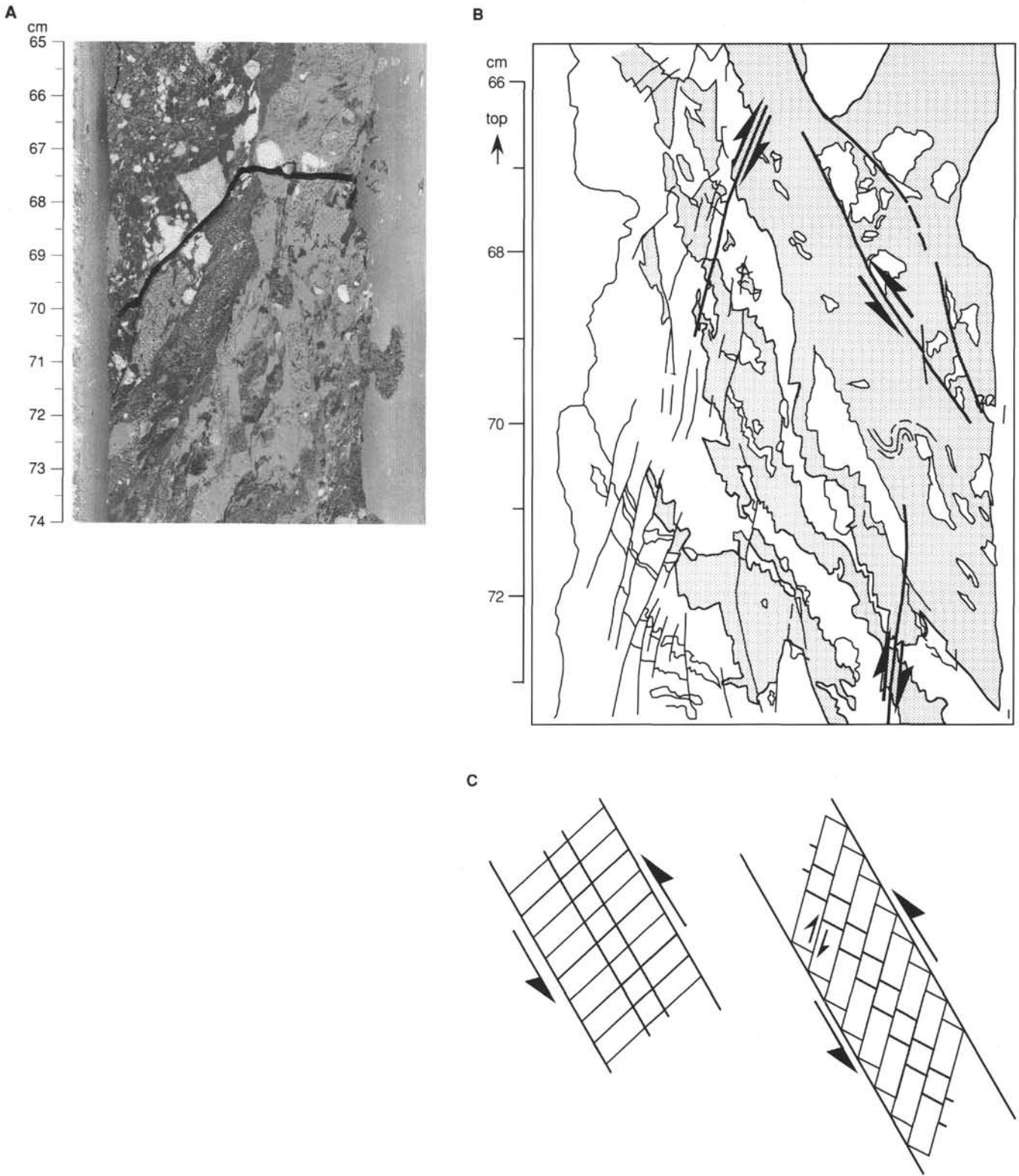


Figure 33. Photograph (A) and sketch (B) of a steeply dipping reverse shear zone with microshear folds in the breccia of tectonic Unit C in interval 134-829A-21R-2, 64–75 cm. The photograph is of the archive half of the core; the sketch represents the working half. The location is indicated in Figure 29. Sketch (C) of the development of the antithetic faults observed in the interval shown in Figure 33B.

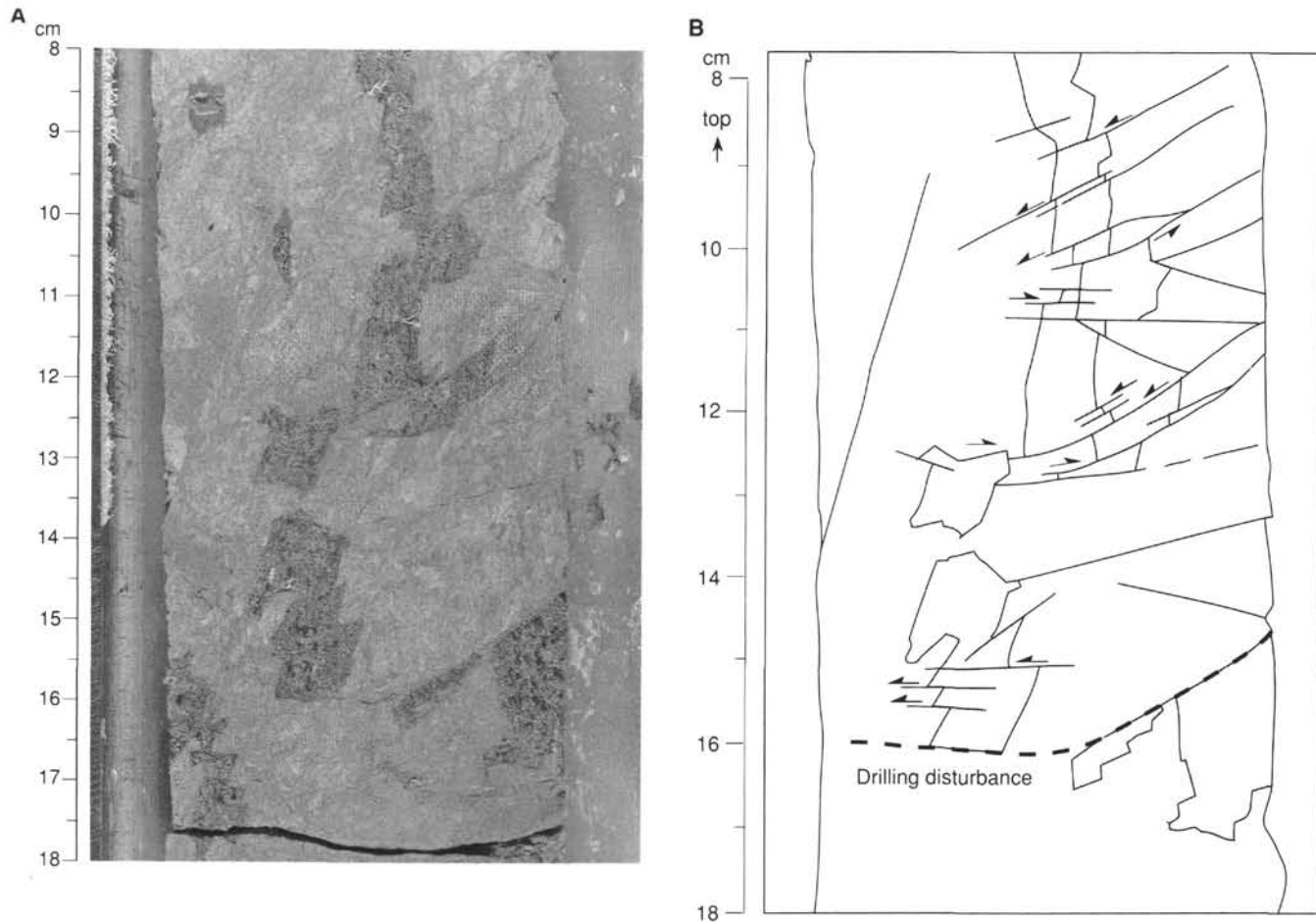


Figure 34. Photograph (A) and sketch (B) of a set of mainly normal faults observed in chalk breccia of tectonic Unit C in interval 134-829A-23R-1, 8–18 cm. The location is indicated in Figure 29.

which may correspond to igneous clasts or rocks (see “Igneous Petrology” section, this chapter).

SEDIMENT ACCUMULATION RATES

Sediment accumulation rates could not be estimated for Holes 829A, 829B, and 829C because of the absence of reliable chronostratigraphic events. These events include both nannofossil and planktonic foraminiferal datum levels (first appearance and last appearance). The incompleteness of the chronostratigraphic record is attributed to repeated displacement of biostratigraphic successions by apparent faults and by tectonic mixing of faunas and floras at various intervals. The use of microfossil zones to establish the age-depth curve in such a sequence would only exaggerate the sedimentation rate.

The first biostratigraphic gap in Hole 829A was recognized approximately between 60.5 and 70.1 mbsf, where middle Pleistocene strata overlie lower Miocene to upper Oligocene deposits. Continuing downhole, major biostratigraphic gaps occur between 99.0 and 108.6 mbsf, where Pleistocene sediments underlie lower Miocene to upper Oligocene deposits, and from 397.7 to 407.4 mbsf (where upper Pliocene–Pleistocene material underlies middle Oligocene sediments).

PHYSICAL PROPERTIES

Measurements of index properties and Hamilton Frame sonic velocities were completed on sediments and rocks at Site 829. Full APC cores from Hole 829C were measured using the gamma-ray attenuation porosity evaluator (GRAPE) and

the *P*-wave logger (PWL) on the multisensor track. Undrained shear-strength measurements were completed on the upper cores of Hole 829A (0–37.5 mbsf) and Hole 829C (0–60.4 mbsf). All measurements at Site 829 were made according to the procedures described in the “Explanatory Notes” chapter (this volume).

Index Properties

Values of porosity (wet and dry), bulk density (wet-, dry-, and grain), and water content (dry and wet) for Site 829 are listed in Table 7. Figure 50 illustrates the variation of porosity, water content, and bulk density as a function of depth below seafloor. Bulk density trends often mirror those of porosity and water content; therefore, bulk density and porosity are plotted against depth, along with the lithostratigraphic units in Figure 51. At Site 829, porosity ranges from 8.2%–66.3%, water content ranges from 3.3%–53.3%, and bulk density ranges from 1.71–2.82 Mg/m³.

The index properties data for Hole 829A can be separated into seven zones. The zones are closely associated with the tectonic and the lithostratigraphic units, with the exception of the boundary between tectonic Units C and D (see “Structural Studies” and “Lithostratigraphy” sections, this chapter). Index zones are correlated with the tectonic and the lithostratigraphic units as follows:

Index Zone 1 (0–171.9 mbsf) = tectonic Units A and B = lithostratigraphic Units I, II, and III;

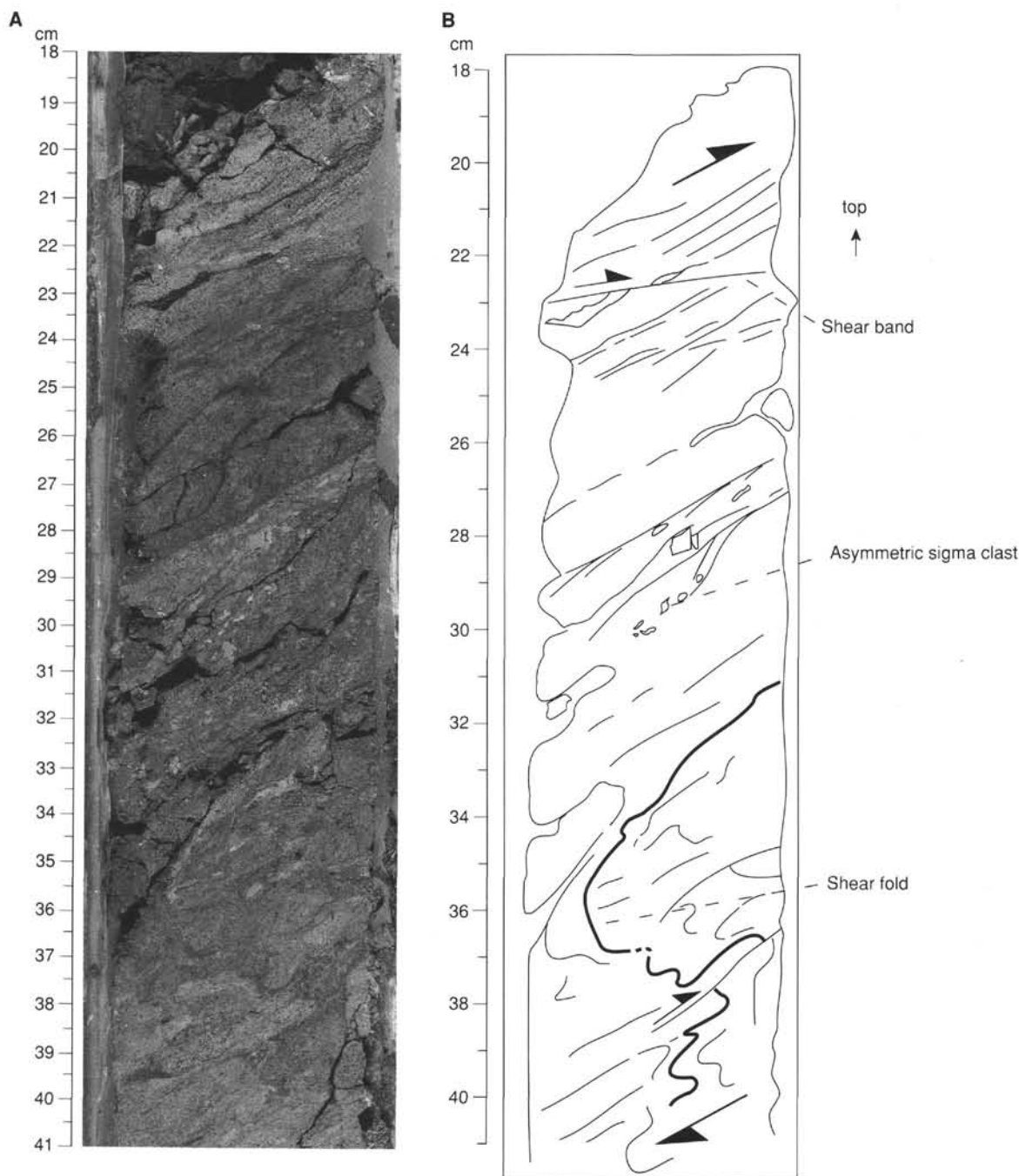


Figure 35. Photograph (A) and sketch (B) of a part of the shear zone with shear band, asymmetric sigma clast, and shear fold observed in chalks at the base of tectonic Unit D in interval 134-829A-43R-1, 18–41 cm. The location is indicated in Figure 29.

Index Zone 2 (171.9–205.2 mbsf) = 171.9–205.2 mbsf in tectonic Unit C = lithostratigraphic Unit IV;

Index Zone 3 (205.2–398.9 mbsf) = 205.2–311.3 mbsf in tectonic Unit C and 311.3–398.8 mbsf in tectonic Unit D = lithostratigraphic Units V and VI;

Index Zone 4 (398.9–462.9 mbsf) = 407.4 mbsf in tectonic Unit D, and tectonic Unit E = lithostratigraphic Units VII to XII;

Index Zone 5 (462.9–494.4 mbsf) = tectonic Unit F = lithostratigraphic Units XIII and XIV;

Index Zone 6 (494.4–524.6 mbsf) = tectonic Unit G = 494.4–495.6 mbsf in lithostratigraphic Unit XIV, Unit XV, and 517.2–524.6 mbsf in Unit XVI; and

Index Zone 7 (524.6–590.3 mbsf) = tectonic Unit H = 524.6–590.3 mbsf in lithostratigraphic Unit XVI.

Porosity and water content decrease very slowly in index Zone 1 (0–171.9 mbsf). All samples, with the exception of one sample of foraminiferal chalk at 80 mbsf, are composed of clayey volcanic silt and partially lithified siltstone. Between the surface and 170.5 mbsf, porosity and water content decrease from 58.1% to 50.7% and 46.5% to 33.5%, respectively. At 1 mbsf, bulk density is 1.92 Mg/m³, a high value for the seafloor (Bryant et al., 1981). Bulk density steadily in-

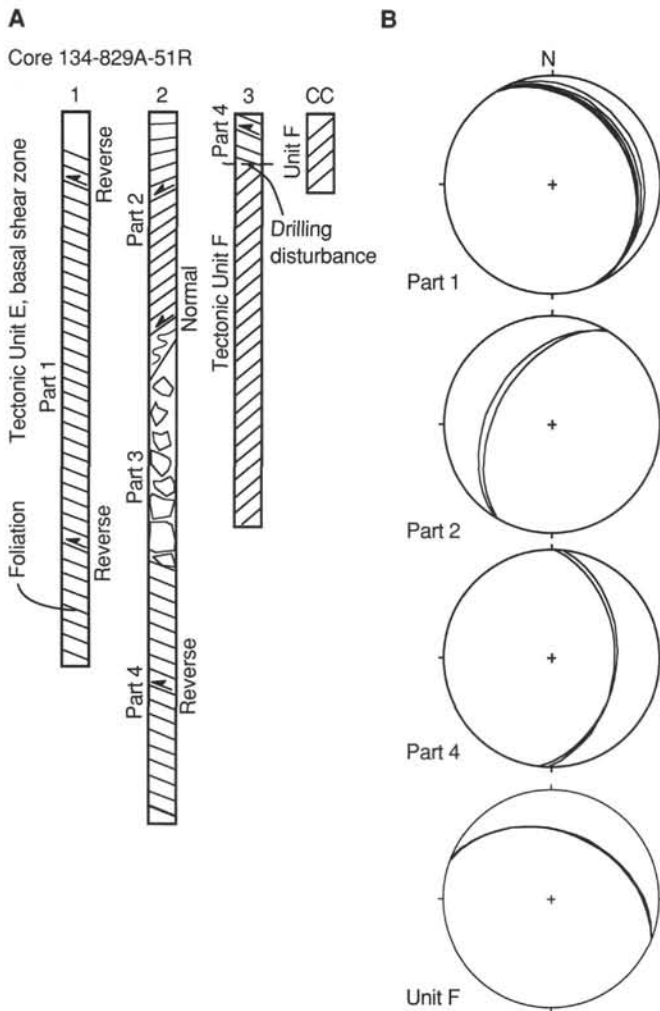


Figure 36. A. Sketch of Core 134-829A-51R showing the different parts of the shear zone at the base of tectonic Unit E. B. Orientation of the planar fabric in these different parts after correction using paleomagnetic measurements.

creases in index Zone 1 (Table 7, Figs. 50 and 51) from 1.88 Mg/m³ at 2.7 mbsf to 2.07 Mg/m³ at 170.5 mbsf. Core recovery below index Zone 1 was much lower. Index Zone 2 (171.9–205.2 mbsf) consists of siltstone-chalk breccia, which is more deformed than the overlying units. Porosity and water content average about 45% and 28%, respectively, with the exception of two measurements from 186–189 mbsf. Bulk density generally increases within index Zone 2, from 1.98 Mg/m³ at 173.5 to 2.25 Mg/m³ at 197.4 mbsf. Between 186–189 mbsf, the location of a major thrust plane (see “Structural Studies” section, this chapter), porosity and water content suddenly increase to 61.8% and 42.1% at 186 mbsf and then decrease anomalously to 8.2% and 3.8% at 189 mbsf. This may be evidence of shear dewatering in this fault zone. The pattern was observed in a number of samples at different tectonically affected sites on Leg 134, in which anomalously high porosity and water content values correlated with thrust planes, and were followed by anomalously low values just below the shear zone.

Index properties vary little in index Zone 3 (205.2–398.9 mbsf), which consists of chalk breccia and brittle, deformed calcareous chalk. Porosity and water content are significantly lower in index Zone 3 than in the zones above, while bulk

density is significantly higher. Between 205.5–398.7 mbsf, porosity and water content values are steady from 29.4% to 37.3% and 14.6% to 18.4%, respectively, while bulk density varies between 2.25 and 2.46 Mg/m³. Index Zone 4 (398.9–462.9 mbsf) is composed of brittle, intensely deformed volcanic breccia (398.9–407.4 mbsf) and chalk of varying ages, silt content, and composition (407.4–462.9 mbsf; Table 2). Porosity, water content, and bulk density values are scattered, ranging from 21.5% to 37.8%, 9.5% to 21.2%, and 2.19 to 2.61 Mg/m³, respectively. Significant exceptions to these ranges occur from 398.9–401.7 mbsf and at 427.1 mbsf, where porosity is 65.3% and 50.0%, water content is 52.9% and 34.9%, and bulk density is 1.94 and 1.98 Mg/m³, respectively. The anomalous index properties can be correlated with possible shear dewatering in a major zone of overthrusting that occurs from 398.7–399.9 mbsf and a thrust plane at 427.3 mbsf. The anomalously high index properties measurements were almost always made in brown clay laminae located in the thrust planes. These brown clay laminae were only observed in shear zones at Site 829 (see “Structural Studies” and “Lithostratigraphy” sections, this chapter), and their origin is undetermined. Only five measurements exist in the volcanic sandstone (462.9–484.5 mbsf) and the highly brecciated chalk (484.5–494.4 mbsf) of index Zone 5; porosity averages 34%, water content 17%, and bulk density 2.37 Mg/m³, respectively. Index Zone 6 (494.4–524.6 mbsf) is composed of volcanic siltstone (495.6–517.2 mbsf) with a minor component of sed-lithic breccia (517.2–524.6 mbsf) and chalk (494.4–495.6 mbsf). Porosity in Zone 6 is 10% higher, averaging 46%, as is water content, which averages 27%. Bulk density varies from 2.05 to 2.24 Mg/m³ in the chalk and in the breccia, and from 2.29–2.39 Mg/m³ in the sandy volcanic siltstone. A biostratigraphic reversal is located at 494.4 mbsf and a major overthrust occurs between 517.2–524.6 mbsf, and these structural features again correlate with significant increase/decrease anomalies in index properties (Table 7 and Figs. 50 and 51). Core recovery was low in index Zone 7, which is composed of breccia. Porosity, water content, and bulk density range from 8.7% to 33.4%, 3.3% to 17.1%, and 2.32 to 2.82 Mg/m³, respectively.

Hole 829C recovered soupy foraminiferal ooze and other sediments in lithostratigraphic Units XVIII–XXI (0–58.4 mbsf) which were not recovered in Hole 829A. Porosity, water content, and bulk density values in this interval were consistent with the upper part of Hole 829A and ranged from 53.1% to 60.1%, 39.0% to 53.3%, and 1.71 to 2.09 Mg/m³.

Sonic Velocity

Sonic velocities were measured with the Hamilton Frame in Holes 829A and 829C. Hamilton Frame velocities are listed in (Table 8) and the variations in velocity with depth is shown in Figure 50. At Site 829, vertical velocity ranges from 1612–6178 m/s and horizontal velocity ranges from 1522–6178 m/s. The vertical and horizontal velocities are anisotropic at several depths, but there is no distinguishable pattern of anisotropy at this site. The velocity data at Hole 829A can be separated into five zones that are associated with the index zones (see previous “Index Properties” subsection), as follows:

- Velocity Zone 1 = Index Zone 1 (0–171.9 mbsf);
- Velocity Zone 2 = Index Zone 2 (171.9–205.2 mbsf);
- Velocity Zone 3 = Index Zone 3 to Index Zone 5 (205.2–494.4 mbsf);
- Velocity Zone 4 = Index Zone 6 (494.4–524.6 mbsf); and
- Velocity Zone 5 = Index Zone 7 (524.6–590.3 mbsf).

The velocities increase very little with depth in the volcanic silt and partially lithified volcanic siltstone of velocity Zone 1

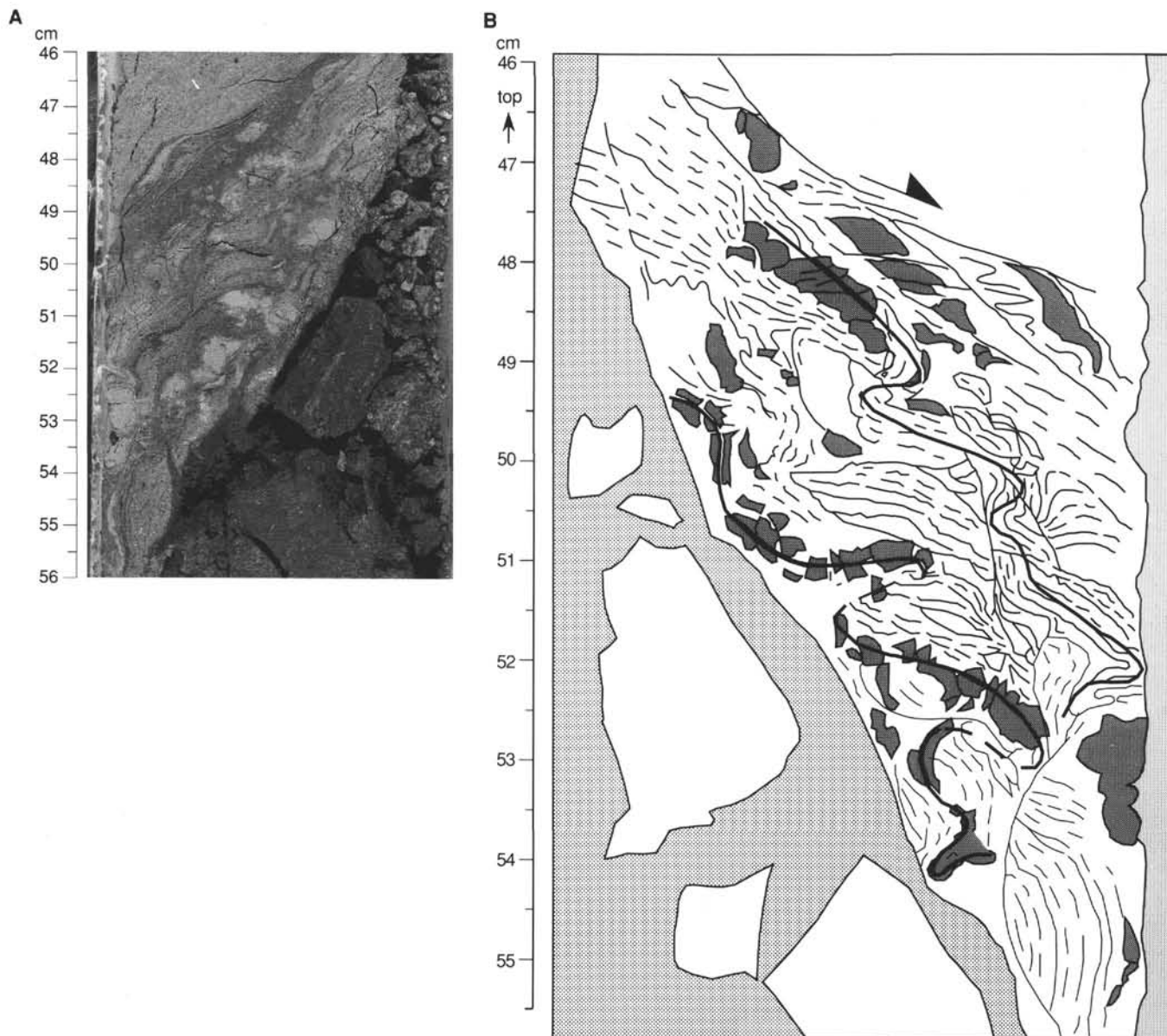


Figure 37. Photograph (A) and sketch (B) of the microshear folds indicating a normal sense of movement in part 3 of the shear zone observed at the base of tectonic Unit E in interval 134-829A-51R-2, 46–56 cm. The solid line is an interpretation of the folded structure. The photograph is of the archive half of the core; the sketch represents the working half. The location is indicated in Figure 29.

(0–171.9 mbsf). Vertical and horizontal velocities range from 1619 to 1755 m/s and 1620 to 1773 m/s between the surface (at 3.7 mbsf) and 169.0 mbsf. Maximum anisotropy (189 m/s) occurs at 122.5 mbsf. Velocity Zone 2 (171.9–205.2 mbsf), which is composed of siltstone chalk breccia, marks an interval in which the data becomes more scattered and continues to be varied in the numerous lithostratigraphic and tectonic units downhole (see “Lithostratigraphy” and “Structural Studies” sections, this chapter). Maximum anisotropy in Zone 2 (264 m/s) occurs at 176.4 mbsf. Vertical velocity data in Zone 3 (205.2–494 mbsf) vary widely from 2065 to 3027 m/s, through numerous lithology changes and biostratigraphic reversals. Maximum anisotropy in Zone 3 (443 m/s), occurs at 388.5 mbsf. In velocity Zone 4, the vertical and horizontal velocities are constant at about 2160 m/s. The sediments of velocity Zone 4 are composed of a biostratigraphically reversed unit of Pliocene or Pleistocene

volcanic siltstone, sed-lithic breccia, and chalk, and are isotropic. Recovery was poor in the sed-lithic breccia of velocity Zone 5 (524.6–590.3 mbsf). Vertical and horizontal velocities are very scattered, ranging from 3585 to 6178 m/s and 4787 to 6178 m/s, respectively. Maximum anisotropy (591 m/s) occurs at 533.6 mbsf.

Hole 829C was APC-cored from 0–58.4 mbsf. Vertical and horizontal velocities vary from 1586 to 1705 m/s and 1612 to 1676 m/s, respectively.

Shear Strength

Shear-strength measurements for Site 829 are listed in Table 9. Figure 52 illustrates the variation of shear strength as a function of depth below seafloor for Hole 829A. In Hole 829A, shear strength increases from 14.7 kPa at the surface (2.6 mbsf) to 77.0 kPa at 34.5 mbsf. Shear strength could not be measured below 40 mbsf in Hole 829A due to the degree of

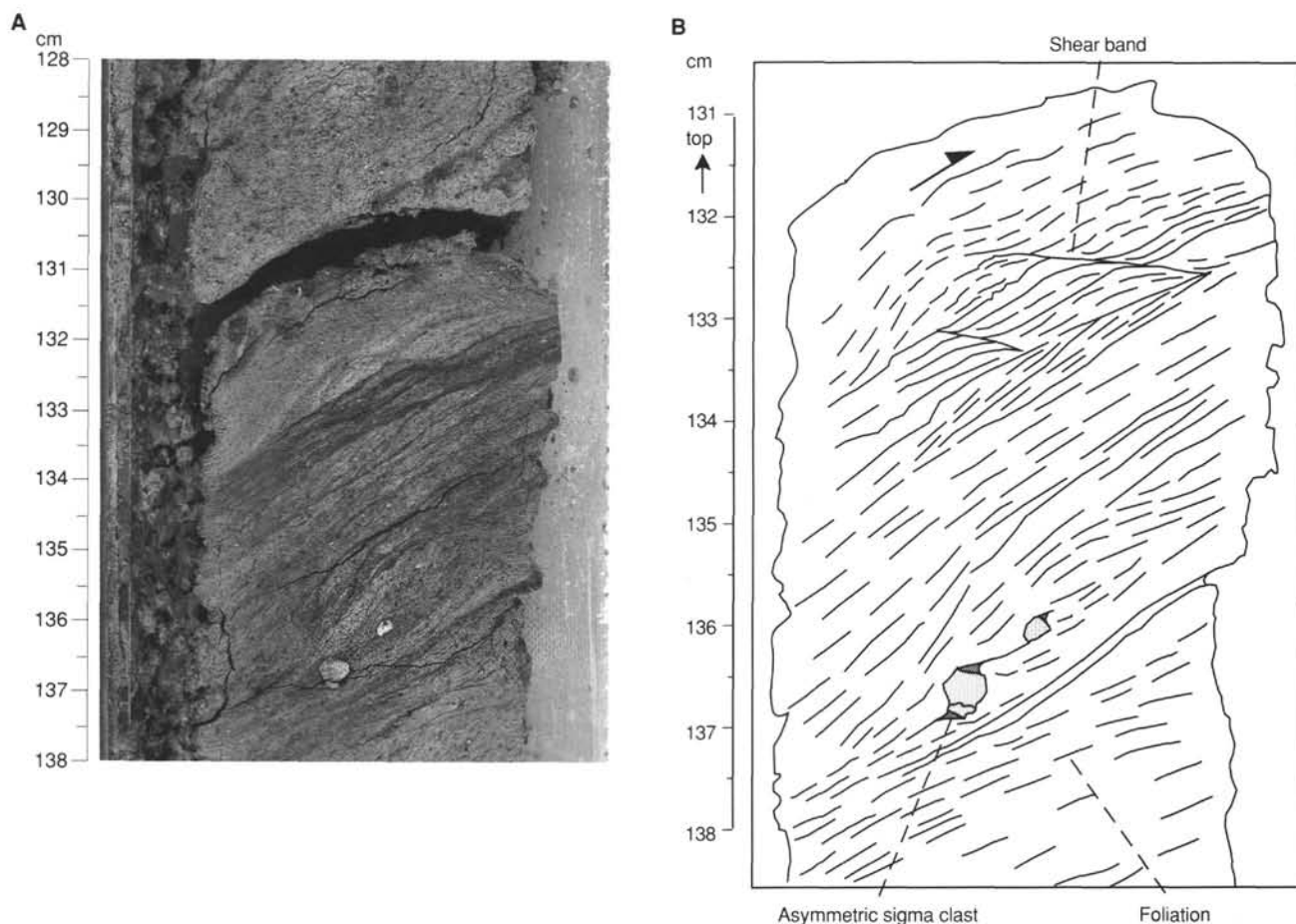


Figure 38. Photograph (A) and sketch (B) of the planar fabric with asymmetric sigma clasts and shear bands in part 4 of the shear zone observed at the base of tectonic Unit E in interval 134-829A-51R-2, 128–138 cm. The location is indicated in Figure 29.

lithification of the cores. Shear strength in Hole 829C was measured between 2.1–58.1 mbsf. Values were scattered and varied between 23.5 and 148.8 kPa in disturbed volcanic silt and soupy foraminiferal ooze.

Thermal Conductivity

At Site 829 thermal conductivity could only be performed to a depth of 60 mbsf. No other thermal conductivity measurements could be completed below 60 mbsf because the cores were too lithified and deformed by tectonics and drilling disturbance. Values range from 0.82 (Hole 829B, 0.25 mbsf) to 1.45 W/(m · K) (Hole 829C, 54.25 mbsf). All thermal conductivity values for Holes 829A, 829B, and 829C are listed in Table 10. Values are consistently between 0.8 and 1.1 W/(m · K) from the seafloor to 40 mbsf, with only minor increases above 1.1 W/(m · K) at several depths (Fig. 53). These slight increases correlate with index properties, corresponding to measurements of decreased water content and increased bulk density. The highest thermal conductivity values recorded were from 50–60 mbsf, where thermal conductivity increases quickly from 1.1 to 1.45 W/(m · K). These measurements correlate with an interval of foraminiferal mixed sediment from 54–60 mbsf.

The observation of increased thermal conductivity in the foraminiferal sediments from 50–60 mbsf is consistent with observations at Site 827 where there is a direct relationship between thermal conductivity and percentage of CaCO₃ in the sediment. Water content was much lower in CaCO₃-rich sediments and thermal conductivity was significantly higher.

This direct correlation between CaCO₃ and thermal conductivity is stronger at Site 829 than at Site 827 because there is less variability in the CaCO₃ percentage data. Rapid shifts and wide variations in CaCO₃ percentage in the lithostratigraphic units make the relationship more difficult to see at Site 827.

Summary

The most notable feature at Site 829 is the distinctly sharp decrease in porosity and water content at the contact between lithostratigraphic Units IV and V (205.2 mbsf) and below (Fig. 50). Porosity and water content range from 29.4% to 37.3% and 14.6% to 18.4%, respectively, from 205.2 mbsf to the bottom of Hole 829A (590.3 mbsf). These ranges are significantly lower than at Site 828 and probably result from the collision of the NDR. Sudden, anomalous increases or decreases of porosity and water content were observed at the locations of major thrust planes and overthrust faults (Fig. 50). For example, porosity and water content suddenly increased by about 20%–25% in the overthrust zone at 397.8–399.9 mbsf. Higher values of porosity and water content were also found in thrust zones at Site 827 (see “Physical Properties” and “Sediment and Fluid Geochemistry” sections, “Site 827” chapter). These data provide evidence that dewatering along shear zones caused by subduction of the NDR may provide a significant path for fluid flow in the DEZ. The significantly lower water contents in the sediments at Site 829 than at either the Nankai (Taira, Hill, Firth, et al., 1991) or Barbados (Taylor and Leonard,

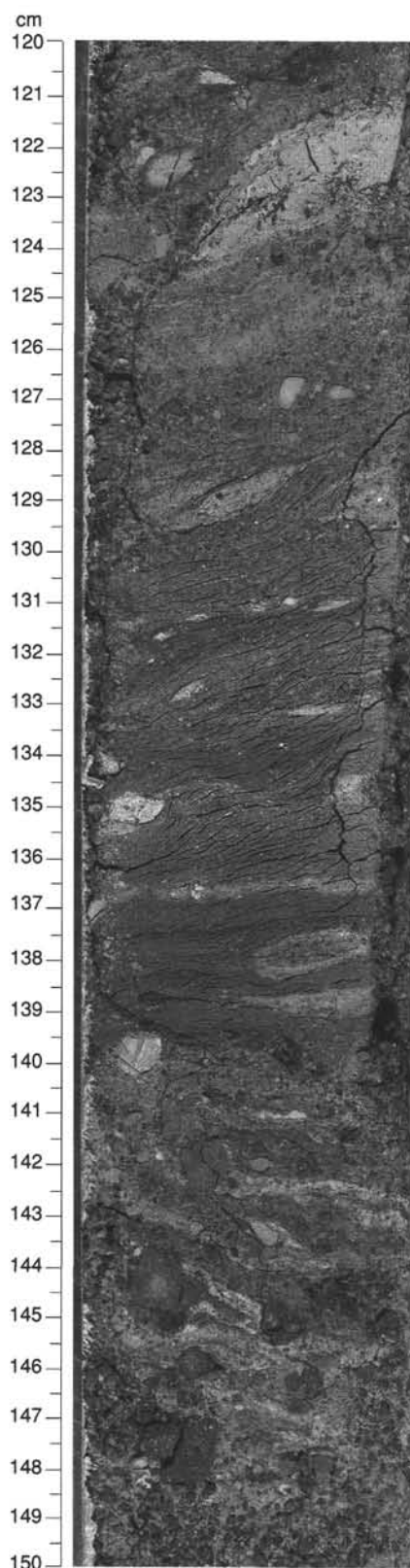


Figure 39. Photograph of the shear zone at the base of tectonic Unit G in interval 134-829A-58R-1, 120–150 cm. The location is indicated in Figure 29.

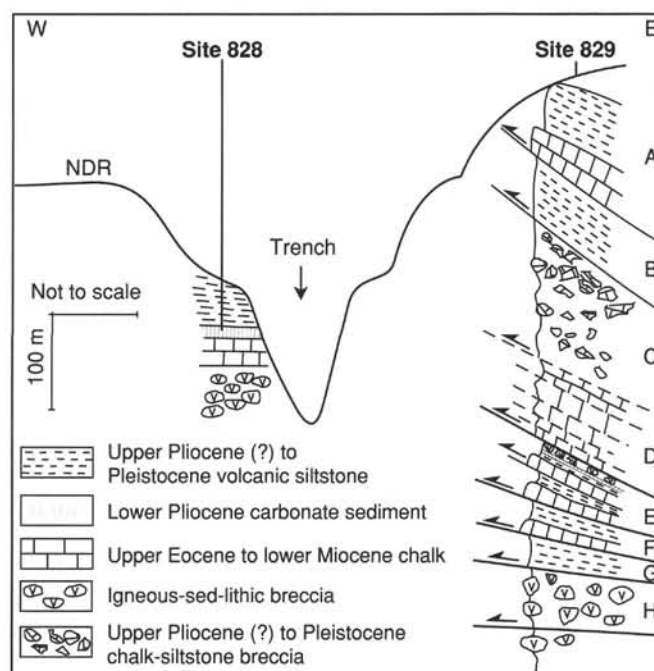


Figure 40. Geologic sketch (not to scale) showing the geological structure of both the accretionary complex at Site 829 and the North d'Entrecasteaux Ridge (NDR) at Site 828. "A" to "H" are the tectonic units. On the ridge, carbonate sediments include upper Eocene to upper Oligocene chalk and lower Pliocene foraminiferal ooze. In the accretionary complex, chalk extends from lower Oligocene (or upper Eocene?) to lower Miocene. A thin interval of lower Pliocene chalk was found in tectonic Unit E.

1990) subduction zones implies that much of the sediment dewatering at convergent margins may result from compressional tectonics caused by topographic features on the seafloor impinging upon the margin (see "Sediment and Fluid Geochemistry" section, this chapter).

DOWNHOLE MEASUREMENTS

Logging Operations

Logging operations in Hole 829A began at 0500 local time (L) on 3 November 1990 and required 32 hr to complete. After a wiper trip between 580 and 91 mbsf, the bottom of the drill pipe was held at 91 mbsf for the duration of logging. The first logging tool string used was the geophysical tool string, which included the long-spaced sonic, lithodensity, natural gamma-ray spectrometry, dual induction resistivity, and the Lamont temperature probe tools. The tool string was lowered to 475 mbsf, about 115 m above the hole depth at the end of drilling. Bridged sections of hole were encountered below 435 mbsf. Log data were recorded as this string was raised at 500 m/hr between 475 and 50 mbsf.

The FMS tool string was the second logging string used, beginning at 1300 L on 3 November. Data were recorded from 473 up to 49 mbsf. A repeat section was recorded from 471 to 156 mbsf. The hole above 156 mbsf had too large a diameter (15 in.) to obtain good FMS data.

The geochemical string was the third logging string run in Hole 829A. The log was run from 476 up to 50 mbsf. A second pass was done from 106 to 0 mbsf, since the geochemical tool can obtain data through the drill pipe. Standard Schlumberger logging operations finished at 0030 L on 4 November 1990.

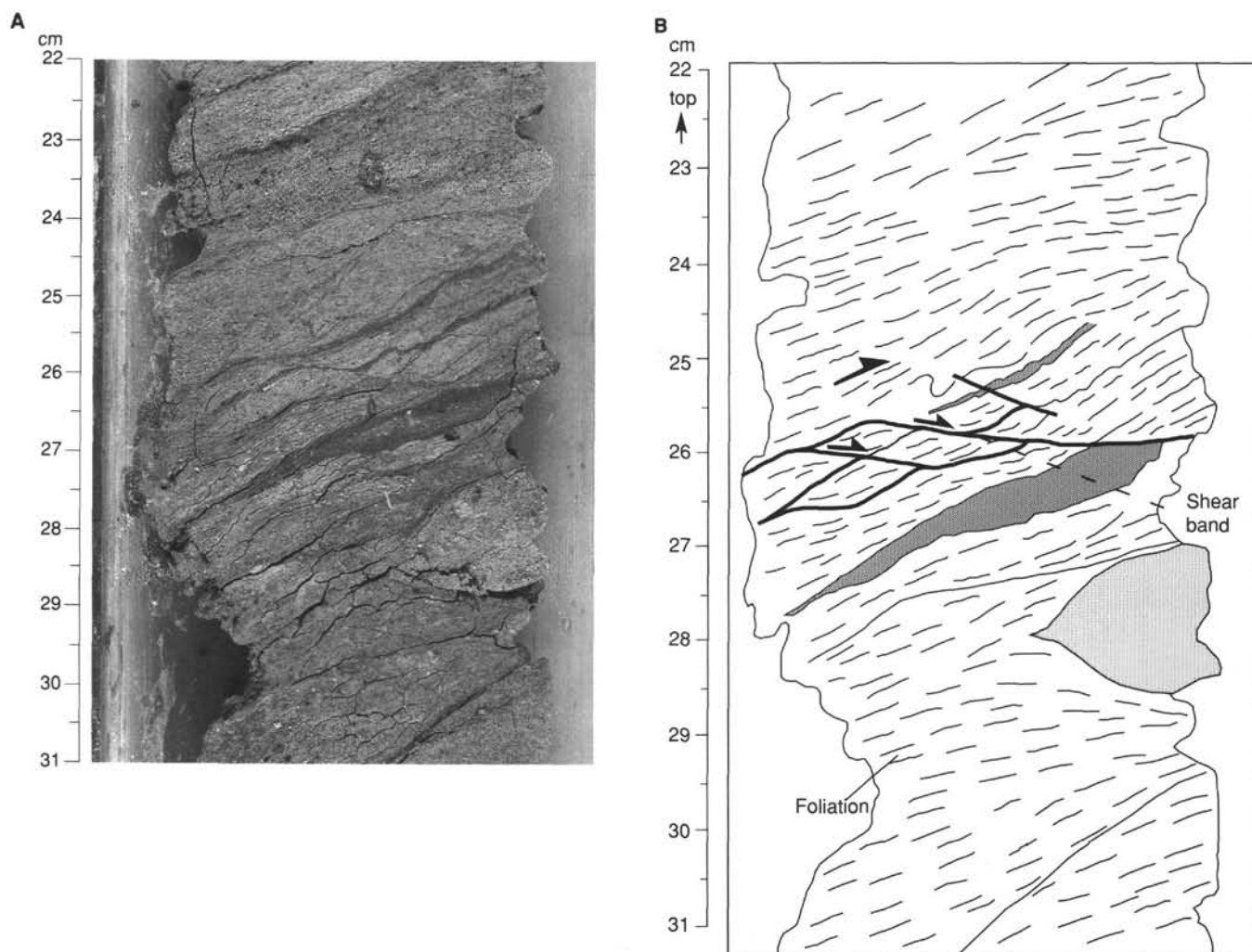


Figure 41. Photograph (A) and sketch (B) of the planar fabric with shear bands in part I of the shear zone observed at the base of tectonic Unit E in interval 134-829A-51R-1, 22–31 cm. The location is indicated in Figure 29.

The fourth logging run was the new BHTV. It could not be lowered below 429 mbsf owing to obstructions in the hole. During the first pass the tool was raised to 155 mbsf with a logging velocity of 150 m/hr; at this velocity stick-slip motion of the tool produced problems in the recorded data. The second pass scanned the borehole from 374 to 166 mbsf, and the logging speed was increased to 318 m/hr, which prevented most of the spurious values due to stick-slip (Fig. 54).

Log Reliability

Logs obtained in Hole 829A are generally of good quality. The hole diameter measured during successive logging efforts shows broad variations at the top and the bottom of the logged interval. Although many of the logs are insensitive to changes in borehole diameter, the gamma-ray and resistivity readings have been revised somewhat during post-cruise processing to correct for these effects. The effects of borehole variations on FMS data are discussed below.

Comparison of Well-Log Data to Core Lithology

In this section the lithostratigraphic units defined from core description ("Lithostratigraphy" section, this chapter) qualitatively are compared to the shapes of well-log curves to describe the generally high level of agreement between litho-

stratigraphic units and rock masses defined on the basis of well-log signatures. The logging results are presented in the Log Summary at the end of this chapter.

This comparison begins with the lowermost part of lithostratigraphic Unit I. Unit I is a Pleistocene clayey volcanic silt and Unit II (60.5–99.4 mbsf) is a foraminiferal chalk; the contact between these units is at 60.5 mbsf. Average core recovery in the chalk was about 10%. Well-log data differentiate lithologies of the silt and chalk units, but the logs also indicate that the contact between the units is gradational over a 5- to 15-m depth interval. This gradation begins at 55 mbsf, about 5 m above the unit boundary that was determined from core description, and the gradation is shown by the slowly increasing velocity and resistivity readings (resistivity–sonic gamma-ray, Log Summary) and the sharply increasing calcium values, as well as by the sharply decreasing iron readings (geochemical Log Summary). Entirely within this zone of gradation, the gamma-ray and aluminum logs reach small peaks, perhaps indicating a clay-rich layer within the gradational contact between Units I and II. The geochemical-log values obtained over Unit II show that the iron and calcium logs vary inversely to each other, indicating a fluctuating silt or clay content throughout the chalk. This fluctuation is borne out by approximately coincident, small changes in velocity

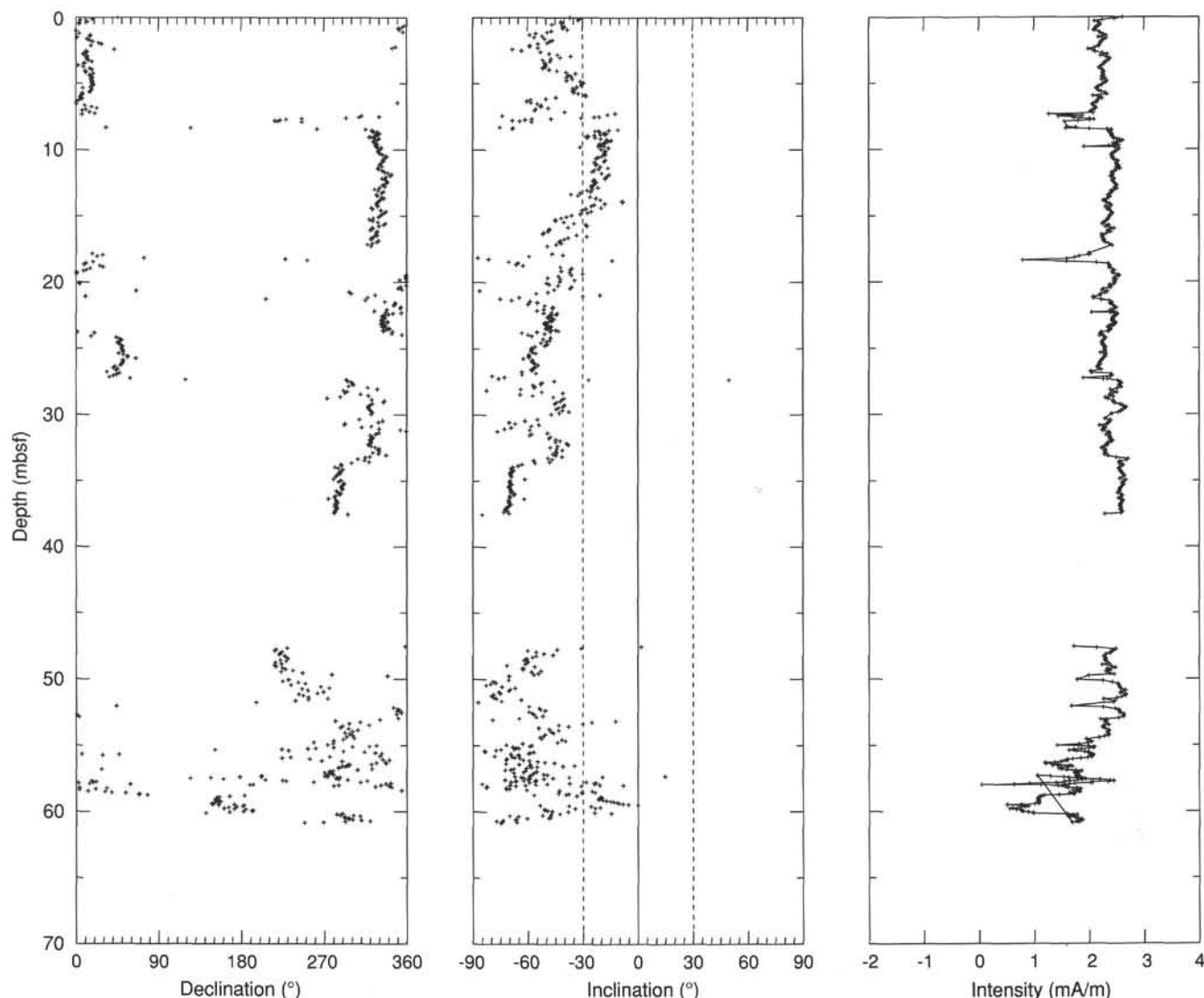


Figure 42. Plot of the remanent magnetization (after AF demagnetization at 10 mT) vs. depth for Hole 829C. Data from the bottom part of the hole are not reliable because the cores were highly disturbed. Sediments from the upper 40 m did not show any evidence of drilling disturbance. Declinations and inclinations vary substantially even after correction using data obtained with the multishot orientation technique. The dispersion in declination may result from the incomplete removal of secondary components of magnetization produced by drilling. The inclinations are quite different from the value expected at this latitude (-29°).

and resistivity. The gamma-ray log yielded uniformly low values, suggesting a low clay content in Unit II.

Lithostratigraphic Unit III (99.4–171.9 mbsf) is a Pleistocene clayey volcanic silt and the contact between Units II and III is a thrust fault at 99.4 mbsf identified from biostratigraphy. Core recovery in Unit III was about 98%. Nearly all logs registered this chalk-silt contact, and they confirm a sharp lithologic break because between 97 and 100 mbsf the calcium, velocity, and resistivity logs all decrease. The calcium log does so sharply, and the gamma-ray, aluminum, silicon, and iron logs increase abruptly in a roughly inverse relationship to the calcium log. The density log shows a small decrease, but this decrease is an artifact in most of the 100–130 mbsf interval caused by the fact that the caliper log is at maximum extension and true hole diameter is not known. The variations in most of these logs can be deduced from the observed change in rock type, but what makes this lithologic contact readily evident in well-log data is the distinctively subdued, smooth readings

obtained over the silt of Unit III by nearly all types of logs (Log Summary).

Unit IV (171.9–205.2 mbsf) is an upper Pliocene to Pleistocene silt and chalk breccia. Core recovery in this unit was about 35%. The upper and lower contacts of Unit IV are not sharply distinguishable because well-log readings in this unit are gradational, representing a more-or-less continuous downhole transition in rock properties from the overlying silt of Unit III through the silt and chalk breccia of Unit IV to the underlying chalk breccia of Unit V. A gradation across Unit IV is present in nearly all logs but not all gradations occur within a common depth interval. The geochemical logs show the pattern expected for a transition from a silt to a chalk: decreasing iron, aluminum, and gamma ray and increasing calcium. Density and resistivity increase. The velocity log increases abruptly at the top of this unit but then gradually decreases toward the base of the chalk units at 400 mbsf.

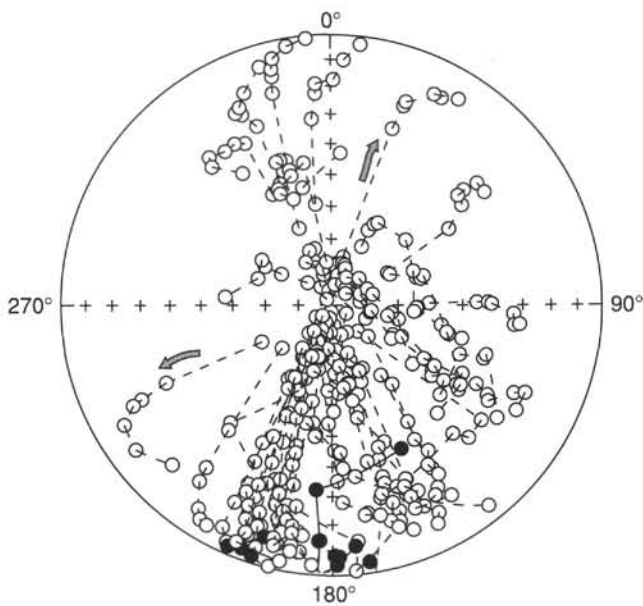


Figure 43. Equal-area projection of the directional variations observed in discrete samples during AF demagnetization.

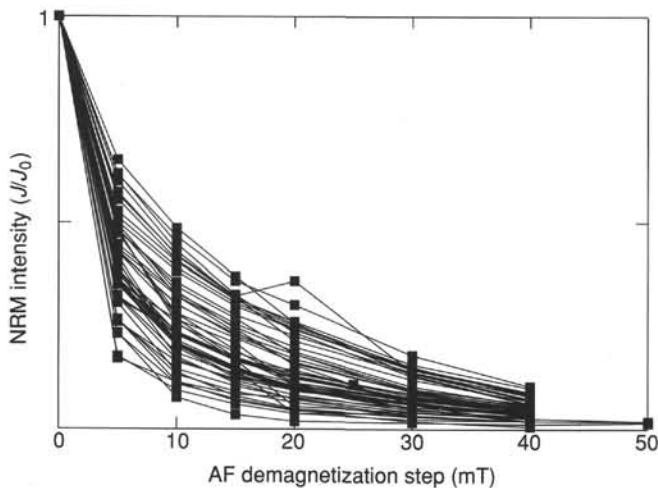


Figure 44. NRM intensity vs. AF demagnetization step for discrete samples from Hole 829B and Hole 829C. J/J_0 is the ratio of magnetic intensity (J) after demagnetization at a particular step to the NRM intensity (J_0). Most of the samples have very low median destructive fields.

Lithostratigraphic Unit V (205.2–311.3 mbsf) is an upper Pliocene to Pleistocene chalk breccia. Core recovery from this unit averaged 20%. In the middle of Unit V (259 mbsf) is an interpreted thrust fault that has marked expression in velocity and resistivity logs. The density log also peaks over this interpreted fault, but this peak coincides with locally decreased hole diameter. The effect of this change in hole diameter on the other logs that registered the thrust fault is unclear. This fault is very prominent in the FMS and BHTV logs (see below). About 4 m above this fault, sharp peaks in the spectral gamma-ray log indicate a peculiar enrichment in potassium, uranium, and thorium relative to surrounding rocks. The type of rock that hosts this enrichment is unknown, but the host's log signature does not appear to be significantly different than the signature from the nearby chalk.

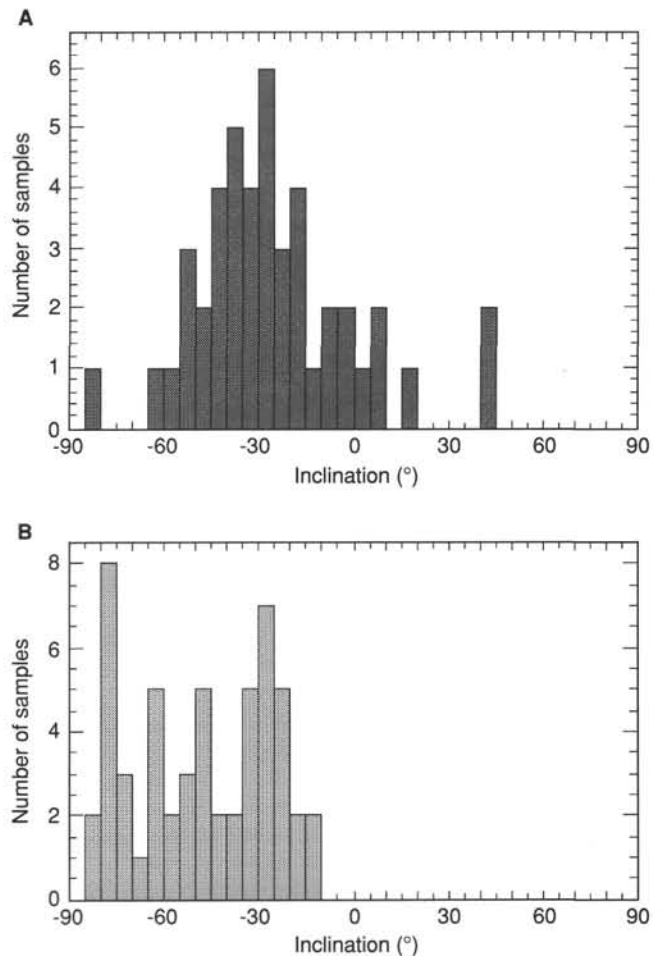


Figure 45. A. Histogram showing the frequency of occurrence of inclinations (plotted in 5° intervals) after AF demagnetization at 10 mT, Hole 829A. B. Histogram showing the frequency of occurrence of inclinations (plotted in 5° intervals) after AF demagnetization at 10 mT, Holes 829B and 829C.

Lithostratigraphic Unit VI (311.3–398.8 mbsf) is a middle Oligocene to lower Miocene calcareous chalk. Core recovery from this unit averaged 15%. None of the logs show any substantial change in readings across the contact between Units V and VI; some logs, however, show gradual changes in average value from 380 mbsf to the base of the unit at about 400 mbsf. Specifically, calcium and velocity decrease gradually; iron varies inversely with them. At 375 mbsf all logs show increasingly variable readings where the hole diameter is irregular. The caliper log shows much variability in the 355–405 mbsf interval, often reaching its maximum extension in the 390–405 mbsf interval. This will decrease the accuracy of logs which must be corrected for borehole diameter.

Lithostratigraphic Unit VII (398.9–407.4 mbsf) is an undated volcanic breccia. Core recovery averaged about 30%. Hole diameter throughout this unit is almost entirely beyond the range of the caliper, so hole corrections cannot be properly applied.

Below 400 mbsf core descriptions suggested as many as six thin, variously colored chalk units, some of which contained silt. These chalks range in age from Oligocene to Pleistocene. Core recovery averaged about 17%. We grouped these units together because the logs reveal that chalk layers alternate with other chalk layers that have a substantial proportion of

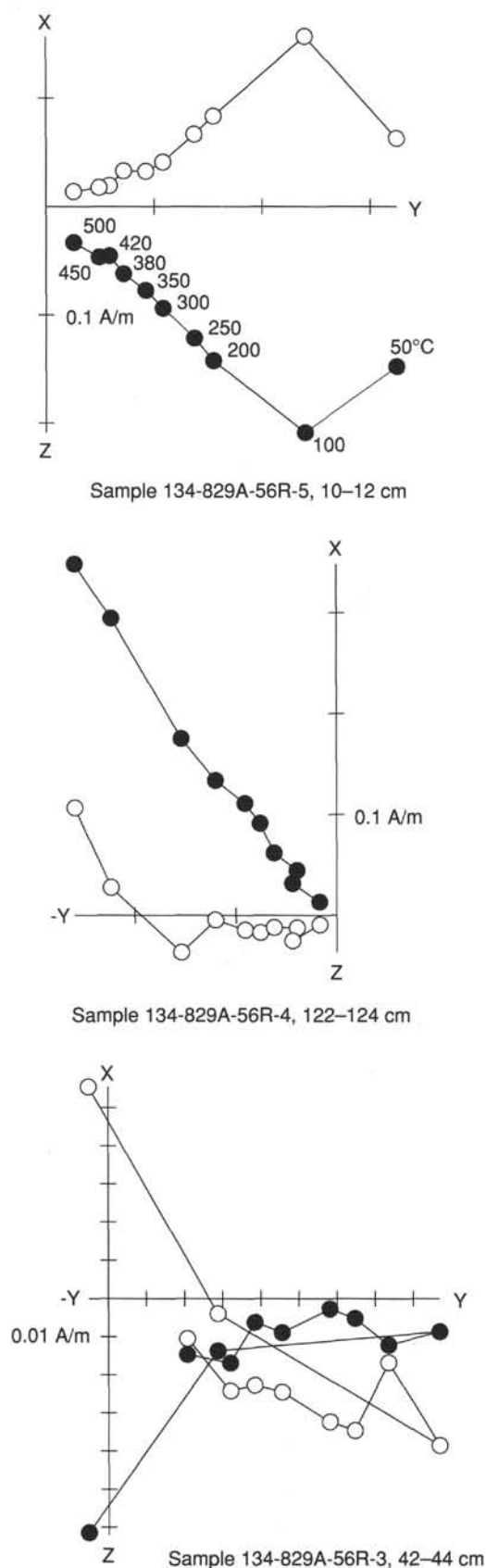


Figure 46. Orthogonal plots of thermal demagnetization data for three samples from Core 134-829A-56R. Open circles correspond to projections onto the vertical plane and solid circles correspond to projections onto the horizontal plane.

silt. The silt-poor units appear relatively low in the iron, aluminum, and gamma-ray readings and high in calcium values. The silt-poor units occur at 405-415 mbsf, 420-437 mbsf, and 440-460 mbsf. The primary evidence that the layers alternate comes from the iron and calcium logs. Furthermore, through each chalk, the resistivity log increases gradually and at the top of silt-rich units, it decreases abruptly; the velocity log shows ragged peaks over the silt-rich zones. Based on this pattern in the velocity and resistivity logs, another alternation between chalk and silty chalk can be inferred to lie below 460 mbsf, below the depth logged by the geochemical logs.

Unfortunately, logging extended no deeper than about 475 mbsf. Consequently, no data are available from the igneous rocks, including basalt and gabbro, that were penetrated deeper in the hole.

FMS Logging

The quality of the FMS data is generally good but suffers locally from two major problems. First, caliper logs reveal places where the hole diameter exceeds 15 in., which is sufficiently large to prevent the tool pads from being in firm contact with the formation; consequently, resistivity measurements are affected by water invading between the electrodes and the borehole wall. Portions of these data affected by large hole diameter appear dark (low resistivity), as can be seen on the reduced dipmeter presentation of FMS data (Fig. 55). Such zones are located principally above 175 mbsf but others occur between 259-260 mbsf, 390-405 mbsf, and 465-470 mbsf. The second problem in FMS data stems from the drill-hole ellipticity, which can be determined from the caliper logs (Fig. 55). For example, between 150 and 400 mbsf the caliper oriented southeast-northwest consistently registers a diameter 2 in. larger than the diameter from the perpendicular caliper. This ellipticity caused the tool to have the same orientation in the hole during the two logging passes, so that nearly half of the borehole wall remains unimaged.

FMS data from Hole 829A were processed aboard ship (see processed FMS data on microfiche at back of this volume). Oriented FMS images, scaled to the core photographs, were produced to correlate core and FMS information. Unfortunately, this correlation was not very successful because of the low core recovery in the main zones where the FMS is most reliable. The second phase in processing FMS data concerns computing the dip and azimuth of dipping features that intersect the borehole. A planar feature intersecting a cylindrical borehole will have sinusoidal expression when the cylindrical FMS image is unwrapped to a flat surface. During this processing, sine waves are cross-correlated with the data from the electrode buttons on the four pads of the FMS. Typical results of such processing are shown in Figure 54. The part of the drill hole from which this example was taken yielded only spotty cores, but FMS images reveal layers that dip 25° to 35° east. Calculated dips were determined automatically over the entire logged interval, and some of the results are presented in an azimuth-frequency diagram and a π -diagram for three separate intervals that correspond to different lithologies where recovery was particularly low (Fig. 55). The validity of these calculated structural attitudes can be determined only by a careful comparison of calculated attitudes with those evident from the original FMS images. This study would establish the reliability in the field of the algorithm and its implementation used in the Schlumberger FMS processing software. Despite the unproven accuracy of the calculated results, a small shift in dip direction, from southeast to northeast, can be discerned by comparing the structure plots from the first and second intervals. Also, dip seems to

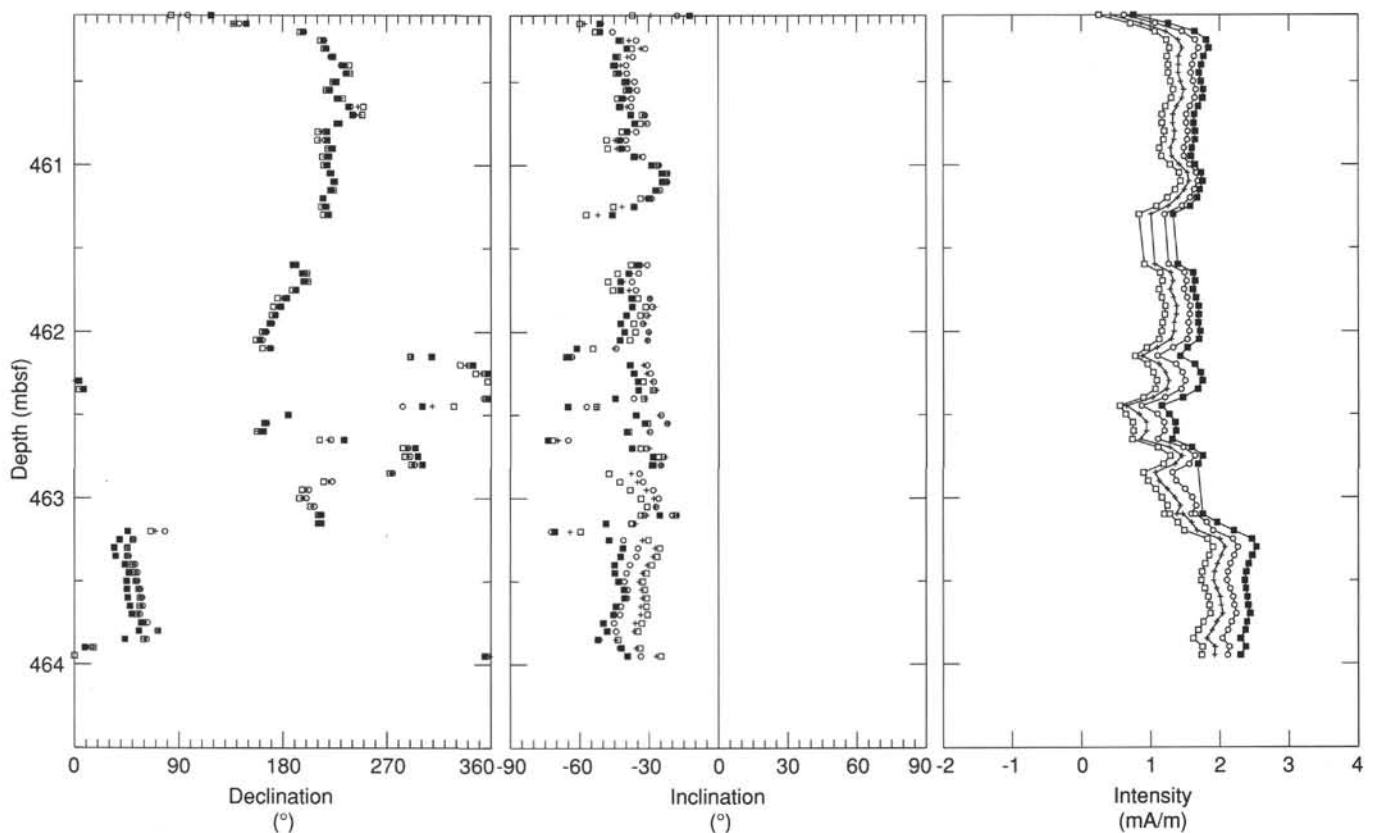


Figure 47. Plot of the remanent magnetization vs. depth for Core 134-829A-51R. Upon demagnetization at 5 (circles), 10 (crosses), and 15 mT (open squares), the inclination shallows toward the value expected at this latitude (-29°). The declination plot confirms that the core was not disturbed much by rotary drilling. Section 134-829A-51R-3 is rotated approximately 180° with respect to Section 134-829A-51R-1.

increase in magnitude together with the shift to northeast dips downward in the hole.

A large open fracture at 259 mbsf appears in FMS data obtained along a chalk unit (Fig. 56). The data indicate an apparent 80-cm width of the fracture in good agreement with the 70-cm estimate from the BHTV (see below). This fracture dips approximately 40° east and seems to separate two rock bodies of slightly different resistivity; the body above the fracture appears to be the more conductive. The upper rock body also appears to be well layered, in contrast to the lower one, but pebbles seem to be more common in the lower body.

Borehole Televiewer

The digital BHTV was used for the first time on an ODP leg during logging operations at Hole 829A. The BHTV scans the borehole wall with ultrasonic pulses, and traveltimes as well as amplitudes are recorded. The images of the BHTV, which are processed and analyzed on an Apple Macintosh II computer, can provide valuable information about structures intersecting the borehole and about the shape of the borehole itself. The later information can then be used to determine the direction of the present stress field if stress indicators such as breakouts and tension cracks are observed.

A preliminary analysis of BHTV data shows that the dip of fractures intersecting the borehole ranges from 30° to 70° (Fig. 57), and most of the dips lie between 30° – 60° . Shallower than 230 mbsf the dips of planar structures vary only slightly between 50° and 70° , whereas deeper than 230 mbsf dips range from 30° to 70° . These two depth zones are separated from each other by a clearly indicated fault that dips east at 40° . The fault having clearest expression in BHTV data occurs at 259

mbsf; this fault is about 70 cm thick and dips 55° southeast. The difference in strike and dip for this fracture from the FMS and the BHTV data will be checked during more detailed analysis of the two data sets. It is probably simply due to the preliminary nature of the shipboard analysis. This fault coincides with the onset of the sedimentary tectonic melange within lithostratigraphic Unit V (See "Lithostratigraphy" section, this chapter).

Although the borehole at Hole 829A has low deviation (between 90 and 100 mbsf the deviation amounts to 5° and for depths greater than 200 mbsf the deviation is less than or equal to 5° ; Fig. 55), the borehole is highly deformed, as shown by the cross-sectional shapes of the borehole (Fig. 58). Between 166 and 374 mbsf these cross sections vary from ellipsoidal to pear shaped. Where the deviation varies between 3° and 5° , the P1-azimuth is constant near 120° . The borehole deviation to the east-southeast and southeast and the softness of the sedimentary rocks affect the cross sectional images of the BHTV because the weight of the drill pipe leads to a pear-shaped cross section. However, above 179 mbsf the borehole is nearly completely washed out over long distances and such forms are no longer observable. No clear stress indicators were observed.

Heat Flow

Two runs of the WSTP temperature tool were performed at Site 829, only one of which was successful. The temperature measurements were extrapolated to equilibrium sediment temperature values using the 1/time approximation technique. The temperature measurements were then combined with the shipboard needle-probe thermal conductivity measurements

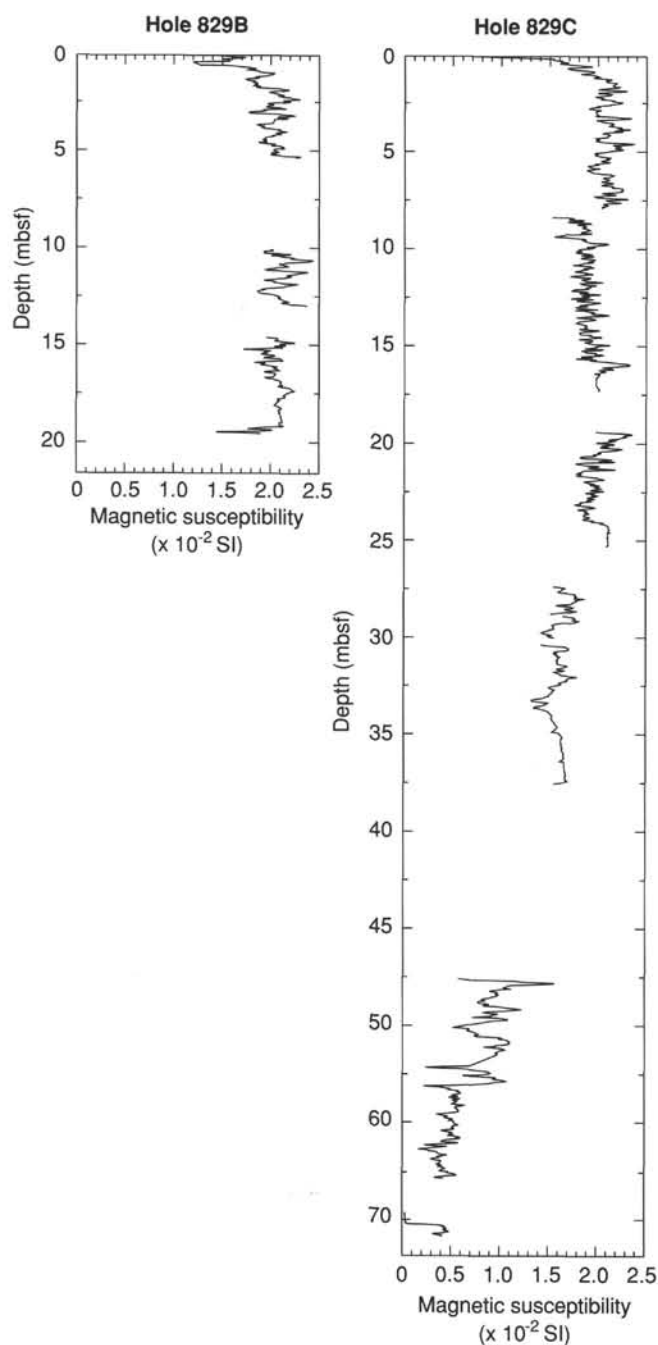


Figure 48. Variation of the magnetic susceptibility vs. depth in Holes 829B and 829C. The decrease in susceptibility observed at the bottom of Hole 829C results from mixing (during coring) of Miocene nanofossil ooze within Pleistocene volcanic siltstone.

(see "Physical Properties" section, Table 10 and Fig. 53, this chapter) to determine the heat flow value. This was done by plotting the temperature values vs. the depth integral of the thermal resistivity (the inverse of the conductivity). The slope of this linear regression is the conductive heat flow.

The individual temperature measurements are discussed below: Run 5H in Hole 829C (Fig. 59) was done at a depth of 30.3 mbsf. The run had a good mudline reference temperature before and after the penetration and no disturbances during the measurement. The reduction to equilibrium temperature is plotted in Figure 60. Run 10H in Hole 829C (Fig. 61) was

unsuccessful as the temperature probe was damaged on penetration when it struck a hard object or layer in the bottom.

The single equilibrium temperature is plotted against integrated thermal resistivity in Figure 62 along with the mudline temperature. The slope of the plotted linear regression indicates that the heat flow is 41.5 mW/m^2 . This is much higher than the value of 23.8 mW/m^2 found at Site 827, but the confidence level given to the Site 829 measurement is low, since it is based upon only one sub-bottom temperature measurement and the bottom-water temperature. If this single measurement had been obtained at a greater depth, its utility would have been higher. There are no other existing heat flow values in the vicinity to compare to this one.

SUMMARY AND CONCLUSIONS

Site 829 (proposed site DEZ-2) is located at $15^{\circ}18.96'S$, $166^{\circ}20.70'E$, at a depth of 2905 mbsf, on the lower part of the forearc slope where the North d'Entrecasteaux Ridge impinges upon the forearc slope of the central New Hebrides Island Arc. The principal objectives of this site were to recover rocks and fluids from within the accretionary complex and to penetrate the décollement and the underlying ridge. More specifically, we wanted to investigate tectonic accretion of ridge fragments, a process not readily evident from drilling at Site 827, and document the chemistry and origin of pore-fluid anomalies discovered at Site 827. Site 829 was our second attempt to drill through the décollement in the collision zone between the NDR and the New Hebrides Island Arc. Although Hole 829A collapsed before we penetrated the décollement, we successfully cored overlying thrust sheets in the accretionary complex. Seismic reflection data (see "Seismic Stratigraphy" section, this chapter) suggest that the zone of décollement lies about 150 m deeper than the total depth of Hole 829A.

Site 829 is located on a small flat area on the 10° west-dipping arc slope, about 330 m on a slope above the trench and is 35 km west of Espiritu Santo Island and about 2 km east from the trace of the subduction zone. Hole 829A was rotary-cored to a total depth of 590.3 mbsf with a recovery rate of 33.4%. Holes 829B and 829C were cored by APC to 19.5 and 58.4 mbsf, with recovery rates of 80% and 90.2%, respectively. Hole 829A started to deteriorate near depths of 525 mbsf and drilling was stopped at 590.3 mbsf. However, the hole remained stable and extensive logging was undertaken, which provided excellent results. Site 829 recovered a 590-m-thick record of the Pleistocene tectonic history of the collision between the NDR and the New Hebrides forearc. In this section, we summarize and discuss the important findings at this site.

Preliminary biostratigraphic data for Site 829 indicate that the sediments are mainly early Oligocene (or late Eocene?) to early Miocene and Pliocene to Pleistocene in age. In addition, 0.4 m of lower Pliocene chalk was recovered in Hole 829A. Middle Miocene through upper Miocene rocks are missing at Site 829.

The lithostratigraphic sequence encountered at Site 829 is complicated by tectonics. Twenty-one lithostratigraphic units were recognized (see "Lithostratigraphy" section, this chapter) and numbered from Unit I to Unit XXI continuously through Holes 829A, 829B, and 829C. Lithologies and ages suggest that 20 of these units can be grouped into four composite units. We named the composite units Bigwan Wan, Bigwan Tu, Bigwan Tri, and Bigwan Fo (Fig. 63). The only unit not included in the four composite units is the short interval (0.4 m) of lower Pliocene chalk (Unit VIII).

Bigwan Wan is comprised of 10 lithostratigraphic units (Fig. 63; see "Lithostratigraphy" section, this chapter) that range in thickness between 0.15 and 72.5 m. Bigwan Wan is

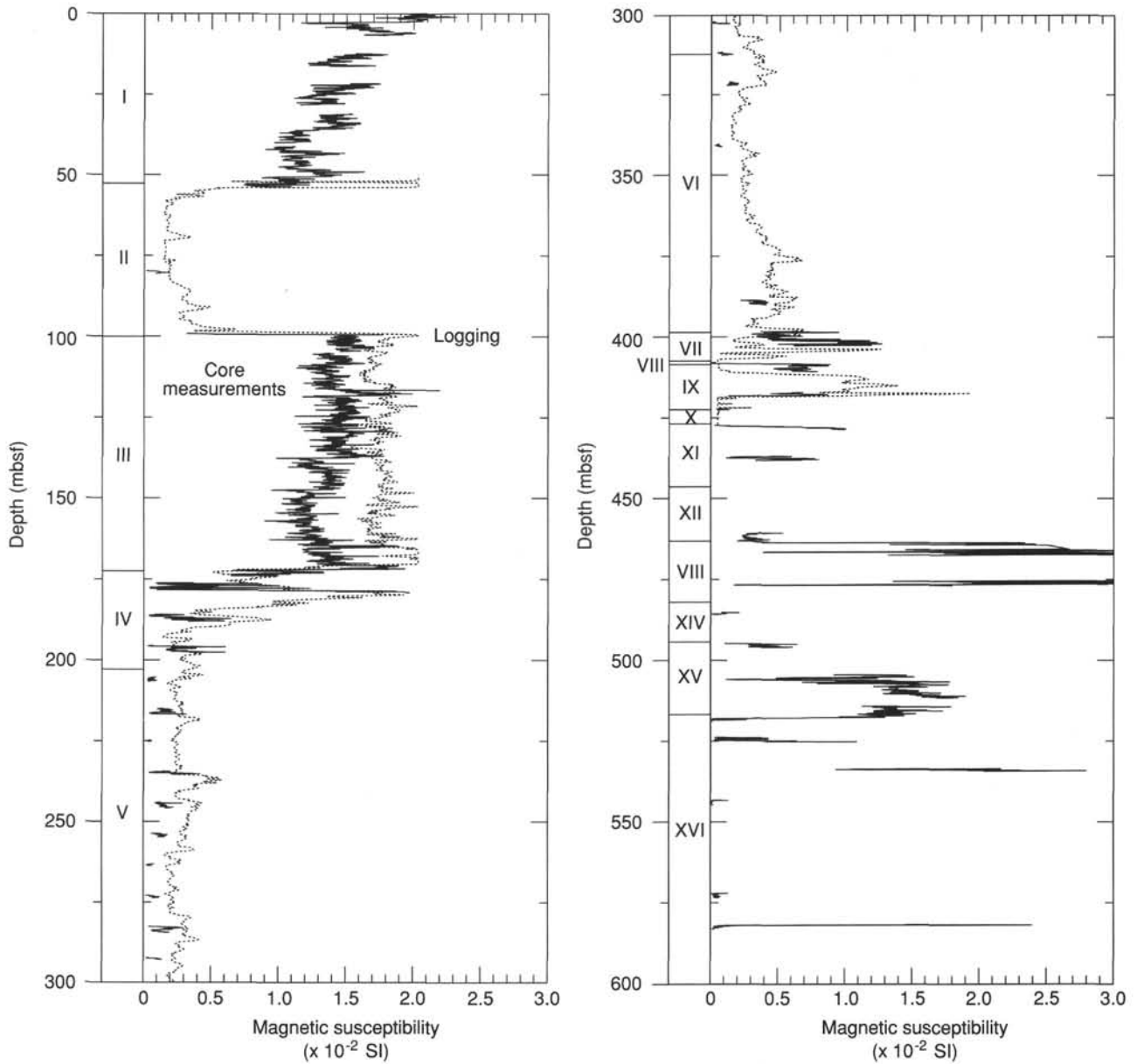


Figure 49. A plot of magnetic susceptibility vs. depth from Hole 829A. The solid line corresponds to whole-core susceptibility measurements and the dashed line corresponds to the downhole log of magnetic susceptibility. These data have not been corrected for the variation in hole diameter, nor has drift been corrected; the absolute susceptibility value was not calculated. Nonetheless, the relative variations in the logging data agree well with measurements of whole cores using the susceptibility meter on the MST. The susceptibility log provides valuable information where core recovery was poor.

composed of dark greenish gray to gray, Pliocene to Pleistocene volcanic silt, siltstone, sandstone, and silty chalk locally interbedded with ash and normally graded volcanic sand. Sediments of Bigwan Wan are interpreted as hemipelagic and turbiditic deposits.

Bigwan Tu consists of six lithostratigraphic units (Fig. 63; see "Lithostratigraphy" section, this chapter) that are 2.7 to 87.6 m thick and which are all pelagic deposits. Bigwan Tu is a light brown to light gray lower Oligocene to lower Miocene foraminiferal to calcareous chalk. Upper Eocene chalk is represented by only one sample in one lithostratigraphic unit (Unit XII, Fig. 63; see also "Biostratigraphy" section, this chapter). The lower contacts of the chalk units in Bigwan Tu are associated with thin (~10 cm) layers of brown clay.

Bigwan Tri is composed of two lithostratigraphic units (Fig. 63; see "Lithostratigraphy" section, this chapter) that are 33.3 and 106.1 m thick. Bigwan Tri is a sed-lithic breccia consisting of chalk breccia and chalk-siltstone breccia; both breccias were deposited between the late Pliocene and Pleistocene and contain reworked upper Oligocene to lower Miocene chalk clasts. The chalk-siltstone breccia also contains angular clasts of dark greenish gray volcanic siltstone, similar to the Pleistocene siltstones of Bigwan Wan. The breccias of Bigwan Tri are sheared and fractured and are interpreted as tectono-sedimentary deposits composed primarily of elements from Bigwan Wan and Bigwan Tu.

Bigwan Fo consists of two lithostratigraphic units (Fig. 63; see "Lithostratigraphy" section, this chapter) that are

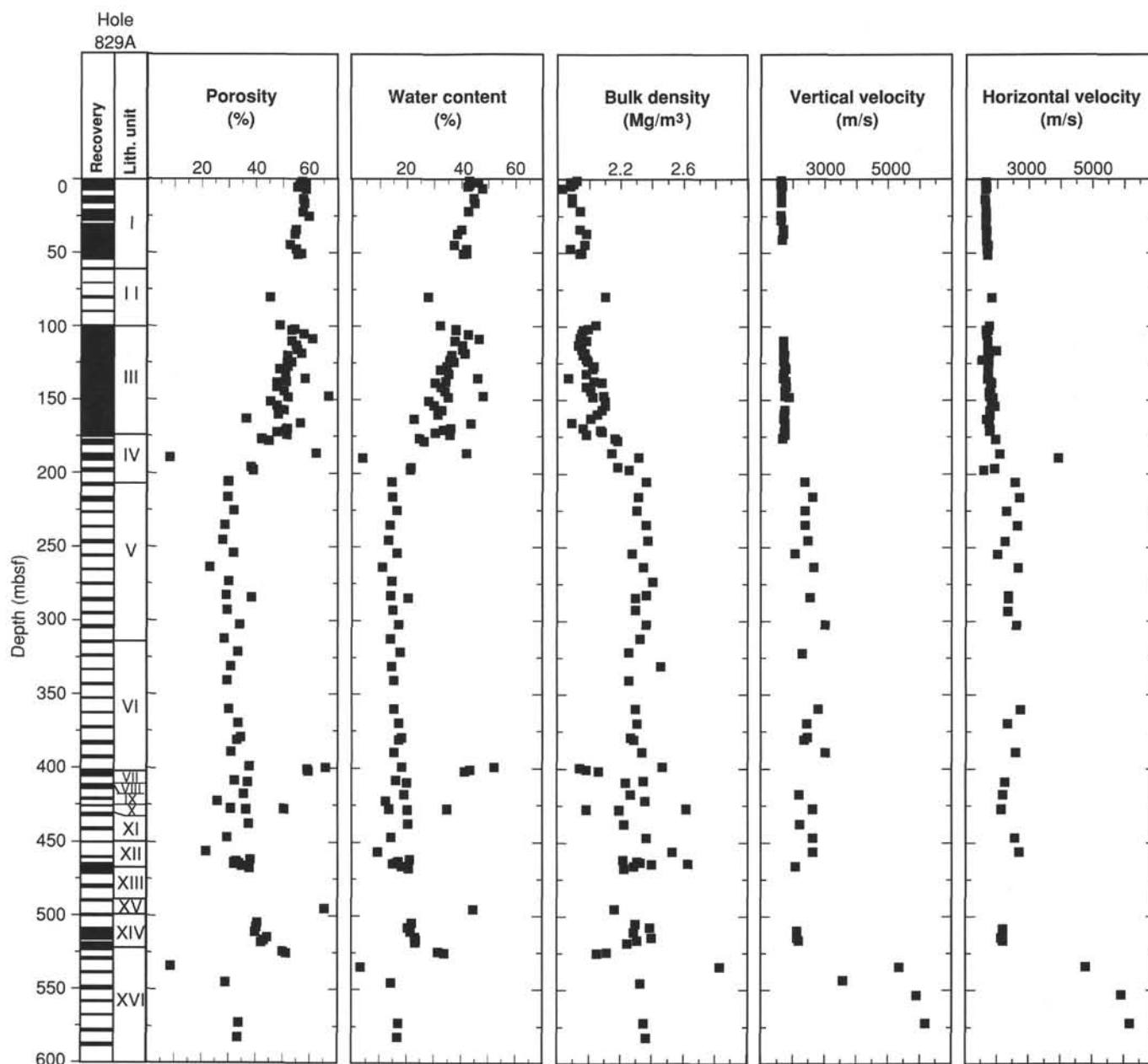


Figure 50. Index properties vs. depth, Hole 829A.

8.5 and 73.1 m thick and comprised of igneous sed-lithic breccia of unknown age. The upper lithostratigraphic unit of Bigwan Fo contains clasts of chalk, basalt, and rare fragments of plutonic rocks in a matrix of gray silt and brown clay. The lower lithostratigraphic unit consists of intervals of sed-lithic breccia interspersed with ig-lithic breccia; clasts in the sed-lithic breccia are mainly siltstone and claystone with rare igneous fragments whereas clasts in the ig-lithic breccia are primarily gabbro, diabase, and basalt.

The 590-m-thick sequence drilled in Hole 829A is characterized by tectonically repeated intervals of the four Bigwan units. Eight major tectonic units are defined by thrust faults.

Tectonic Unit A (0–99.4 mbsf) consists of dark volcanic Pleistocene silt (Bigwan Wan) overlying upper Oligocene to lower Miocene chalk (Bigwan Tu). This tectonic unit is relatively undeformed with respect to the other tectonic units. At the base of tectonic Unit A, Bigwan Tu is in sharp contact with a lower

interval of Bigwan Wan in tectonic Unit B, but no direct evidence of faulting was observed in the cores. The contact is interpreted here as a thrust fault, however, because of the inverted stratigraphy and a brown clay layer found between tectonic Units A and B and because of possible reverse faults in the lower part of tectonic Unit A (Fig. 63; see “Lithostratigraphy” and “Structural Studies” sections, this chapter).

Tectonic Unit B (99.4–172 mbsf) is an interval of Bigwan Wan that indicates brittle deformation. The base of tectonic Unit B is marked by a lithologic change from the volcanic silt of Bigwan Wan to highly deformed sed-lithic breccia (Bigwan Tri) in the underlying tectonic Unit C.

Tectonic Unit C (172–311 mbsf) is equivalent to Bigwan Tri and consists of upper Pliocene(?) to Pleistocene chalk-siltstone and chalk breccia containing reworked clasts of late Oligocene to early Miocene age (Fig. 63). Near the top of tectonic Unit C (172–187 mbsf), brittle-ductile microshear

Table 7. Index properties data, Site 829.

Sample (cm)	Depth (mbsf)	Unit	Wet-bulk density (Mg/m ³)	Dry-bulk density (Mg/m ³)	Grain density (Mg/m ³)	Porosity		Water content	
						Wet (%)	Dry (%)	Wet (%)	Dry (%)
134-829A-									
1R-1, 130	1.30	I	1.92	1.35	2.77	56.6	54.1	30.1	43.1
1R-2, 120	2.70	I	1.88	1.28	2.74	58.1	55.7	31.7	46.5
2R-1, 87	3.67	I	1.90	1.33	2.72	55.8	53.6	30.1	43.1
2R-2, 87	5.17	I	1.88	1.32	2.72	54.8	53.2	29.8	42.5
2R-3, 87	6.67	I	1.83	1.24	2.64	57.9	55.5	32.4	47.9
3R-1, 100	13.30	I	1.89	1.31	2.73	57.0	54.6	30.8	44.6
3R-3, 100	16.30	I	1.89	1.30	2.71	57.4	54.7	31.1	45.1
4R-1, 37	21.97	I	1.94	1.36	2.72	56.8	53.4	30.0	42.8
5R-3, 37	34.37	I	1.94	1.38	2.56	54.4	50.5	28.7	40.3
5R-5, 37	37.37	I	1.98	1.43	2.68	54.0	50.6	27.9	38.8
6R-3, 37	44.47	I	1.97	1.43	2.75	52.3	50.3	27.2	37.4
6R-5, 37	47.47	I	1.88	1.32	2.55	54.4	51.5	29.6	42.1
6R-7, 37	50.47	I	1.95	1.37	2.76	56.4	53.4	29.6	42.1
7R-1, 37	51.17	I	1.94	1.38	2.73	55.0	52.3	29.0	40.9
10R-1, 33	80.03	II	2.10	1.64	2.72	44.8	42.8	21.8	28.0
12R-1, 27	99.27	II	2.04	1.54	2.74	48.5	46.5	24.4	32.2
12R-2, 137	101.87	III	1.99	1.44	2.74	53.7	50.8	27.7	38.2
12R-3, 37	102.37	III	1.96	1.42	2.72	52.7	50.5	27.5	38.0
12R-5, 37	105.37	III	1.95	1.37	2.71	57.2	53.4	30.0	42.8
12R-7, 37	108.37	III	1.94	1.32	2.71	60.3	55.6	31.8	46.7
13R-1, 120	109.80	III	1.98	1.44	2.71	52.8	50.2	27.4	37.7
13R-3, 120	112.80	III	1.93	1.38	2.70	54.4	51.9	28.8	40.5
13R-5, 120	115.80	III	1.95	1.39	2.71	54.7	51.9	28.8	40.4
13R-7, 65	118.25	III	1.97	1.39	2.45	56.3	50.0	29.3	41.5
14R-1, 130	119.50	III	1.96	1.44	2.74	51.1	49.5	26.7	36.4
14R-3, 130	122.50	III	1.98	1.46	2.72	51.1	49.0	26.4	35.9
14R-4, 130	124.00	III	1.99	1.45	2.76	52.9	50.5	27.3	37.5
14R-6, 130	127.00	III	2.03	1.50	2.72	51.4	48.4	25.9	35.0
15R-1, 115	129.05	III	2.02	1.52	2.67	48.4	46.2	24.6	32.5
15R-3, 115	132.05	III	1.98	1.46	2.65	50.6	48.1	26.2	35.4
15R-5, 115	135.05	III	1.87	1.28	2.76	57.8	55.7	31.6	46.2
15R-7, 60	137.50	III	2.03	1.51	2.68	50.8	47.6	25.7	34.5
16R-1, 57	138.07	III	2.08	1.60	2.77	47.5	45.5	23.4	30.5
16R-3, 57	141.07	III	1.98	1.49	2.57	47.6	45.4	24.7	32.8
16R-5, 57	144.07	III	2.01	1.50	2.74	50.0	48.0	25.4	34.1
16R-7, 57	147.07	III	2.09	1.41	2.44	66.3	53.7	32.5	48.2
17R-1, 55	147.75	III	2.02	1.49	2.66	51.4	48.1	26.1	35.3
17R-3, 55	150.75	III	2.10	1.64	2.71	45.1	43.0	22.0	28.2
17R-5, 55	153.75	III	2.10	1.61	2.71	47.5	44.6	23.2	30.2
17R-7, 55	156.75	III	2.08	1.56	2.68	50.1	46.4	24.7	32.9
18R-2, 137	159.67	III	2.05	1.56	2.73	47.8	45.8	23.9	31.5
18R-4, 137	162.67	III	2.01	1.64	2.92	36.5	39.7	18.6	22.8
18R-6, 137	165.67	III	1.89	1.32	2.70	56.1	53.7	30.3	43.6
19R-2, 97	168.97	III	1.96	1.44	2.72	51.1	49.3	26.6	36.3
19R-3, 97	170.47	III	2.07	1.55	2.76	50.7	47.7	25.1	33.5
19R-4, 97	171.97	IV	2.08	1.59	2.72	47.4	45.0	23.4	30.5
19R-5, 97	173.47	IV	1.98	1.46	2.74	51.0	49.2	26.4	35.9
20R-1, 26	176.36	IV	2.16	1.73	2.74	41.8	40.1	19.8	24.8
20R-2, 23	177.83	IV	2.18	1.73	2.86	44.4	42.6	20.8	26.3
21R-1, 24	186.04	IV	2.14	1.51	2.75	61.8	53.3	29.6	42.1
21R-3, 28	189.08	IV	2.31	2.22	2.68	8.2	9.1	3.7	3.8
22R-1, 37	195.87	IV	2.18	1.79	2.68	37.9	36.3	17.8	21.6
22R-2, 36	197.36	IV	2.25	1.85	2.70	38.7	36.3	17.6	21.4
23R-1, 33	205.53	V	2.36	2.06	2.70	29.4	28.0	12.8	14.6
24R-1, 84	215.74	V	2.31	2.01	2.71	29.4	28.6	13.1	15.0
25R-1, 28	224.88	V	2.30	1.97	2.70	31.8	30.5	14.2	16.5
26R-1, 64	234.94	V	2.36	2.07	2.69	28.4	27.1	12.3	14.0
27R-1, 133	245.23	V	2.37	2.09	2.64	27.5	26.0	11.9	13.5
28R-1, 30	253.90	V	2.27	1.95	2.70	31.5	30.5	14.2	16.6
29R-1, 30	263.40	V	2.34	2.10	2.72	22.9	23.0	10.1	11.2
30R-1, 30	273.10	V	2.40	2.10	2.61	29.9	27.3	12.7	14.6
31R-1, 23	282.63	V	2.36	2.07	2.71	28.8	27.5	12.5	14.2
31R-2, 29	284.17	V	2.29	1.90	2.75	38.2	35.9	17.1	20.7
32R-1, 31	292.41	V	2.29	1.99	2.67	29.2	28.4	13.1	15.0
33R-1, 54	302.34	V	2.36	2.01	2.75	33.9	31.8	14.7	17.2

folds and shear-band structures suggest thrusting and reverse faulting along steeply dipping (50°–80°) planes (see “Structural Studies” section, this chapter). These data are evidence that tectonic Units B and C are separated by a thrust fault zone. Near 244–260 mbsf, a second zone of tectonic deformation is implied by a brittle-ductile shear zone and brittle

deformation that has produced highly brecciated rocks, and minor thrust faults may also occur here (Fig. 63).

Tectonic Unit D (311–405 mbsf) consists of chalk (Bigwan Tu) overlying volcanic breccia (Bigwan Fo; Fig. 63). These rocks are highly brecciated as a result of brittle deformation. The occurrence of a 2-m-thick shear zone with a planar fabric

Table 7 (continued).

Sample (cm)	Depth (mbsf)	Unit	Wet-bulk density (Mg/m ³)	Dry-bulk density (Mg/m ³)	Grain density (Mg/m ³)	Porosity		Water content	
						Wet (%)	Dry (%)	Wet (%)	Dry (%)
34R-1, 33	311.63	VI	2.32	2.04	2.67	28.2	27.2	12.4	14.2
35R-1, 38	320.88	VI	2.25	1.91	2.71	33.2	32.2	15.1	17.8
36R-CC, 14	330.34	VI	2.45	2.13	2.75	30.7	28.5	12.8	14.7
37R-1, 29	340.09	VI	2.25	1.95	2.60	29.3	28.3	13.4	15.4
39R-1, 40	359.50	VI	2.29	1.98	2.65	29.8	28.7	13.3	15.4
40R-1, 34	369.14	VI	2.30	1.96	2.72	33.1	31.7	14.8	17.3
41R-1, 30	378.70	VI	2.26	1.91	2.65	34.1	32.4	15.5	18.3
41R-3, 30	380.21	VI	2.28	1.95	2.70	32.9	31.5	14.8	17.3
42R-1, 40	388.50	VI	2.33	2.05	2.67	30.6	28.9	13.4	15.5
43R-1, 103	398.73	VI	2.46	2.07	2.59	37.3	31.9	15.5	18.4
43R-1, 120	398.90	VII	1.94	1.27	2.58	65.3	57.2	34.4	52.5
43R-2, 103	400.23	VII	1.98	1.38	2.58	58.5	52.6	30.3	43.5
43R-3, 95	401.65	VII	2.06	1.46	2.40	59.1	49.6	29.3	41.5
44R-1, 35	407.75	VIII	2.34	2.01	2.69	32.0	30.2	14.0	16.3
44R-2, 35	409.25	IX	2.23	1.85	2.67	36.7	34.7	16.8	20.2
45R-1, 57	417.17	IX	2.26	1.90	2.74	35.4	34.0	16.1	19.1
46R-1, 27	421.87	X	2.35	2.09	2.70	25.6	25.0	11.1	12.5
47R-1, 10	426.70	X	2.61	2.29	3.00	30.7	28.8	12.1	13.7
47R-1, 48	427.08	X	1.98	1.47	2.70	50.0	48.1	25.8	34.9
47R-1, 93	427.53	XI	2.19	1.82	2.64	36.2	34.7	16.9	20.4
48R-1, 37	436.67	XI	2.22	1.84	2.70	37.2	35.5	17.2	20.7
49R-CC, 10	446.00	XII	2.36	2.06	2.76	29.2	28.4	12.7	14.5
50R-1, 20	455.80	XII	2.52	2.30	2.73	21.5	20.4	8.7	9.5
51R-1, 100	461.10	XII	2.21	1.83	2.63	37.8	35.5	17.5	21.2
51R-2, 72	462.32	XII	2.30	1.96	2.73	32.6	31.3	14.5	17.0
51R-3, 0	463.10	XIII	2.32	2.00	2.71	31.9	30.4	14.1	16.4
51R-3, 72	463.82	XIII	2.62	2.28	3.12	33.6	31.6	13.1	15.1
51R-CC, 13	464.09	XIII	2.39	2.06	2.70	31.8	29.6	13.6	15.8
52R-1, 27	465.47	XIII	2.28	1.93	2.75	34.5	33.1	15.5	18.3
52R-2, 30	467.00	XIII	2.22	1.84	2.67	37.4	35.4	17.2	20.8
55R-1, 38	494.48	XIV	2.16	1.49	1.89	65.0	45.6	30.9	44.6
56R-1, 37	504.17	XV	2.29	1.88	2.72	40.4	37.1	18.0	22.0
56R-3, 28	507.08	XV	2.38	1.97	2.78	39.9	36.2	17.2	20.7
56R-5, 37	510.17	XV	2.28	1.87	2.72	39.5	36.7	17.8	21.6
57R-1, 46	513.96	XV	2.39	1.94	2.75	44.0	38.5	18.8	23.2
57R-2, 73	515.73	XV	2.30	1.86	2.80	42.8	39.5	19.1	23.6
57R-3, 82	517.32	XVI	2.24	1.82	2.78	41.6	39.1	19.0	23.4
58R-1, 24	523.44	XVI	2.11	1.60	2.68	49.7	45.7	24.1	31.8
58R-1, 137	524.57	XVI	2.05	1.53	2.60	50.8	46.6	25.4	34.0
59R-1, 74	533.64	XVI	2.82	2.73	2.85	8.7	8.4	3.2	3.3
60R-2, 20	544.30	XVI	2.32	2.02	2.71	28.6	27.9	12.6	14.5
63R-1, 37	571.87	XVI	2.34	2.00	2.69	33.4	31.2	14.6	17.1
64R-1, 49	581.69	XVI	2.36	2.02	2.72	33.1	31.0	14.4	16.8
134-829C-									
1H-2, 60	2.10	XVIII	1.91	1.34	2.68	55.3	52.8	29.7	42.2
1H-4, 60	5.10	XVIII	2.00	1.43	2.66	55.6	51.1	28.5	39.8
2H-1, 140	9.70	XVIII	2.09	1.47	2.68	60.1	52.4	29.5	41.8
2H-4, 140	14.20	XVIII	1.93	1.36	2.63	55.2	51.9	29.4	41.6
2H-6, 140	17.20	XVIII	2.00	1.41	2.69	57.0	52.3	29.2	41.3
3H-2, 125	20.55	XVIII	1.96	1.39	2.71	55.5	52.2	29.0	40.9
3H-4, 135	23.65	XVIII	1.96	1.38	2.71	56.4	52.8	29.5	41.8
3H-6, 140	26.70	XVIII	1.94	1.37	2.70	55.8	52.7	29.5	41.8
4H-2, 110	29.90	XVIII	1.97	1.41	2.73	54.1	51.3	28.2	39.2
5H-1, 130	31.60	XVIII	1.71	1.15	2.23	54.5	51.6	32.6	48.5
5H-3, 130	34.60	XVIII	1.89	1.30	2.69	57.9	54.8	31.4	45.7
5H-5, 120	37.50	XVIII	1.96	1.37	2.74	57.3	53.7	30.0	42.9
7H-1, 105	48.55	XVIII	1.86	1.27	2.69	57.6	55.2	31.7	46.5
8H-1, 135	51.35	XVIII	1.94	1.40	2.70	53.1	50.9	28.0	39.0
9H-2, 130	54.80	XIX	1.94	1.38	2.34	54.8	48.4	28.9	40.7
9H-4, 132	57.82	XX	1.94	1.38	2.72	54.5	52.1	28.8	40.5
9H-5, 117	59.17	XXI	1.77	1.15	2.70	60.1	58.7	34.8	53.3
9H-6, 76	60.26	XXI	2.01	1.51	2.73	48.4	46.9	24.7	32.8
10H-1, 42	57.72?	XXI	1.93	1.36	2.71	56.1	53.0	29.7	42.2

dipping 20°–40° at the base of tectonic Unit D suggests the presence of a major thrust zone. Clay minerals in this interval are evidence that ductile deformation did not occur under high temperature.

Tectonic Unit E (405–463 mbsf) is a highly sheared and deformed unit consisting of two repeated sections (Subunits E₁ and E₂, Fig. 63) of Pliocene to Pleistocene silty chalk

(Bigwan Wan) overlying Oligocene chalk (Bigwan Tu). The two subunits are separated by a minor shear zone that dips 20° and which is composed of laminae of brown clay. The base of tectonic Unit E is marked by a 3.1-m-thick, well-preserved shear zone that may have undergone two stages of deformation and brown clay laminae (see “Structural Studies” section, this chapter).

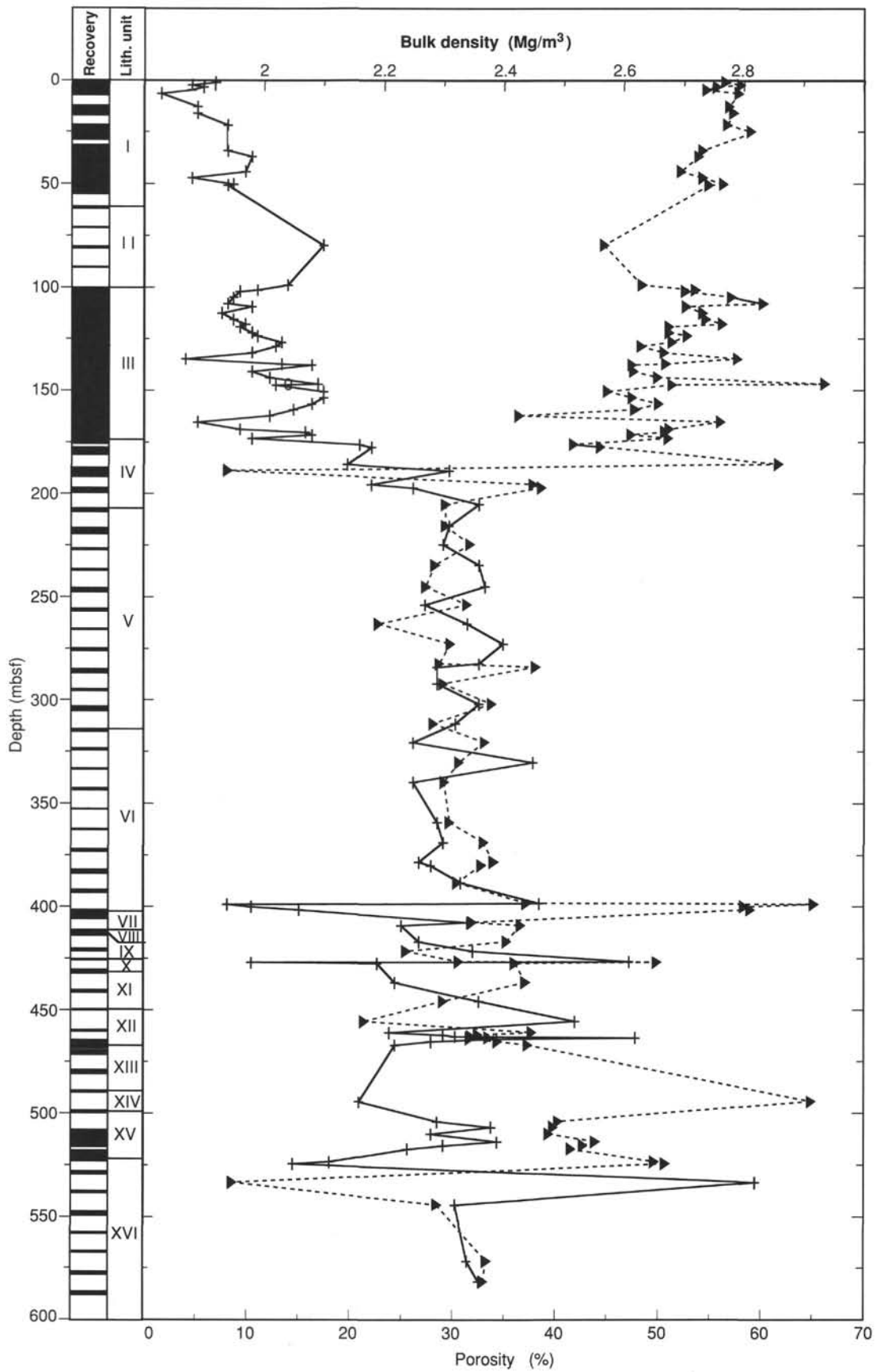


Figure 51. Bulk density (crosses) and porosity (triangles) vs. depth, Site 829.

Table 8. Vertical and horizontal velocity data, Site 829.

Core, section, interval (cm)	Depth (mbsf)	Unit	Vertical velocity (m/s)	Wave type ^a	Horizontal velocity (m/s)	Wave type ^a
134-829A-						
1R-1, 130	1.30	I	1640	C	1639	C
1R-2, 120	2.70	I			1638	C
2R-1, 87	3.67	I	1619	C	1620	C
2R-2, 87	5.17	I	1652	C	1658	C
2R-3, 87	6.67	I	1627	C	1627	C
3R-1, 100	13.30	I	1625	C	1605	C
3R-3, 100	16.30	I	1641	C	1622	C
4R-1, 37	21.97	I			1636	C
4R-3, 37	24.97	I	1613	C	1626	C
4R-5, 37	27.97	I	1626	C	1633	C
5R-1, 37	31.37	I			1641	C
5R-3, 37	34.37	I	1704	C	1672	C
5R-5, 37	37.37	I	1688	C	1656	C
6R-1, 37	41.47	I	1659	C	1656	C
6R-3, 30	44.40	I			1701	C
6R-5, 37	47.47	I			1667	C
6R-7, 30	50.40	I			1677	C
7R-1, 37	51.17	I			1695	C
10R-1, 33	80.03	II			1816	C
12R-1, 10	99.10	II			1737	C
12R-2, 143	101.93	III			1700	C
12R-3, 30	102.30	III			1638	C
12R-5, 37	105.37	III			1662	C
13R-1, 120	109.80	III	1703	C	1693	C
13R-3, 120	112.80	III	1691	C	1686	C
13R-5, 120	115.80	III	1691	S	1965	S
13R-7, 65	118.25	III	1702	C	1694	C
14R-1, 130	119.50	III	1733	C	1734	C
14R-3, 130	122.50	III	1711	C	1522	C
14R-4, 130	124.00	III	1717	C	1726	C
14R-6, 130	127.00	III	1750	C	1719	C
15R-1, 115	129.05	III	1769	S	1700	C
15R-3, 115	132.05	III	1721	C	1722	C
15R-5, 115	135.05	III	1685	C	1680	C
15R-7, 60	137.50	III	1774	C	1778	C
16R-1, 57	138.07	III			1831	C
16R-3, 57	141.07	III	1798	C	1781	C
16R-5, 60	144.10	III	1738	C	1745	C
16R-7, 57	147.07	III	1738	C	1748	C
17R-1, 55	147.75	III	1889	C	1851	C
17R-3, 58	150.78	III			1820	C
17R-5, 58	153.78	III			1930	C
17R-7, 55	156.75	III	1736	C	1776	C
18R-2, 137	159.67	III	1733	C	1761	C
18R-4, 137	162.67	III	1708	C	1645	S
18R-6, 137	165.67	III	1746	C	1741	C
19R-2, 97	168.97	III	1755	C	1773	C
19R-3, 97	170.47	III			1754	C
19R-4, 97	171.97	IV	1732	C		
19R-5, 97	173.47	IV	1736	C		
20R-1, 26	176.36	IV	1678	C	1942	C
21R-1, 18	185.98	IV			2078	C
21R-3, 20	189.00	IV			3915	C

Tectonic Unit F (463–494.4 mbsf) is another interval in which Bigwan Wan overlies Bigwan Tu. At the top of tectonic Unit F, well-stratified volcanic sandstone of Bigwan Wan is strongly deformed. Foliation dips 20°–30°, parallel to the bedding of the sandstone. The chalk of tectonic Unit F is a tectonic breccia and contains a possible thrust plane that marks the contact with the underlying tectonic Unit G.

Tectonic Unit G (494.4–524.6 mbsf) is an interval of Bigwan Wan overlying Bigwan Fo (Fig. 63). This tectonic unit displays fractures and microshear folds; some microfolds may be the result of syndimentary processes. The base of tectonic Unit G is marked by a major 3-m-thick shear zone composed of intensely deformed horizons with planar fabrics dipping 0°–30°; this deformation occurs within the igneous sed-lithic breccia of Bigwan Fo.

Table 8 (continued).

Core, section, interval (cm)	Depth (mbsf)	Unit	Vertical velocity (m/s)	Wave type ^a	Horizontal velocity (m/s)	Wave type ^a
134-829C-						
22R-1, 40	195.90	IV			1915	C
22R-2, 23	197.23	IV			1571	C
23R-1, 33	205.53	V	2377	C	2554	C
24R-1, 84	215.74	V	2626	C	2701	C
25R-1, 28	224.88	V	2388	C	2290	C
26R-1, 64	234.94	V	2400	C	2632	C
27R-1, 133	245.23	V	2479	C	2237	S
28R-1, 30	253.90	V	2065	C	2015	C
29R-1, 30	263.40	V	2664	C	2653	C
31R-1, 30	282.70	V			2353	C
31R-1, 125	283.65	V	2543	C		
31R-2, 30	284.18	V			2343	C
32R-1, 52	292.62	V			2339	C
33R-1, 55	302.35	V	3027	C	2597	C
35R-1, 91	321.41	VI	2305	C		
39R-1, 40	359.50	VI	2812	C	2728	C
40R-1, 34	369.14	VI	2449	C	2320	C
41R-1, 0	378.40	VI	2461	C		
41R-3, 30	380.21	VI	2371	C		
42R-1, 40	388.50	VI	3022	C	2579	C
44R-1, 142	408.82	VIII			2239	C
45R-1, 57	417.17	IX	2210	C	2177	C
47R-1, 10	426.70	X	2628	C	2131	S
48R-1, 37	436.67	XI	2215	C		
49R-CC, 10	446.00	XII	2627	C	2545	C
50R-1, 20	455.80	XII	2644	C	2678	C
52R-1, 30	465.50	XIII	2082	C		
56R-3, 91	507.71	XV			2187	C
56R-4, 95	509.25	XV	2149	C	2178	C
57R-1, 46	513.96	XV	2138	C	2129	C
57R-2, 73	515.73	XV	2191	C	2177	C
59R-1, 74	533.64	XVI	5358	C	4787	C
60R-1, 20	542.80	XVI	3585	C		
61R-1, 30	552.60	XVI	5902	C	5902	C
63R-1, 7	571.57	XVI	6178	C	6178	C
134-829C-						
1H-2, 60	2.10	XVIII	1660	C	1655	C
1H-4, 60	5.10	XVIII	1665	C	1679	C
2H-1, 140	9.70	XVIII	1645	C	1651	C
2H-4, 140	14.20	XVIII	1612	C	1601	C
2H-6, 140	17.20	XVIII	1642	C	1652	C
3H-2, 125	20.55	XVIII	1660	C	1651	C
3H-4, 135	23.65	XVIII	1676	C	1684	S
3H-6, 140	26.70	XVIII	1672	C	1664	C
4H-2, 110	29.90	XVIII	1666	C	1586	C
5H-1, 130	31.60	XVIII	1660	C	1642	C
5H-3, 130	34.60	XVIII	1657	C	1647	C
5H-5, 120	37.50	XVIII	1662	C	1685	S
8H-1, 135	51.35	XVIII			1705	C
9H-2, 130	54.80	XIX			1686	C
9H-4, 132	57.82	XX	1683	C	1646	C
10H-1, 42	57.72?	XX	1717	C	1709	C

^a C = compressional (P-wave) and S = shear (S-wave).

Tectonic Unit H (524.6–590.6 mbsf) consists of undated igneous sed-lithic breccia in Bigwan Fo. Near 590.6 mbsf, the total depth of Hole 829A, the breccias are deformed by sheared horizons with planar fabrics dipping 0°–30°.

In summary, the section recovered at Site 829 is characterized by tectonically repeated intervals of Bigwan Wan overlying Bigwan Tu. However, in one case, Bigwan Wan (tectonic Unit B) is separated from Bigwan Tu (tectonic Unit D) by Bigwan Tri (tectonic Unit C). Bigwan Tri is interpreted as a tectono-sedimentary melange formed by erosion of previously imbricated thrust sheets (see “Structural Studies” section, this chapter). In another case, within tectonic Unit G, Bigwan Wan directly overthrusts Bigwan Fo; here, Bigwan Wan could have been incorporated into the accretionary complex as an individual thrust.

Table 9. Shear-strength data, Site 829.

Sample (cm)	Depth (mbsf)	Unit	Shear strength ^a (kPa)
134-829A-			
1R-1, 126	1.26	I	25.7
1R-2, 114	2.64	I	14.7
2R-1, 94	3.74	I	27.1
2R-2, 94	5.24	I	27.1
2R-3, 82	6.62	I	29.3
3R-1, 106	13.36	I	33.0
3R-3, 96	16.26	I	23.1
4R-1, 35	21.95	I	22.7
4R-3, 31	24.91	I	63.1
4R-5, 32	27.92	I	49.1
5R-1, 35	31.35	I	58.7
5R-3, 31	34.31	I	77.0
5R-5, 45	37.45	I	66.7
134-829C-			
1H-2, 55	2.05	XVIII	53.5
1H-4, 55	5.05	XVIII	98.2
2H-1, 136	9.66	XVIII	77.7
2H-4, 147	14.27	XVIII	96.0
2H-6, 146	17.26	XVIII	44.0
3H-2, 112	20.42	XVIII	142.2
3H-4, 141	23.71	XVIII	112.2
3H-6, 136	26.66	XVIII	71.1
4H-2, 96	29.76	XVIII	90.2
5H-1, 139	31.69	XVIII	148.8
5H-3, 130	34.60	XVIII	90.9
5H-3, 137	34.67	XVIII	90.9
5H-5, 95	37.25	XVIII	122.4
7H-1, 97	48.47	XVIII	81.4
8H-1, 145	51.45	XVIII	112.9
9H-2, 125	54.75	XIX	31.5
9H-4, 127	57.77	XX	23.5
9H-5, 13	58.13	XX	2.2
9H-6, 91	60.41	XX	41.1
10H-1, 28	57.58?	XX	75.5

^aValues determined by Wykeham-Farrance spring vane-shear apparatus.

The dip of the thrusts that separates the eight tectonic units in Hole 829A is constrained by structural, paleomagnetic, and FMS data. Structures in a core oriented by paleomagnetism indicate that the thrust zone at the base of tectonic Unit E dips northeast. The FMS data indicate that most of the structures between 190 and 460 mbsf dip northeast to southeast. From these observations, we assume that all tectonic units dip eastward. Based on structural data, thrust dip angle decreases downhole from 50°–80° near 180 mbsf to 0°–30° at the bottom of Hole 829A. This decrease in dip angle is not obvious on FMS dipmeter data because these data do not discriminate between bedding plane and fault plane dips.

Petrologic and geochemical analyses indicate that the igneous rocks occurring as clasts in the breccias of Bigwan Fo at Site 829 are transitional in composition between MORB and IAT. The upper interval of Bigwan Fo (lithostratigraphic Unit VII) contains clasts of pyroxenite and vesicular porphyritic basalt; a fragment of serpentinite was also recovered in this interval. Geochemical analyses of the basalt in Unit VII show that many of the trace elements concentrations (Ce to V; Table 3) are similar to MORB, whereas a negative Nb anomaly and enrichment in Rb and K (Fig. 17) are characteristic of IAT.

The lower interval of Bigwan Fo (lithostratigraphic Unit XVI) contains clasts of microgabbro, diabase, and less abundant gabbro and nonvesicular basalt. The gabbros have been significantly altered as indicated by serpentinized olivine and development of secondary pyrite. Although most igneous rocks in this lower interval were recovered without matrix, all pieces of gabbro have alteration rims, which suggests that

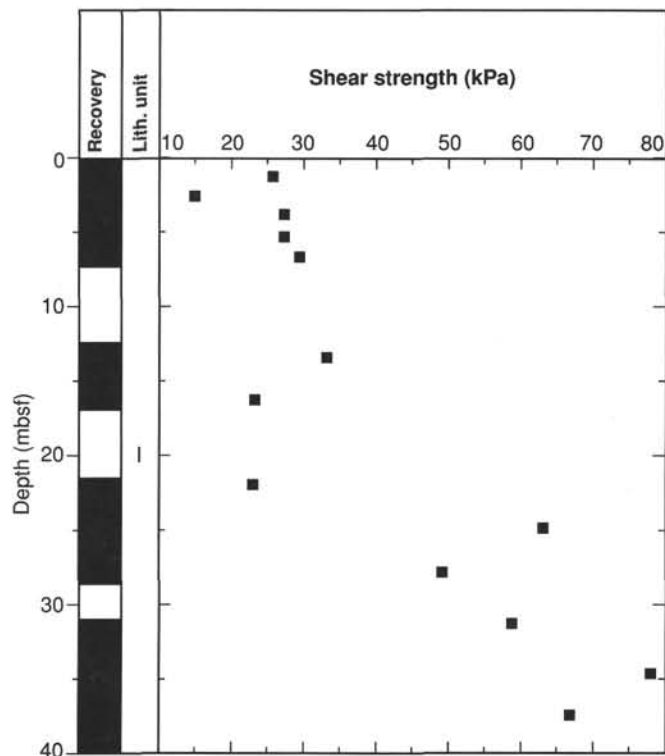


Figure 52. Shear strength vs. depth, Hole 829A.

they are clasts in a breccia. Basalt in the lower interval (lithostratigraphic Unit XVI) of Bigwan Fo differs from basalt in the upper interval (lithostratigraphic Unit VII) in that it lacks clinopyroxene phenocrysts but contains plagioclase. Geochemical analyses of the gabbro, microgabbro, and diabase from the lower interval show negative Nb anomalies (Table 3) typical of IAT, and Ni vs. Ti ratios (Fig. 20) that are indicative of MORB.

Because of obstructions downhole, Hole 829A was logged only to 475 mbsf, 115 m above total depth. The geophysical and geochemical tool strings, the FMS, the magnetic susceptibility tool, and the digital BHTV were run successively between 50 and 475 mbsf (see “Downhole Measurements” section, this chapter).

The logs are generally of good quality and help define the nature of the contacts between lithostratigraphic units. For example, a gradational contact between silty lithostratigraphic Unit I and chalky Unit II is suggested by increasing values of velocity and resistivity and a sharply increasing value of calcium. In addition, most logs recorded a sharp contact between the chalk of Unit II and the volcanic silt of Unit III. Finally, a progressive increase in velocity, density, and resistivity and an irregular decrease in magnetic susceptibility (see “Paleomagnetism” section, this chapter) between 170–200 mbsf suggest that the siltstone-chalk breccia of Unit IV represents a continuous downhole transition from the silt of Unit III to the chalk breccia of Unit V.

The complex lithostratigraphic and tectonic sequence of Units VII to XII is better defined using Fe, Ca, and resistivity logs than core descriptions. The lithologic sequence shows several alternations of Oligocene chalk with upper Pliocene(?) to Pleistocene silty chalk but thicknesses of the units are poorly defined by core description because of low (17%) recovery. The Fe, Ca, and resistivity signatures suggest that the silty chalk intervals (Units IX and XI) are thinner and the chalk intervals (Units VIII, X, and XII) are thicker than

Table 10. Thermal conductivity data, Site 829.

Sample (cm)	Depth (mbsf)	Unit	Value (W/[m · K])
134-829A-			
1R-1, 75	0.75	I	1.0676
1R-2, 75	2.25	I	0.9390
2R-2, 75	5.05	I	1.0685
2R-3, 50	6.30	I	0.9739
3R-3, 45	15.75	I	0.9672
134-829B-			
1H-1, 25	0.25	I	0.8263
2H-1, 75	1.25	I	1.0616
2H-2, 75	2.75	I	1.0770
2H-3, 75	4.25	I	1.0610
2H-4, 21	5.21	I	1.0761
3H-2, 75	12.25	I	1.0795
3H-4, 75	15.25	I	1.0791
3H-5, 75	16.75	I	1.0418
3H-6, 75	18.25	I	1.0599
134-829C-			
1H-2, 75	2.25	XVIII	1.0792
1H-3, 75	3.75	XVIII	1.0888
1H-4, 75	5.25	XVIII	1.0580
1H-5, 75	6.75	XVIII	1.0920
2H-2, 75	10.55	XVIII	1.1116
2H-3, 75	12.05	XVIII	1.0914
2H-4, 75	13.55	XVIII	1.0357
2H-5, 75	15.05	XVIII	1.0498
3H-2, 75	20.05	XVIII	1.1358
3H-3, 75	21.55	XVIII	1.0980
3H-4, 75	23.05	XVIII	1.0493
3H-5, 75	24.55	XVIII	1.0726
4H-1, 75	28.05	XVIII	1.0553
4H-2, 50	29.30	XVIII	1.0685
5H-1, 75	31.05	XVIII	1.0225
5H-2, 75	32.55	XVIII	0.9928
5H-3, 75	34.05	XVIII	1.0209
5H-5, 75	37.05	XVIII	0.9238
5H-5, 75	37.05	XVIII	0.9591
7H-1, 75	48.25	XVIII	1.0613
8H-1, 75	50.75	XVIII	1.3346
9H-1, 75	52.75	XVIII	1.0882
9H-2, 75	54.25	XVIII	1.4551
9H-3, 75	55.75	XIX	1.3820
9H-4, 75	57.25	XIX	1.2415
10H-1, 43	57.73	XX	1.3190

suggested by core descriptions. For example, the logs define intervals of silty chalk at 415–420 and 437–440 mbsf, rather than at 407.8–421.6 (Unit IX) and 427.3–445.9 mbsf (Unit XI; Fig. 63). Correspondingly, the logs suggest that chalk occurs at 405–415, 420–437, and 440–460 mbsf, rather than at 407.4–407.8 (Unit VIII), 421.6–427.3 (Unit X), and 445.9–462.9 mbsf (Unit XII; Fig. 63). However, the logging data must be further processed before true intervals can be calculated. Nevertheless, the initial implication of the log data is that the silty chalk units are 5 and 3 m thick, rather than 13.8 and 18.6 m thick, as suggested by the core description and that the chalk units are 10, 17, and 20 m thick, rather than 0.4, 5.7, and 17 m thick.

FMS data contribute information about stress and structure. During the FMS run between 150 and 400 mbsf, the southeast-northwest-oriented caliper consistently registered a diameter 2 in. larger than the southwest-northeast-oriented caliper. If this ellipticity in the hole results from tectonic stress, rather than drilling, the maximum compressive stress would be oriented northeast-southwest. Calculations based on FMS data indicate that structures intersecting the borehole dip generally eastward. For example, these data show a fault dipping 40° east at 259 mbsf in the chalk breccia of lithostratigraphic Unit V. This fault is also seen in BHTV data and is marked by a downhole increase in velocity and resistivity and

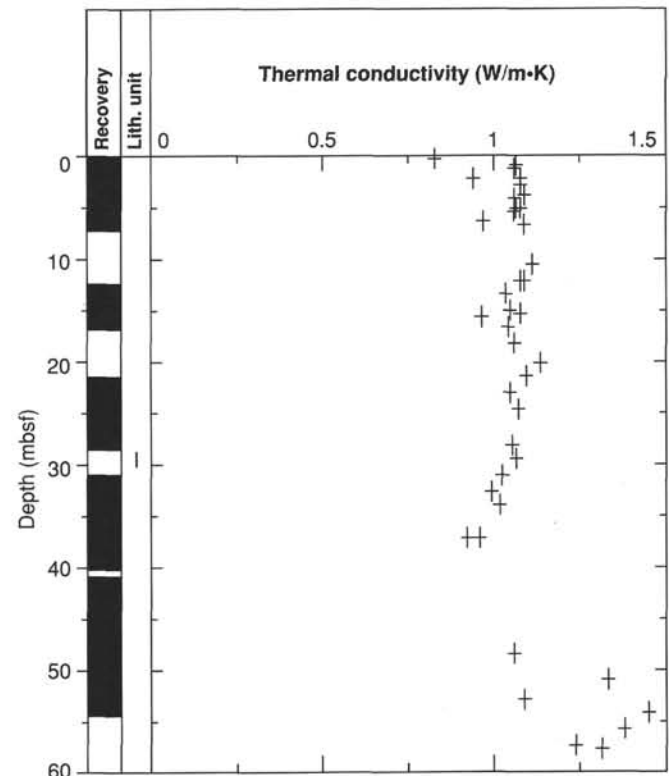


Figure 53. Thermal conductivity vs. depth, Site 829.

correlates with a zone of scaly fabric observed in the cores. Indications of a stress field possibly oriented northeast-southwest, together with evidence for eastward-dipping structures, are consistent with stresses and dips that would be expected across an eastward-dipping subduction zone.

Geochemical analyses of fluids and physical properties of rocks at Site 829 suggest that fluid content is related to structural deformation and that fluid hydrology is fault-controlled. In addition, geochemical analyses can be used to characterize the fluids in the thrust zones.

Relatively undeformed silt, siltstone, and chalk in the interval 0–170 mbsf (lithostratigraphic Units I–III) show a general downhole decrease in water content, from 42% to 30%, and a corresponding decrease in porosity, from 58% to 48% (Fig. 63). Fluid yields are consistent with water content measurements, decreasing from about 8 cm³/cm at the surface to <1 cm³/cm at 200 mbsf (see Fig. 22, “Sediment and Fluid Geochemistry” section, this chapter). The chalk in Unit II was poorly recovered but the few available analyses suggest that the chalk is drier than the silt, with a water content of about 28% and a porosity of about 45%. The thrust contact between chalk and silt at 99 mbsf is marked by distinctly higher water content (up to 38%) and porosity (up to 54%). In addition, concentration gradients of ammonia, phosphate, alkalinity, sulfate, calcium, and magnesium all exhibit discontinuities across this thrust fault (Fig. 25).

The interval between 170 and 200 mbsf records a transition from wet rocks above 170 mbsf, to rocks below 200 mbsf that are dry except at thrust faults. The transitional interval is a thrust fault consisting of highly deformed and sheared chalk-siltstone breccia (lithostratigraphic Unit IV). This zone is characterized by wide-ranging values of water content (4%–40%) and porosity (8%–60%; Fig. 63).

Below 200 mbsf, highly deformed and sheared rocks (i.e., chalk breccia, chalk, and volcanic breccia, siltstone, sand-

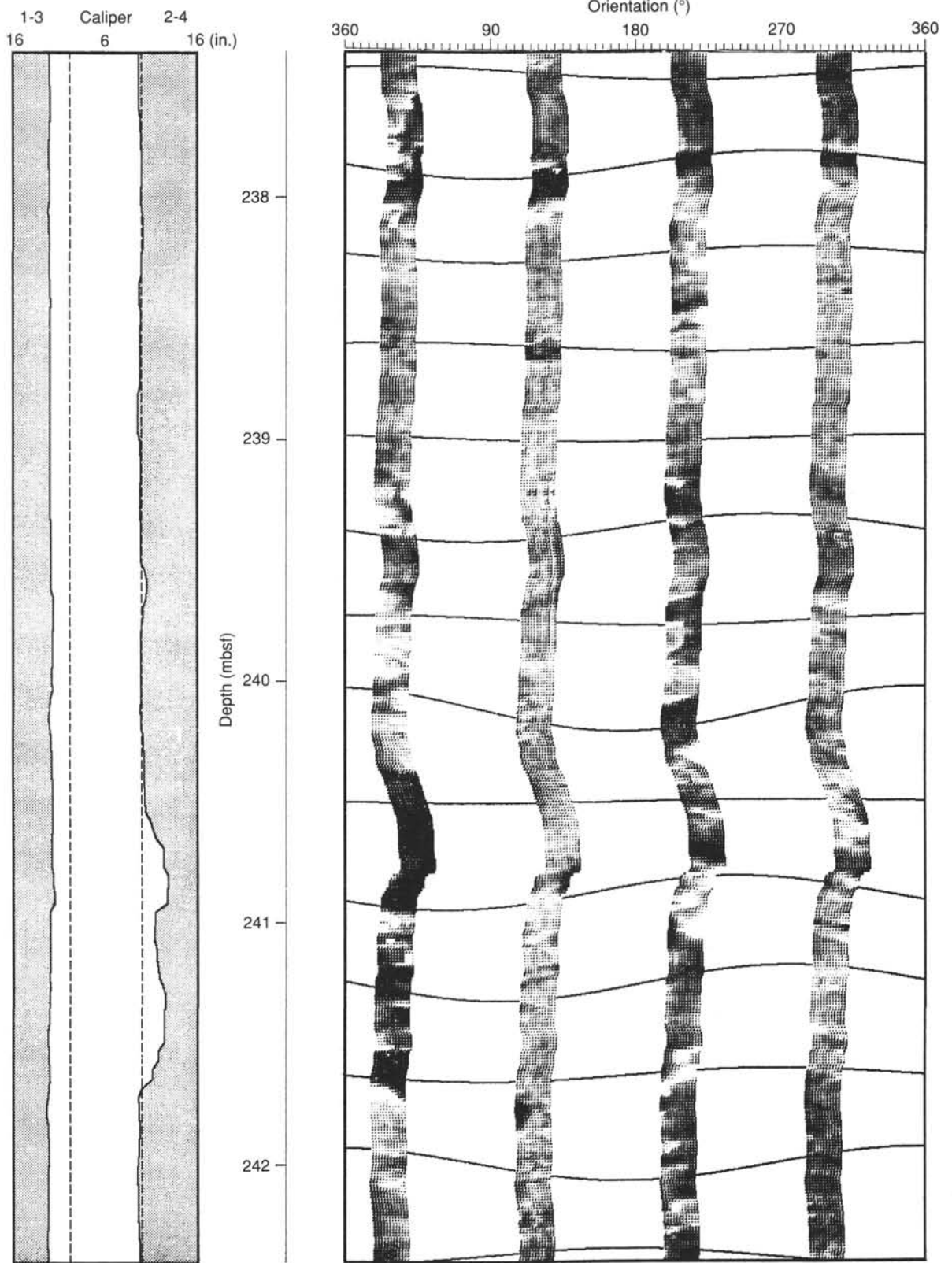


Figure 54. FMS image from the depth interval 237-242 mbsf.

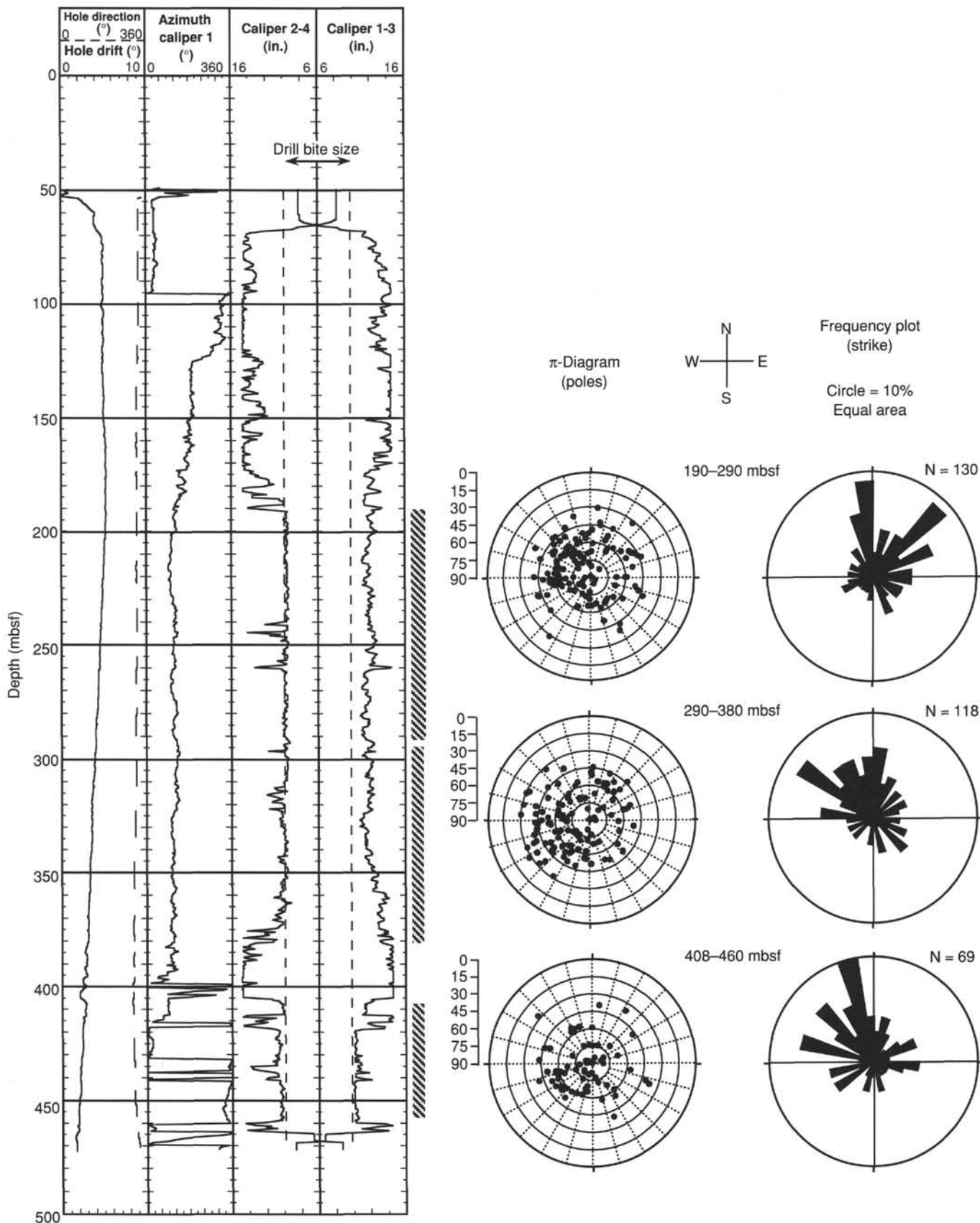


Figure 55. The chart on the left shows the variation in the borehole size, drift, and direction recorded by caliper logs in two perpendicular directions. The π -diagrams and rose diagrams show the strikes and dips of structures as calculated from dipmeter results (FMS data) in three different depth intervals of the drill hole.

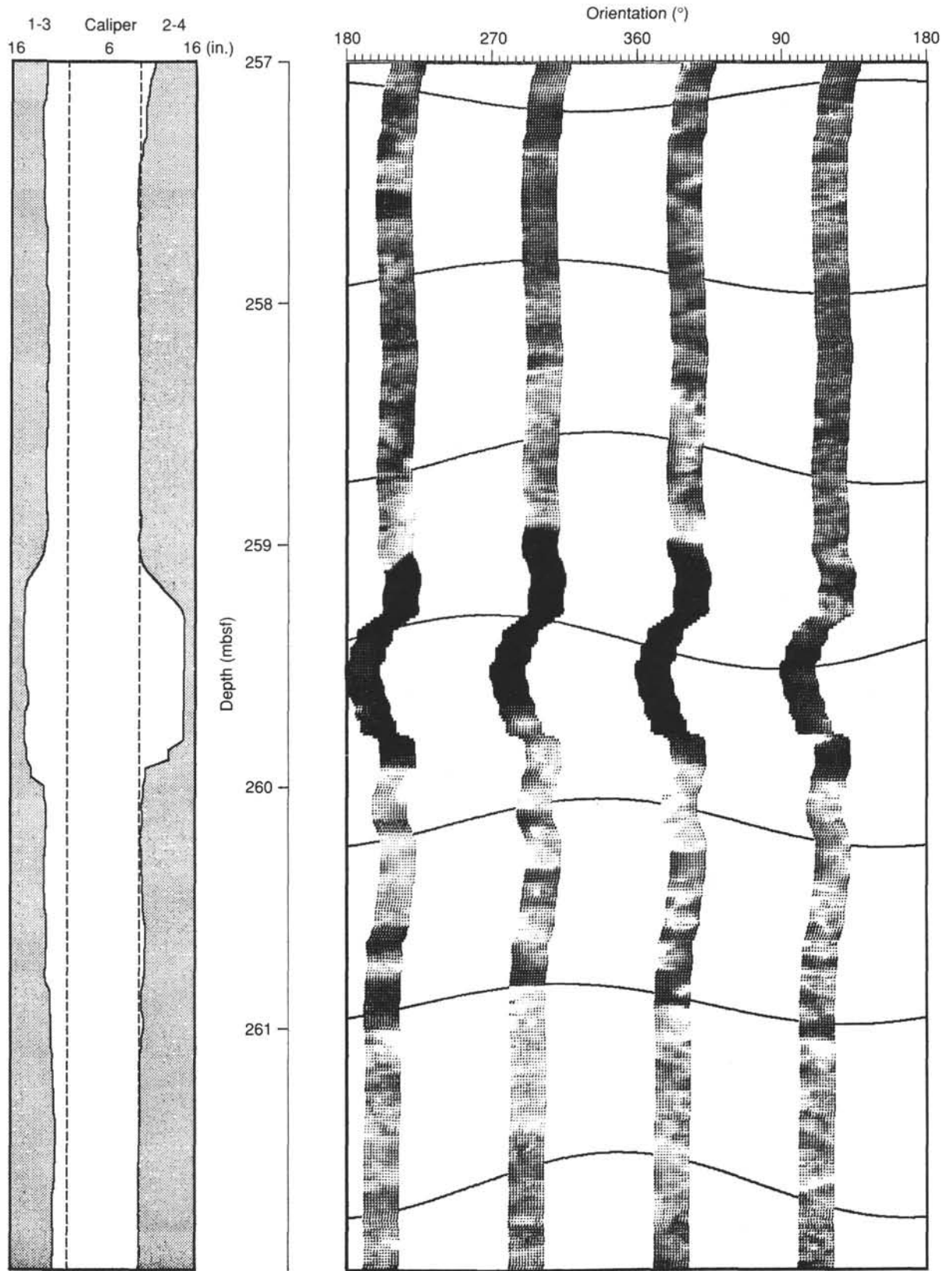


Figure 56. FMS image from the depth interval 257–262 mbsf, which shows an open fracture (black) that dips 40° east. Changes in resistivity across the fracture probably reflect differences in layering and pebble content.

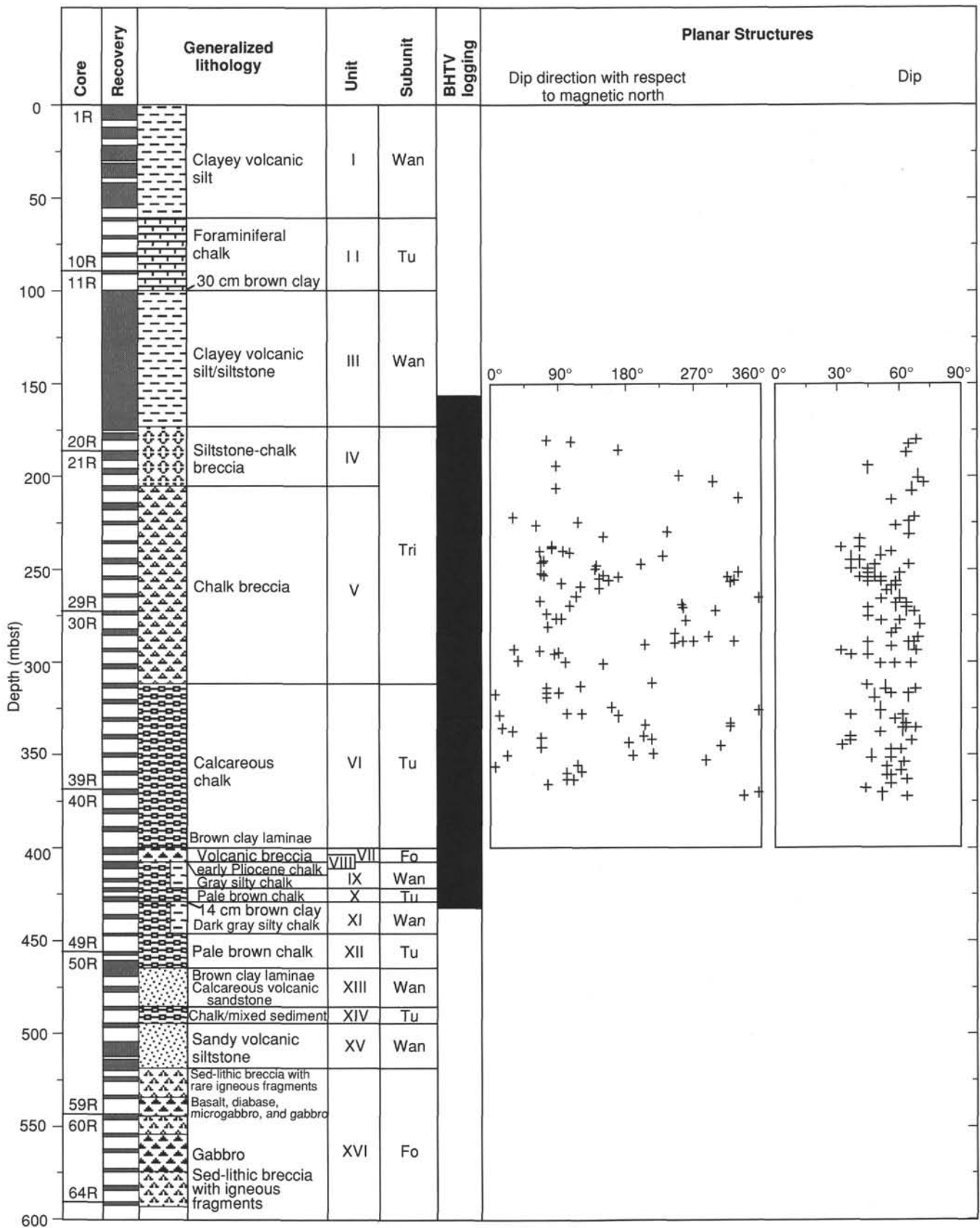


Figure 57. Azimuthal variation of planar structures intersecting the borehole and dip of planar structures.

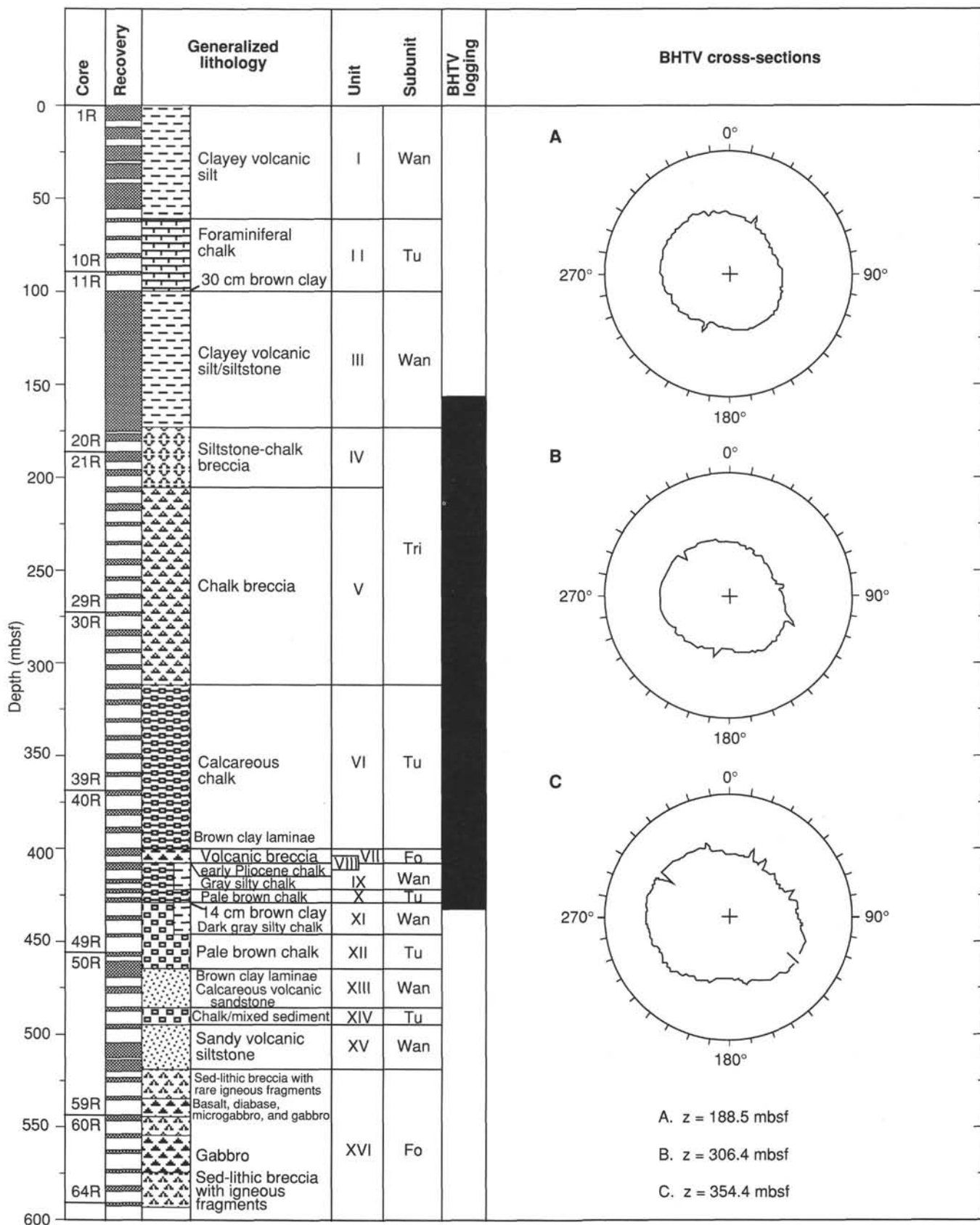


Figure 58. Cross-sections indicating the high deformation and ellipticity of the borehole. Azimuths are with respect to magnetic north.

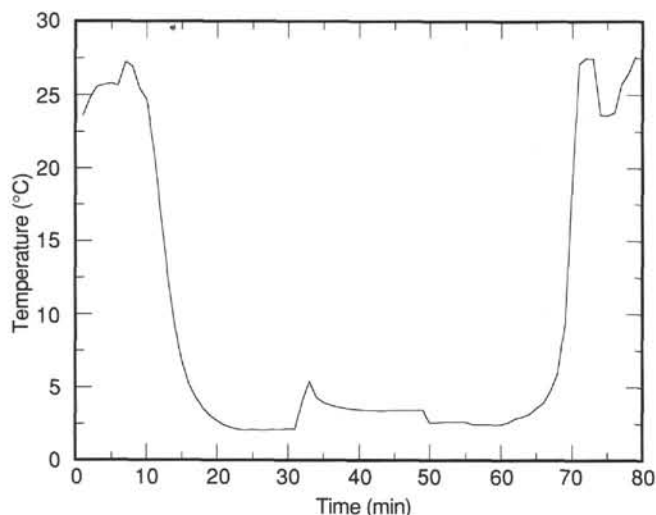


Figure 59. Temperature vs. time for WSTP run 5H in Hole 829C at a depth of 30.3 mbsf.

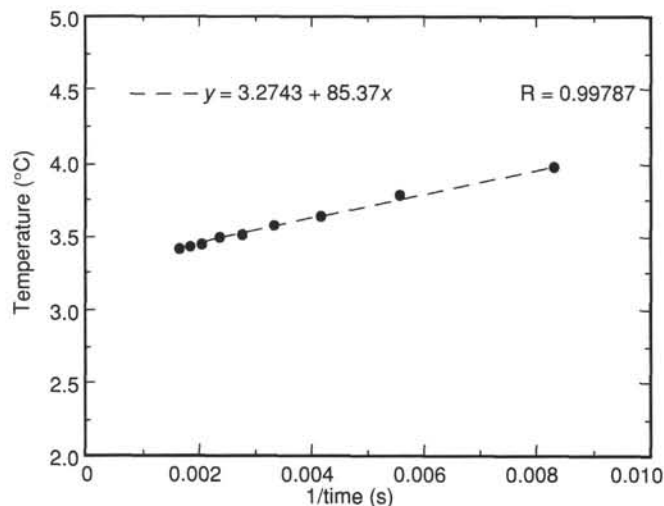


Figure 60. Reduction to equilibrium temperature for WSTP run 5H in Hole 829C. The temperature value at $1/\text{time} = 0$ is the equilibrium value.

stone and silty chalk in lithostratigraphic Units V to XVI) generally have very low water content (10%–20%) and very low porosity (20%–30%). However, in thrust fault zones, which occur in the interval from 400–600 mbsf, water content and porosity increase to 30%–50% and 50%–65%, respectively (Fig. 63). Fluid yields from samples below 200 mbsf are consistent with water content measurements: samples were dry except for those collected immediately below thrust faults, which yielded small amounts of water ($<1 \text{ cm}^3/\text{cm}$; Fig. 22).

The occurrence of relatively undeformed wet rocks above 170 mbsf and highly deformed rocks below 200 mbsf that are dry except at thrust faults suggests that rocks below 200 mbsf have been dewatered and that fluid hydrology is fault-controlled. Dewatering is inferred to result from compressional stress accompanying tectonic accretion rather than from overburden pressure, because the water contents are unusually low. For example, values of 10%–20% water content in chalk between 200 and 400 mbsf at Site 829 contrast with 20%–40% water content in chalk at equivalent depths in the Exmouth Plateau (Haq, von Rad, O'Connell, et al., 1990) and Mas-

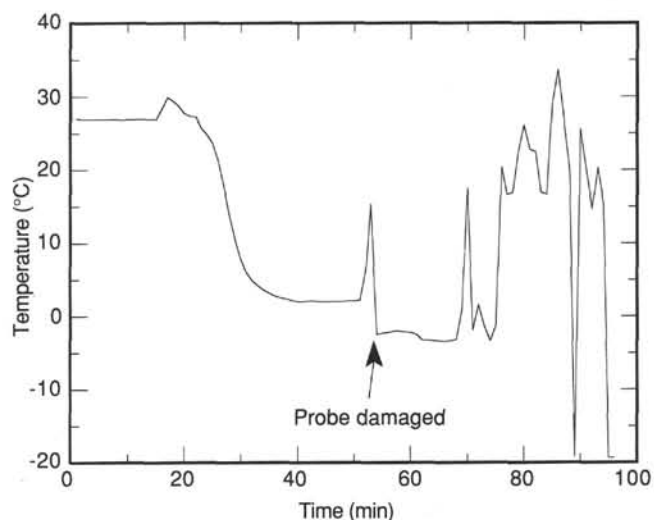


Figure 61. Temperature vs. time for WSTP run 10H in Hole 829C. The arrow indicates the point at which the probe was damaged.

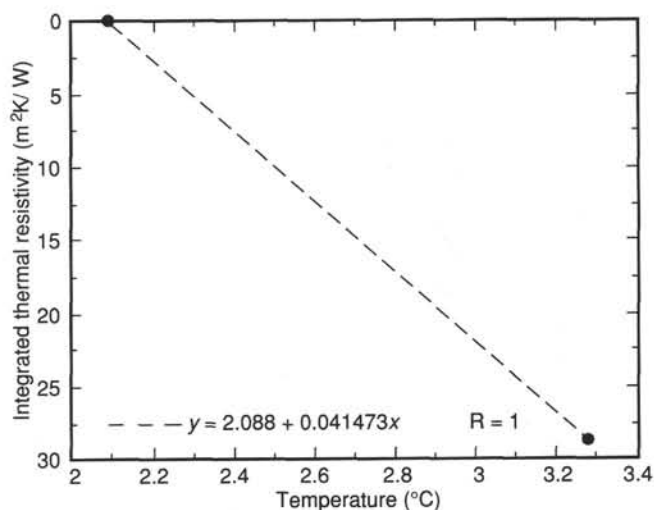


Figure 62. Temperature vs. the depth integral of thermal resistivity. The slope of the linear regression line is the conductive heat flow.

carene Plateau (Backman, Duncan, et al., 1988). In addition, comparison with other active margins shows that water contents at Site 829 are significantly lower than, for example, those in the Barbados accretionary prism, where claystone and mudstone contain about 30% water (Masle, Moore, et al., 1988). Differences in water contents at Site 829 and Barbados could result at least in part from lithologic variations between the two sites. However, the lower values of water content at Site 829 may be an indication that compressional stresses associated with collision between a ridge and an arc are greater than those associated with normal subduction of ocean floor. The mechanism of dewatering at Site 829 is not known, but restriction of fluids at depths greater than 200 mbsf to thrust fault zones suggests that, as in Barbados, the thrust faults act as preferential paths for fluid migration or are impermeable barriers preventing upward fluid migration.

Geochemical analyses of fluids at Site 829 show variations in fluid composition above and below 400 mbsf. In particular, chloride concentrations above 400 mbsf have relatively constant values of about 550 mM, whereas below 400 mbsf chloride concentrations drop to 400–410 mM (Fig. 25). In

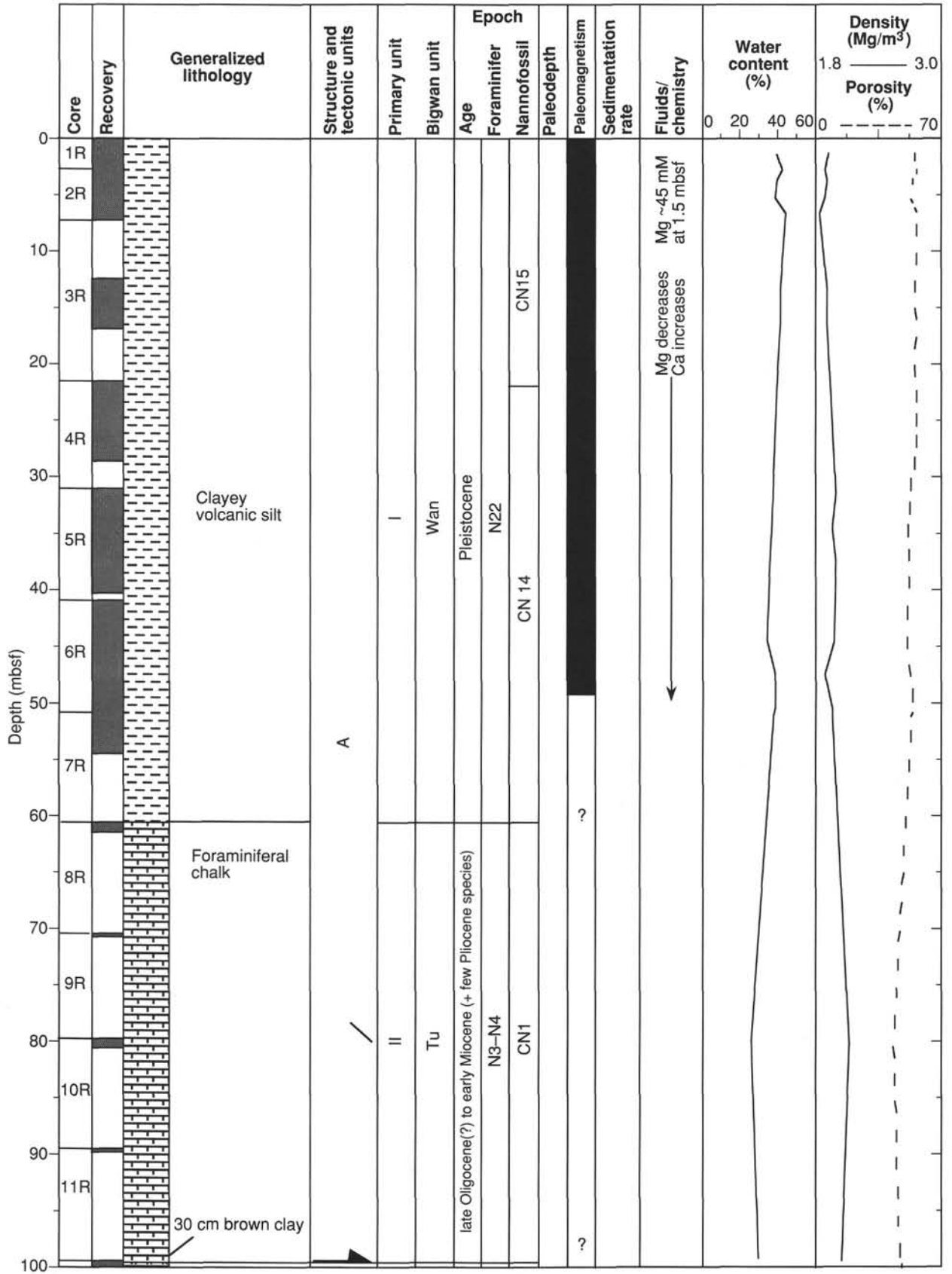


Figure 63. Generalized summary of Hole 829A. If no data or annotations appear in a particular column, refer to the appropriate section of this chapter for details.

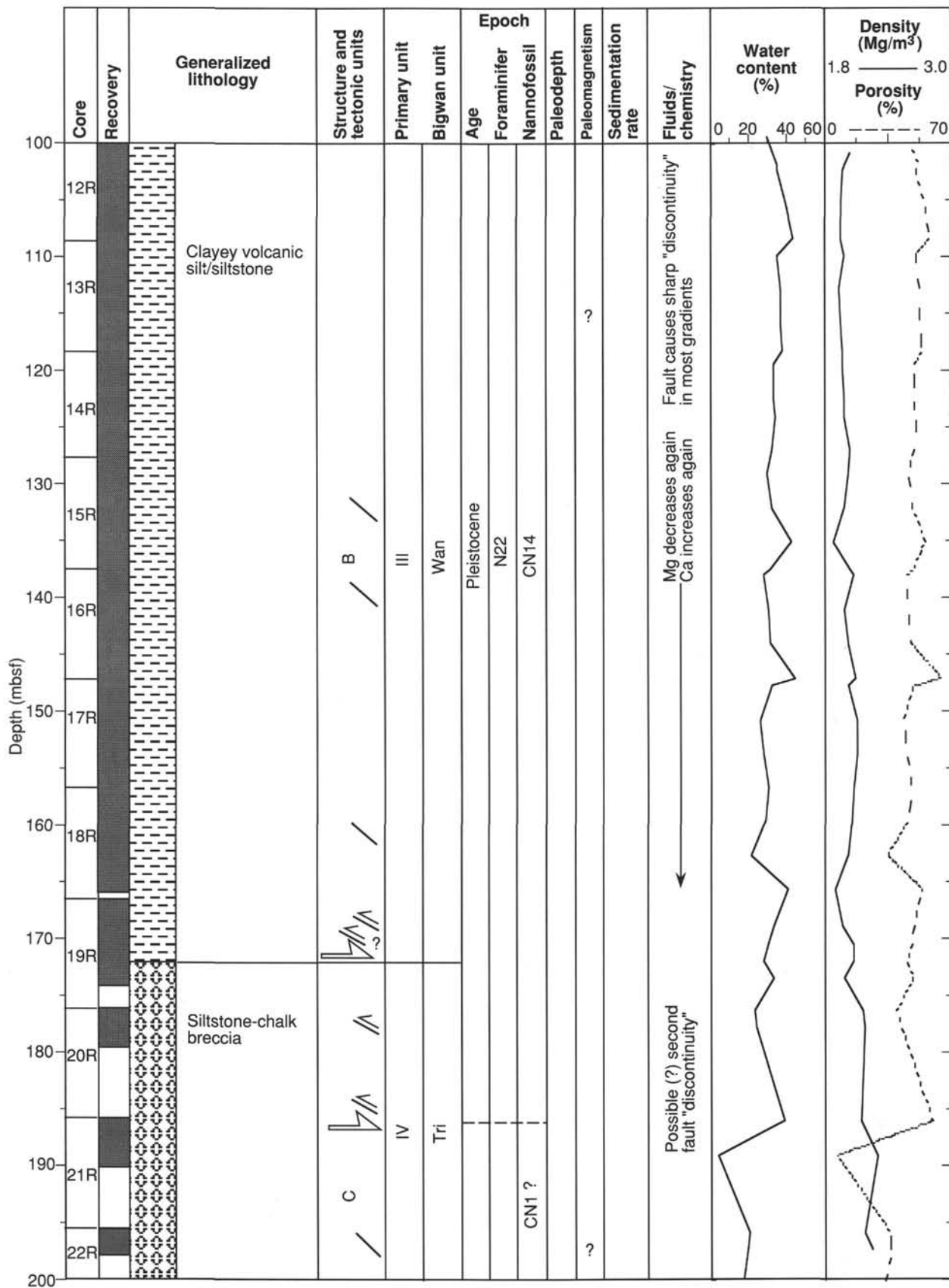


Figure 63 (continued).

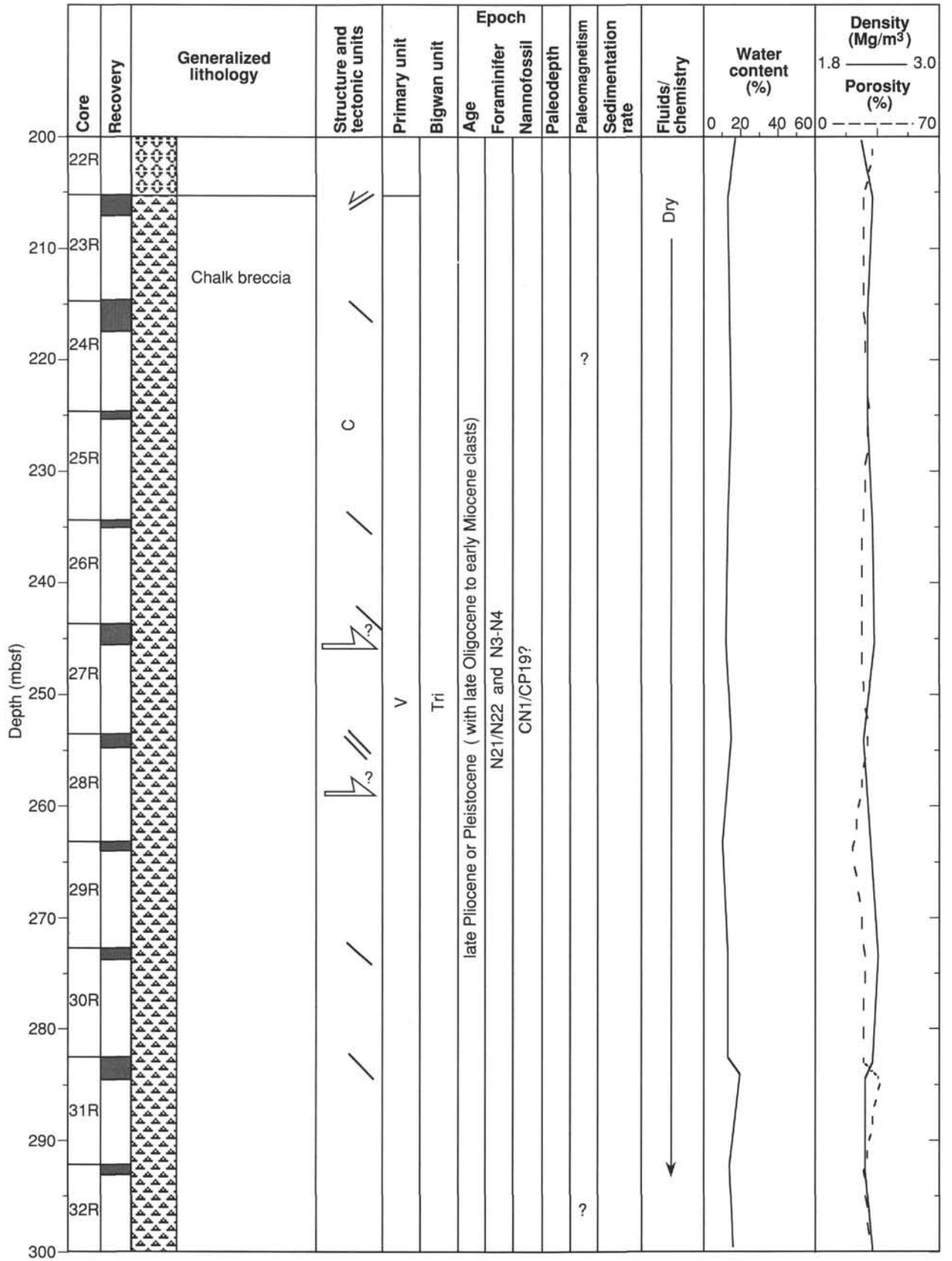


Figure 63 (continued).

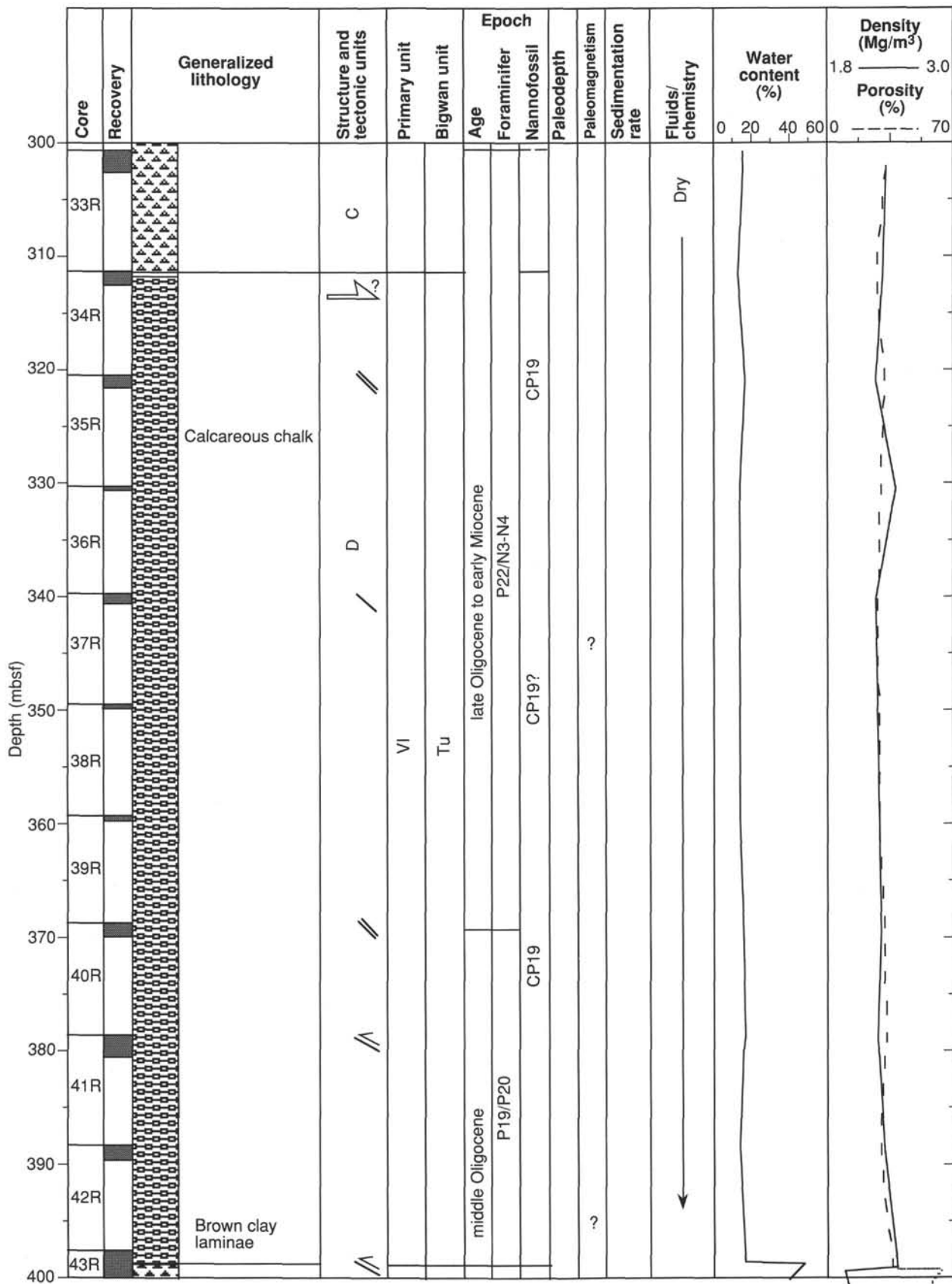


Figure 63 (continued).

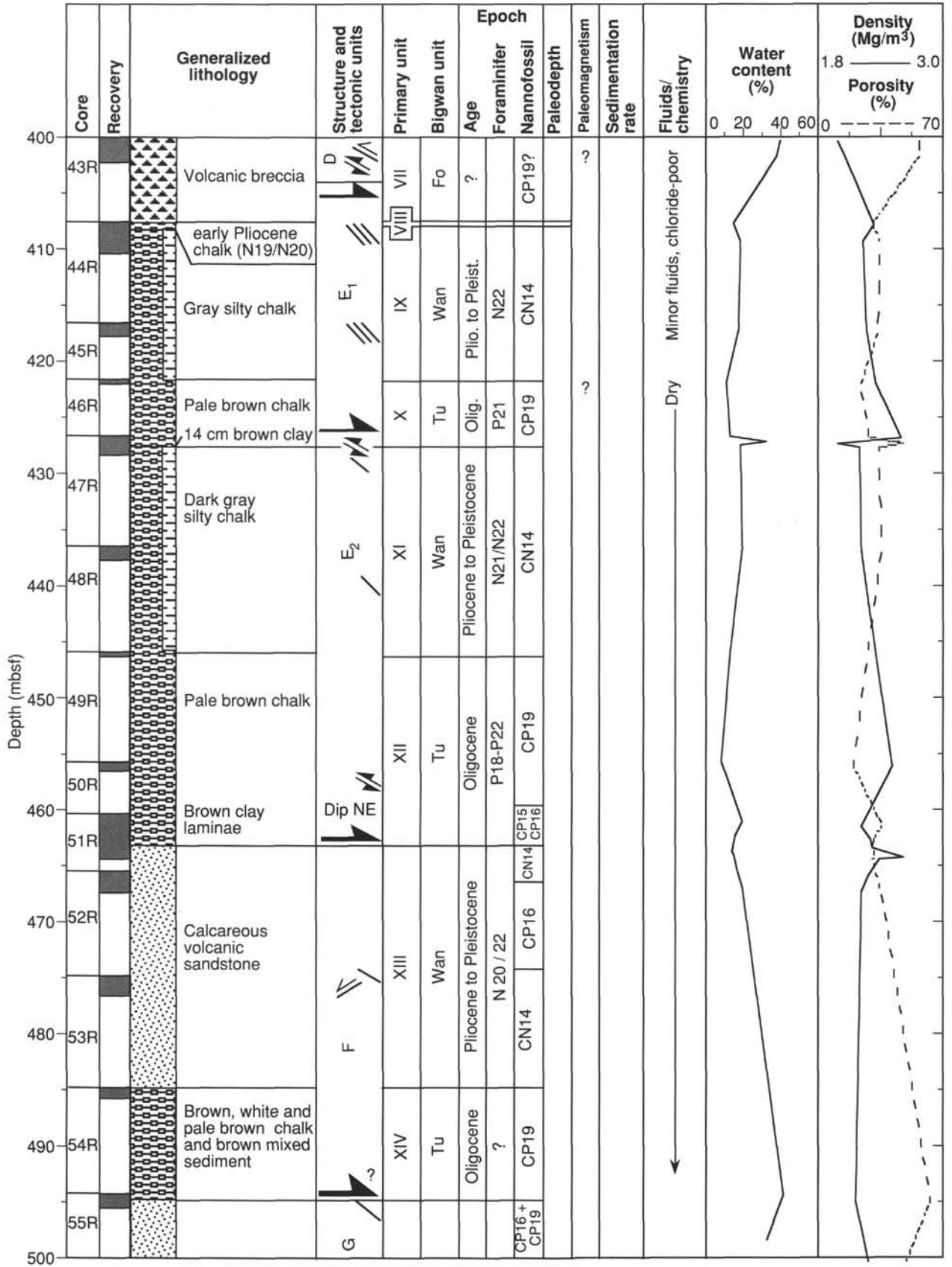


Figure 63 (continued).

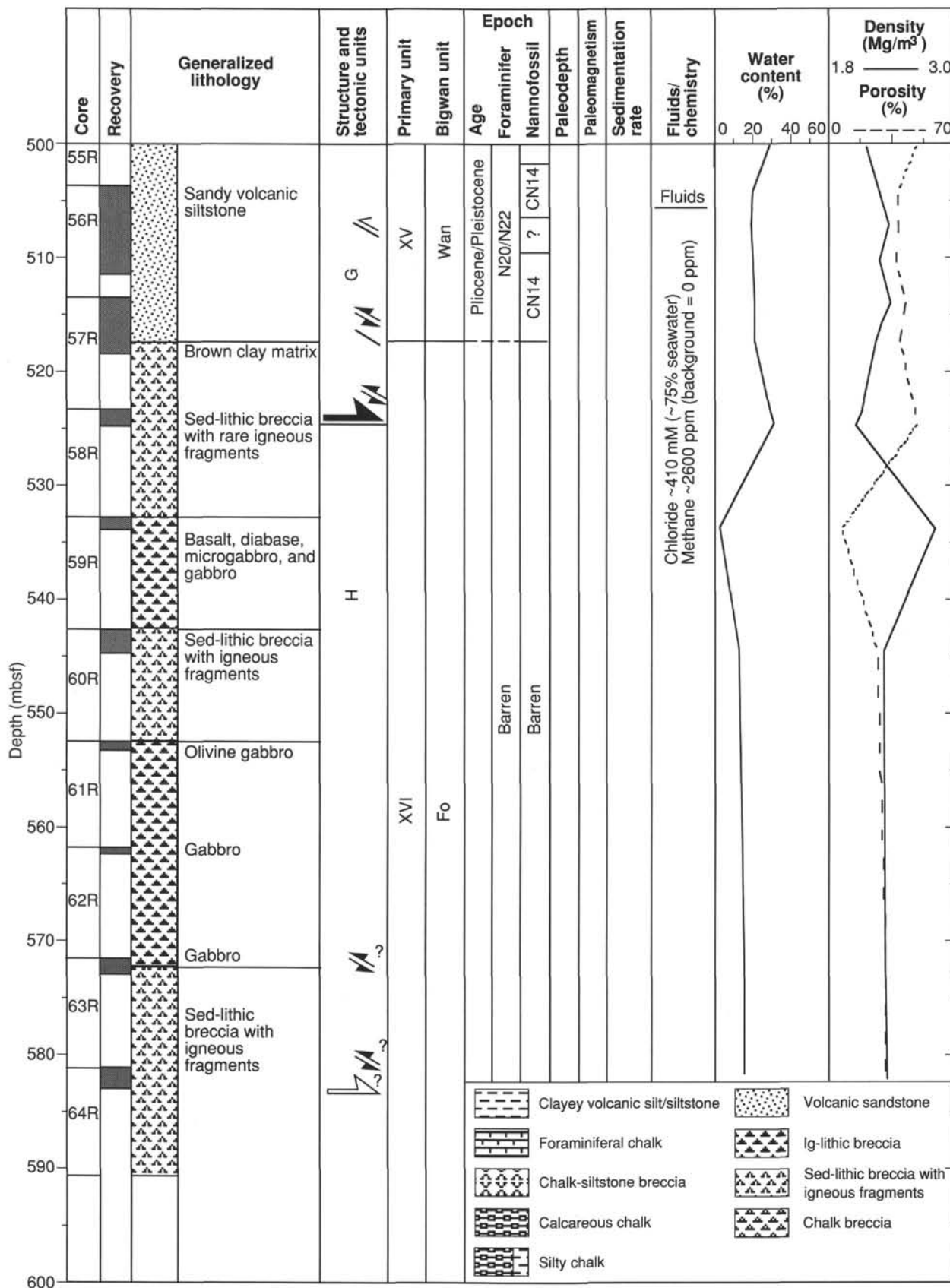


Figure 63 (continued).

addition, methane is absent at Site 829, except near 510 mbsf in Hole 829A, where it has a concentration of 2600 ppm (Fig. 28). Similar occurrences of low chloride and high methane in the décollement zone at Barbados (Masle, Moore, et al., 1988; Gieskes et al., 1990a) suggest that fluids below 400 mbsf at Site 829 may originate in the décollement zone.

Fluid geochemistry also provides evidence that surficial slumping may have occurred at Site 829. A difference between seawater magnesium concentration (55 mM) and the initial magnesium concentration at the sediment-water interface (45 mM; Fig. 27) suggests that 25–50 m of sediment may have been recently removed.

Tectonic, lithostratigraphic, and biostratigraphic data suggest that the sequence of rocks recovered at Site 829 represents an accretionary complex consisting of at least eight imbricated thrust sheets, each consisting of less than 120 m of deformed Cenozoic sediment (Fig. 40). This accretionary complex has resulted from collision between the NDR and the central New Hebrides Island Arc. Although the décollement was not reached at Site 829, it is the first penetration of an accretionary complex in a subduction zone where a ridge collides with an island arc.

Structural observations of the cores from Site 829 indicate that deformation within the accretionary complex is concentrated along major thrust zones marked by intervals of cataclasite ranging in thickness from a few centimeters to 3 m. This cataclasite results from extreme fracturing, grinding, and shearing of rocks during the collision process.

Pore-fluid, physical properties, and structural data indicate that the collision between the NDR and the arc has compressed and dewatered the accreted sediments. Fluid flow concentrates along thrust planes and facilitates movement along the faults. Dewatering of rocks by compressional stress associated with tectonic accretion is suggested by lower water contents at Site 829 than in tectonically undisturbed sediments of equivalent lithology and depth at Site 828. The upper 100 m at both sites consists of silt and chalk, but water contents in the silt and chalk at Site 829 are about 40% and 28%, compared to 50% and 55% in the silt and chalk at Site 828 (see Table 7 in "Physical Properties" section, "Site 828" chapter). In addition, the unusually low fluid content at Site 829, which is even lower than in the Barbados complex (see Masle, Moore, et al., 1988) suggests that extremely high compressive stresses may be associated with collision between a topographic feature and an island arc.

Sediments recovered in the imbricated thrusts at Site 829 are similar to sediments deposited on the NDR at Site 828. The lithostratigraphy of both sites indicates that (1) sediments consist mainly of upper Pliocene(?) to Pleistocene volcanic siltstone and Oligocene chalk, and (2) most of the Miocene section is missing. Thin (less than 10-m-thick) intervals of lower Pliocene and upper Eocene carbonate sediment were also recovered at both sites. In addition, igneous rocks recovered in breccias and conglomerates at Sites 829 and 828 are both transitional between MORB and IAT. The similarities between the sedimentary and igneous rocks at Sites 829 and 828 suggest that rocks of the NDR were incorporated into the accretionary complex.

Despite the general similarities of the lithologies and ages of the rocks at Sites 828 and 829, there are a few differences. First, the length of the hiatus represented by the missing Miocene sediments is different at the two sites. At Site 828 on the ridge, the hiatus extends from the upper Oligocene (~24 Ma) to lower Pliocene (~6 Ma; see "Summary and Conclusions" section, "Site 828" chapter). In contrast, the hiatus at Site 829 in the accretionary complex is shorter, extending only from middle (~15 Ma) to late (~6 Ma) Miocene. However,

recovery of lower Miocene sediments at DSDP Site 286 (Shipboard Scientific Party, 1975), located in the North Loyalty Basin approximately 120 km south of Site 828, suggests that the regional Miocene unconformity is of variable age. Therefore, we infer that lower Miocene sediments, even though not found at Site 828, could be present at other places on the ridge and could have been accreted into the forearc or could represent New Hebrides Island Arc forearc rocks.

A second difference between Site 828 and Site 829 involves the degree of lithification and the stratigraphic position of the lower Pliocene carbonate sediments. The lower Pliocene sediment on the ridge is soupy foraminiferal ooze, but in the accretionary complex this sediment is foraminiferal chalk. The difference in lithification of these sediments could be a result of dewatering of the ooze by compressional stress during tectonic accretion. In addition, the lower Pliocene ooze on the ridge occurs in its correct stratigraphic position, between Oligocene chalk and Pleistocene volcanic silt. In contrast, lower Pliocene chalk in the accretionary complex was not recovered in correct stratigraphic position, but was found in only one interval between volcanic breccia of unknown age and Pleistocene silty chalk. The apparent lack of lower Pliocene chalk stratigraphically located between Oligocene chalk and Pleistocene silt in the accretionary complex may be a result of poor recovery or infrequent paleontological sampling.

Finally, thicknesses of equivalent lithostratigraphic units at Sites 828 and 829 vary. For example, the Oligocene chalk at Site 828 on the ridge is only 20 m thick, whereas it is 87 m thick in tectonic Unit D at Site 829. The increased thickness of chalk at Site 829 could be a function of depositional variability on the ridge or could result from thickening of the section at Site 829 by thrust faulting.

Comparisons between Sites 829 and 827, both located on the arc slope, indicate that in addition to thrust sheets accreted from the ridge the accretionary complex includes arc-derived rocks. Sediment recovered at Site 827, located only 3 km north of Site 829, consists mainly of upper Pliocene(?) to Pleistocene volcanic silt and sed-lithic conglomerate of unknown age. The presence of andesitic clasts with arc affinities in the sed-lithic conglomerate at Site 827, together with the absence of Oligocene to lower Miocene chalk, are evidence that the rocks drilled at Site 827 were derived from the arc rather than from the ridge.

REFERENCES

- Akimoto, K., 1990. Distribution of Recent benthic foraminiferal faunas in the Pacific off Southwest Japan and around Hachijojima Island. *Sci. Rep. Tohoku Univ., Ser. 2*, 60:139–223.
- Backman, J., Duncan, R. A., et al., 1988. *Proc. ODP, Init. Repts.*, 115: College Station, TX (Ocean Drilling Program).
- Bolli, H. M., and Saunders, J. B., 1985. Oligocene to Holocene low latitude planktonic foraminifera. In Bolli, H. M., Saunders, J. B., and Perch-Nielsen, K. (Eds.), *Plankton Stratigraphy*: Cambridge (Cambridge Univ. Press), 155–262.
- Bougault, H., Cambon, P., Corre, O., Joron, J. L., and Treuil, M., 1980. Evidence for variability of magmatic processes and upper mantle heterogeneity in the axial region of the Mid-Atlantic Ridge near 22° and 36°N in oceanic ridges and arcs. In Toksök, M. N., Uyeda, S., and Francheteau, J. (Eds.), *Geodynamic Processes*: Amsterdam (Elsevier), 227–250.
- Briqueu, L., Bougault, H., and Joron, J. L., 1984. Quantification of Nb, Ta, Ti and V anomalies in magmas associated with subduction zones: petrogenetic implications. *Earth Planet. Sci. Lett.*, 68:297–308.
- Bryant, W. R., Bennett, R. H., and Katherman, C. E., 1981. Shear strength, consolidation, porosity, and permeability of oceanic sediments. In Emiliani, C. (Ed.), *The Sea* (Vol. 7): New York (Wiley), 1555–1616.

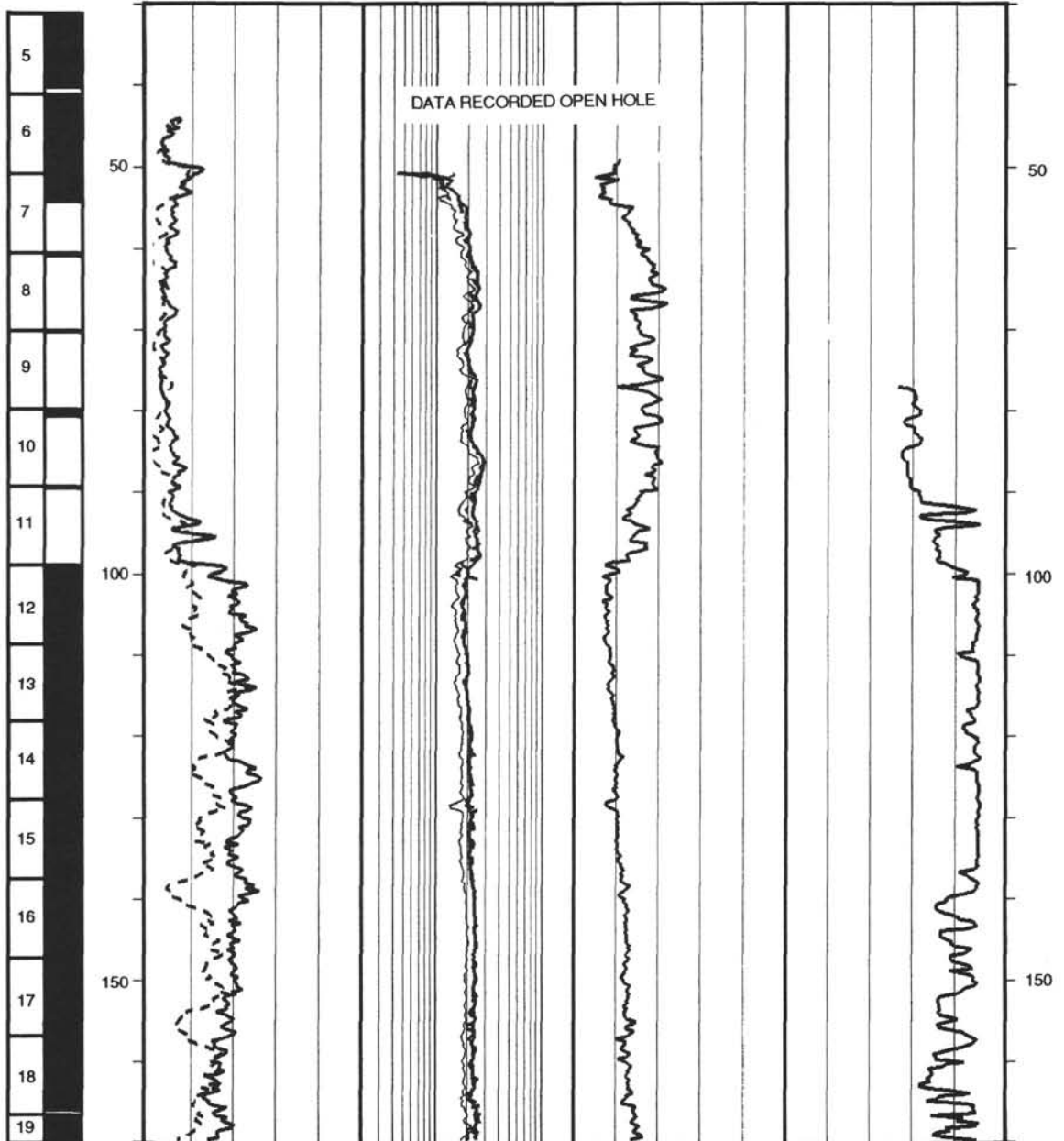
- Carney, J. N., Macfarlane, A., and Mallick, D.I.J., 1985. The Vanuatu island arc—an outline of the stratigraphy, structure, and petrology. In Nairn, A.E.M., Stehli, F. G., and Uyeda, S. (Eds.), *The Ocean Basins and Margins* (Vol. 7): New York (Plenum), 685–718.
- Collot, J.-Y., Daniel, J., and Burne, R. V., 1985. Recent tectonics associated with the subduction/collision of the d'Entrecasteaux zone in the central New Hebrides. *Tectonophysics*, 112:325–356.
- Collot, J.-Y., and Fisher, M. A., 1991. The collision zone between the North d'Entrecasteaux Ridge and the New Hebrides Island Arc. Part 1: Seabeam morphology and shallow structure. *J. Geophys. Res.*, 96:4457–4478.
- Collot, J.-Y., Pelletier, B., Boulin, J., Daniel, J., Eissen, J.-P., Fisher, M. A., Greene, H. G., Lallemand, S., and Monzier, M., 1989. Premiers résultats des plongées de la campagne SUBPSO1 dans la zone de collision des rides d'Entrecasteaux et de l'arc des Nouvelles Hébrides. *C. R. Acad. Sci. Ser. 2*, 309:1947–1954.
- Crowley, T., 1990. *An Illustrated Bislama-English and English-Bislama Dictionary*: Vila, Vanuatu (Pacific Unit and the Vanuatu Extension Centre of the University of the South Pacific).
- Dupuy, C., Dostal, J., Marcellot, G., Bougault, H., Joron, J. L., and Treuil, M., 1982. Geochemistry of basalts from central and southern New Hebrides arc: implication for their source rock composition. *Earth Planet. Sci. Lett.*, 60:207–225.
- Etoubleau, J., Corre, O., Joron, J. L., Bougault, H., and Treuil, M., 1983. Costa Rica Rift: variably depleted basalt in the same Hole. In Cann, J. R., Langseth, M. G., Honnorez, J., Von Herzen, R. P., White, S. M., et al., *Init. Repts. DSDP*, 69: Washington (U.S. Govt. Printing Office), 765–773.
- Fisher, M. A., Collot, J.-Y., and Geist, E. L., 1991. The collision zone between the North d'Entrecasteaux Ridge and the New Hebrides Island Arc. Part 2: structure from multichannel seismic data. *J. Geophys. Res.*, 96:4479–4495.
- Fisher, M. A., Collot, J.-Y., Smith, G. L., 1986. Possible causes for structural variation where the New Hebrides island arc and the d'Entrecasteaux Zone collide. *Geology*, 14:951–954.
- Gieskes, J., and Gamo, T., in press. Chemical methods for interstitial water analysis on *JOIDES Resolution*. *ODP Tech. Note*.
- Gieskes, J. M., 1981. Deep-sea drilling interstitial water studies: implications for chemical alteration of the oceanic crust, layers I and II. In Warne, J. E., Douglas, R. G., and Winterer, E. L. (Eds.), *The Deep Sea Drilling Project: A Decade of Progress*. Soc. Econ. Paleontol. Mineral. Spec. Publ., 32:149–167.
- Gieskes, J. M., Blanc, G., Vrolijk, P., Elderfield, H., and Barnes, R., 1990a. Interstitial water chemistry—major constituents. In Moore, J. C., Mascle, A., et al., *Proc. ODP, Sci. Results*, 110: College Station, TX (Ocean Drilling Program), 155–178.
- Gieskes, J. M., Vrolijk, P., and Blanc, G., 1990b. Hydrogeochemistry of the northern Barbados accretionary complex transect: Ocean Drilling Program Leg 110. *J. Geophys. Res.*, 95:8809–8818.
- Gorton, M., 1974. The geochemistry and geochronology of the New Hebrides. Unpubl. Ph.D thesis, Australian National Univ., Canberra.
- Haq, B. U., von Rad, U., O'Connell, S., et al., 1990. *Proc. ODP, Init. Repts.*, 122: College Station, TX (Ocean Drilling Program).
- Kennett, J. P., and Srinivasan, M. S., 1983. *Neogene Planktonic Foraminifera: A Phylogenetic Atlas*: Stroudsburg, PA (Hutchinson Ross).
- Le Pichon, X., Foucher, J.-P., Boulegue, J., Henry, P., Lallemand, S., Benedetti, M., Avedik, F., and Mariotti, A., 1990. Mud volcano field seaward of the Barbados accretionary complex: a submersible survey. *J. Geophys. Res.*, 95:8931–8943.
- Mascle, A., Moore, J. C., et al., 1988. *Proc. ODP, Init. Repts.*, 110: College Station, TX (Ocean Drilling Program).
- Mottl, M. J., in press. Pore waters from serpentinite seamounts in the Mariana and Izu-Bonin forearcs, ODP Leg 125: evidence for volatiles from the subducting slab. In Fryer, P., Pearce, J. A., et al., *Proc. ODP, Sci., Results*, 125: College Station, TX (Ocean Drilling Program).
- Passchier, C. W., and Simpson, C., 1986. Porphyroclast systems as kinematic indicators. *J. Struct. Geol.*, 8:831–843.
- Ramsay, J. G., and Huber, M. I. (Eds.), 1987. *Techniques of Modern Structural Geology* (Vol. II): Oxford (Academic Press).
- Shipboard Scientific Party, 1975. Site 286. In Andrews, J. E., Packham, G., et al., *Init. Repts. DSDP*, 30: Washington (U.S. Govt. Printing Office), 69–131.
- _____, 1988. Site 504, Costa Rica Rift. In Becker, K., Sakai, H., et al., *Proc. ODP, Init. Repts.*, 111: College Station, TX (Ocean Drilling Program), 35–251.
- Sun, S. S., 1980. Lead isotopic study of young volcanic rocks from mid-ocean ridges, ocean islands and island arcs. *Philos. Trans. R. Soc. London*, A297:409–445.
- Taira, A., Hill, I., Firth, J., et al., 1991. *Proc. ODP, Init. Repts.*, 131: College Station, TX (Ocean Drilling Program).
- Taylor, E., and Leonard, J., 1990. Sediment consolidation and permeability at the Barbados forearc. In Moore, J. C., Mascle, A., et al., *Proc. ODP, Sci. Results*, 110: College Station, TX (Ocean Drilling Program), 289–308.

Ms 134A-109

NOTE: All core description forms (“barrel sheets”) and core photographs have been printed on coated paper and bound as Section 4, near the back of this volume, beginning on page 581.

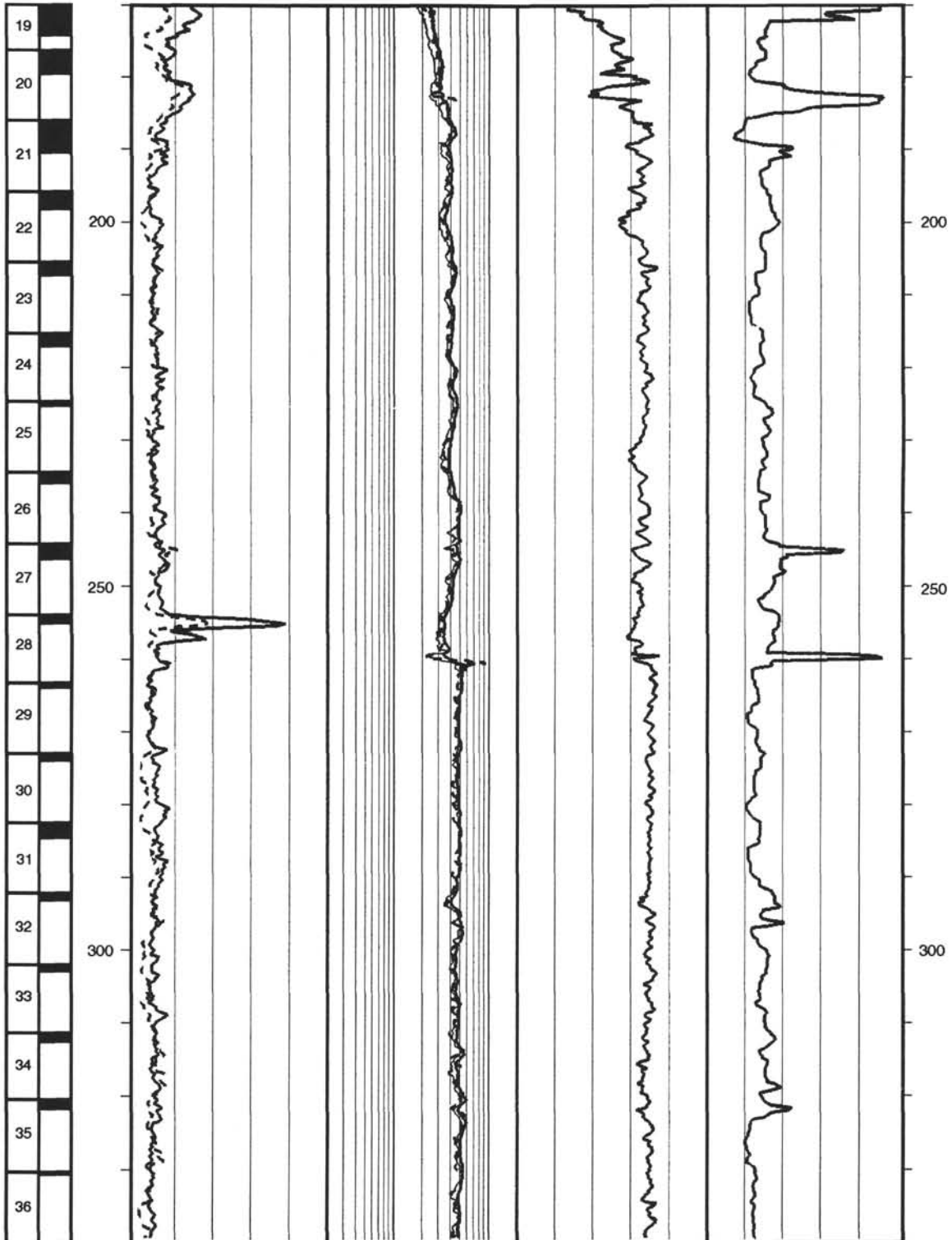
Hole 829A: Resistivity-Sonic-Natural Gamma Ray Log Summary

CORE RECOVERY	DEPTH BELOW SEA FLOOR (m)	RESISTIVITY								DEPTH BELOW SEA FLOOR (m)		
		SPECTRAL GAMMA RAY			FOCUSED							
		0	50	0.2	ohm*m	20						
		COMPUTED			SHALLOW							
	0	API units	50	0.2	ohm*m	20	TRANSIT TIME					
							200	µs/ft	50	9	in	19
		TOTAL			DEEP					CALIPER		
		0	API units	50	0.2	ohm*m	20					



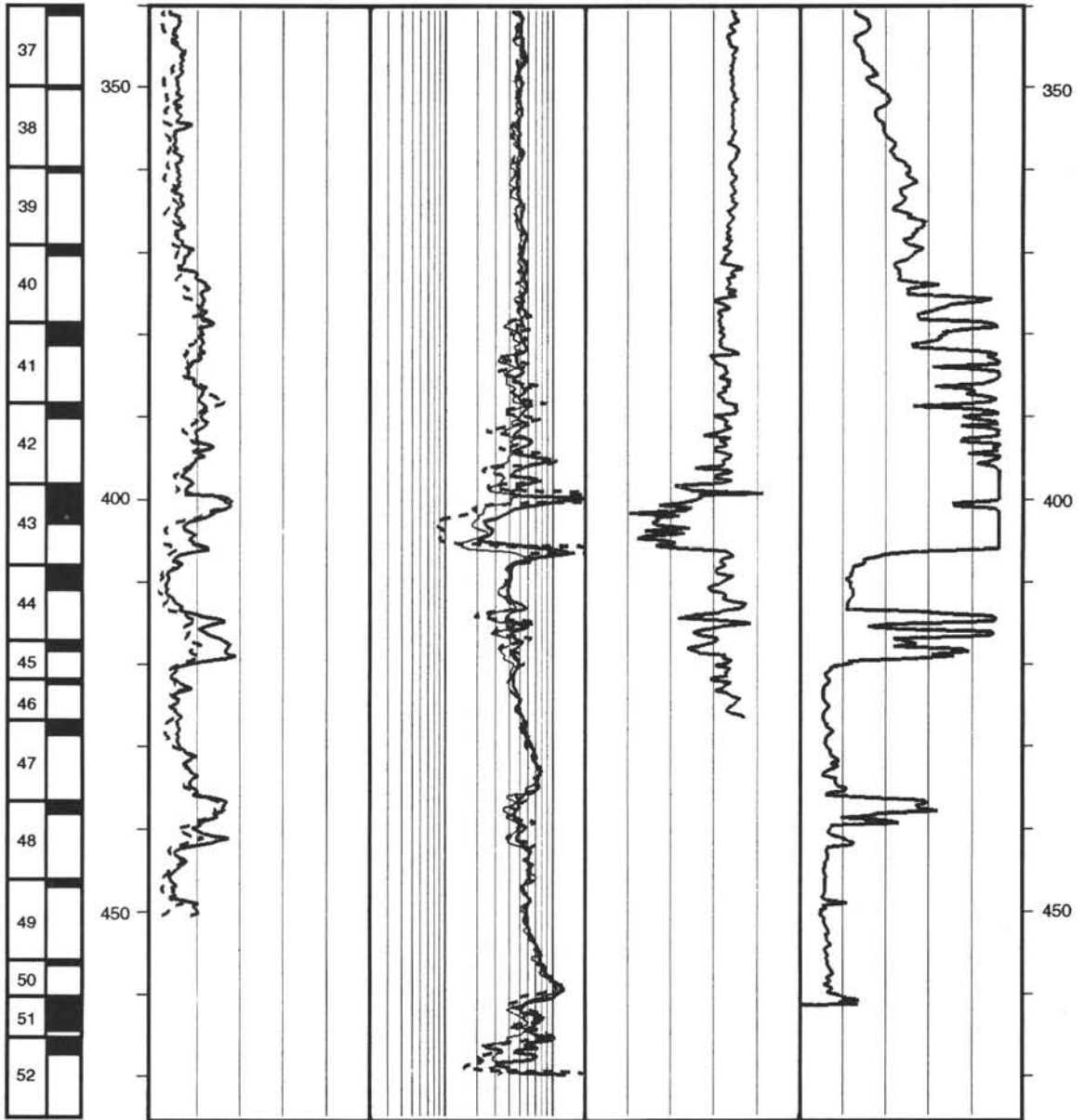
Hole 829A: Resistivity-Sonic-Natural Gamma Ray Log Summary (continued)

CORE RECOVERY	DEPTH BELOW SEA FLOOR (m)	RESISTIVITY						DEPTH BELOW SEA FLOOR (m)		
		SPECTRAL GAMMA RAY		FOCUSED		SHALLOW				
		0	50	0.2	20	0.2	20			
		COMPUTED API units		SHALLOW ohm•m		DEEP ohm•m		TRANSIT TIME μs/ft	CALIPER in	
		0	50	0.2	20	200	50	9	19	



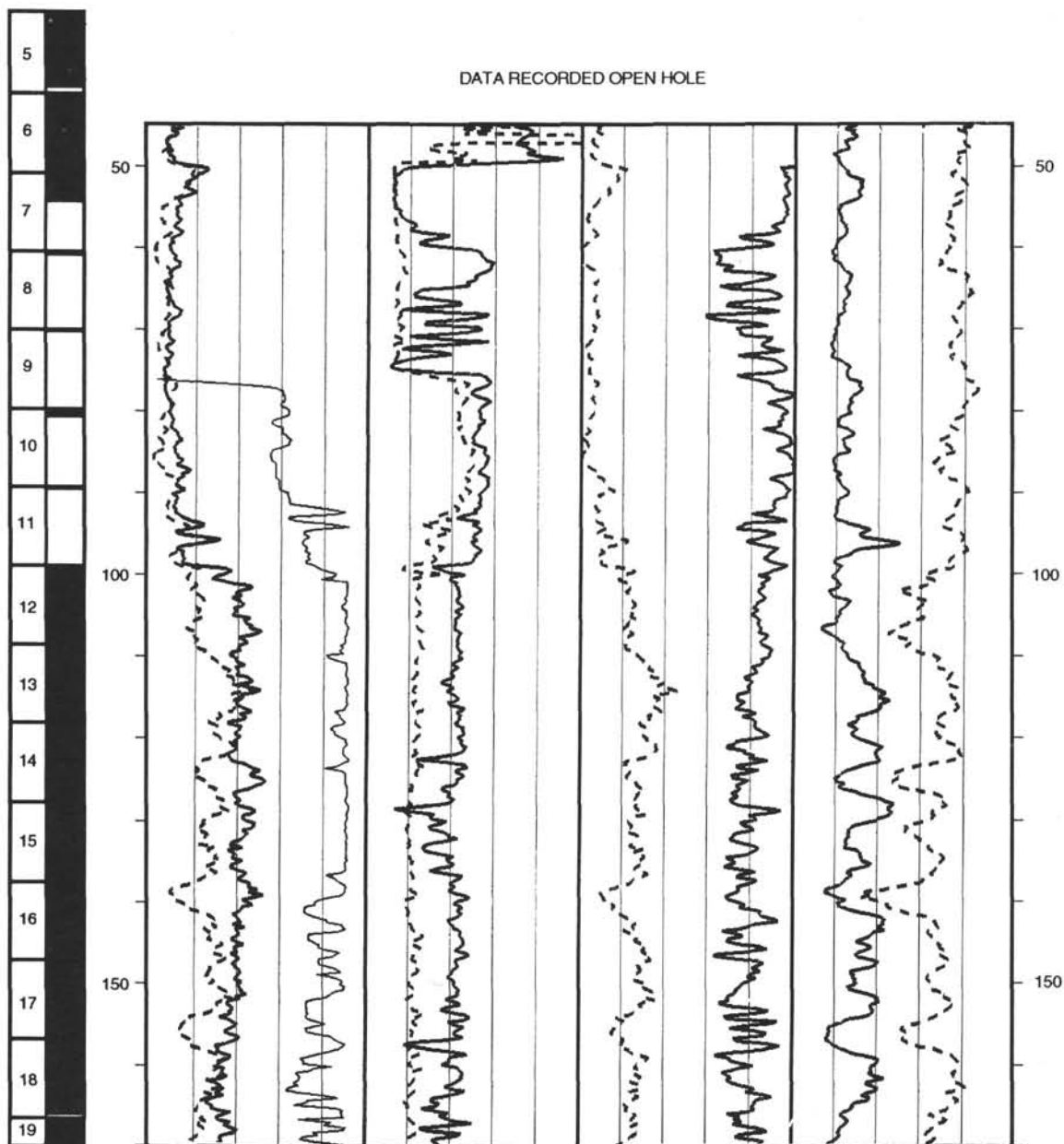
Hole 829A: Resistivity-Sonic-Natural Gamma Ray Log Summary (continued)

CORE RECOVERY	DEPTH BELOW SEA FLOOR (m)	RESISTIVITY								DEPTH BELOW SEA FLOOR (m)		
		SPECTRAL GAMMA RAY				FOCUSED						
		COMPUTED		SHALLOW		DEEP		TRANSIT TIME			CALIPER	
		0	50	0.2	20	0.2	20	200	50		9	19
	API units		ohm*m		ohm*m		μs/ft		in			

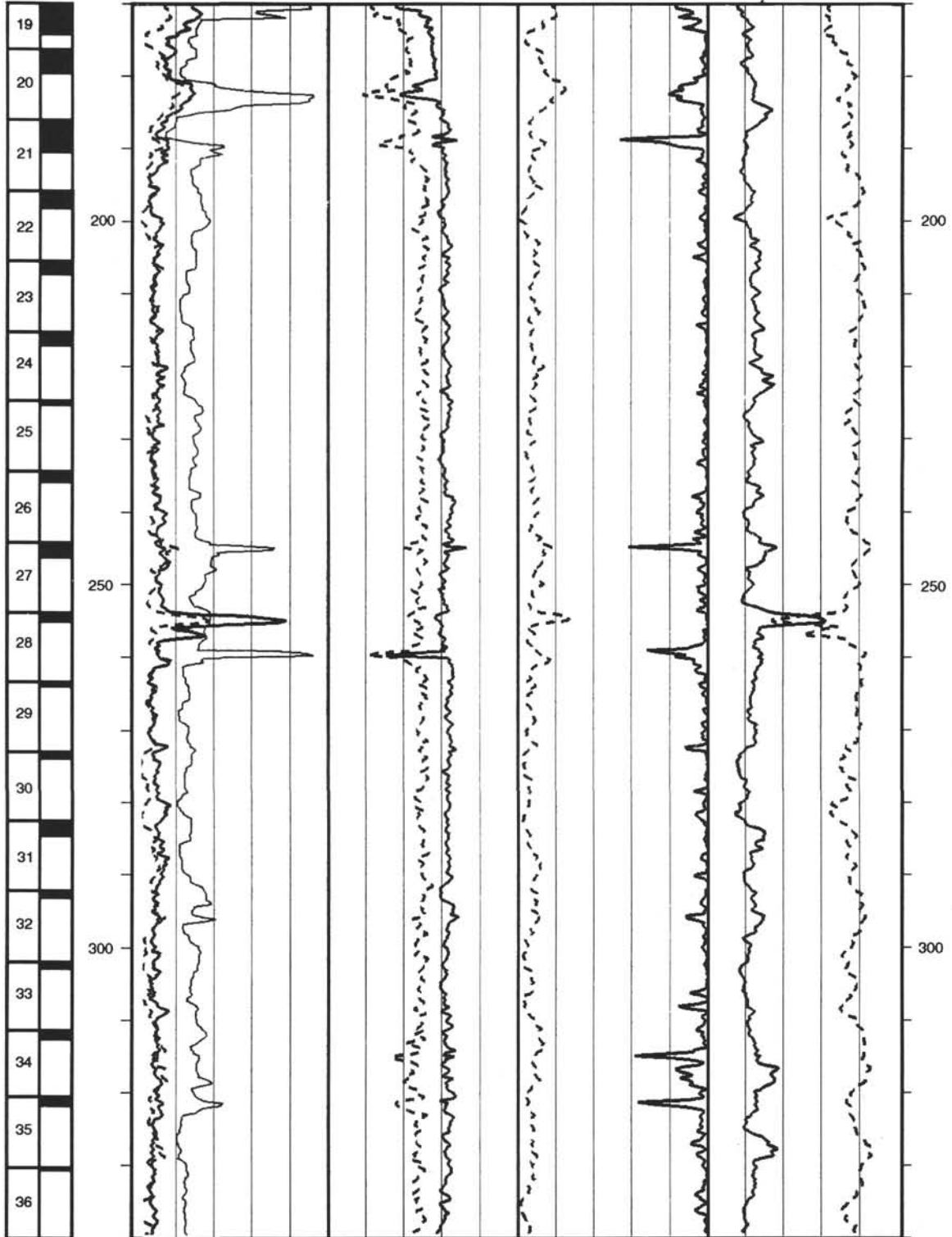
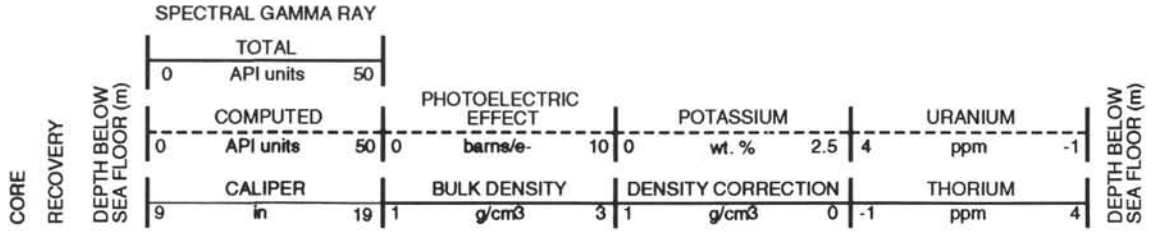


Hole 829A: Density-Natural Gamma Ray Log Summary

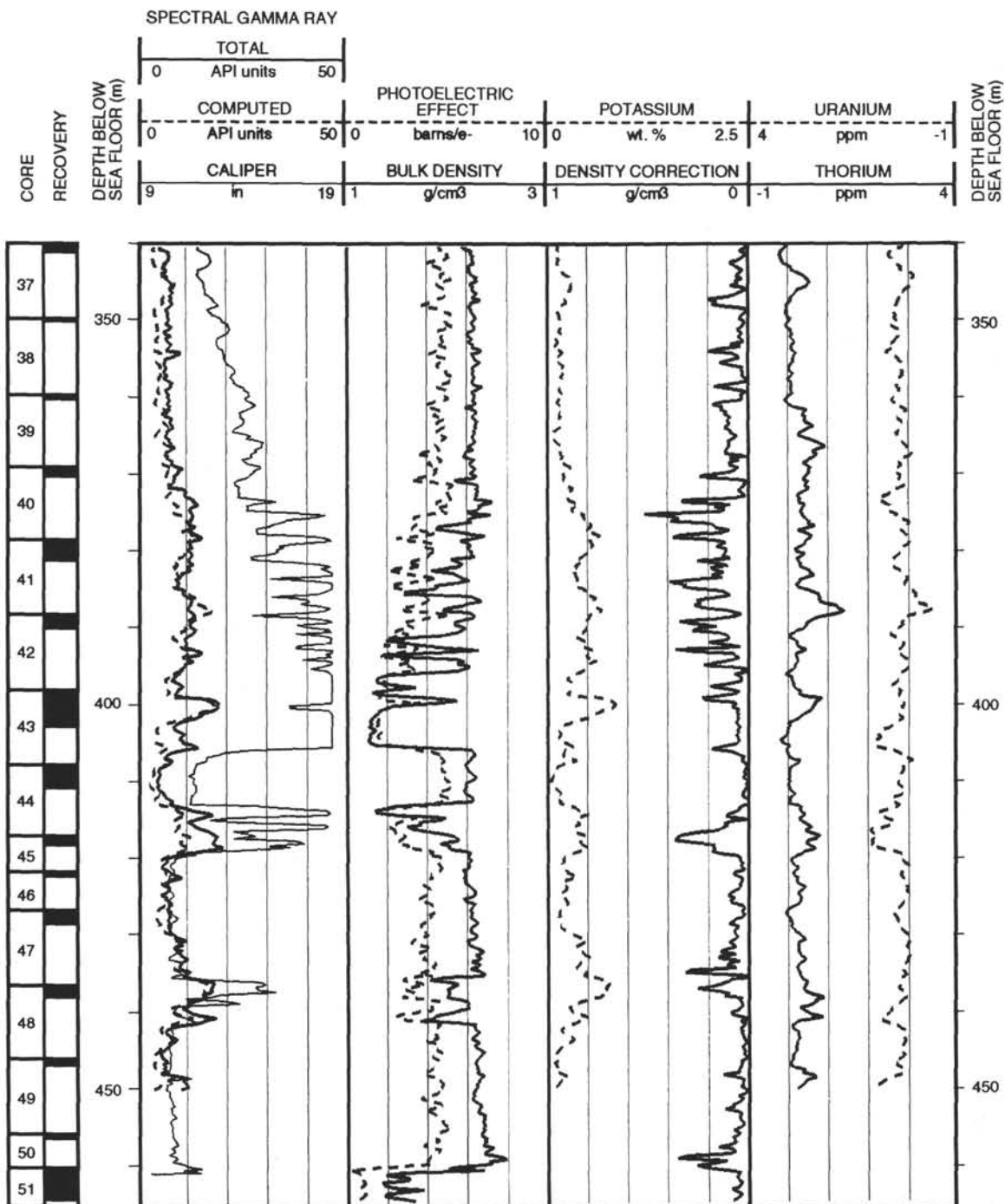
		SPECTRAL GAMMA RAY								
		TOTAL		PHOTOELECTRIC EFFECT		POTASSIUM		URANIUM		
CORE RECOVERY	DEPTH BELOW SEA FLOOR (m)	API units		barns/e-		wt. %		ppm		DEPTH BELOW SEA FLOOR (m)
		0	50	0	10	0	2.5	4	-1	
		COMPUTED		BULK DENSITY		DENSITY CORRECTION		THORIUM		
		API units		g/cm ³		g/cm ³		ppm		
		0 50		0 10		0 2.5 4		-1		
		9		1		1		-1		
		in		g/cm ³		g/cm ³		ppm		
		19		3		0		4		



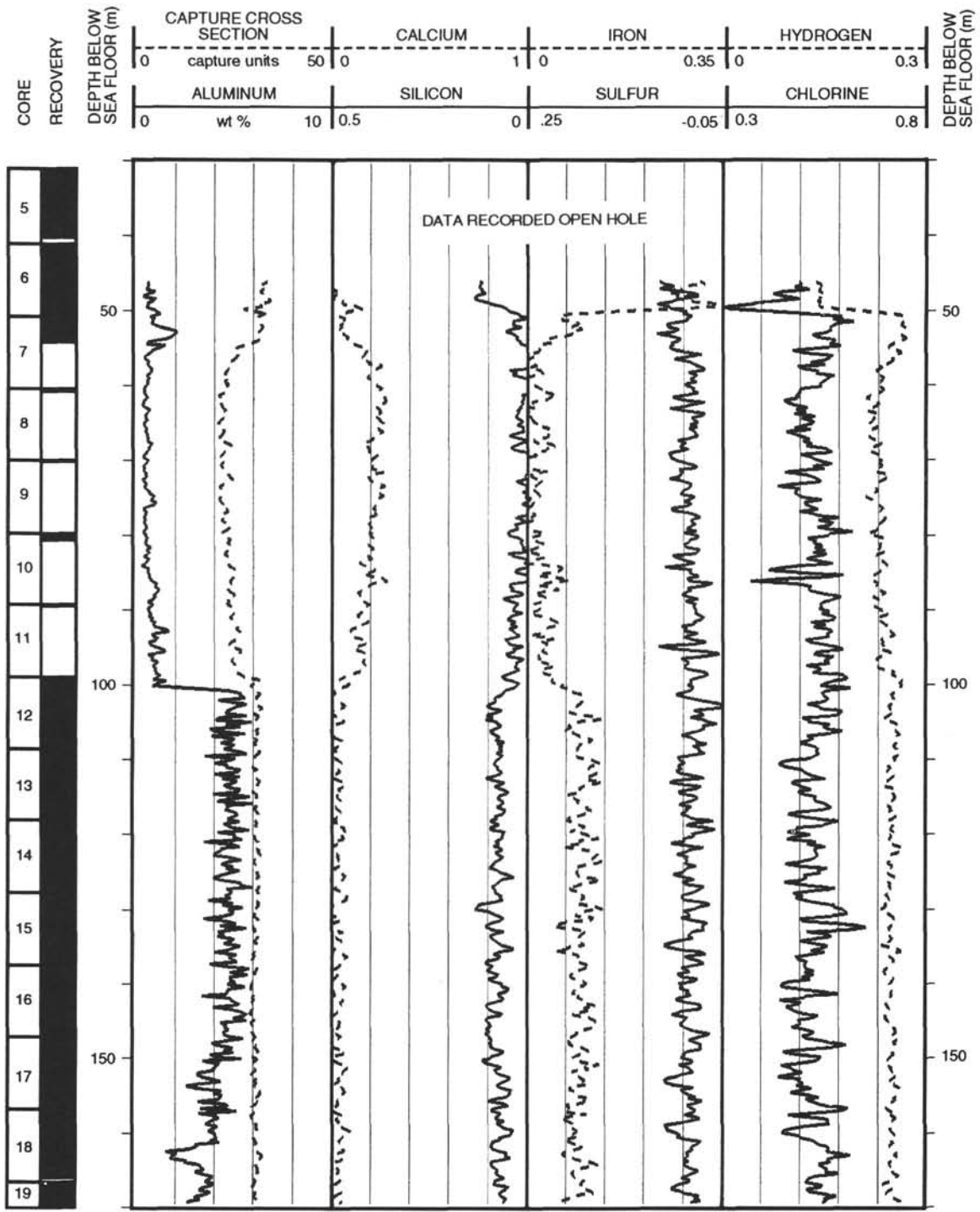
Hole 829A: Density-Natural Gamma Ray Log Summary (continued)



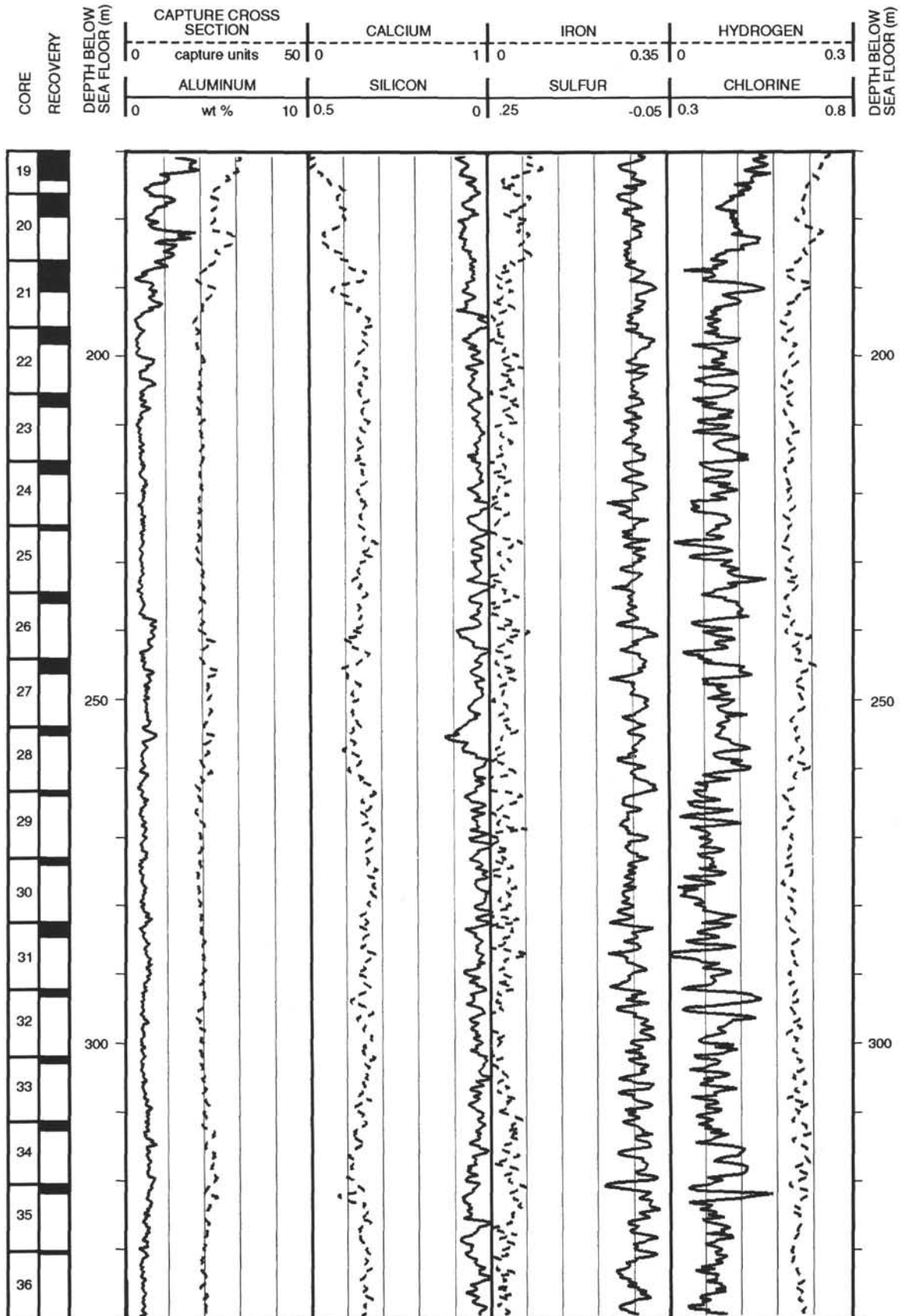
Hole 829A: Density-Natural Gamma Ray Log Summary (continued)



Hole 829A: Geochemical Log Summary



Hole 829A: Geochemical Log Summary (continued)



Hole 829A: Geochemical Log Summary (continued)

